LMSC-A959837
VOL III
DECEMBER 22, 1969

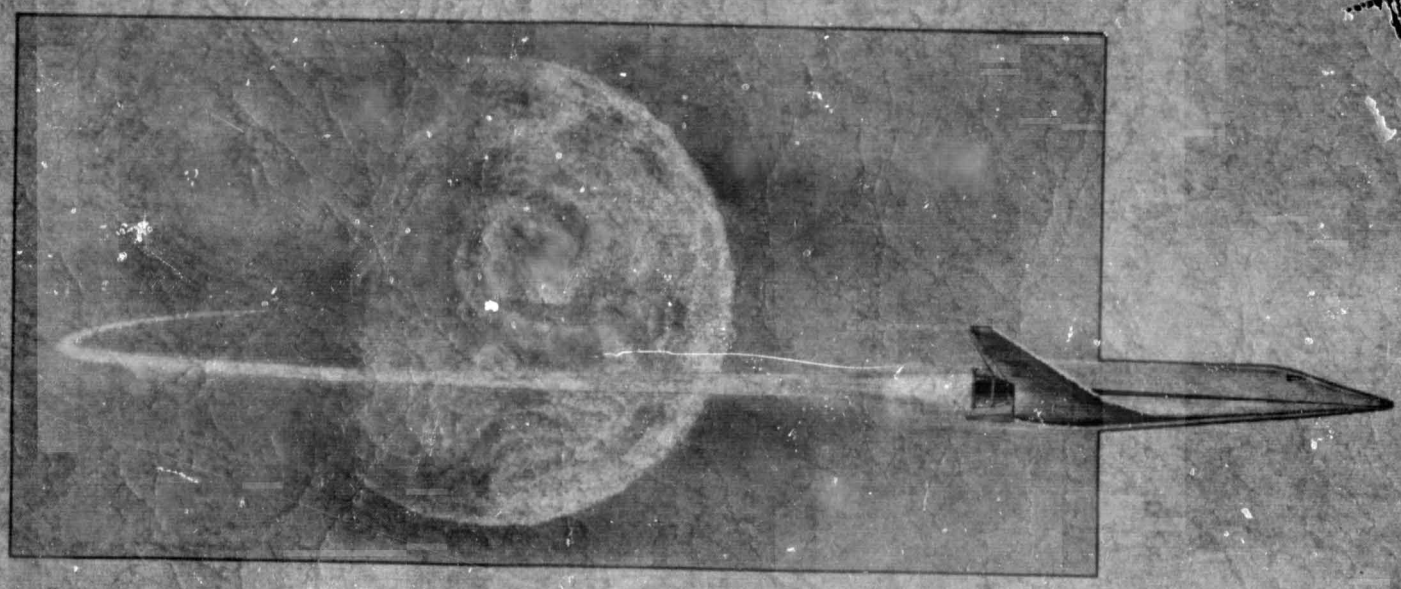

LOCKHEED
LMSC
SPACE SYSTEMS
DIVISION

FINAL REPORT
INTEGRAL LAUNCH AND REENTRY VEHICLE

VOLUME III
SPECIAL STUDIES

PART A - SECTION 1 THROUGH 3 AND APPENDIX A

FINAL REPORT

INTEGRAL LAUNCH AND

REENTRY VEHICLE

Volume III

Special Studies

Part A - Sections 1 Through 3

and Appendix A

FOREWORD

This final report for the Integral Launch and Reentry Vehicle (ILRV) Study, conducted under Contract NAS9-9206 by Lockheed Missiles & Space Company under direction of the NASA Marshall Space Flight Center, is presented in three volumes. Volume I, Configuration Definition and Planning, contains results of the preliminary cost analyses, conceptual design, mission analyses, program planning, cost and schedule analyses, and sensitivity analyses, accomplished under Tasks 1 through 6. Volume II covers Task 7, Technology Identification; and Volume III contains results of the Special Studies conducted under Task 8.

Principal LMSC task leaders and contributors in performance of this study include:

Systems Integration	T. E. Wedge	Primary Engines	A. J. Hief
System Synthesis	J. E. Torrillo	Propulsion	L. L. Morgan
Mission Analysis	D. W. Fellenz	Integrated Avionics	J. J. Herman
Design	G. Havrisik	Safety	J. A. Donnelly
Cost	J. Dippel	Structures	P. P. Plank
Schedule	W. James	Thermodynamics	F. L. Guard
Test	R. W. Benninger	Aerodynamics	C. F. Ehrlich
Operations	K. Urbach	Weights	A. P. Tilley

The three volumes are organized as follows:

Volume I - Configuration Definition and Planning

Section	
1	Introduction and Summary
2	System Requirements
3	Configuration Summary
4	Vehicle Design
5	Performance and Flight Mechanics
6	Aerodynamics
7	Aerothermodynamics
8	Structures and Materials
9	Propulsion

CONTENTS
(See individual sections for detailed contents)

Section 1

INTRODUCTION

This volume documents the Special Emphasis Studies performed as part of the Integral Launch and Reentry Vehicle (ILRV) systems study under contract NAS 9-9206. The study tasks were established under contract redirection of June 30, 1969, to explore selected aspects of systems design, development, and operation in more detail than normally done in a Phase A study.

CONTENTS

Section 2

PROPULSION SYSTEM STUDIES

2.1 INTRODUCTION

The propulsion system studies consisted of an evaluation of propulsion system parameters and propulsion/vehicle system interfaces. Propulsion system parameter studies included thrust-level considerations, engine-configuration effects, and orbital operation mode. Propulsion/vehicle interface studies were associated with establishment of rocket-engine criteria for the engine-system specification.

2.2 PROPULSION/SYSTEM PARAMETERS

Both the aerospike and bell-type engines were examined in various phases of the study. Examinations were made of the system interfaces associated with these two types of engines. The two configurations considered were a Two-Stage arrangement, shown in Fig. 2.2-1, and a dissimilar Triamese arrangement, shown in Fig. 2.2-2. Also, payload, liftoff weight and stage weight descriptions, listed in Table 2.2-1, were established.

2.2.1 Thrust-Level Considerations. Studies early in the contract were performed to determine the most desirable thrust-level requirements. These studies tended to indicate that the optimum engine thrust levels were above 600,000 pounds. Later, however, a maximum of 400,000 pounds was adopted as a ground rule. The basic approach adopted for the study was to provide desirable commonality in the orbiter and booster engines by maintaining the same turbomachinery and thrust chamber but with variations in the nozzle. Studies involving such considerations as base area, expansion ratio (and

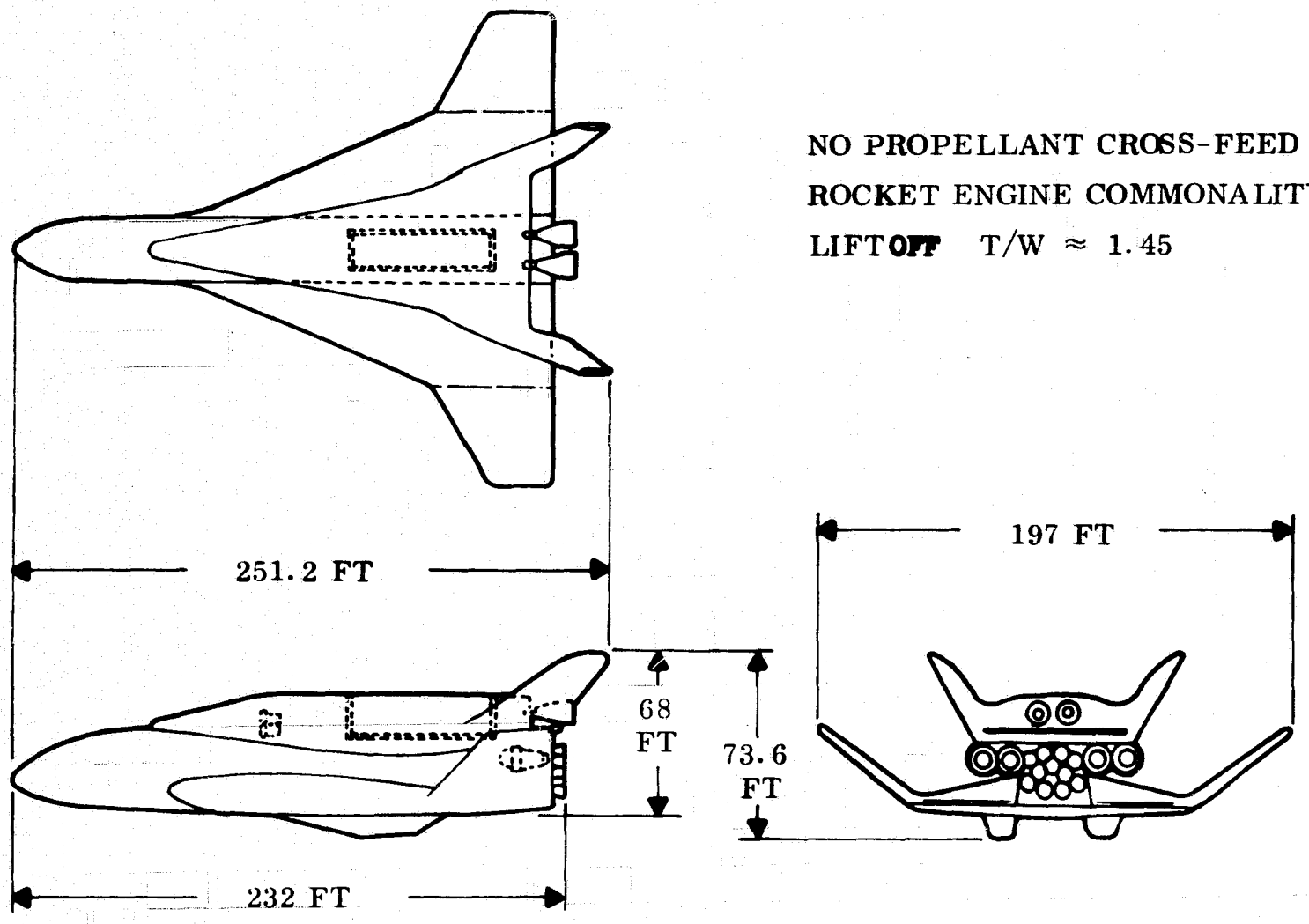

NO PROPELLANT CROSS-FEED
ROCKET ENGINE COMMONALITY
LIFTOFF T/W ≈ 1.45

FIG. 2.2-1 TWO-STAGE VEHICLE SYSTEM

- DISSIMILAR ELEMENTS
- NO PROPELLANT CROSS-FEED
- ROCKET ENGINE COMMONALITY
- LIFTOFF T/W ≈ 1.45

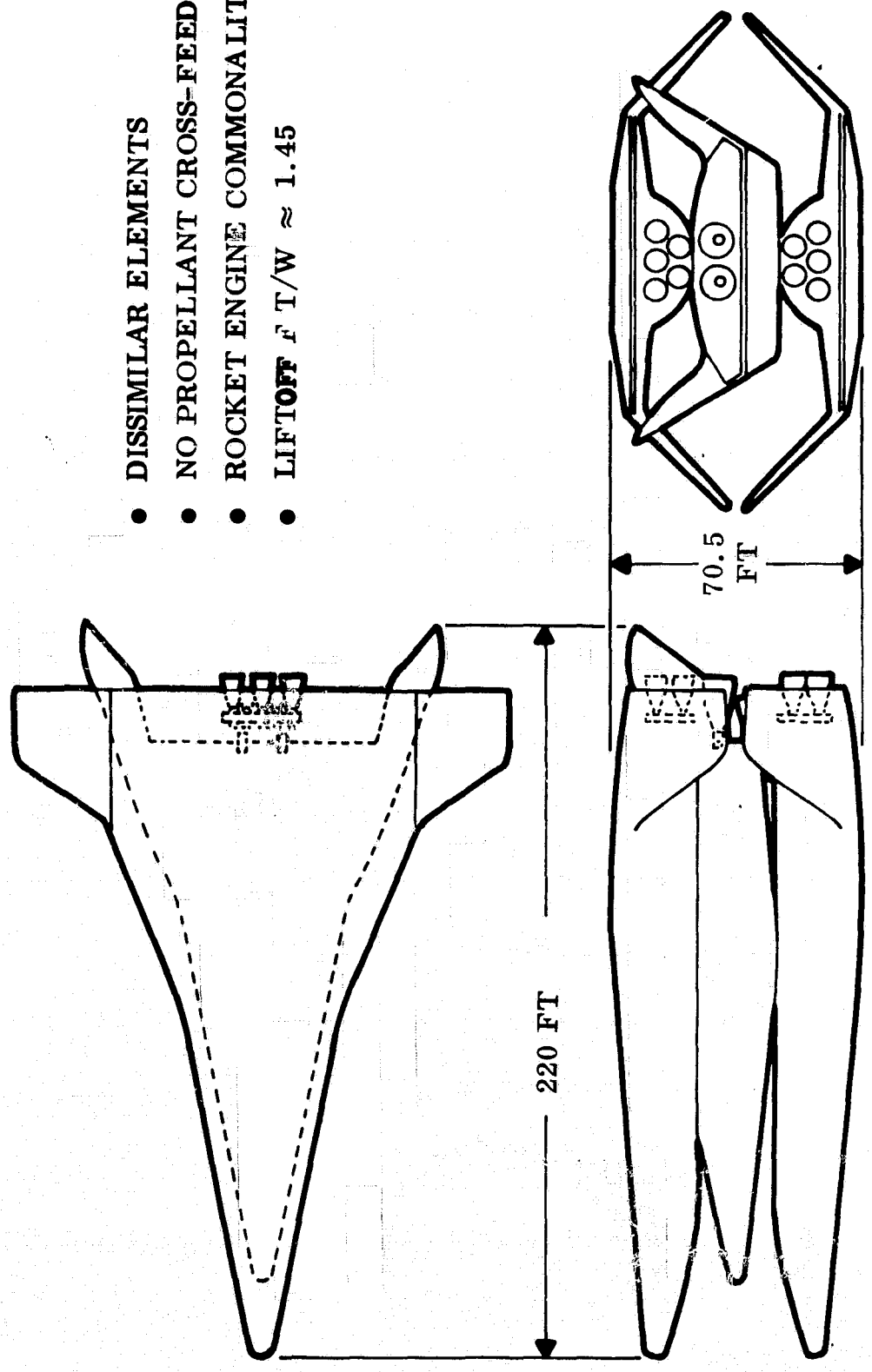

FIG. 2.2-2 TRIAMESE VEHICLE SYSTEM

Table 2.2-1

VEHICLE WEIGHTS SUMMARY

	Two-Stage		Triamese	
Payload	25 K	50 K	25 K	50 K
Liftoff	3.3×10^6	4.0×10^6	3.5×10^6	4.2×10^6
Orbital Spacecraft				
Propellant	0.500×10^6	0.610×10^6	0.500×10^6	0.610×10^6
Inert	0.188×10^6	0.208×10^6	0.188×10^6	0.208×10^6
	0.688×10^6	0.818×10^6	0.688×10^6	0.818×10^6
Booster Stage				
Propellant	2.207×10^6	2.687×10^6	2.376×10^6	2.857×10^6
Inert	0.405×10^6	0.495×10^6	0.436×10^6	0.525×10^6
	2.612×10^6	3.182×10^6	2.812×10^6	3.382×10^6

Conditions: O/F Ratio = 7.0
No propellant crossfeed between stages

resulting specific impulse), and gimbal angle reported in Section 2.2.2, indicated that the booster expansion ratio should be approximately 35:1. The thrust of the booster engine with an optimized 35:1 area ratio nozzle was established at a sea level thrust of 400,000 pounds. The thrusts vary for the different nozzles as presented in Section 2.2.2.

Thrust levels for two payload sizes on each of the two vehicle configurations, determined in accordance with the criteria listed above, are presented in Table 2.2-2. To illustrate the sensitivity of thrust level to payload weight and to liftoff thrust/weight ratio, a second set of rocket engine sizes were computed on the basis of thrust/weight ratio of 1.38. Figure 2.2-3 shows these two sets of data plotted and that rocket-engine thrust level is more sensitive to payload size than to the thrust/weight ratio in the range of parameters between 1.38 and 1.45. While the ground rule for operating the orbiter engine at 10 percent of normal rated thrust at liftoff has been set aside, the sensitivity factors displayed in this analysis should not be significantly modified.

KEY

50,000 LB PAYLOAD

25,000 LB PAYLOAD

LIFTOFF T/W = 1.38

LIFTOFF T/W = 1.45

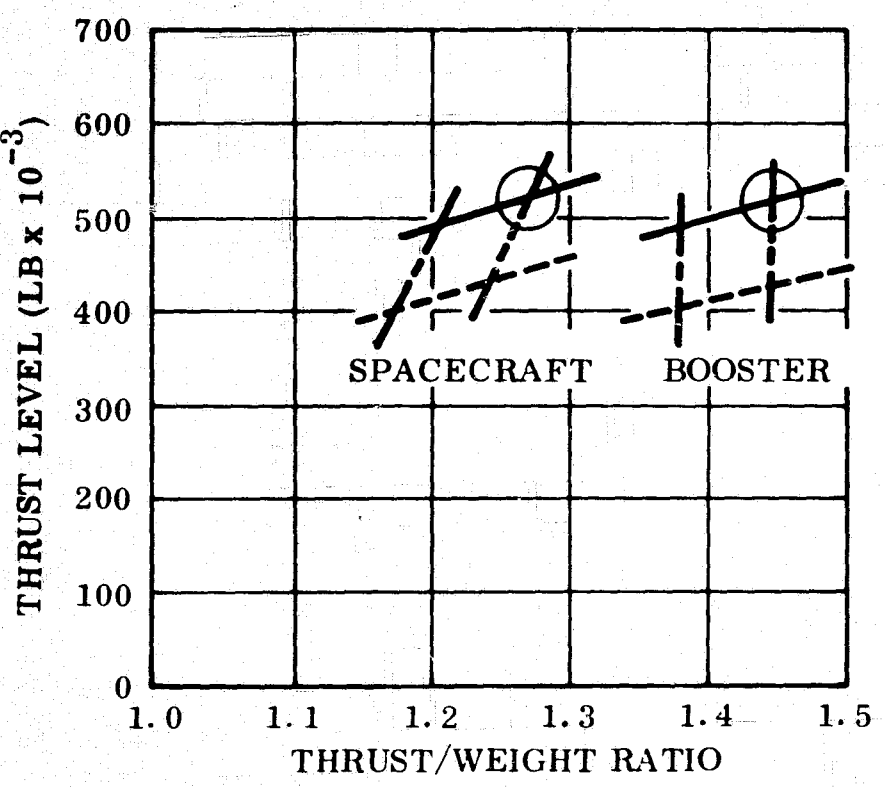

TWO-STAGE

11 ENGINE BOOSTER
2 ENGINE SPACECRAFT

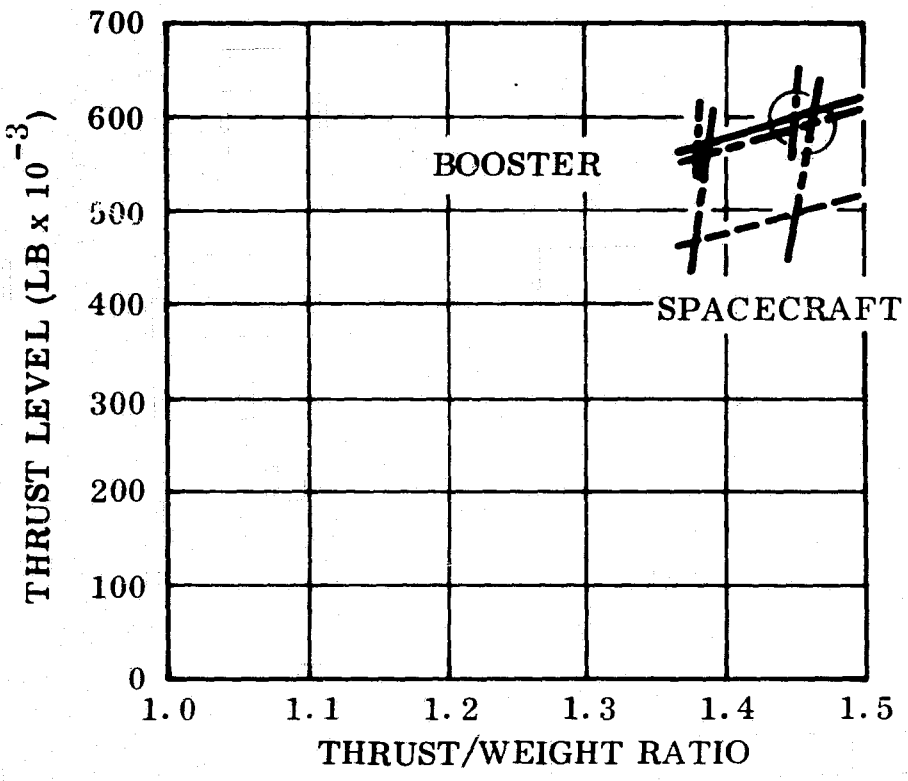

TRIAMESE

2 – 5 ENGINE BOOSTERS
2 ENGINE SPACECRAFT

FIG. 2.2-3 EFFECT OF THRUST/WEIGHT RATIO

Table 2.2-2

ROCKET ENGINE THRUST LEVEL SUMMARY

	Two-Stage		Triamese	
Payload Weight	25 K	50 K	25 K	50 K
Liftoff Weight	3.3×10^6	4.0×10^6	3.5×10^6	4.2×10^6
Liftoff Thrust @ T/W 1.45	4.78	5.80	5.07	6.09
Number of Engines	11/2	11/2	5/2/5	5/2/5
Thrust Level (Sea Level)	426 K	517 K	497 K	596 K

2.2.2 Engine Configuration Effects. The engine configurations were, of course, major design factors. The various engine configurations evaluated are cited in Table 2.2-3 and the characteristics of various engines are shown in Table 2.2-4. Dimensional details of the engines are shown in Figs. 2.2-4, 2.2-5, and 2.2-6. Figure 2.2-4 presents three Pratt & Whitney 400,000-pound bell-type engines with optimized 35:1 and 100:1 nozzles and a two-position 35/150 nozzle. In Fig. 2.2-5, the Rocketdyne 400,000-pound and 800,000-pound engines are shown. The Aerojet-General bell-type engine configurations presented in Fig. 2.2-6 illustrate the three expansion ratios of optimized 35:1 and 100:1 nozzles and a two position 35/150 nozzle.

Table 2.2-3

ENGINE CONFIGURATION STUDY CASES

Configurations	Number of Engines
Booster Optimized for Bell-Type Engine	13 - 400,000-lb
Booster Optimized for Aerospike Engine	7 - 800,000-lb
Booster Compromise Design	
Either aerospike engine or bell-type engine	7 - 800,000-lb 13 - 400,000-lb
Booster Compromise Design	
Either aerospike engine or bell-type engine	13 - 400,000-lb 13 - 400,000-lb
Orbiter Optimized for Aerospike Engine	3 - 400,000-lb
Orbiter Compromise Design	
Either aerospike engine or bell-type engine	3 - 400,000-lb 3 - 400,000-lb

Table 2.2-4

ENGINE CHARACTERISTICS

Engine Type and Manufacturer	SL Thrust (lb)	Length (inch)	Nozzle Exit Diameter (inch)	Weight (lb)
Pratt & Whitney				
Bell-Type 35:1	400 K	132	61	4140
35/150 (with 35:1 chamber)	391 K	210/273	124	4700
100:1	400 K	233	108	4980
35/150 (with 100:1 chamber)	451 K	223/289	134	5250
Rocketdyne	400 K	52	136	4450
Aerospike	800 K	52	139	7800
Aerojet-General				
Bell-Type 35:1	400 K	130	69	4100
35/150	400 K	207/272	123	5300
100:1	400 K	223	100	4400

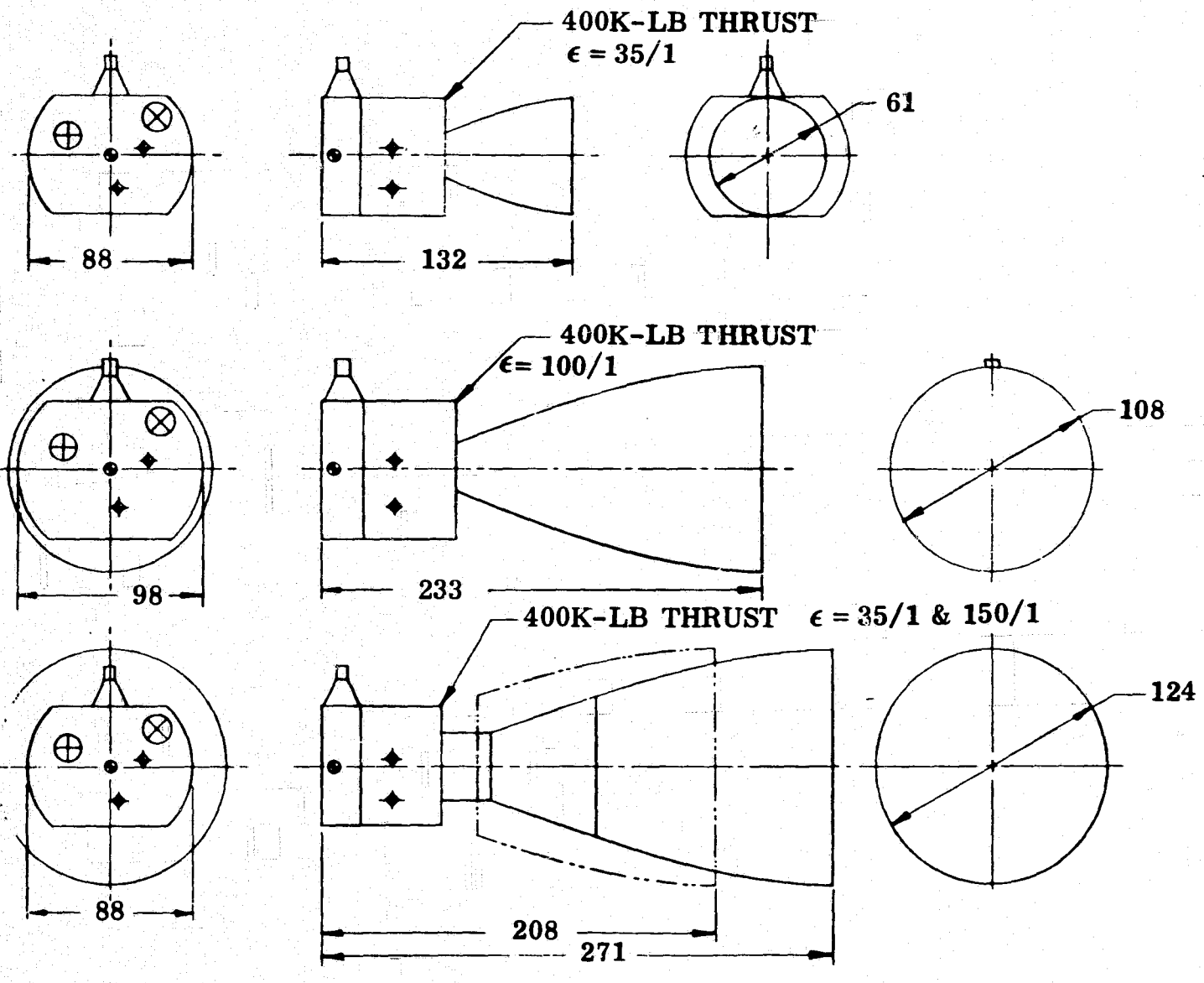

FIG. 2.2-4 PRATT & WHITNEY BELL ENGINES

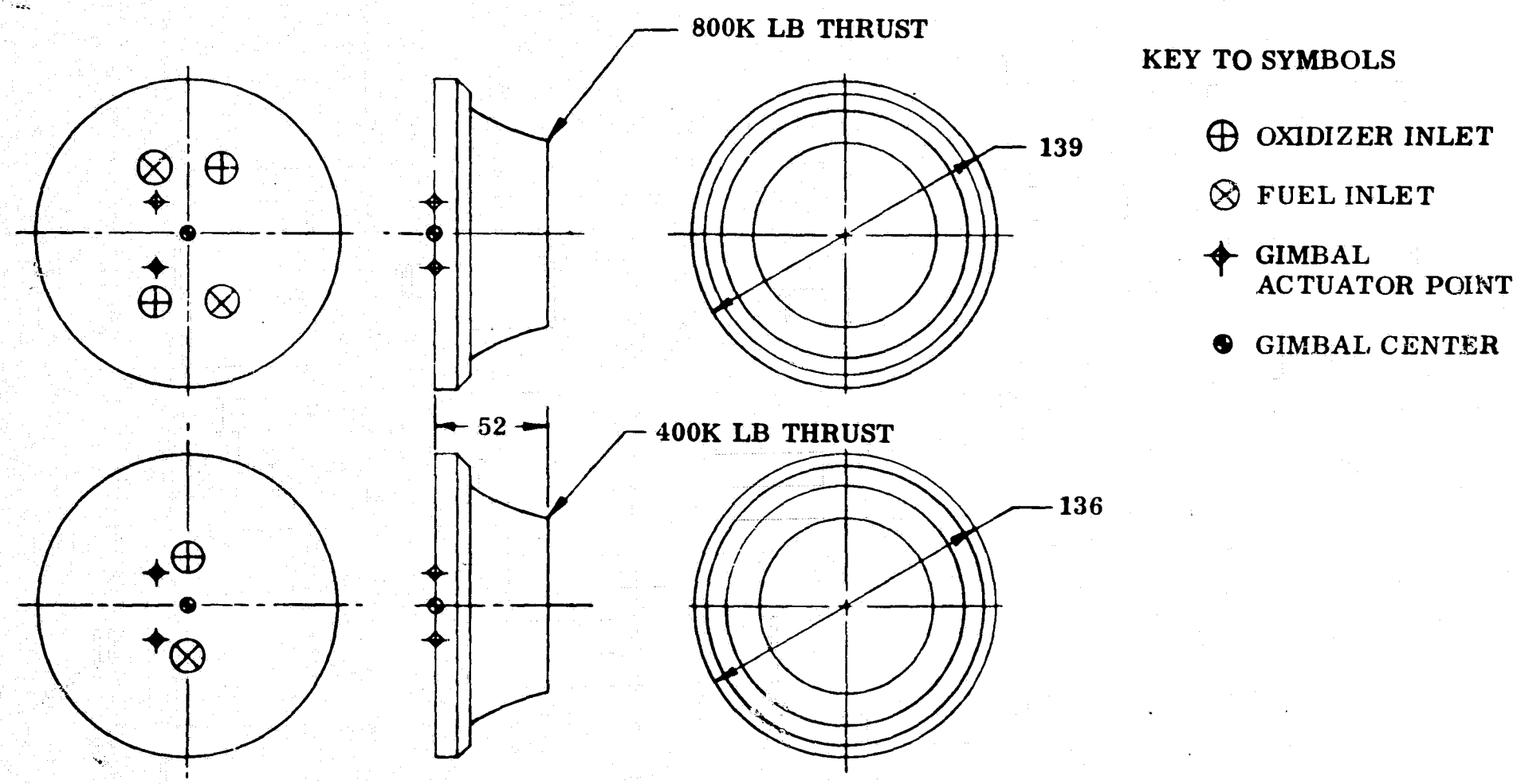

FIG. 2.2-5 ROCKETDYNE AEROSPIKE ENGINES

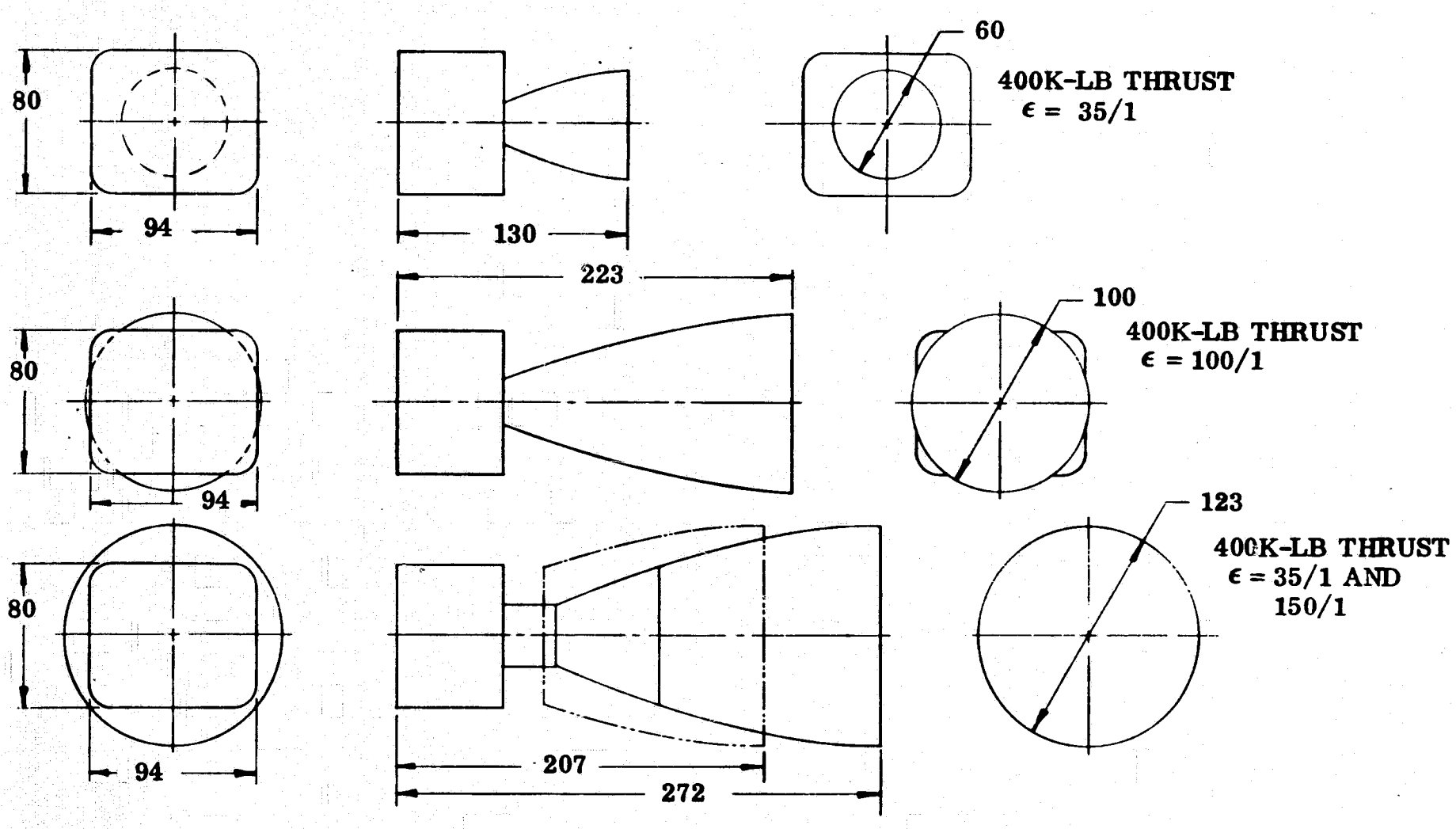

FIG. 2.2-6 AEROJET BELL TYPE ENGINES

It is noteworthy that the two aerospike engines have essentially the same overall dimensions. The diameter of the 800,000-pound engine is made 3 inches larger than that of the 400,000-pound engine to accommodate the second 400,000-pound annular combustion chamber. The 800,000-pound engine is modular in design and consists of two 400,000-pound engines, each with its own turbopump. The 400,000-pound aerospike engine has only one turbopump.

Figure 2.2-7 illustrates the dynamic characteristics of the two types of engines, with a 7-degree gimbal angle in a square pattern assumed.

Preliminary evaluation indicates that a desirable increase in booster engine performance can be achieved by increasing the nozzle expansion ratio for the bell-type engine from 35:1 to 100:1. Tests at Pratt & Whitney reportedly indicate that no flow separation occurs in the 100:1 nozzle at 100 percent thrust at sea level. The base areas for two bell-type engine configurations (13 - 400,000-lb thrust) and for the aerospike configuration (13 - 400,000-lb thrust) have been compared, as shown in Fig. 2.2-8. It is evident that the base area for the bell-type engine with 35:1 nozzle is considerably smaller than for the other configurations. Actually, the base areas for the 100:1 bell-type engine and aerospike configuration are almost identical when the necessary gimbal area is included for the bell-type engine. Because of the small expansion ratio, the size of the chamber near the turbopump is the controlling diameter. The seven 800,000-pound optimum aerospike arrangement is also shown. The compromise arrangement allows use of either the 800,000-pound aerospike or the 400,000-pound bell-type engines. Gross base areas for these various configurations, as well as for the 400,000-pound configuration shown in Fig. 2.2-8 are tabulated in Table 2.2-5.

The effects of these base areas on complete vehicle drag coefficients and on booster flyback drag coefficients have been determined. The values of

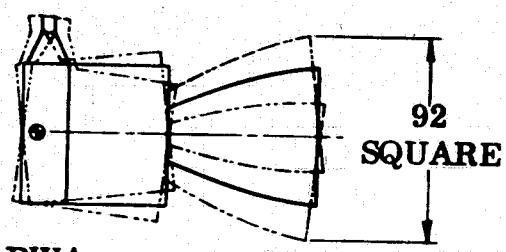

PWA
ϵ = 35/1
THRUST = 400K AT SL

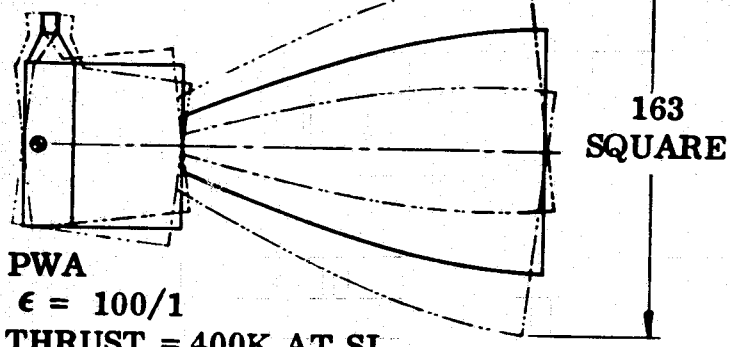

PWA
ϵ = 100/1
THRUST = 400K AT SL

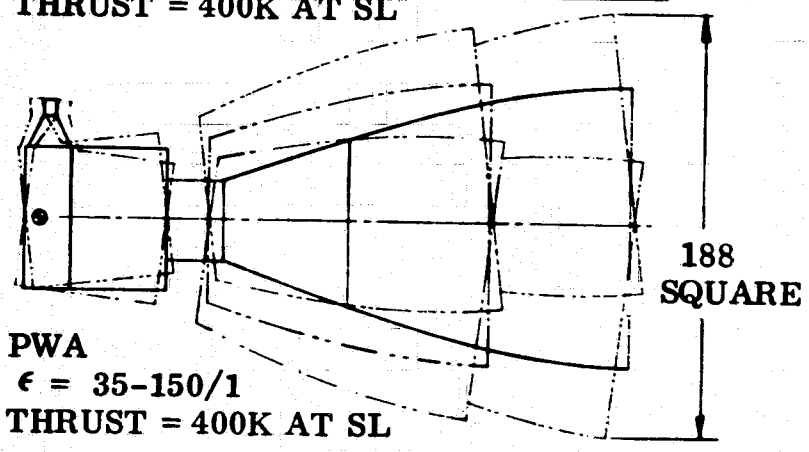

PWA
ϵ = 35-150/1
THRUST = 400K AT SL

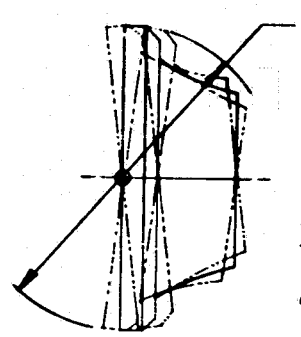

ROCKETDYNE
ϵ = 124
THRUST = 400K AT SL

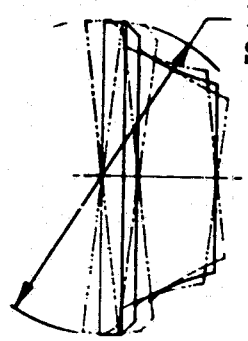

ROCKETDYNE
ϵ = 66-122/1
THRUST = 800K AT SL

FIG. 2.2-7 ENGINE DYNAMIC INSTALLATION ENVELOPES (± 7 DEGREE ANGULAR DISPLACEMENT - SQUARE PATTERN)

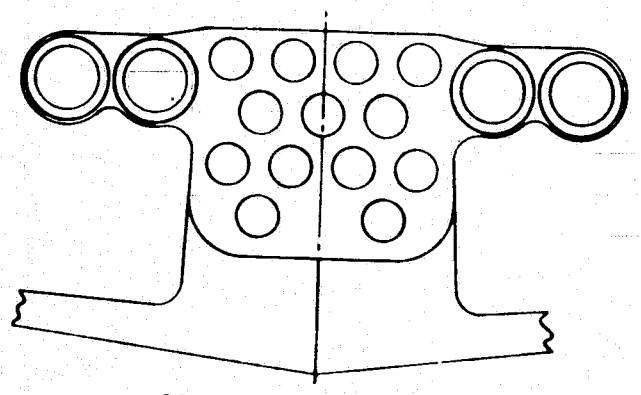

13 - 400K ENGINES
BELL NOZZLE ϵ = 35/1
(1262 SQ FT GROSS)

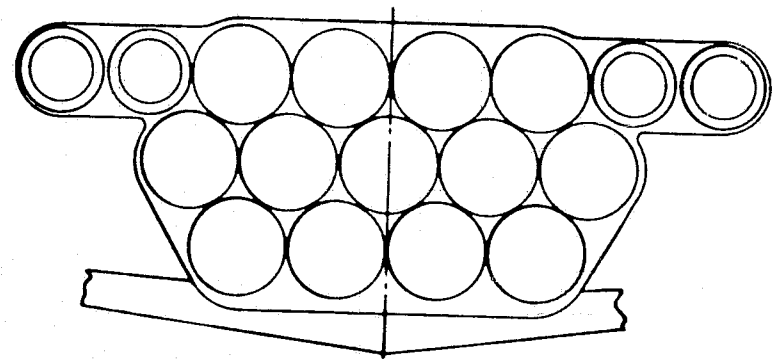

13 - 400K ENGINES
AEROSPIKE ϵ = 124
(2210 SQ FT GROSS)

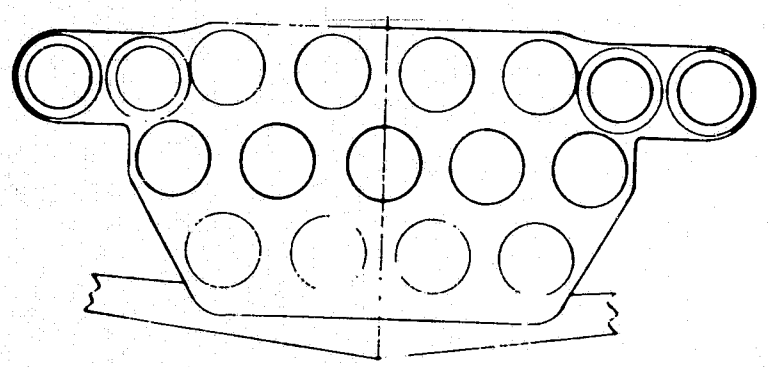

13 - 400 K ENGINES
BELL NOZZLE ϵ = 100/1
(2210 SQ FT GROSS)

FIG. 22-8 BOOSTER BASE AREA COMPARISON

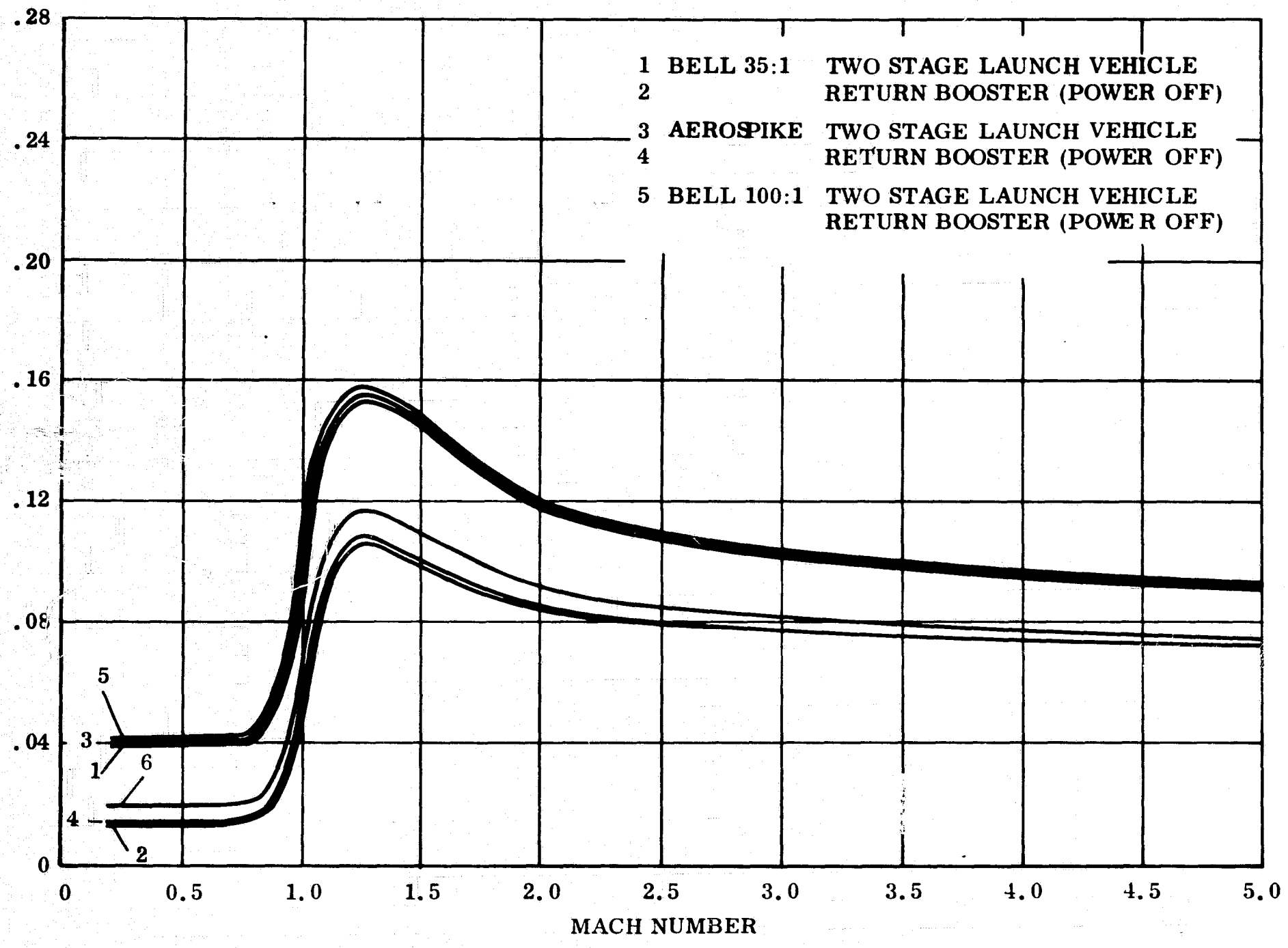

FIG. 2.2-9 DRAG COEFFICIENT EFFECTS

these coefficients versus Mach number are shown in Fig. 2.2-9. The increased drag coefficients due to the increased base area may modestly affect the ascent trajectory of the vehicle, and the flyback capability of the returning booster may be more significantly affected.

Table 2.2-5

BOOSTER BASE AREA

Engine Configuration	Engine Size (lb)	Gross Base Area (ft^2)
Optimum Bell-Type (35:1)	13 - 400,000	1262
Optimum Aerospike	7 - 800,000	1430
Compromise Aerospike	7 - 800,000	1430
Bell-Type (35:1)	13 - 400,000	1430
Compromise Aerospike	13 - 400,000	2210
Bell-Type (100:1)	13 - 400,000	2210

Results of the Evaluation of Alternate Configurations on the Booster. Evaluation studies were conducted for the various booster bell-type engine and Aerospike engine configurations. The baseline configuration used for this study was the 560,000-pound bell-type engine configuration evaluated as reported in LMSC-A955317A. The alternate configurations to be considered are as follows:

Configuration	Engines	Figure No.
Optimum Bell-Type (35:1)	13 - 400K	2.1-11
Optimum Aerospike	7 - 800K	2.1-12
Compromise Bell-Type (35:1)	13 - 400K	2.1-13
Compromise Aerospike	7 - 800K	2.1-14
Compromise Bell-Type (100:1)	13 - 400K	2.1-8
Compromise Aerospike	13 - 400K	2.1-8

In the evaluations, the booster configuration was held constant to a point immediately aft of the LH_2 tank. Any changes in booster shape to accommodate

the enlarged base area for the various engine configurations are reported as changes in structural weight. Fairing changes to protect the various bell nozzle configurations have been evaluated. Changes in thrust structure to spread the thrust loads are minimal for the various configurations except for the compromise bell-type (100:1) and the 400,000-pound aerospike engine.

The commonality of design in these various engine configurations can be readily observed in Figs. 2.2-10 through 2.2.-13. A structure to spread the loads from the engines into the main booster structure lies aft of the LH_2 sump. A second structural element lies midway between the first structural element and the engine gimbal axis, and the engines are directly mounted to this second element by tubular mounts. A typical thrust structure design is shown in Fig. 2.2-14. The designs of these structural elements are similar between configurations. It should be noted that studies are underway to eliminate the first structural element so as to minimize structural weights. The increased height of the base section required for introduction of the aerospike engine is evident in Figs. 2.2-10 and 2.2-11. The general approach to plumbing installations is shown in Fig. 2.2-12. Fuel lines to the engines connect directly to the LH_2 sump. The LO_2 lines run from the engines to two manifolds located between the upper and lower rows of engines. Since the 800,000-pound thrust aerospike engines have two turbopump units per engine, 14 pairs of inlet lines are required for the aerospike engines versus 13 pairs of lines for the bell-type engines. Pressure volume compensators are located on all inlets to the engines to minimize feed inlet fluctuations and to provide flexibility of design. The commonality of the propellant lines is readily apparent.

The difference in booster fairing to protect the bell-type engine nozzle is shown in Figs. 2.2-12 and 2.2-13. As shown in Fig. 2.2-12, the fairing at the bottom of the booster must be intact to avoid nozzle heating during the high angle-of-attack reentry. As shown in Fig. 2.2-13, this fairing is removed to eliminate exhaust plume impingement and to reduce weight. The short nozzle length of the aerospike does not require fairing protection during the reentry phase.

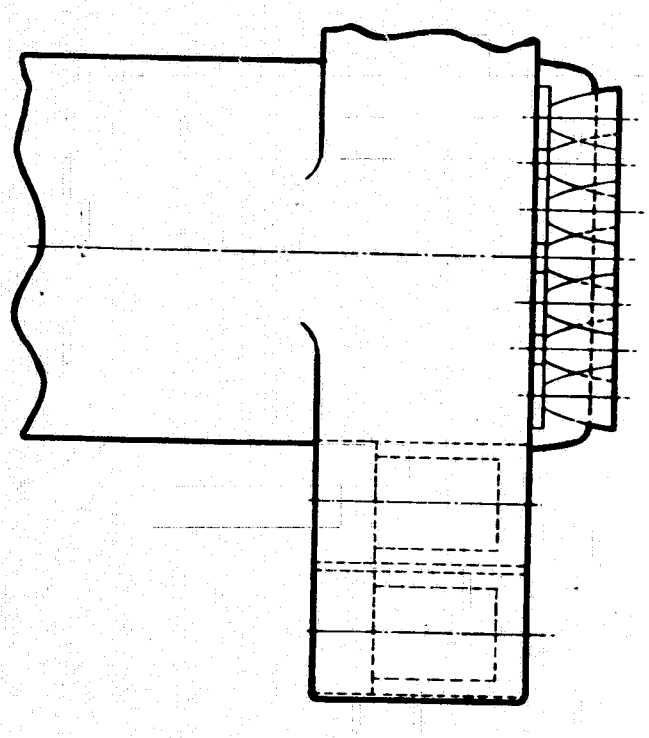

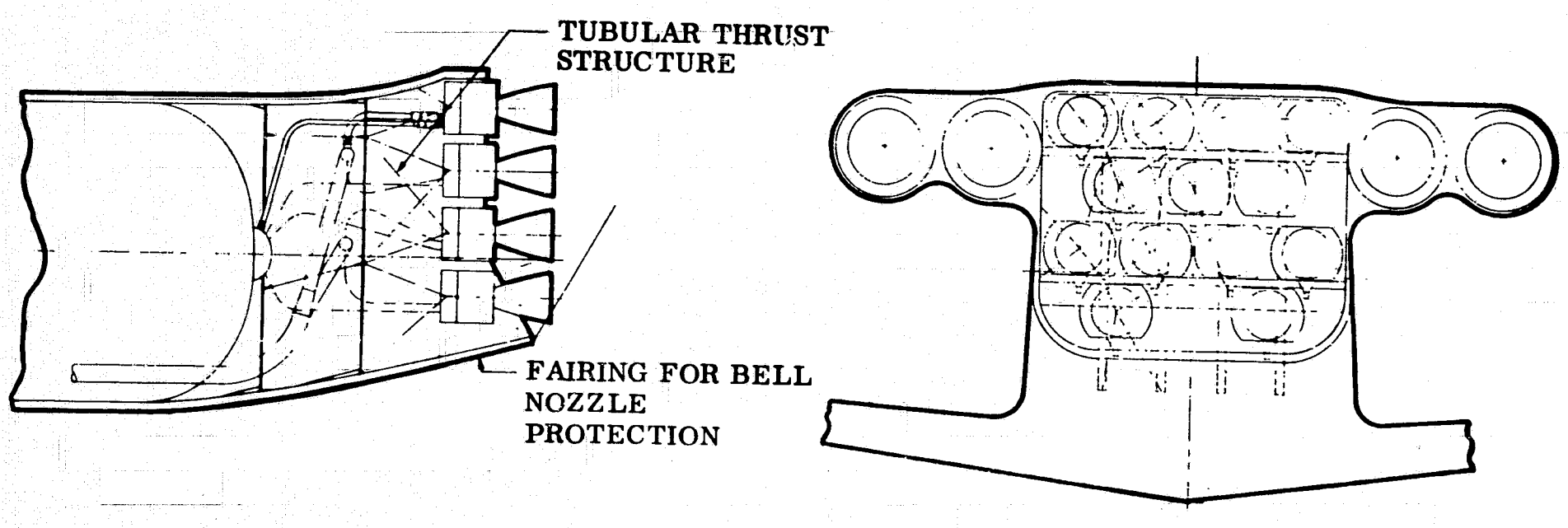

FIG. 2.2-10 BOOSTER OPTIMUM BELL ENGINE INSTALLATION

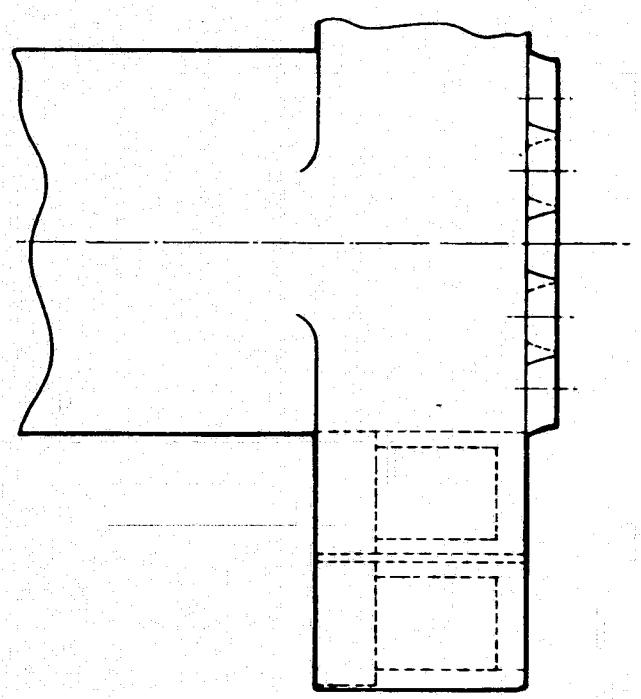

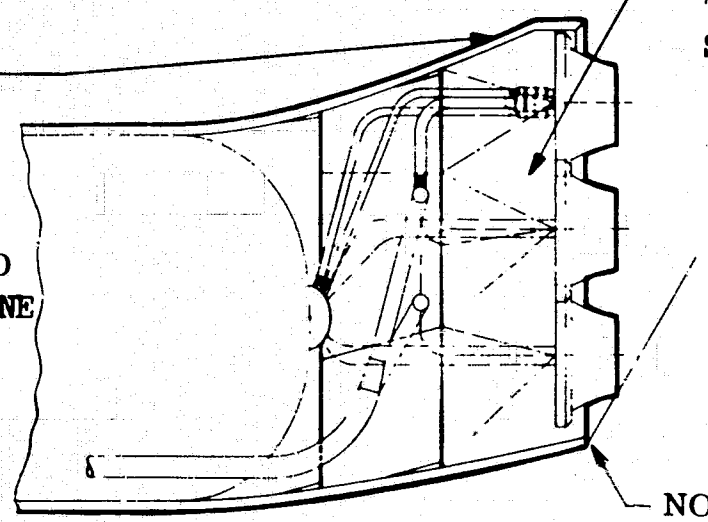

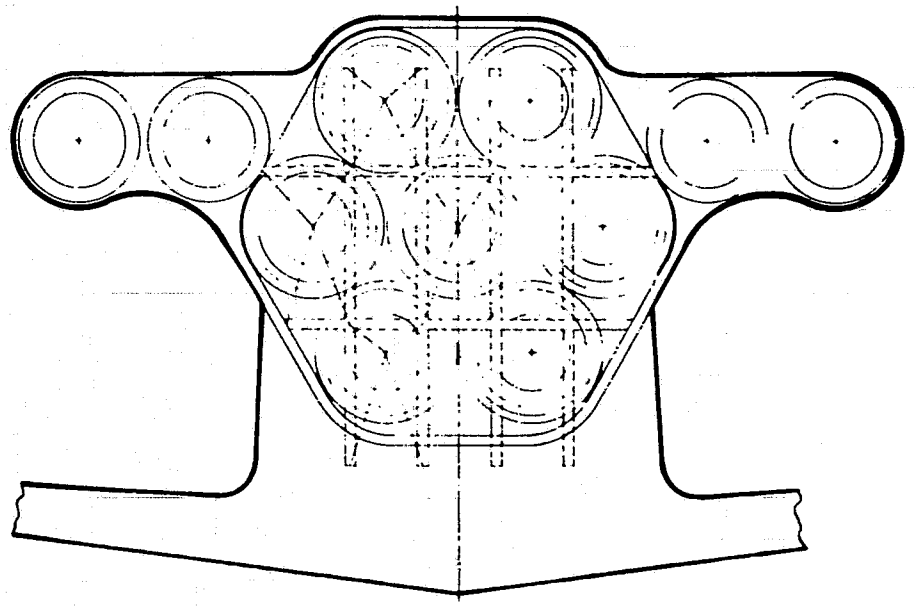

FIG. 2.7-11 BOOSTER OPTIMUM AEROSPIKE ENGINE INSTALLATION

KEY

1. VALVE
2. GIMBAL JOINT
3. SLIDING EXPANSION JOINT
4. SLIDING SUPPORT
5. FIXED SUPPORT
6. SWINGING SUPPORT
7. PRESSURE-VOLUME COMPENSATOR
8. LO_2 TRUNK LINE (22 IN.)
9. LO_2 MANIFOLD (17 IN.)
10. ENGINE LO_2 FEED LINE. (8 IN.)
11. ENGINE LH_2 FEED LINE (8 IN.)
12. THRUST STRUCTURE
13. GIMBAL ACTUATOR

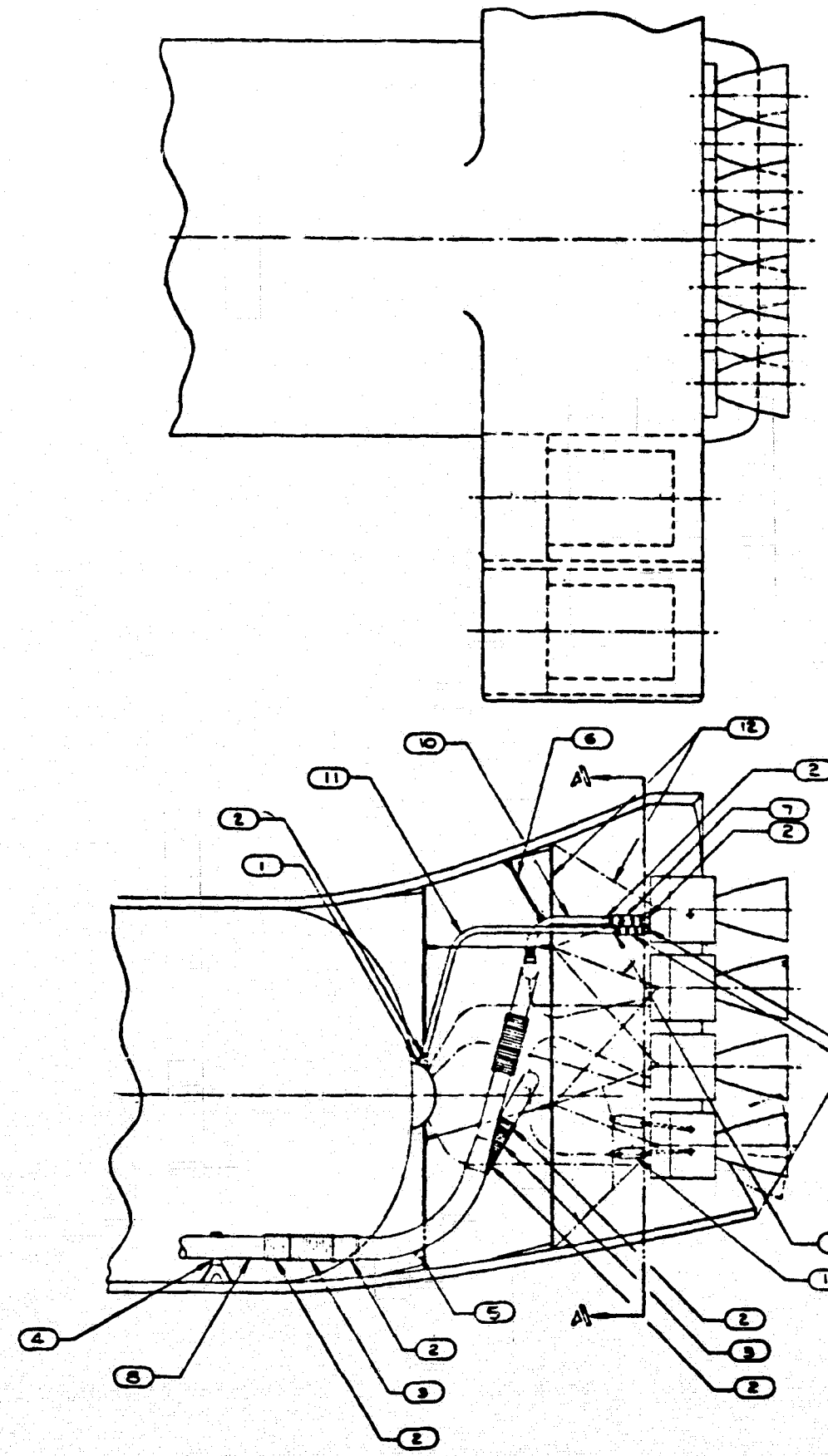

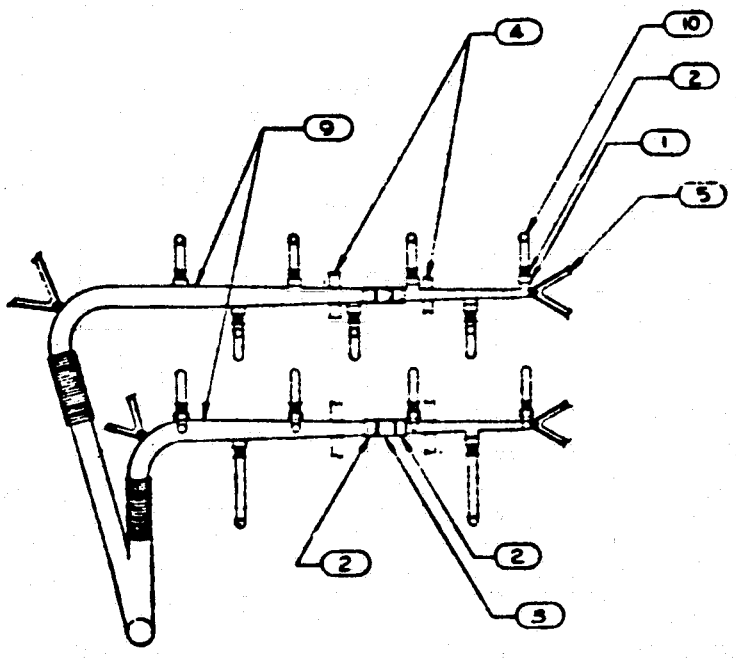

SECT A-A
OXIDIZER MANIFOLDING

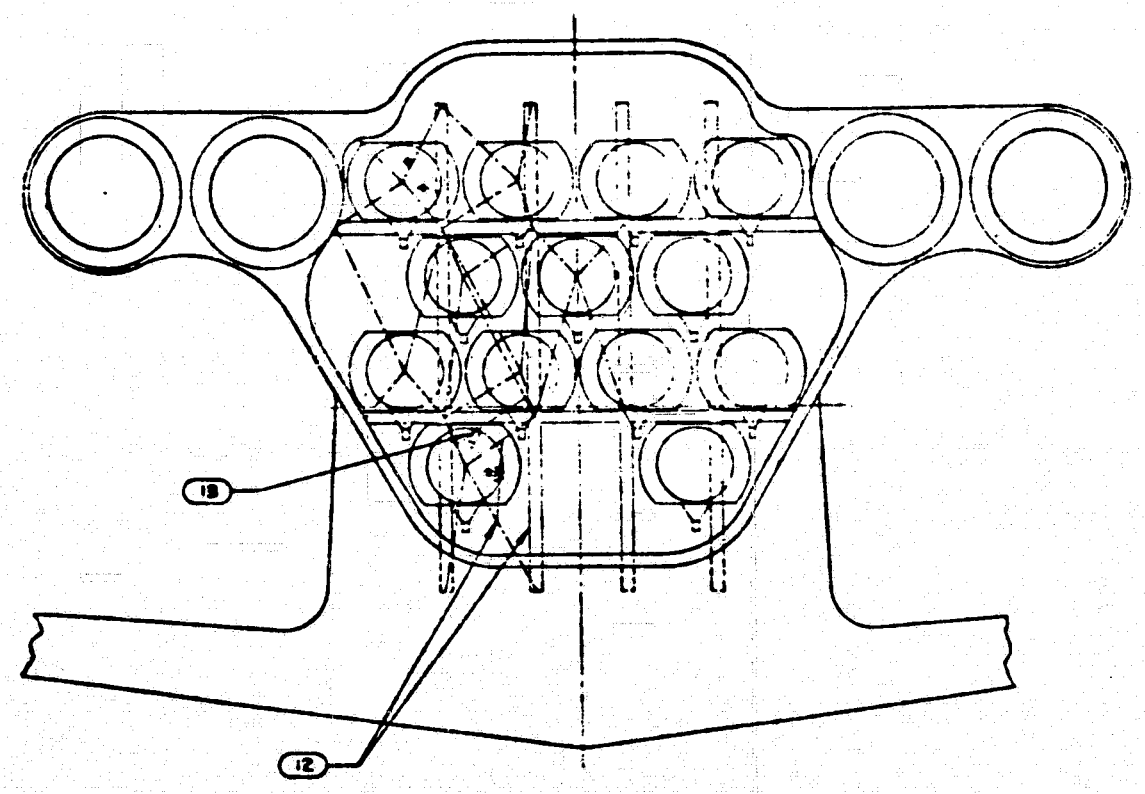

FIG. 2.2-12 COMPROMISE BELL

FOLDOUT FRAME 2

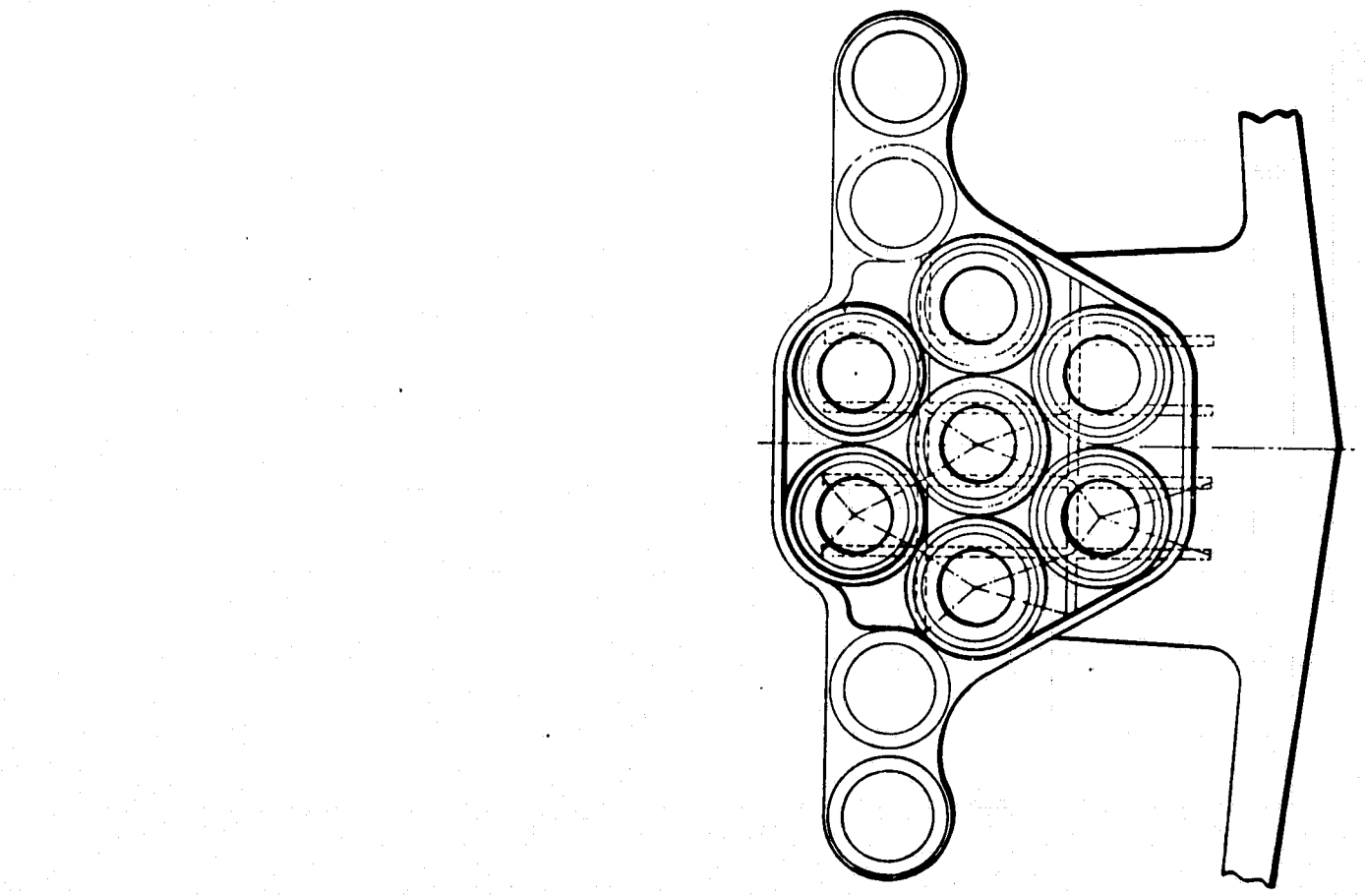

FIG. 2.2-13 BOOSTER COMPROMISE AEROSPIKE ENGINE INSTALLATION

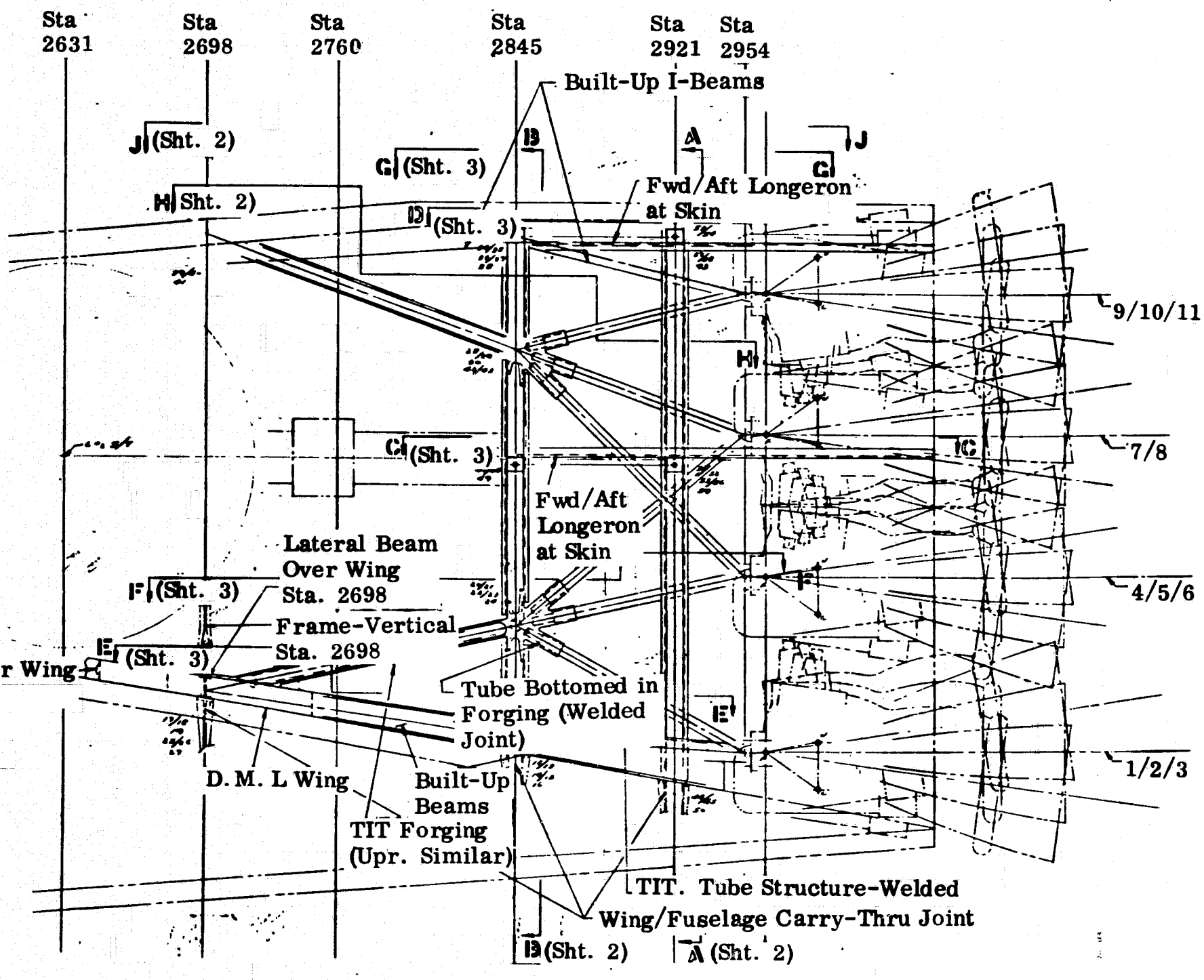

FIG. 2.[illegible]-14 TYPICAL THRUST STRUCTURE CONFIGURATION

The data in Table 2.2-6 indicate that there are no significant differences in weights between the 35:1 bell-type configurations and the 800,000-pound Aerospike configurations. The compromise design involving use of either of these engines without involving any significant changes in structure shows that there is a very slight weight penalty (1940 lb) over the optimum bell-type configuration. The compromise configurations involving 100:1 bell-type engines and 400,000-pound aerospike engines have 14,000 to 22,000 pound weight penalties over the compromise designs involving 35:1 bell-type or 800,000-pound aerospike engines. These weight penalties may not be significant alone; but, when combined with the increased drag during flyback, a performance degradation may result from a complete vehicle re-evaluation.

Results of the Evaluation of Alternate Engine Configurations on the Orbiter. The orbiter was examined for the effects of the bell-type and aerospike engine configurations. The approach was similar to that for the booster, as discussed previously. The following were considered in these evaluations:

- Optimum orbiter aft vehicle region for the bell-type engine (which resulted in the optimum configuration for adaptation to the aerospike engine)
- Compromise orbiter aft region employing the aerospike engine (same as optimum bell-type configuration)
- Optimum orbiter aft region optimized for the aerospike configuration

The results, which are reported in the subsequent discussion, indicate that the optimum bell-type installation also satisfies the general requirements for the compromise system for either the bell-type or the aerospike installation. The optimum aft vehicle region for the aerospike configuration indicated that additional volume is available in the aft section to hold propellant or equipment.

Orbiter Optimized for the Bell-Type Engine (and Resulting Compromise Design). The orbiter optimized for the bell-type engine is illustrated in Fig. 2.2-15. The design is based on engine operation at a nominal 10 percent thrust up to

Table 2.2-6

COMPARISON OF WEIGHTS RELATED TO BOOSTER ENGINE ALTERNATIVES

Engine Configuration	Figure No.	Structural Weight, lb	Fairing Weight, lb	Thrust Structure, lb	Engine Weight, lb	Total Weight, lb	Weight Change, lb
Baseline Bell-Type	LMSC-A955317A	8,507	605	15,850	65,321	90,283	–
Optimum Bell-Type (35:1)	2.2-10	10,290	550	16,250	53,820	80,910	-9,373
Optimum Aerospike (800K)	2.2-11	12,000	–	15,450	54,600	82,050	-7,833
Compromise Bell-Type (35:1)	2.2-12	12,546	495	16,250	53,820	83,111	-7,172
Compromise Aerospike (800K)	2.2-13	12,546	–	15,450	54,600	82,596	-7,287
Compromixe Bell-Type (100:1)	2.2-8	20,700	1,000	18,800	64,740	105,240	+14,957
Compromise Aerospike (400K)	2.2-8	20,700	–	18,000	57,850	96,550	+6,667

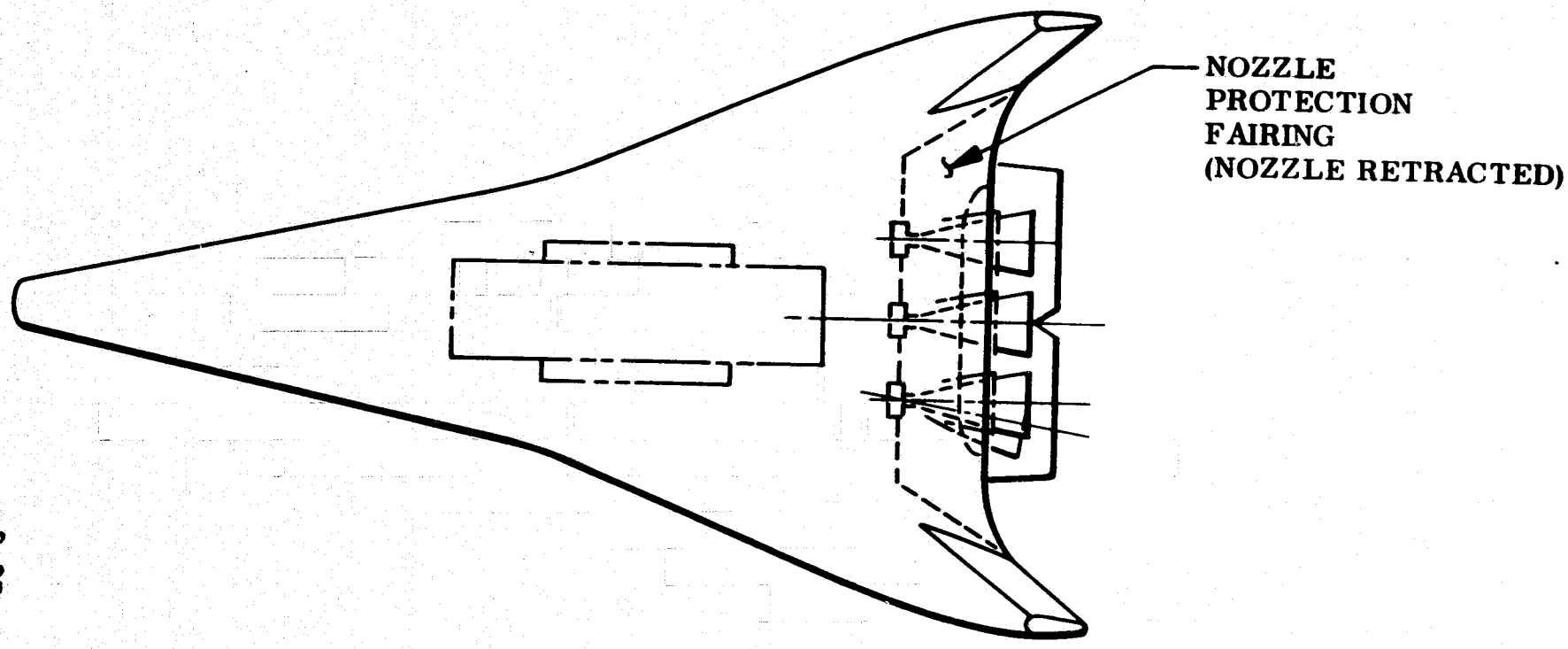

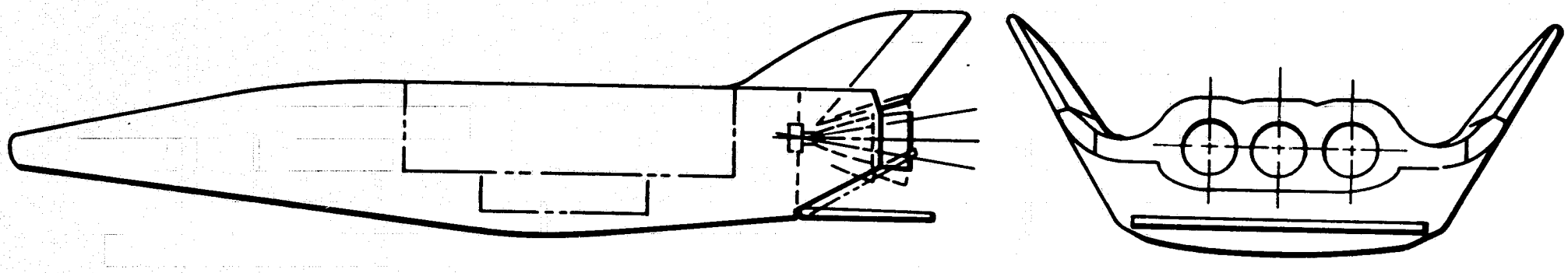

FIG. 2.2-15 ORBITER OPTIMIZED FOR BELL-TYPE ENGINE (RESULTING COMPROMISE DESIGN)

stability. Aerospike exhaust plume characteristics data (shown in Fig. 2.2-17) furnished by Rocketdyne were used to determine that during the ascent trajectory with the aerospike engines generating full thrust, the pressure forces generated on the elevons by the exhaust plume could be counteracted by an angular displacement of the thrust vector less than 0.1 degree. This analysis is considered to be conservative, and an accurate analysis may approach angular displacements of 0.01 degree. The effect appears to be insignificant.

An additional study was undertaken to evaluate the thermal effect of exhaust plume impingement on the elevon. Rocketdyne data shown in Fig. 2.2-17 defining aerospike exhaust plume characteristics were used for the thermal data. A general parametric analysis was undertaken, since the elevon design has not been frozen. However, the location of the elevon with respect to the engine mount is specific, as shown on Fig. 2.2-16. In the thermal model developed, two limiting cases were derived and are reported in Fig. 2.2-18.

Other than the fairing required for nozzle protection, the engine thrust structure and plumbing requirements for use of either the bell-type engine or the aerospike engine are very similar; the elevon temperature capability must be greater for the aerospike engine. The arrangement of the propellant feedlines are somewhat different, as a result of the inlet location differences, as shown in Figs. 2.2-4, 2.2-5, and 2.2-6. However, it was determined that this could be considered in the initial manifold design. The use of pressure volume compensating bellows is considered to be an integral feature of the plumbing design for commonality between the two engines. These allow stabilization of the manifolds and more flexibility in the design of the feedlines from the manifolds to the engines.

These data show that the compromise aerospike engine has about a 1600-pound weight advantage over the optimum/compromise bell design. This weight decrease results primarily from the removal of the nozzle fairing over the bell nozzles. The optimum aerospike design, which provides additional propellant or cargo space, is about 2200 pounds heavier than the compromise aerospike design because of extra structural mounting in the rear of the orbiter.

the point of booster separation in accordance with the ground rules. It was also considered that the nozzle extension would be retracted at all times when air or thermal loads of sufficient magnitude to cause nozzle damage are possible.

A major consideration in this design is the fairing to protect the nozzle from air loads during ascent and reentry with the nozzle extension retracted. Since this fairing represents considerable weight, its removal is considered in the compromise aerospike configuration.

The engine installation provides for the required gimbal angles and prevents temperatures from the bell-type engine in excess of 2000°F on all surfaces accessible to the plume, both at full thrust and at a nominal 10 percent thrust.

Orbiter Compromise Aerospike Design. As discussed earlier, the optimum bell-type engine design also results in the compromise design for the aerospike engine. The design is shown in Fig. 2.2-16. The upper surface fairing for engine protection is not required for this design. As discussed, the thrust structure, plumbing, and related structure are very similar between the designs.

There are effects on the elevon from plume impingement from the aerospike engine. The bell-type installation is arranged so as to minimize the effects of the plume at 10 percent thrust. The effects of the aerospike may be categorized into plume pressure effects, thermal effects, and acoustic vibration effects. Since sufficient data to evaluate the acoustic environment are not presently available, no further discussion of this subject is offered.

In the orbital spacecraft configuration, the exhaust gases of the three 400K thrust aerospike rocket engines impinge on the extended elevon assembly. An analysis was performed to determine the magnitude of the pressure force generated on the upper suface of the elevon by the rocket exhaust plume, the magnitude of the torsional disturbance imposed on the vehicle by this pressure force, and the gimbal angle displacement required to restore the spacecraft

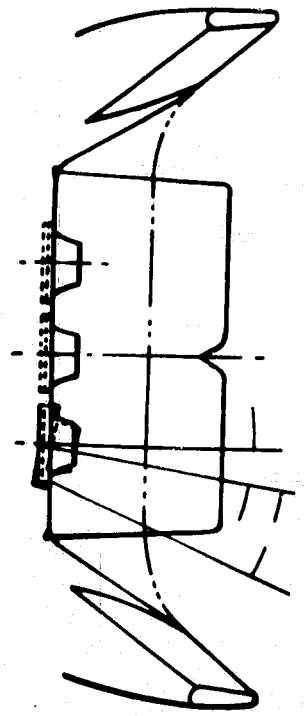

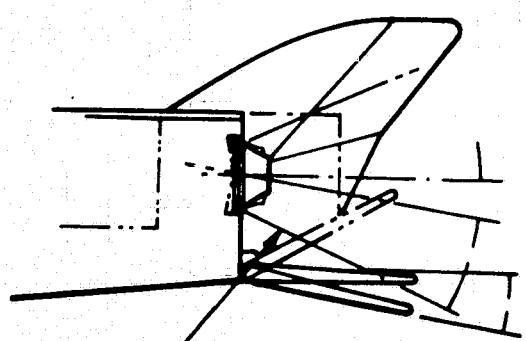

PLUME IMPINGEMENT
CONSIDERATIONS

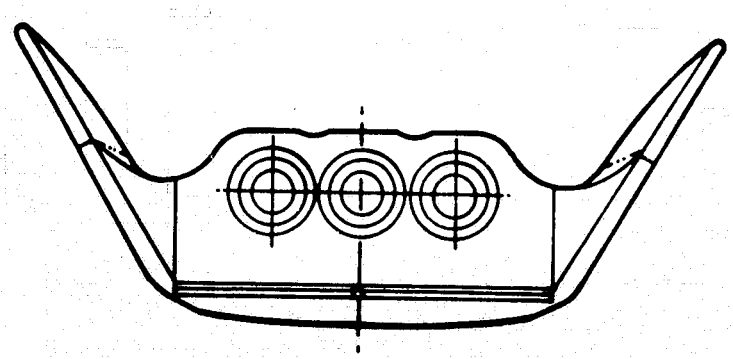

FIG. 2.2-16 COMPROMISE AEROSPIKE

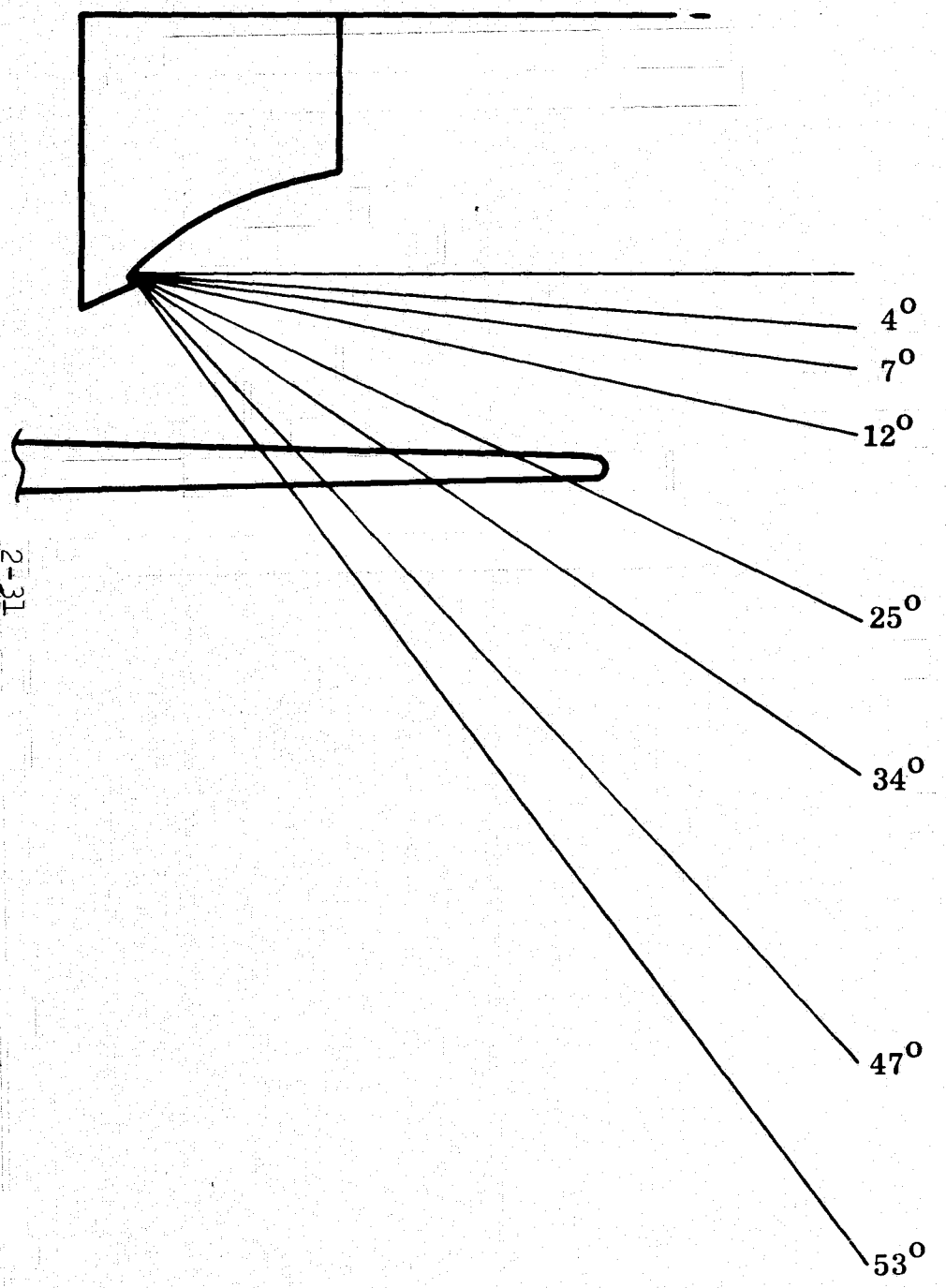

Angle (deg)	Plume Density ($lb/in.^3$)	Plume Static Pressure (psia)	Mass Velocity ($lb/in.^2$-sec)	Heat Flux ($Btu/in.^2$-sec)
4	$.40 \times 10^{-6}$	1.00	.074	.410
7	$.29 \times 10^{-6}$	0.63	.054	.316
12	$.16 \times 10^{-6}$	0.31	.031	.247
25	$.30 \times 10^{-7}$	0.034	.0057	.094
34	$.78 \times 10^{-8}$	0.0056	.0015	.035
47	$.58 \times 10^{-9}$	0.00020	.00011	.008
53	$.89 \times 10^{-10}$	0.00017	.000017	.002

*Rocketdyne Report R-8003, "Design and Operational Data for the Reusable O_2/H_2 Aerospike Engine," Sept 22, 1969

FIG. 2.2-17 AEROSPIKE EXHAUST PLUME CHARACTERISTICS*

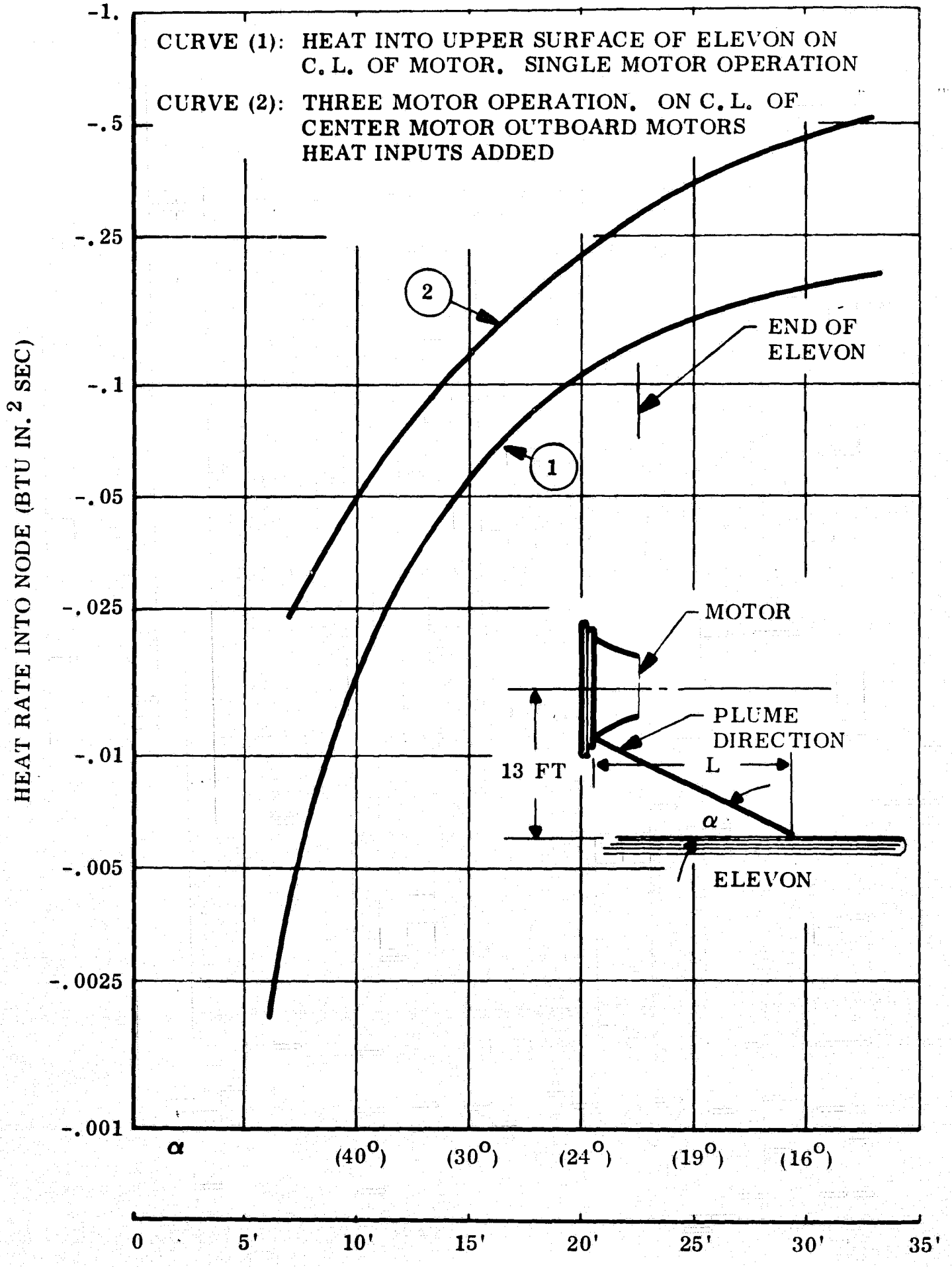

FIG. 2.2-18 PLUME IMPINGEMENT HEATING RATES

In curve 1 of this figure, the heat input to an elevon immediately below the center line of a given engine was calculated. For curve 2, it was assumed that the heat input from the center motor was augmented by heat from the two outboard motors. In the actual case, it is believed that the heating value lies somewhere between the two curves but generally near curve 1, since the plume interference flow pattern limits interaction of the plumes. In Fig. 2.2-19, the equilibrium temperature attained by the elevon (with radiation to space from one side of the elevon assumed) is plotted against heat flux into the elevon. The limiting angle of the impingement of the Aerospike plume on the orbiter elevon is about 22 degrees; therefore, heat flux into the elevon lies between about 0.13 and 0.28 Btu/in^2-sec. With an average value of 0.20 Btu/in^2-sec and an emissivity of 0.8 assumed, an elevon equilibrium temperature of almost 2500°F is obtained. If subsequent test results substantiate these temperatures, the elevon will have to be designed to withstand these conditions, as related to the overall heat shield. One additional corrective action is possible in that, in vacuum, the elevon can be rotated outboard to increase the spacing to the engine.

Orbiter Optimum Aerospike Design. The optimum aerospike engine installation, presented in Fig. 2.2-20, is not optimum from the standpoint of weight, based upon the criteria used in the investigations. However, this design will provide for potential redesign of the orbiter to accommodate additional propellant or equipment; and will minimize the potential plume effects.

This design requires additional structure to mount the engine in the position, which is a major influence on the weights shown in Table 2.2-7.

2.2.3 Operational Characteristics

Base Heat Considerations. The thermal environment in the base region of a rocket stage, consisting of a multiengine cluster, results in a relatively severe heating environment for temperature-sensitive engine components exposed to the combined convection and radiation (primarily from exhaust gases) as a result of nozzle plume interaction. Considerable flight data have been

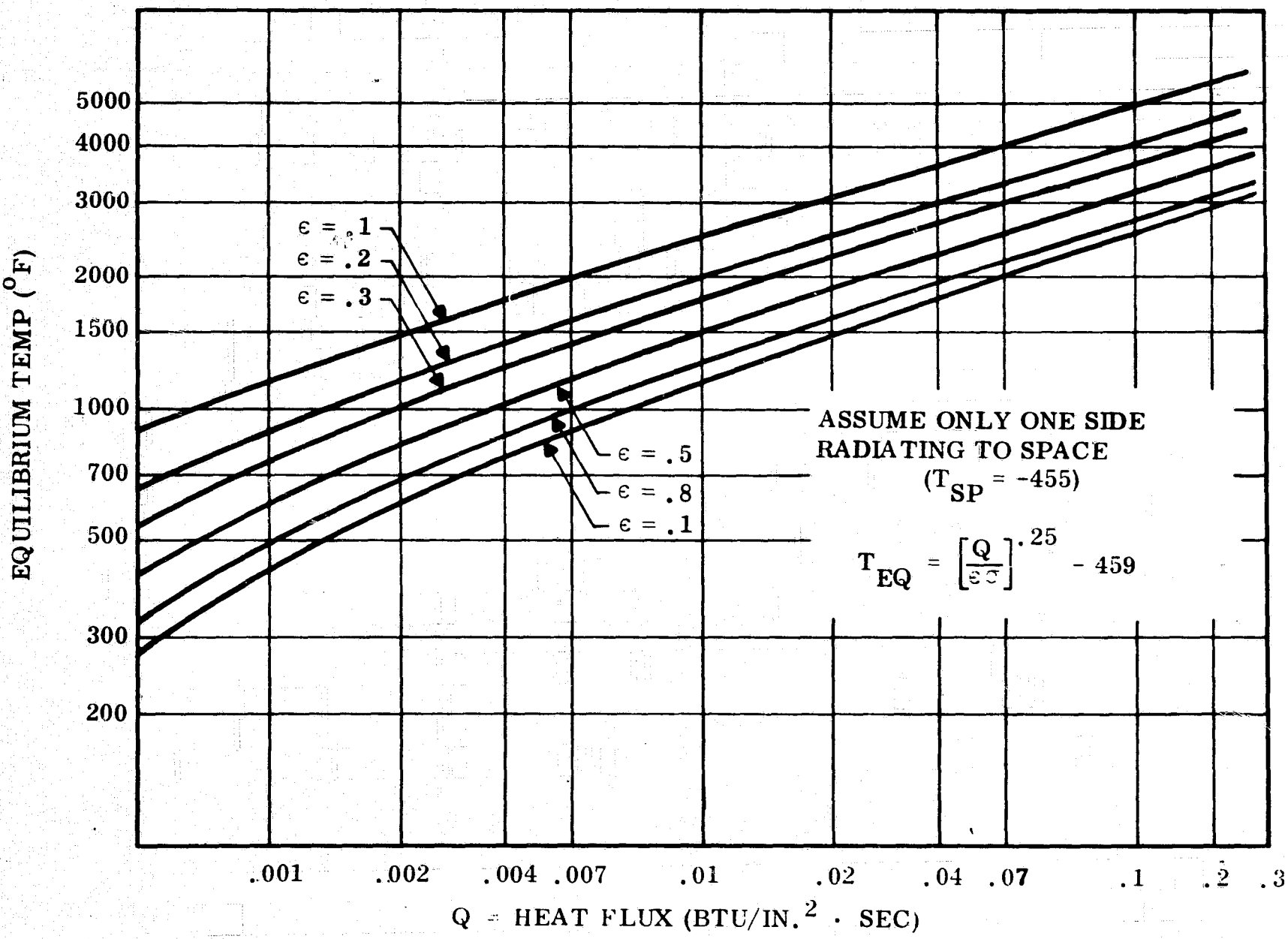

FIG. 2.3-19 ELEVON EQUILIBRIUM TEMPERATURES

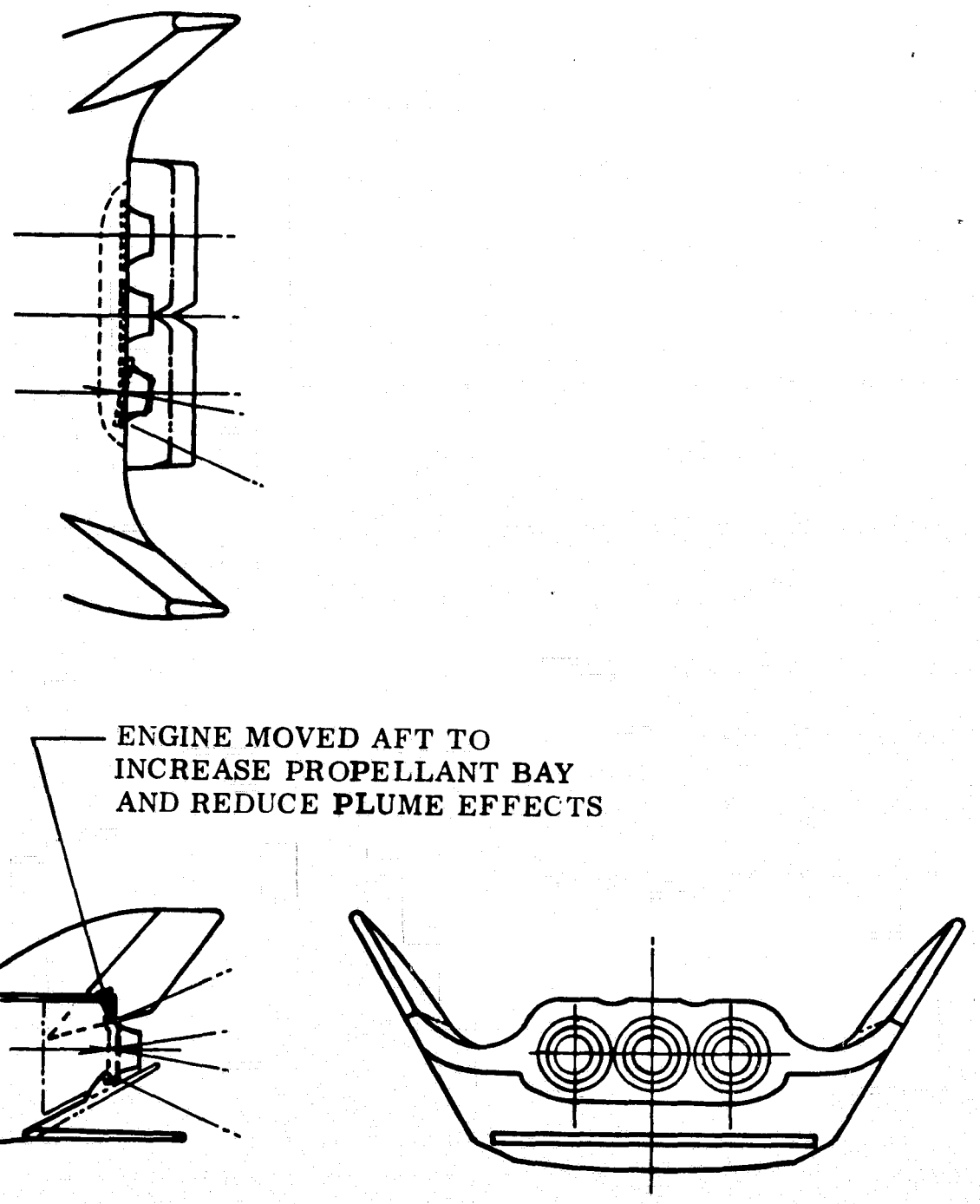

FIG. 2.2-20 OPTIMUM AEROSPIKE CONFIGURATION

Table 2.2-7

COMPARISON OF WEIGHTS RELATED TO ORBITER ENGINE ALTERNATIVES

Configuration	Figure No.	Structural Weight (lb)	Fairing Weight (lb)	Thrust Structure (lb)	Engine Weight (lb)	Total Weight (lb)	Weight Change (lb)
Baseline Bell-Type	LMSC-A955317A	–	1,800	2,740	13,280	17,820	–
Optimum Bell-Type (and resulting compromise)	2.2-15	–	1,850	2,740	13,800	18,390	+570
Compromise Aerospike	2.2-16	675	–	2,740	13,350	16,765	-1,055
Optimum Aerospike	2.2-20	–	2,935	2,740	13,350	19,025	+1,205

accumulated from the Fleet Ballistic Missile, Minuteman, and Saturn. For example, an empirical correlation of a considerable quantity of base heating data for four-nozzle clusters provides one of the most severe heating environments for the vehicle base region.* These methods have been applied to Minuteman and Saturn vehicles with equal success; therefore, it represents a suitable method for a first estimate of the heat transfer when the major contribution to the total heat is a result of reverse flow into the base region from nozzle interaction without combustion. The estimated peak heating environments are presented in Table 2.2-8 for the candidate booster and orbiter configurations. The gas temperature near the base shield surface is on the order of 50 percent (3250°R) of the chamber temperature; therefore, the actual convective heat transfer to the heat shield surface and flame curtains will be significantly less than those presented in Table 2.2-8 for a cold wall (temperature = 70°F). Estimates of the combustion effect on the total heat transfer to the base heat shield, which constitutes an engine compartment protective cover, were made based on S-I and S-IV data. An analysis will be made to establish an upper limit value of the hydrogen burning contribution to the base heat transfer during the entire ascent phase.

Regions of flow separation provide for recirculation of hydrogen from the base region (for an oxidizer/fuel ratio of 7:1) with resultant localized burning and associated radiative heat transfer. For asymmetrical vehicles (mated booster and orbiter), large separated regions could exist, particularly at angles of attack, between a booster and orbiter. The extent of this region will be defined on the basis of tunnel test programs; and, dependent upon the estimated combustion contributed heat rate levels, reconfiguring to minimize this effect may be considered. It is pointed out that the amount of free hydrogen in the nozzle exhaust is essentially identical for both the bell-type and the Aerospike engines.

Candidate material systems may be used for the combined booster base heat shield and flexible flame curtains. These are presented in Tables 2.2-9 and

*"An Empirical Correlation of Polaris Base Heating Data," by D.M. Tellep and Y. Kawamura, LMSC-801511, March 20, 1962.

Table 2.2-8

BASE HEAT SHIELD* PEAK HEAT RATE LEVELS

	Number of Engines	Nominal Sea Level Thrust, Klb	Expansion Ratio	Location Measured From Nozzle Exit Plane, in.	Convective Heat Rate BTU/ft^{2}sec, Cold Wall (T_w=70°F)	Combustion Effect on Base Environment, BTU/ft^{2}sec**	Total Heat, BTU/ft^{2}sec
BELL NOZZLE CONFIGURATION							
BOOSTER	13	400	35/1	68	10	10-30	20-40
ORBITER	3	400	150/1	208	<2.5	Small	<5
AEROSPIKE NOZZLE CONFIGURATION							
BOOSTER	7	800	–	32	100	10-30	110-130
ORBITER	3	400	–	32	10-20	Small	10-20

*Base heat shield or engine compartment enclosure.
**Preliminary estimates, based on S-I and S-IV data.

Table 2.2-9

BASE HEAT SHIELD CONCEPTS

	Maximum Reuse Temperature, °F	Working Maximum Heat Rate Level, Btu /ft^{2}sec
REUSABLE CANDIDATE MATERIAL SYSTEMS		
Stainless Steel – Fiberglas Insulation	1400	5
Haynes 25 – Fiberglas Insulation	1800	10
TD-NiCr – Fiberglas Insulation	2200	20
Rigid Light Weight Silica Insulation (LI-15)	2500	30
Columbium/Disilicide Coating	2500	30
Tantalum/Disilicide Coating	3000	60
Regeneratively Cooled Liquid Hydrogen	—	150+
NONREUSABLE CANDIDATE MATERIAL SYSTEMS		
Open Faced Honeycomb-Cells Filled with Lightweight Silicone Elastomer*	4000 a	125 (ρ =25 lb/ft^3)
	4000 b	200 (ρ =55 lb/ft^3)
Silicone Elastomer Reinforced With Silica Cloth or Rigid Silica Matrix*	4000	125 (ρ =25 lb/ft^3)
Refrasil Phenolic or Carbon Phenolic	4000 and up	200 and up

*Substrate – Phenolic Fiberglass

2.2-10. A promising stage-of-the-art system consists of a rigid heat shield of silicone elastomer in an open-celled honeycomb of phenolic Fiberglas, supported by a reinforced phenolic Fiberglas honeycomb structure. The flame curtains are composed of a flexible silicone elastomer, reinforced by silica fibers and covered on both surfaces with silica cloth covers. They are attached between the rigid heat shield and movable nozzles, similar to that for the S-I vehicle. The corresponding typical heat protective material and compartment structure section weight are presented for both bell-type and the Aerospike engine systems in Figs. 2.2-21 and 2.2-22.

In addition to these systems, a variety of refractory metallic (reradiative), high-temperature insulative materials, regeneratively cooled liquid hydrogen, and ablative materials may be used for the base heat shield, as outlined in Table 2.2-9. Each of these systems will be considered for application in the base region, dependent upon the localized heating environment and upon weight and cost of the protective system.

Candidate systems for flame curtains are quite limited because of the requirement for flexibility. While flexible metallic (accordion like) structures and metallic shingle systems are potential candidates for further consideration, they do not appear to be very promising.

Evaluation of Crossfeed of Propellants Between Booster and Orbiter.

Performance studies indicating the weight penalities for orbiter engine operations at liftoff are discussed elsewhere in the report. These and previous studies at LMSC have indicated considerable penalties for operation of the orbiter engines without consideration of crossfeed of propellants between the booster and the orbiter.

Crossfeeding of propellants was discussed at the Management Council, Space Shuttle Design Criteria Review, September 10-11, 1969. In the presentation, the crossfeed assessment showed (1) significant increase in design complexity, (2) complex staging transients, (3) significant additional development and testing, (4) penetration of thermal protection system, (5) significant in-

Table 2.2-10

FLAME CURTAIN HEAT PROTECTION CONCEPTS

	Maximum Use Temperature, ^{o}F	Maximum Use Heat Rate, Btu/ft^2 sec
Silicone Elastomer, Reinforced with Silica Fibers or Cloth and Sandwiched between Fiberglas Cloth	4000-4300	125-200
Flexible Metallic (Accordion Like) Structure	<3000	<60
Metallic Shingle System	<3000	<60

BELL-TYPE SYSTEM

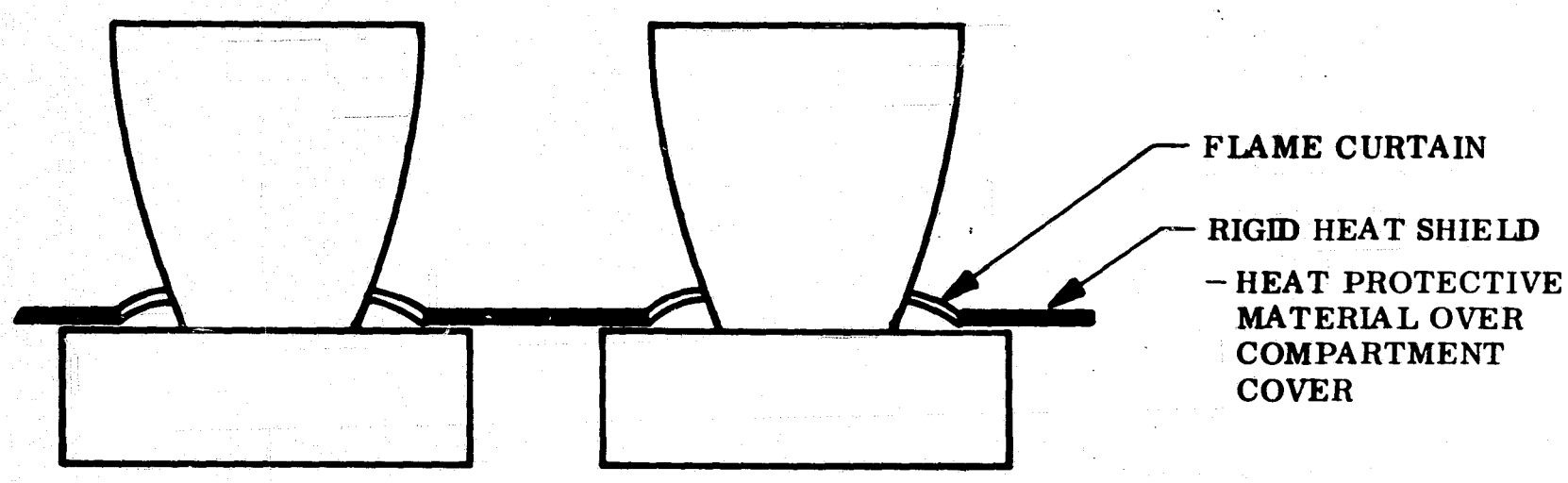

TYPICAL SECTION WEIGHTS

HEAT SHIELD	
• HEAT PROTECTIVE MATERIAL – SILICONE ELASTOMER/ PHENOLIC FIBERGLAS HONEYCOMB – EXTERNAL SURFACE OPEN CELL	2.0 LB/FT^2
• REINFORCED PHENOLIC FIBERGLAS HONEYCOMB STRUCTURE	1.0 LB/FT^2
FLAME CURTAIN	
• FLEXIBLE HEAT PROTECTIVE MATERIAL – REINFORCED SILICONE ELASTOMER WITH SILICA CLOTH COVERS	1.0 LB/FT^2

Fig. 2.2-21 Typical Booster Base Protective System

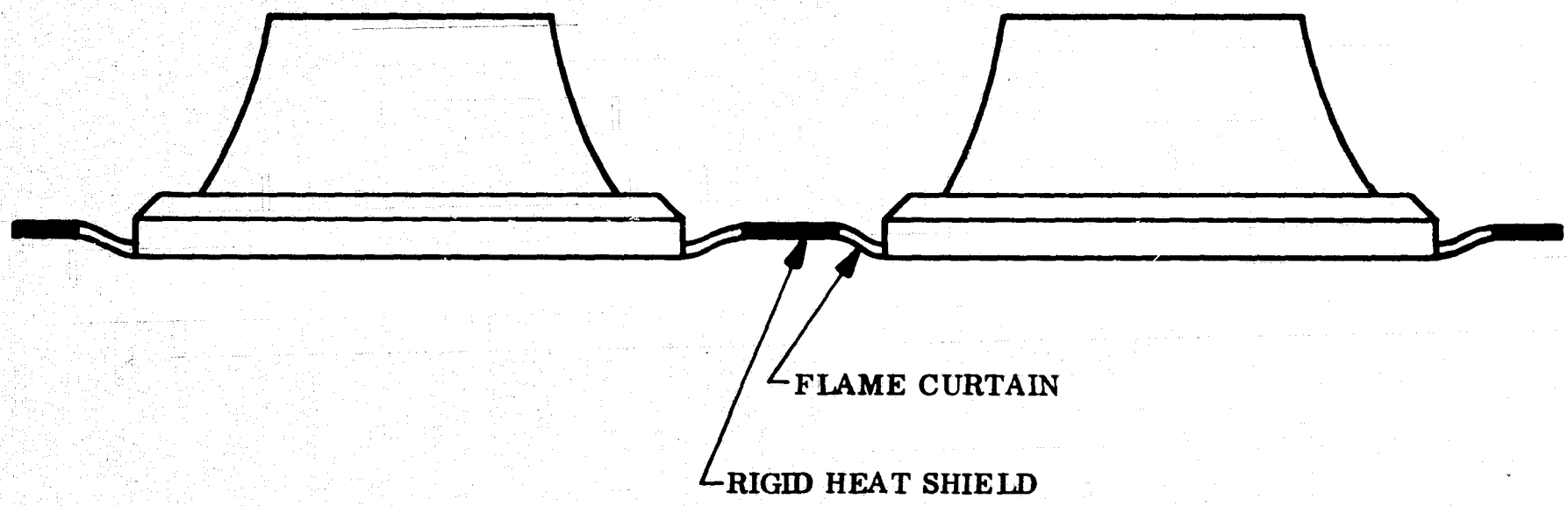

TYPICAL SECTION WEIGHTS

HEAT SHIELD	
• HEAT PROTECTIVE MATERIAL – SILICONE ELASTOMER/ PHENOLIC FIBERGLAS HONEYCOMB – EXTERNAL SURFACE OPEN CELL	4.0 LB/FT^2
• REINFORCED PHENOLIC FIBERGLAS HONEYCOMB STRUCTURE	1.0 LB/FT^2
FLAME CURTAIN	
• FLEXIBLE HEAT PROTECTIVE MATERIAL – REINFORCED SILICONE ELASTOMER WITH SILICA CLOTH COVERS	4.0 LB/FT^2

Fig. 2.2-22 Aerospike System

crease in program cost, (6) zero leakage seal technology required, (7) pre-launch checkout complexity increased, and (8) some potential reduction in liftoff weight for certain configurations.

Although some of the problems indicated cannot be overcome, LMSC has considered what appears to be an improved design approach. An evaluation of the crossfeed lines was undertaken to provide a design for easy separation of the crossfeed lines between the orbiter and booster without generating any debris and without protrusion of the plumbing beyond the orbiter or booster. A design has been developed as depicted in Fig. 2.2-23. In this design, one propellant line on each side of the booster passes inside each of the orbiter support pylons to the orbiter. Joining of the feed lines within the orbiter involves a snorkel-type connection, which can be released at staging. Before staging, valves on each side of the crossfeed lines are closed and the propellants in between the valves are drained through small separate lines. A hydraulic actuator disengages the snorkel fitting.

Although it appears to be technically feasible to develop a crossfeed capability, the reduction in launch vehicle system weight (principally the reduction in rocket engine thrust level or number of units) may not warrant its development when compared with the greater inherent simplicity of a tandem-burn, Two-Stage vehicle system.

Total system weight is 2475, as shown in Table 2.2-11.

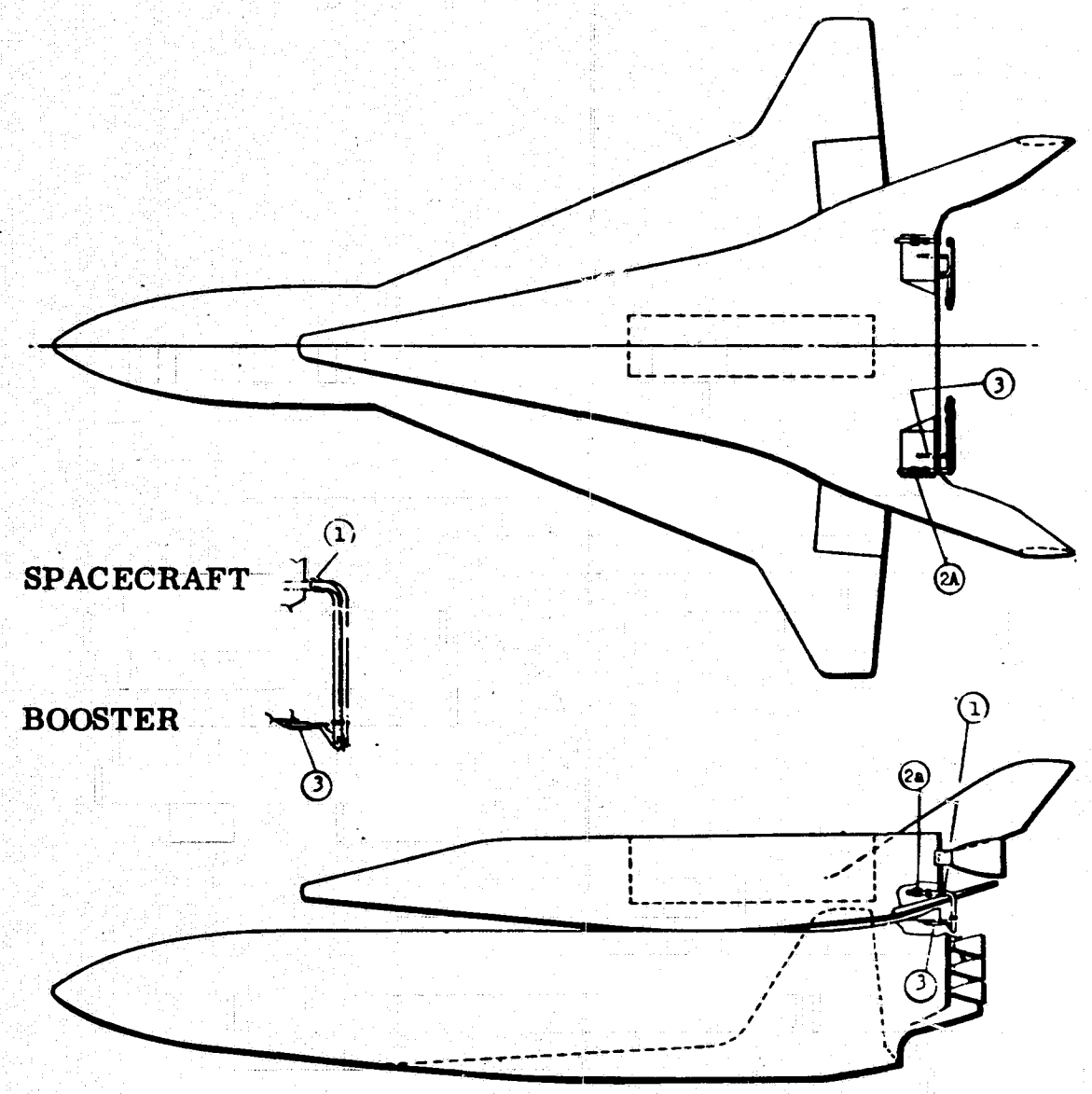

1 REUSABLE PROPELLANT TRANSFER COUPLING MATED DURING PRELAUNCH ASSEMBLY OPERATIONS

2a 2b ORBITER AND BOOSTER SHUTOFF VALVES ACTUATED BEFORE DECOUPLING/ SEPARATION AND PROPELLANT TRAPPED BETWEEN THESE VALVES IS DRAINED

3 ACTUATOR DISENGAGES PROPELLANT TRANSFER COUPLING PRIOR TO VEHICLE SEPARATION

4 EXTENDED BOOSTER PROPELLANT LINE RETRACTED TO REDUCE REENTRY HEATING EFFECTS

Fig. 2.2-23 Propellant Crossfeed Scheme

Table 2.2-11

WEIGHT BREAKDOWN - CROSSFEED SYSTEM

	Wt (lb)
Liquid Oxygen System	
Orbiter shutoff valve	50
Snorkel fitting	35
Flange and clamp	20
Drain valve	25
Shutoff valve	50
Line and supports	780
Pneumatic actuators	25
	985
Liquid Hydrogen System	
Orbiter shutoff valve	110
Snorkel fitting	60
Flange and clamp	35
Drain valve	10
Shutoff valve	110
Line and supports	1120
Pneumatic actuator	45
	1490

Reliability and Abort Consideration. The requirement for fail-operational/fail-safe operation will be evaluated for the various bell-type and aerospike engine configurations.

It should be noted that the aerospike 800K engine has two turbopump assemblies operating separate combustion chambers, so the seven aerospike engines actually become fourteen engines.

For one engine out on the booster, the remaining engines can be increased in thrust approximately 8 percent to compensate. In the event that the engine outage occurs during the worst gimbal loads, it may be necessary to shut down

a second opposite engine to compensate. For two engines out on the booster, the engine thrust of the remaining engine must be increased about 18 percent to compensate. The engine manufacturers have stated that the engines have the capability of increasing the thrust to 115 percent on a reusable basis. Thus the remaining 11 or 12 engines can probably compensate enough for two engines out to permit mission completion and certainly to compensate sufficiently to permit an abort operation.

The orbiter is equipped with three engines so that with one engine out, the remaining engines would have the capability of providing the necessary thrust/weight ratio. It appears to be desirable to assure that adequate thrust/weight ratio is provided in the initial design. For two engines out, if failures occur after 100 seconds of full thrust burning, the mission can be accomplished at a reduced thrust/weight ratio. An abort operation can be accomplished in any event with two engines out because of the high altitude at which normal stage separation occurs.

Alternate Means of Performing Orbital Maneuvers. The following ways of performing the orbit maneuvers defined for the Space Shuttle were considered:

- One main engine throttled to 10 percent of rated thrust (pumped idle)
- One main engine at unpumped idle (pressure-fed)
- Three maneuvering/translation RCS thrusters

The unpumped idle mode is operation of the main engine while using tank pressure only. No cooldown is required prior to entering this mode. In the pumped idle mode, the turbomachinery delivers propellants at a rate appropriate to the commanded 10 percent of rated thrust. A start to steady-state pumped idle operation has a transient with a plateau at the unpumped state. The plateau is held long enough to cool the engine adequately to permit operation at pumped idle. Shutdown occurs without such a plateau. The third

propulsion mode involves use of the three aft-firing maneuvering/translation thrusters of the orbiter reaction control system. After startup, some propellant is diverted to operate pumps and heat exchangers necessary for extended continuous operation.

The maneuvers and ΔV requirements projected for the orbital operations are listed in Table 2.2-11a. Also listed in Table 2.2-11a is the reentry weight assumed for this work. The loaded quantities of the fluids that are normally expended on orbit (prime power reactants, environmental control system fluids, and RCS propellants for attitude maneuvers) are included in this figure and not adjusted for normal usage.

The following assumptions were made for the calculations performed in this study:

- o No impulse was provided by the propellants used for cooldown, diverted for operation of the RCS pumps and heat exchangers, or consumed during start and stop transients.
- o A complete cooldown cycle for each engine firing was required prior to pumped idle mode operation.
- o The propellants designated for the contingency ΔV were carried until the deorbit maneuver was completed. Then, the contingency ΔV was supplied without transients or cooldown. In other words, the contingency ΔV was provided in a fifth "firing" after the deorbit maneuver.

The numerical results of this analysis are shown in Table 2.2-11b (along with the assumed values of specific impulse for each mode). Propellant consumption

is the sole basis for the tabulated results. In no case was the change in any present system design or tank and component weight assessed. The lower thrust capability of the RCS implies that long-duration firings (on the order of 1600 seconds) would be necessary to perform each maneuver, thus reducing the number of missions that can be completed before the limit of engine life is reached. Changes in tank volumes, tank weights, and required subsystem components were not examined.

It was assumed, as for the RCS, that operation in either of the two main engine modes is feasible; and the necessary modifications, if any, were not considered. The pumped idle mode of operation offers the advantage of the availability of engine bleed for tank pressurization, which is not possible for the unpumped idle mode. The pumped idle mode requires that liquid propellants be provided to the engine immediately following cooldown. This requirement suggests some type of propellant orientation system. One possible technique is to apply an unpumped idle mode with cooldown propellants.

In terms of propellant expenditure, the pumped idle mode is superior to the other two modes considered. This is true even though transients and cooldown were assumed to make no contribution to impulse. Inclusion of the nonimpulsive propellants results in an approximate effective specific impulse of 418 sec (about 93.5 percent of the assumed value). Therefore, the pumped idle mode will remain superior as long as the effective specific impulse of neither of the other two modes exceeds this value. The unpumped idle mode is not essential to the pumped idle mode. However, it offers the possibility of obtaining impulse performance from the cooldown propellants. If used in this

manner, 1210 fewer pounds of impulse propellant would be required, raising the effective specific impulse to near 431 seconds.

2.2.4. Performance. A study was conducted to determine the comparative performance of various bell-type and aerospike engine configurations for the Space Shuttle, For this study, a constant launch weight for the vehicle of 3.5 million pounds was selected, and the payload was allowed to vary as necessary to perform the missions. The parameters whose effects were evaluated were booster cruise lift/drag ratio, booster inert weight, orbiter inert weight, thrust/weight ratio, booster specific impulse, and orbiter specific impulse. The payload sensitivities as determined by computer studies are recorded in Table 2.2-12 for each of these parameters.

Table 2.2-11a

ORBIT MANEUVERS

Maneuver	ΔV, fps	No. of Firings
Plane change due to launch dispersion	200	1
Circularization at 100 nm	100	1
Transfer to 260 nm phasing orbit	558	2
Deorbit	500	1
Contingencies	500	-
Total	1858	

Weights

Payload	50,000 lb
Entry Weight	272,698 lb

Table 2.2-11b

PROPELLANT REQUIREMENTS

Mode	Impulse Propellant, lb	Other Propellant, lb	Total, lb
Pumped Idle	36,240	2500 (1)	38,740
Unpumped Idle	40,760	80 (2)	40,840
ECS Thrusters	40,480	3520 (3)	44,000

(1) includes propellant expended during cooldown and start/stop transients

(2) includes only start/stop transients

(3) includes propellant required for heat exchangers and pumps

PERFORMANCE ASSUMPTIONS

Mode	Specific Impulse, sec
Pumped Idle	446.5
Unpumped Idle	380.
RCS Thrusters	386.

Table 2.2-12

RUBBER VEHICLE PAYLOAD SENSITIVITIES

Parameter	Payload Sensitivity
Booster cruise lift/drag ratio	2590 lb/unit
Booster inert weight	-0.189 lb/lb
Orbiter inert weight	-1.13 lb/lb
Thrust/weight ratio	38,800 lb/unit
Booster specific impulse	665 lb/unit
Orbiter specific impulse	765 lb/unit

The vehicles listed in Table 2.2-13 were evaluated. A number of these configurations are discussed in Section 2.2.2.

Table 2.2-13

ENGINE CONFIGURATIONS

Vehicle	Engine Configuration	Booster Engine	Orbiter Engines
1	Optimum bell	13-400K (35:1)	3-400K bell (35/150)
2	Compromise bell	13-400K (35:1)	3-400K bell (35/150)
3	Optimum bell	13-400K (50:1)	3-400K bell (35/150)
4	Optimum bell	13-400K (65:1)	3-400K bell (35/150)
5	Optimum bell	13-400K (80:1)	3-400K bell (35-150)
6	Compromise bell	13-400K (100:1)	3-400K bell (35/150)
7	Compromise aerospike	13-400K (8 ft)	3-400K A/S (8 ft)
8	Compromise aerospike	13-400K (10 ft)	3-400K A/S (10 ft)
9	Compromise aerospike	13-400K (11.5 ft)	3-400K A/S (11.5 ft)
10	Optimum aerospike	7-800K (11.5 ft)	3-400K A/S (11.5 ft)
11	Compromise aerospike	7-800K (11.5 ft)	3-400K A/S (11.5 ft)

In the tradeoff study, the optimum bell (35:1) was selected as the baseline configuration. All of the bell-type engine configurations call for the same two-position engine on the orbiter. Three of the aerospike configurations have identical engines on the two vehicle elements. The remaining two have related engines of different thrust levels. Payload weight changes resulting from variations in the parameters are shown in Table 2.2-14.

Table 2.2-14

PAYLOAD WEIGHT CHANGES

CONFIGURATION*	VEHICLE NO.	P/L NET CHANGE, LB	L/D EFFECT	BOOSTER INERT WT. EFFECT	ORBITER INERT WT. EFFECT	T/W EFFECT	BOOSTER I_{sp} EFFECT	ORBITER I_{sp} EFFECT
35:1 Optimum bell	1	0	0	0	0	0	0	0
400K A/S (8 ft)	7	-3601	0	1667	5057	0	2128	-12,453
800K Optimum A/S	10	+7098	-1554	-367	2599	4423	3525	-1,528
800K Comp. A/S	11	+6995	-1554	-470	2599	4423	3525	-1,528
35:1 Comp. bell	2	-1970	-1554	-416	0	0	0	0
50:1 bell	3	-2418	-2850	-1763	0	0	2195	0
400K A/S (10 ft)	8	-1727	-4144	-1641	4322	0	4855	-3,119
65:1 bell	4	-5189	-4144	-2907	0	0	1862	0
80:1 bell	5	-6912	-4792	-3650	0	0	1530	0
400K A/S (11.5 ft)	9	-1098	-5180	-3107	2599	0	6118	-1,528
100:1 bell	6	-9578	-5180	-4598	0	0	200	0

*Listed in order of increasing base area, and grouped if identical

The L/D effect includes adjustment of the subsonic cruise propulsion system to overcome any loss in L/D. Evaluation of this table yields the following observations:

- The best bell-type engine configuration is number 1, having an area ratio of 35:1. As area ratio is increased, there is a reduction in payload delivered. Although the vacuum specific impulse improves as the area ratio increases, the average delivered specific impulse over the flight of the booster first improves and then begins to deteriorate. Over the same range of area ratio, the penalty associated with the necessarily larger base area steadily increases. The net effect is most favorable for configuration number 1.

- Configuration 9 is the best aerospike engine configuration when the thrust is limited to 400K. This engine has the largest diameter; therefore, in contrast to the bell configurations, there is an increase in the payload delivered as the area ratio (diameter) is increased. The significant weight penalties associated with larger base area are more than compensated for by the improvement in specific impulse.

- Configurations 10 and 11 deliver more payload than the baseline. The principal contributing effect is the thrust/weight ratio difference for these two configurations, which results from the greater liftoff thrust provided by the seven Aerospike engines. To compensate for this effect as a first approximation, the payload gain from the increased thrust/weight ratio may be subtracted. However, there is no change in the rankings. Furthermore, the gain due to inert weight savings in the orbiter is attributable to the use of the 400K, 11.5 foot engines. Use of these engines implies a premium in cost for the development of an engine derivative. If this payload gain is removed, configurations 10 and 11 are essentially equivalent to the baseline.

- In configurations 9 and 10, the 400K engine and the 800K engine have approximately the same diameter. The additional 400K engines required to meet the liftoff thrust entail a weight penalty slightly larger than

the payload gain because of the improved specific impulse. The difference in net payload change is small enough to suggest that these two configurations fall in the same performance class.

- Three bell engine configurations may be paired with Aerospike configurations having the same base area. They are 1/7, 4/8, and 6/9 in order of increasing area. In the last two cases, the Aerospike configuration is superior. For the smallest base area, however, the bell is superior. The turnaround is caused by an especially severe degradation of Aerospike specific impulse at the smallest diameter.

- Configurations 1 and 9 represent the best of each engine type when the thrust levels are limited to 400K. If the 800K aerospike payload change is adjusted as discussed earlier, configurations 1, 9, 10 and 11 are capable of delivering approximately the same payload. Based on configuration 1, the net weight increases caused by larger base areas is about offset by the gain due to increased specific impulse. Hence, the best of both types of engines are evidently in the same performance class as measured by payload delivered.

Evaluation of these configurations and others that may be defined should continue. The present conclusions are based principally on analytic studies. Future work should include design layouts to verify earlier analytical results and assist in further differentiating among the configurations.

2.2.5 Cost Considerations. A preliminary analysis was performed to assess the impact on system costs of carrying both the bell-type engine and aerospike engine into the design and development phases for the Space Shuttle. The analysis was based on the 4.1 million-pound Two-Stage reusable vehicle and its development schedule, as described in Volume IX of "Space Shuttle Data" (LMSC-A954317A).

For this purpose, the first 18 months subsequent to Phase C go-ahead were divided into six increments of 3 months each. Each increment was then examined to determine the areas of effort that would be impacted by a delay in

engine selection. Estimates were then made of the additional effort imposed on the vehicle contractor as a result of carrying parallel designs to accommodate either the bell-type or Aerospike engine configuration. These areas and the estimates of the percentages of additional effort required are shown in the activity matrix of Table 2.2-15.

Based on LMSC estimates, the RDT&E costs for the baseline vehicle are $5310 million after the development costs of the 673,000-pound vacuum thrust engine are subtracted. This cost estimate, which was derived by using the parametric cost model developed for the ILRV, agrees very closely with costs arrived at by using the Air Force CERs for Space Shuttle vehicles. The RDT&E cost was then spread over the first 18 months of the Phase C effort in accordance with an idealized 50/50 cost distribution when 50 percent cost is expended at 50 percent time elapsed. The percentage of additional effort required to support the dual-engine capability was then added to the baseline expenditure costs. The curves in Fig. 2.2-24 show the cumulative costs for both baseline and dual-engine programs as a function of time for the first 18 months of Phase C. Figure 2.2-25 is a plot of the delta-cost as a function of time.

As could be expected, the analysis shows that relatively minor cost penalties are incurred if the engine selection is made while the vehicle is still in the analysis and early design phases. However, these penalties can become significant as the program progresses into tooling and hardware.

2.2.6. Summary and Conclusions. The principal considerations in the LMSC analysis were the following:

- Engine configuration factors affecting vehicle design
- Effects on design from engine installation
- Engine performance
- Costs

Engine Configuration Factors. Considered in the investigations was the basic groundrule that only one bell-type engine and one Aerospike engine would exist and only modifications of these would be candidates.

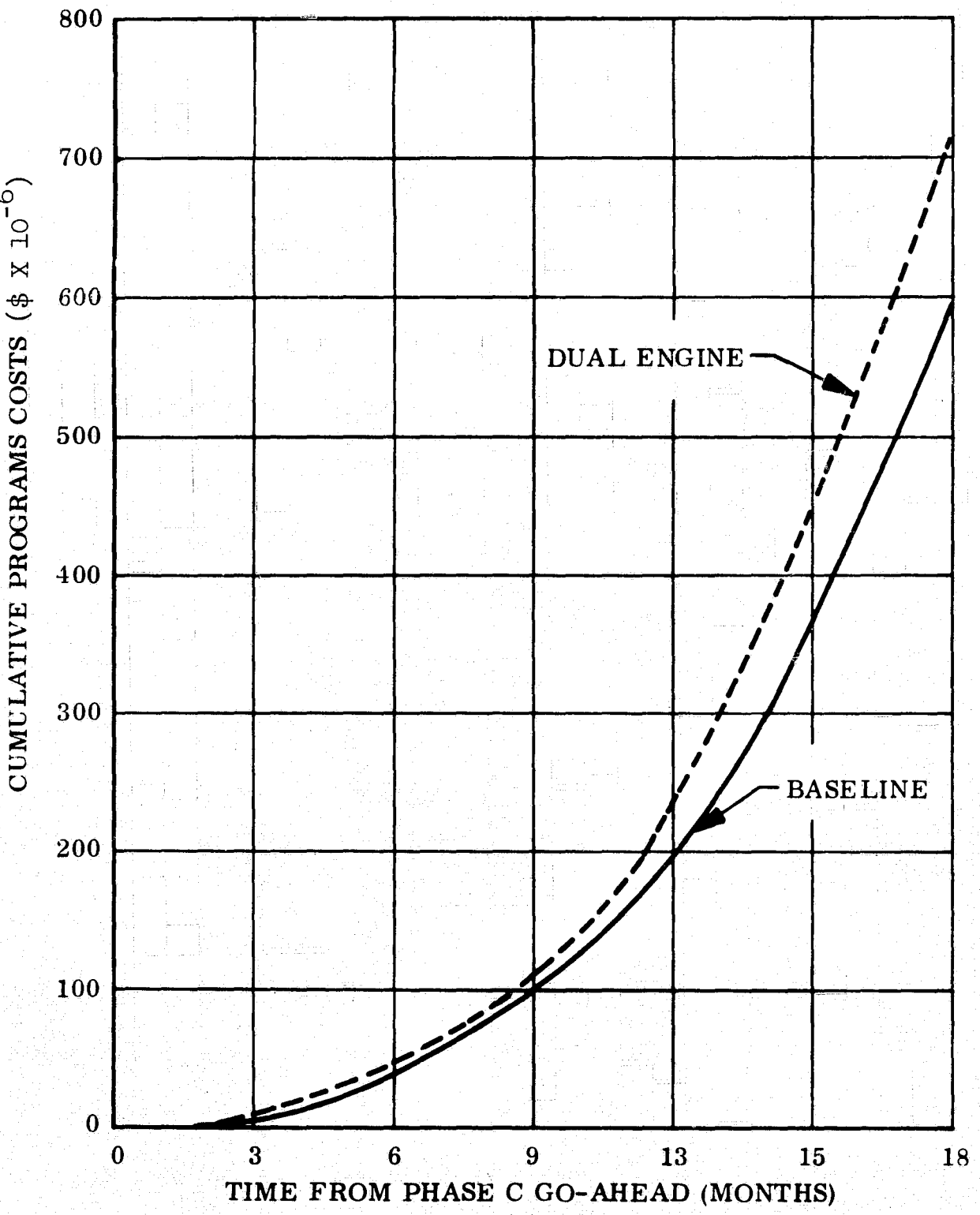

Fig. 2.2-24 Cumulative Costs vs Time

Table 2.2-15

TWO-STAGE ACTIVITY MATRIX

Period	Sys Eng and Integration	Prelim Design	Specifications	Wind Tunnel Model Testing	AGE Analyses	Detail Design	Tool Design	Procurement	GSE Analysis	Fab Engineering Mockup	Tool Fab	STV Fab	Breadboard Testing	ETV Fab	Component Testing	GSE Design	Tooling Mockup Fab	Flight Prototype No. 1 Fab	Flight Prototype No. 2 Fab	Flight Prototype No. 3 Fab	GSE Fab	Percent of Additional Effort
1	X	X	X	X	X				X													5
2	X		X	X	X	X	X	X	X													8
3	X		X	X		X	X	X	X	X	X	X	X									15
4	X		X	X		X	X	X	X		X	X		X	X	X	X					20
5	X		X	X		X	X	X			X	X		X	X	X	X	X				25
6	X		X	X		X	X	X			X	X		X	X	X		X	X		X	30

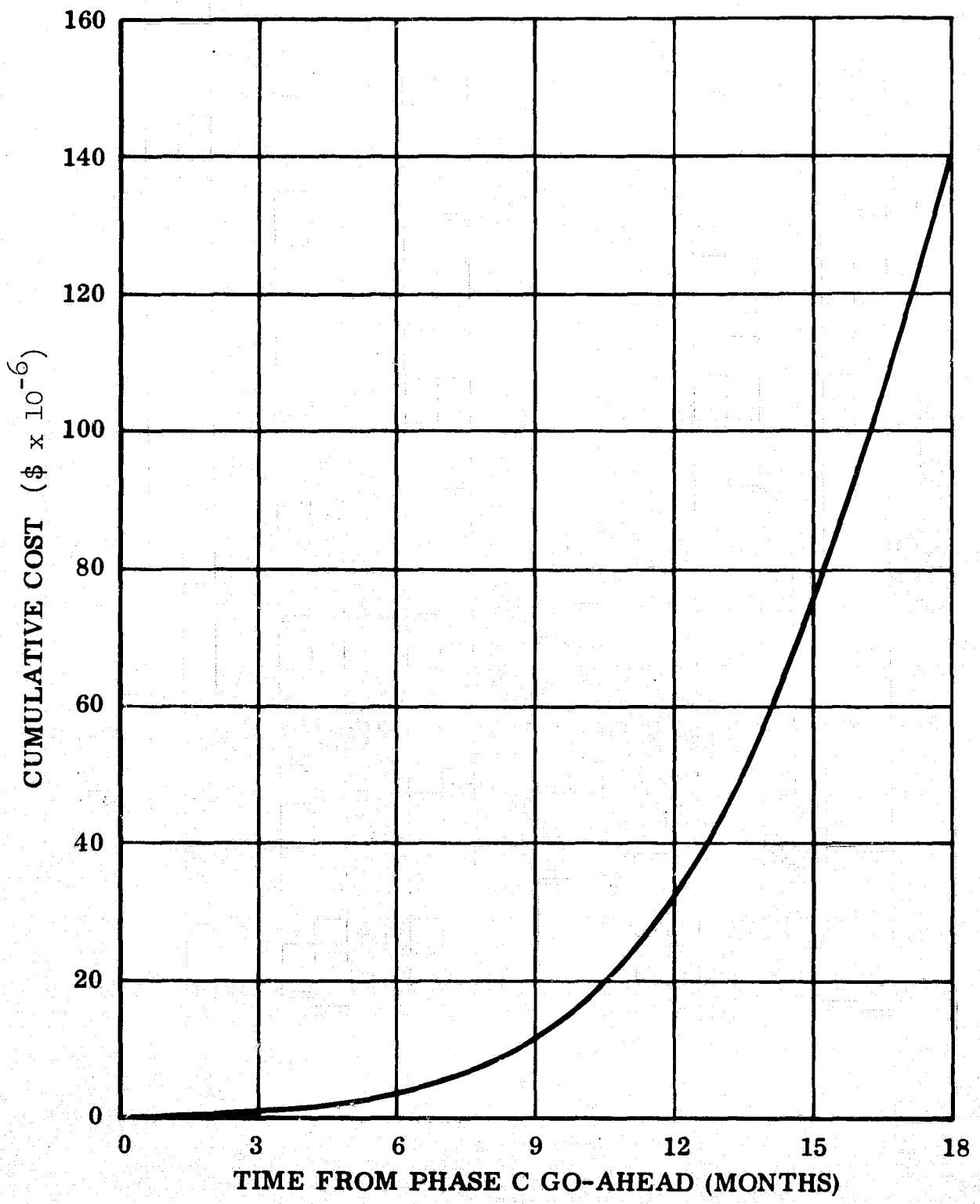

Fig 2.6-25 Cumulative Costs vs Time

For example, the bell-type engine could have a 35:1 nozzle with an extension to obtain higher specific impulse for vacuum performance, and the Aerospike engine could add another ring of combustion chambers to double the thrust. It should be noted that a bell-type engine can be increased in specific impulse through the use of the nozzle extension, but the aerospike engine must increase in diameter in order to increase specific impulse. Sufficient tradeoff comparisons of overall booster and orbiter performance, including the effects related to L/D ratio and flyback propellant requirements, are not available to indicate fully all of the effects on the booster. However, judgments based on available data tend to favor smaller booster base areas and, therefore, the bell-type engines at lower expansion ratios (35:1).

If the aerospike is employed, it appears more desirable to replace two bell-type engines of lower expansion ratio (35:1) with one aerospike engine of twice the thrust; otherwise, the booster vehicle base areas will have to be increased if engines of equal thrust are substituted. Engine configuration effects are summarized in Table 2.2-16.

Table 2.2-16

SUMMARY OF ENGINE CONFIGURATION EFFECTS
ON A TWO-STAGE VEHICLE SYSTEM

	BOOSTER		SPACECRAFT	
	Aerospike	Bell-nozzle	Aerospike	Bell-nozzle
Engine Configuration				
Length (inches)	52 in	132 in	52 in	210/273
Nozzle Dia {Static	139 in	61 in	136 in	124 in
Nozzle Dia {Dynamic	141 in	92 in	137 in	188 in
Weight (ea-lb)	7800	4140	4450	4700
Engine Installation				
No. of Engines	7	13	3	3
Thrust Level (lb)	800K	400K	400K	400K
Base Area (sq ft)	1430	1262	common	
Structure Weight, etc. (lb)	+1500	baseline	+635	baseline
Performance				
Specific Impulse	-6.0 sec	sea level baseline	-1.6 sec	vacuum baseline
Payload Increment	≈1800 pounds less payload for Aerospike installation where nominal payload is 40,8000 pounds at a launch weight of 3.5×10^6 pounds			

Engine Installation Factors. Conslusions resulting from the examination factors, other than booster base area effects, did not indicate large penalties to provide for the capability of using either the aerospike or the bell-type engines. Thrust structures, plumbing, and related hardware can be modified at fixed aft vehicle stations to accept either engine. Fairings required to protect the bell-type engines from air loads are a major contributor to the weight differences. The relevance of engine installation factors on the shuttle vehicle are summarized in Table 2.2-17.

Table 2.2-17

SUMMARY OF ENGINE INSTALLATION EFFECTS
ON A TWO-STAGE VEHICLE SYSTEM

	Minimum Installation Differences	Significant Installation Differences
TVC Gimbal Angle	X	
TVC Actuators	X	
Feed Line Size	X	
Propellant Tank Pressure (Based on NPSH) - Booster	X	7-800K Aerospike Engines vs. 13-400K bell-nozzle engines
Thrust Structure - Spacecraft	X	
Engine Installation Fairings - Booster		Not required for Aerospike
Exhaust Plume Press. Effects	X	
Exhaust Plume Thermal Effects		Aerospike creates severe environment on elevons
Exhaust Plume Acoustic Effects	(insufficient data)	
Base Area - Booster		Minimum Aerospike larger than minimum bell nozzle
Base Area - Spacecraft	X	

Engine Performance. The engine performance factors did not produce significant differences. The reportedly inherent idle mode capability of the aerospike engine may be an advantage, but further study is required to establish the total magnitude of this feature.

Cost Estimates. The cost to the Space Shuttle contractors of maintaining the capability of using either engine in the program has been estimated to be approximately $30 million through the first year.

2.3 PROPULSION/VEHICLE SYSTEM INTERFACE

In establishing detailed propulsion system parameters, engine that are equally applicable both to the booster and orbiter stages of either the Two-Stage or Triamese vehicles must be considered. The requirements of engine commonality, efficient engine operation at both sea level and altitude, and reusability of engines for extended periods impose significant innovations; and the development of criteria that are definitive and responsive to requirements becomes the program objective.

The tasks to be accomplished in this program include:

- Examine the reusable vehicle configurations and their mission requirements.
- Determine rocket engine size and performance characteristics that meet vehicle and mission requirements.
- Establish operational criteria for start and stop sequences, throttling, propellant feed condition, TVC, engine control and instrumentation, environments imposed on the engine and created by the engine, etc.
- Identify rocket engine reusability criteria for preflight and postflight checkouts, maintenance, overhaul, etc.
- Correlate rocket engine physical dimensions with vehicle limitations.
- Evaluate basic criteria for the compatibility of the engine control system with the vehicle integrated electronic system.

From each of these tasks, rocket engine requirements and engine operational and performance criteria can be specified. On the basis of studies conducted and the data generated to date, rocket engine criteria for a reusable space transport system document have been prepared. The latest version of this document is presented in Appendix A; the bases for selection of the criteria are discussed in the following section.

2.3.1 Bases for Rocket Engine Criteria Selection

As a result of the task studies conducted, the bases for the rocket engine criteria have been derived. These bases are discussed in the following paragraphs. For convenience, the paragraphs are numbered to correspond to the paragraphs of Appendix A, the Rocket Engine Criteria Document.

(3.1.1.1.1) Thrust. Thrust ratings and mixture ratios required for the rocket engine are shown in Fig. 2.3-1. Ratings are derived from mission analyses shown in Refs. 1(a) and 1(d). The requirement for the emergency rating (115%) are based on abort analyses reported in Ref. 1(e). Data showing these requirements for the Two-Stage and Triamese vehicles are shown in Fig. 2.3-2 and 2.3-3. Normal thrust rating for the two vehicles is derived from data shown in Fig. 2.3-4. Mixture ratio requirements are shown in Fig. 2.3-5. Spacecraft configurations that make use of these engines are shown in Ref. 1.

(3.1.1.1.2) Specific Impulse. The required minimum engine specific impulses listed in the Rocket Engine Criteria, Appendix A, are based on analytic studies whose results are discussed below.

Fig. 2.3-6 is a presentation of the effect of booster and orbiter mixture ratios on launch weight and total dry weight. Although a common mixture ratio of 6:1 minimizes the launch weight, a mixture ratio of 7:1 was selected in order to minimize the dry weight and hence vehicle size and cost. Fig. 2.3-6 indicates that there are relatively small variations in launch weight and dry weight as the mixture ratio changes from 6:1 to 7:1. The mixture ratio that is ultimately selected for the Space Shuttle engines will depend on other important criteria.

(3.1.1.2.1) Duty Cycle. Burn times and rocket engine power settings for selected missions calculated at LMSC are given in Table 2.3-1. Typical orbital operations data, which are based on a preliminary allotment of 2000 ft/sec of total incremental velocity, are presented in Table 2.3-2.

Calculations show that it is more economical in terms of propellants to use primary propulsion for orbital maneuvers in excess of 500,000 lb/sec when the cooldown propellants are used in an unpumped idle mode having a specific impulse of 300 lb/sec. It was assumed that the main engine and the RCS have specific impulses of 446.5 and 389 lbf-sec/lbm, respectively. Recent information indicates that the specific impulse of the unpumped idle mode will be greater than 300 lbf-sec/lbm and that the specific impulse of the RCS will be slightly lower than 389 lbf-sec/lbm. If either one of these trends occurs, the point (total impulse) at which the primary propulsion mode becomes superior will fall.

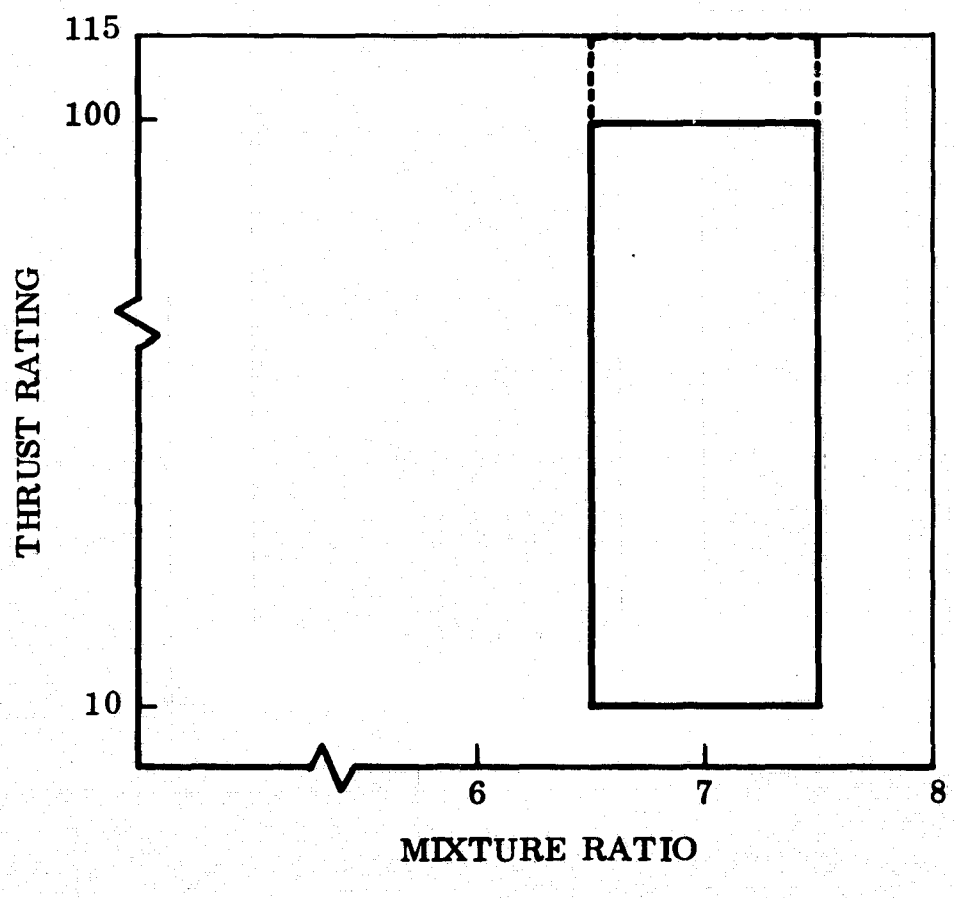

Fig. 2.3-1 Engine Thrust Regime

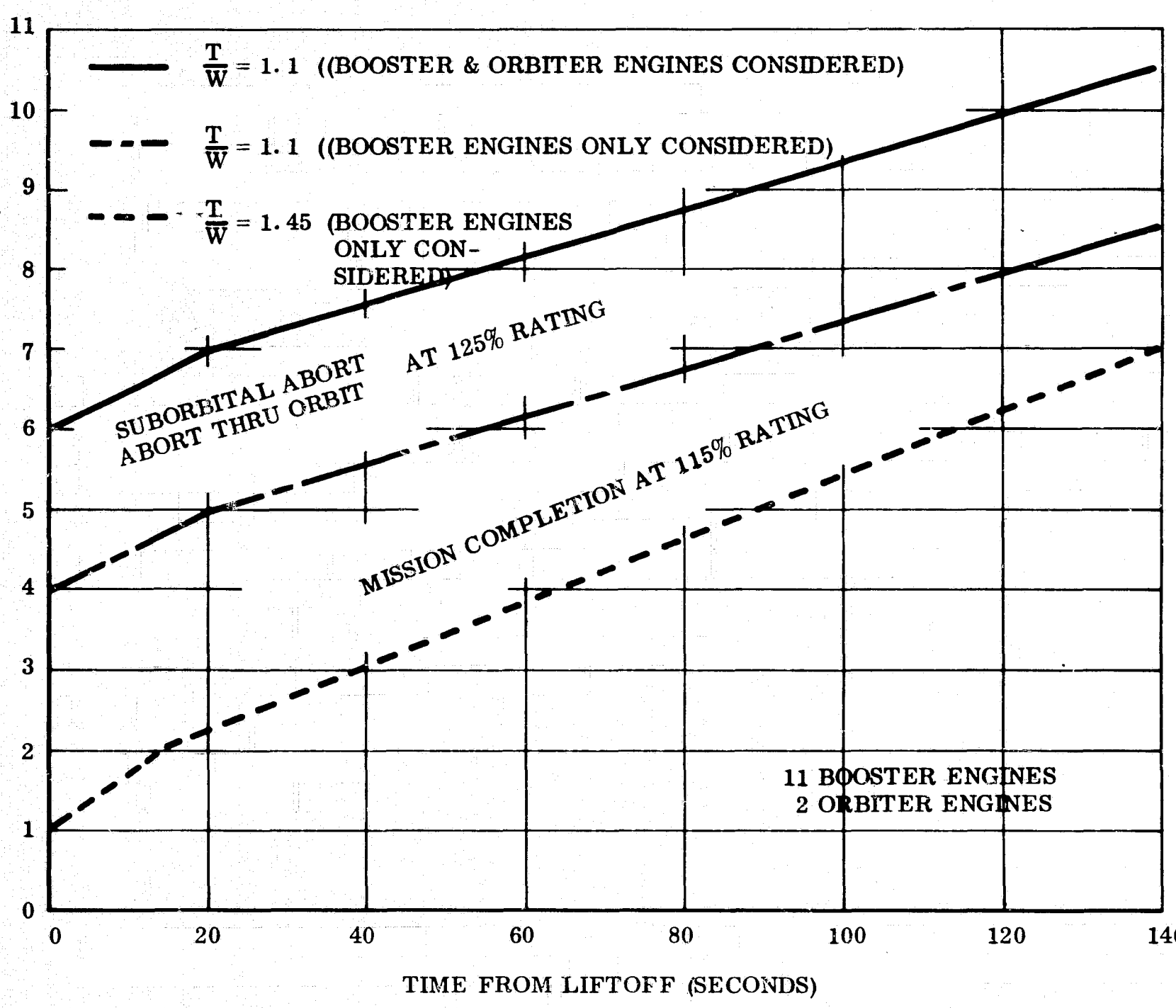

CONTINUOUS THROTTLING BEGINS (3G)

Fig. 2.3-2 Allowable Engines Out vs Time From Liftoff – Two-Stage Configuration

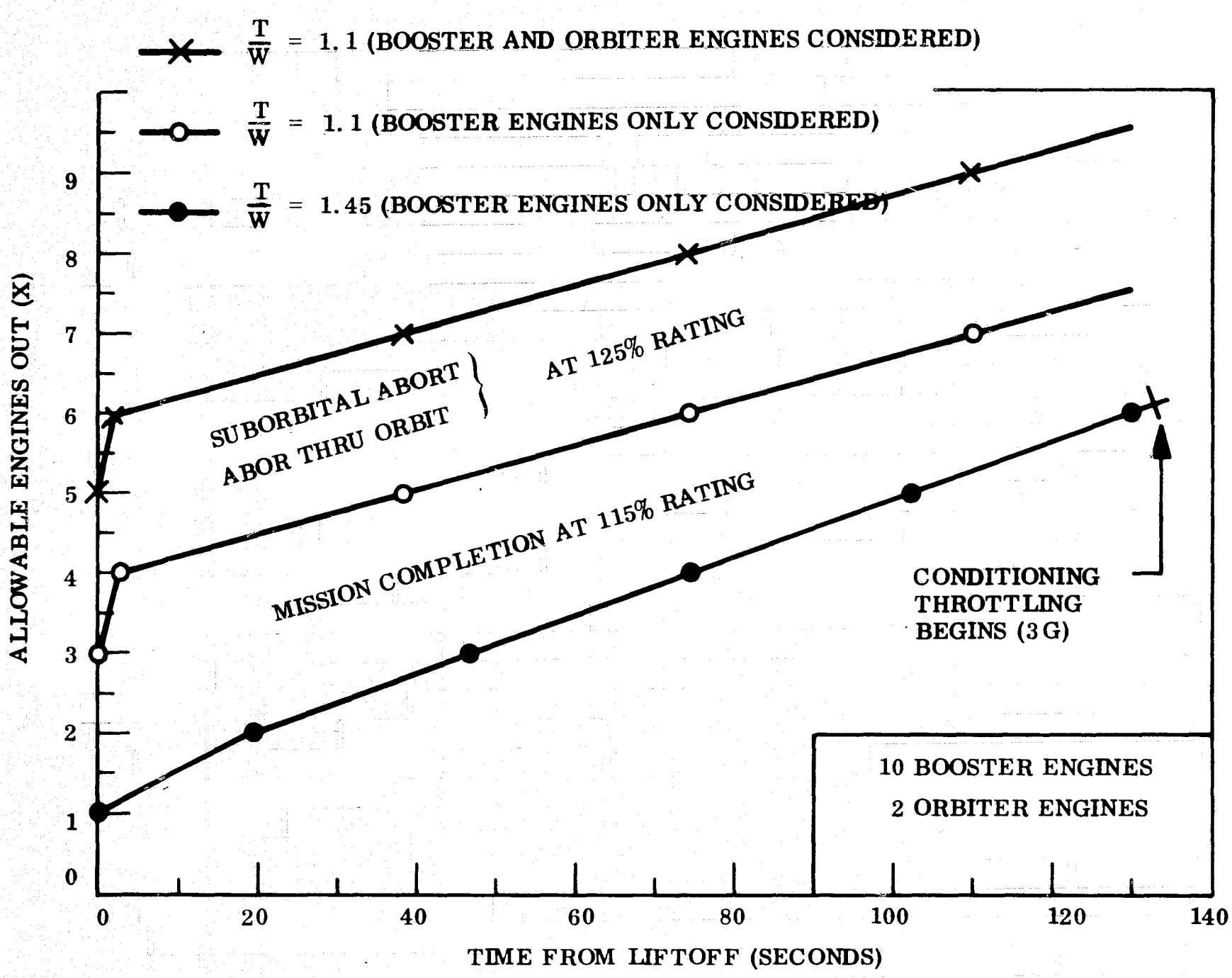

Fig. 2.3 3 Allowable Engines Out vs Time From Liftoff – Triamese Configuration

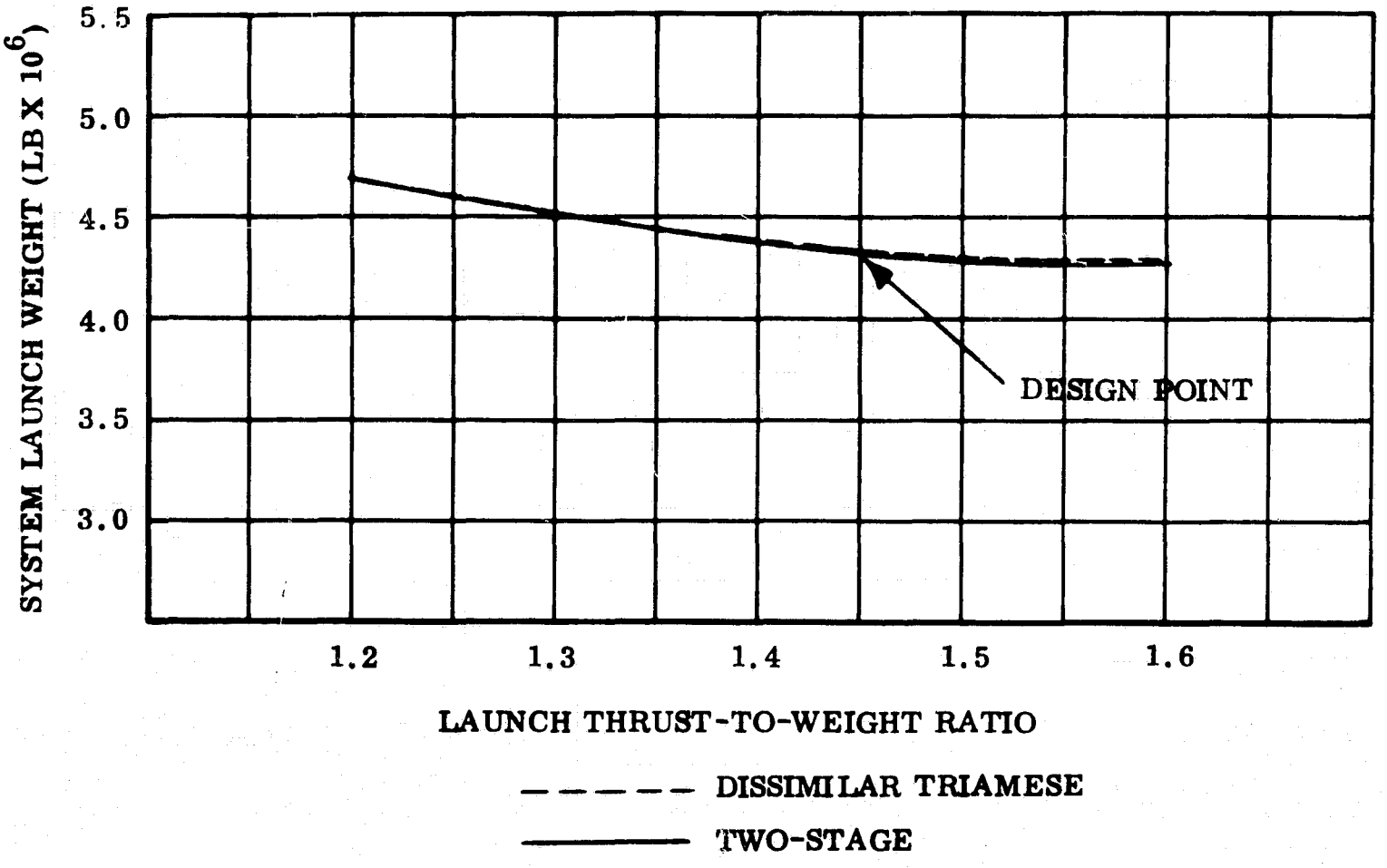

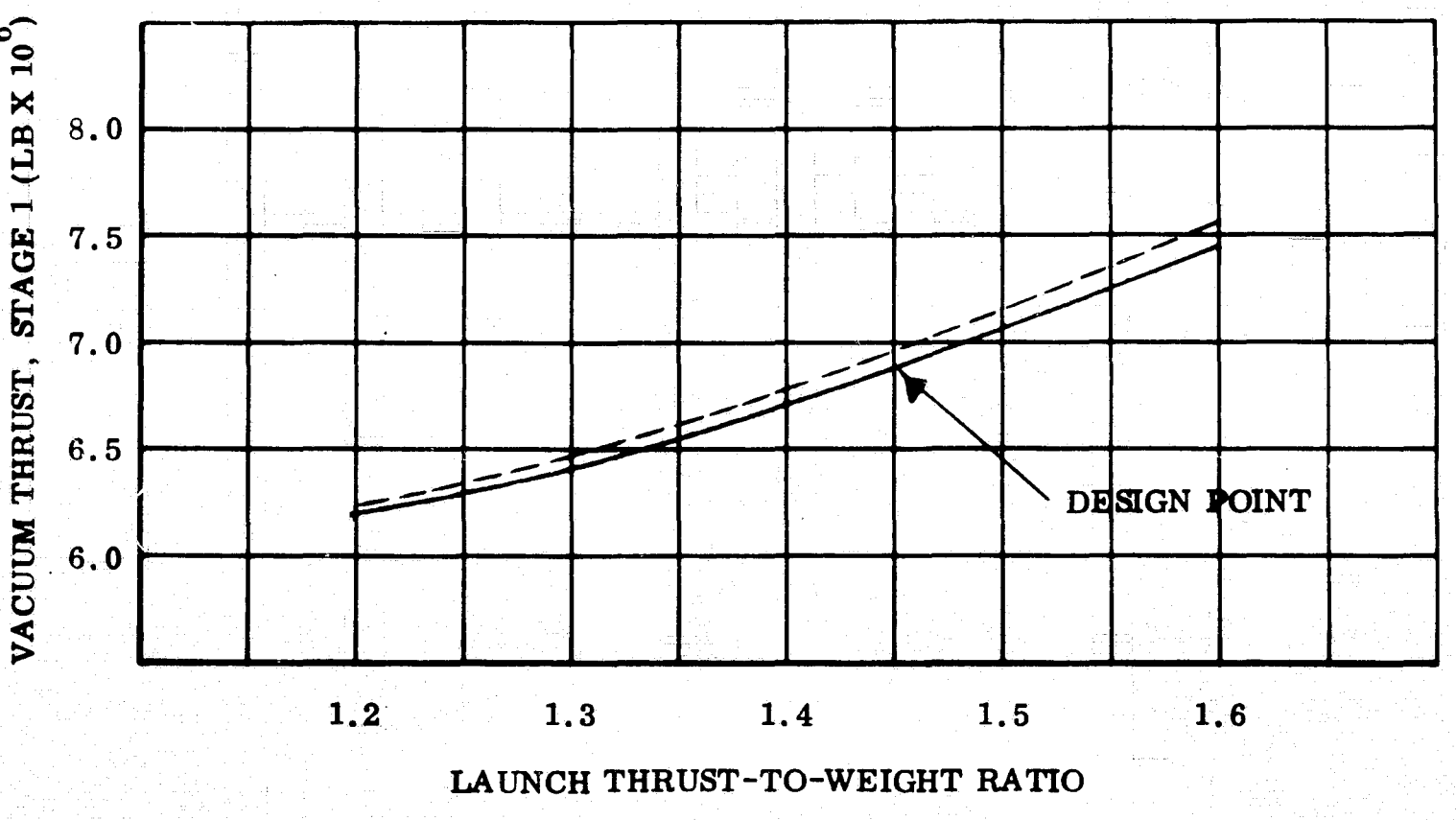

Fig. 2.3-4 Launch Thrust-to-Weight Ratio Effects
(Stage 1 Vacuum Thrust, System Launch Weight)

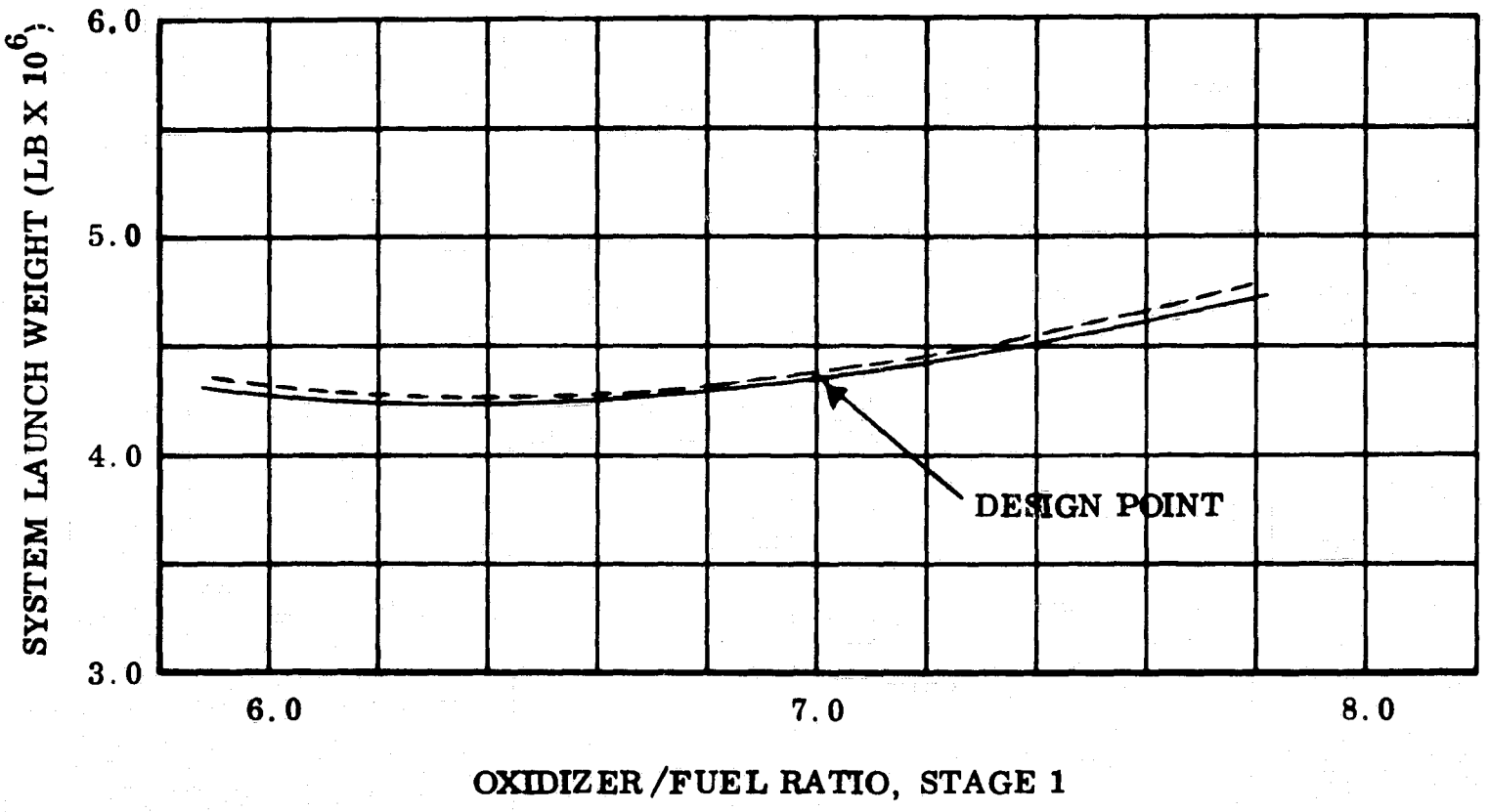

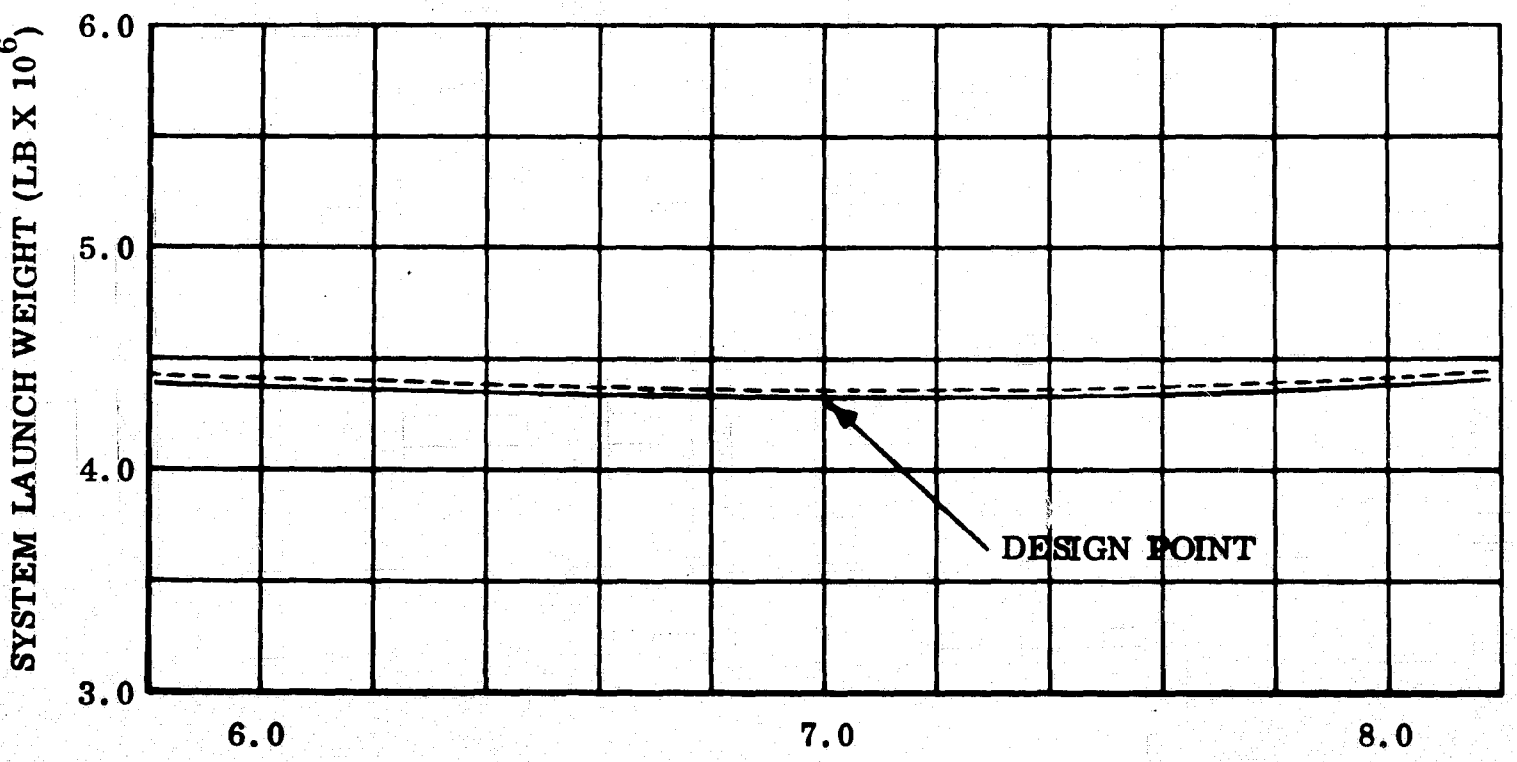

Fig. 2.3.-50xidizer/Fuel Ratio Effects

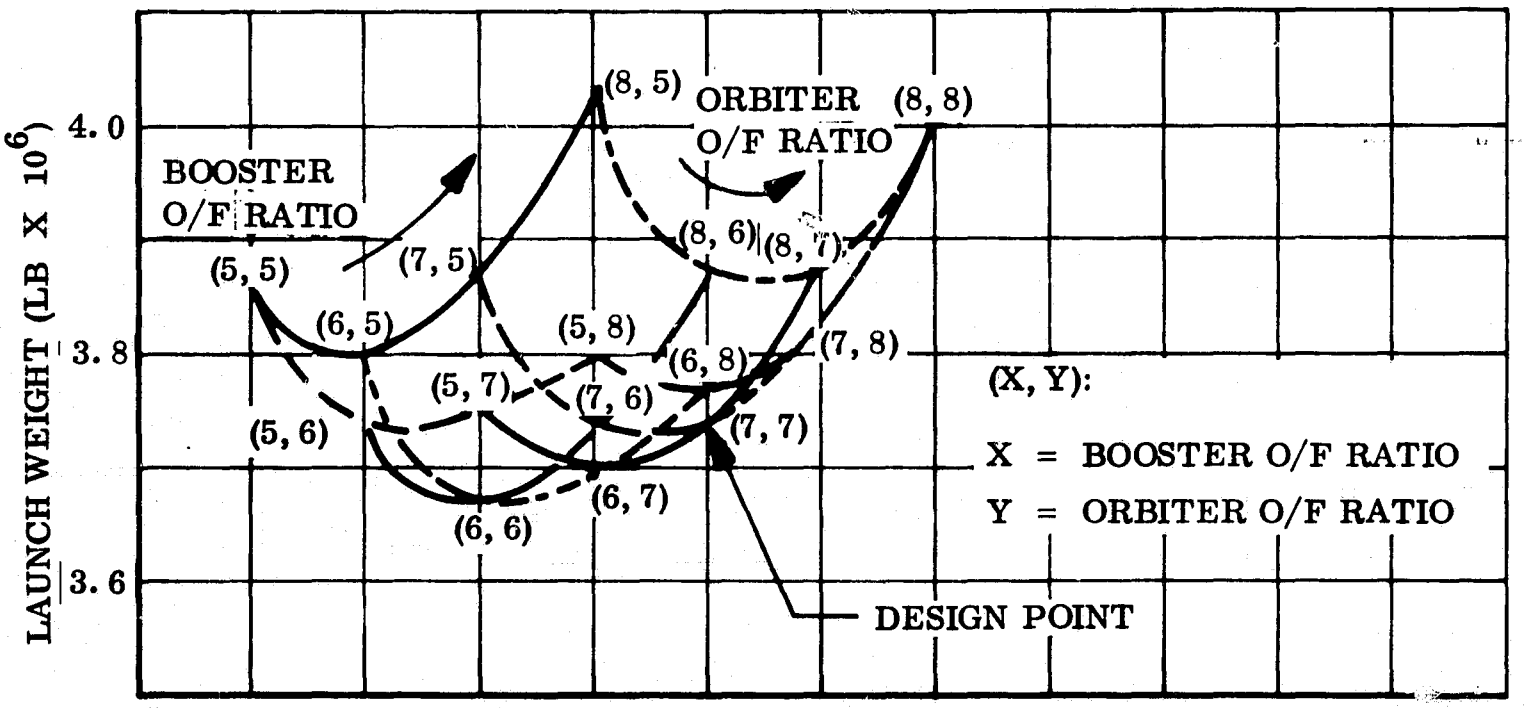

——— CONSTANT O/F RATIO IN ORBITER
VARIABLE O/F RATIO IN BOOSTER

– – – – CONSTANT O/F RATIO IN ORBITER
VARIABLE O/F RATIO IN BOOSTER

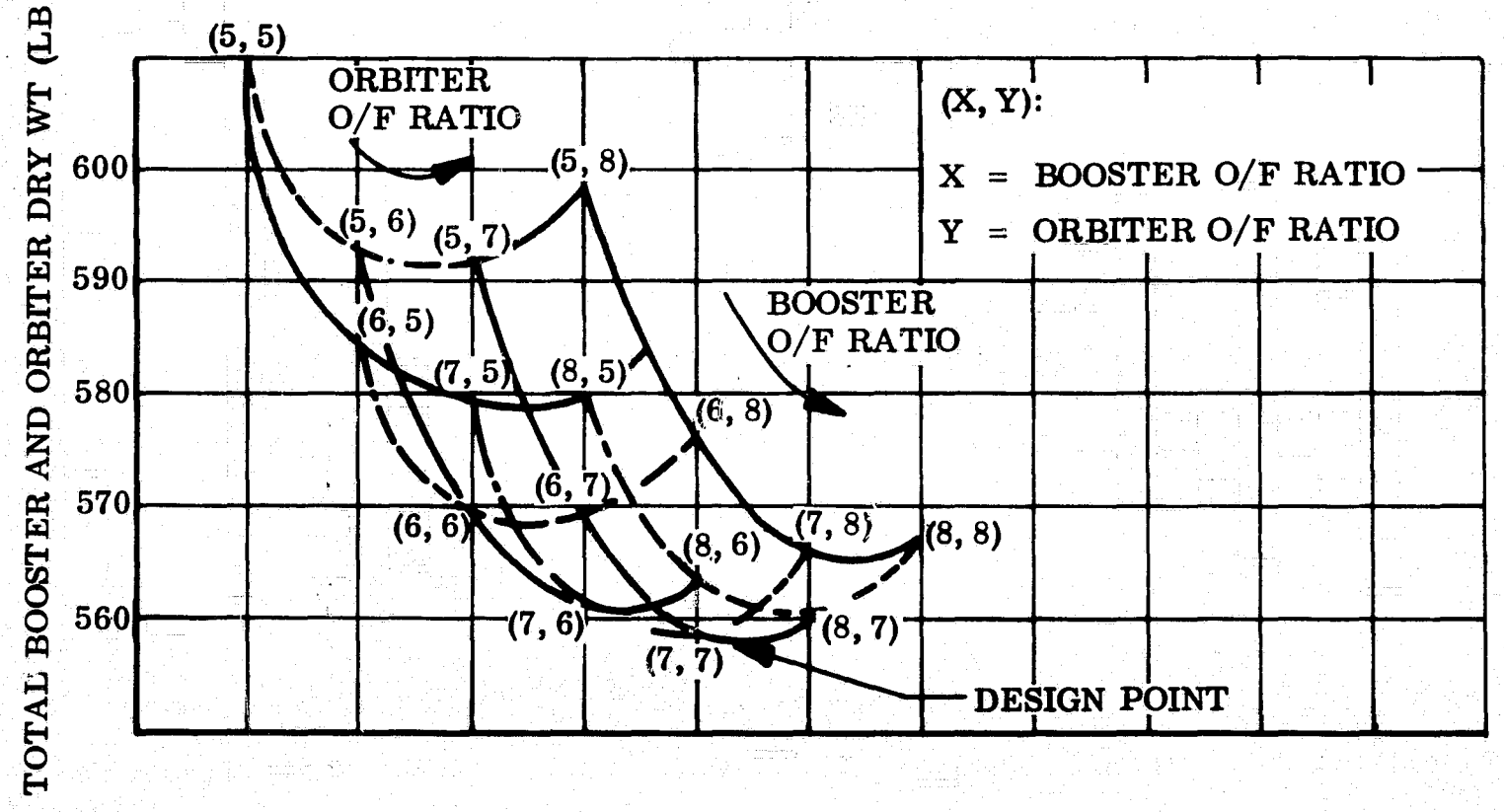

Fig. 2.3-6 Oxidizer/Fuel Ratio Effect for Two-Stage 50 K Payload

Table 2.3-1

ESTIMATED DUTY CYCLE, VEHICLE WITH 50,000-LB PAYLOAD, 3-G LIMIT, CONTINUOUS THROTTLING, ETR LAUNCH TO 55° INCLINATION, 45x100-NM ELLIPTICAL ORBIT

TWO-STAGE		TRIAMESE	
Burn Time (sec)	Thrust Rating (%)	Burn Time (sec)	Thrust Rating (%)
0	100 (SL)	0	100 (SL)
115 (throttled)	100 (VAC)	125 (throttled)	100 (VAC)
196	62 (VAC)	184	65 (VAC)
Staging		Staging	
196	100 (VAC)	184	100 (VAC)
420 (throttled)	100	411 (throttled)	100
436 (orbit injection)	90	443 (orbit injection)	81

Table 2.3-2

ORBITAL MANEUVER

Maneuver	Incremental Velocity (ft/sec)	Propellant Impulse (lb)	Weight* Total (lb)	Nominal Impulse (lb-sec)	Nominal** Burn Time (sec)
Plane change due to launch dispersion	200	4,240	4,740	$1.89 \cdot 10^6$	41
Circularization at 100nm	100	2,110	2,610	$0.94 \cdot 10^6$	20
Transfer to 260 nm phasing orbit	558	10,910	11,910	$4.88 \cdot 10^6$	105
Terminal rendezvous, docking, and undocking (RCS)	142	4,070	4,500	$1.55 \cdot 10^6$	-
Deorbit	500	9,650	10,150	$4.31 \cdot 10^6$	93
Contingency	500	9,330	9,330	$4.16 \cdot 10^6$	90
TOTAL	2,000	40,310	43,240		

*Total propellant, including start/stop transients and cooldown propellants.

**With one engine throttled to 10 percent normal rating.

(3.1.1.2.1.1) Starting, (3.1.1.3.1.3) Shutdown. Start and shutdown characteristics of the rocket engines are based on predicted performance.

(3.1.1.2.2) Thrust Vector Control. Results of LMSC preliminary calculations (Ref. 2) to determine the thrust vector control requirements for the Two-Stage vehicle to 45 x 100-nm orbit with all engines operating normally are as follows:

Angular Displacement	Booster (deg)	Orbiter (deg)
Pitch	±7.5	±5
Yaw	±7.5	±5
Pitch Cant Angle	±3	
Yaw Cant Angle	0	

The location of the center of gravity of this vehicle is shown in Fig. 2.3-7. The location of the center of gravity with respect to the aerodynamic center (i.e., center of pressure) at takeoff is such that the vehicle is inherently stable. Thus, angular acceleration rate variations have no significant effect upon the angular displacement limits.

The TVC capabilities of selected rocket engines, including XLR129, M-1, J-2S, XLR-81BA-15, and RL-10, are shown in Table 2.3-3. It would appear that engines are generally capable of providing the necessary capability for normal vehicle operation.

(3.1.1.2.4) Thrust Transients. Data on thrust transients for the engine operational modes are based on predicted performance.

(3.1.1.2.6) Mixture Ratio Control. The engine mixture ratio requirements have been defined in 3.1.1.1.1. Control requirements for propellant utilization are discussed in Ref. 1(c).

(3.1.1.2.8) Propellant Dump. The requirements for propellant dump through the engine without ignition has not been established. However, the J-2S engine has this capability, as cited in Ref. 3, and the capability may be desirable for these missions.

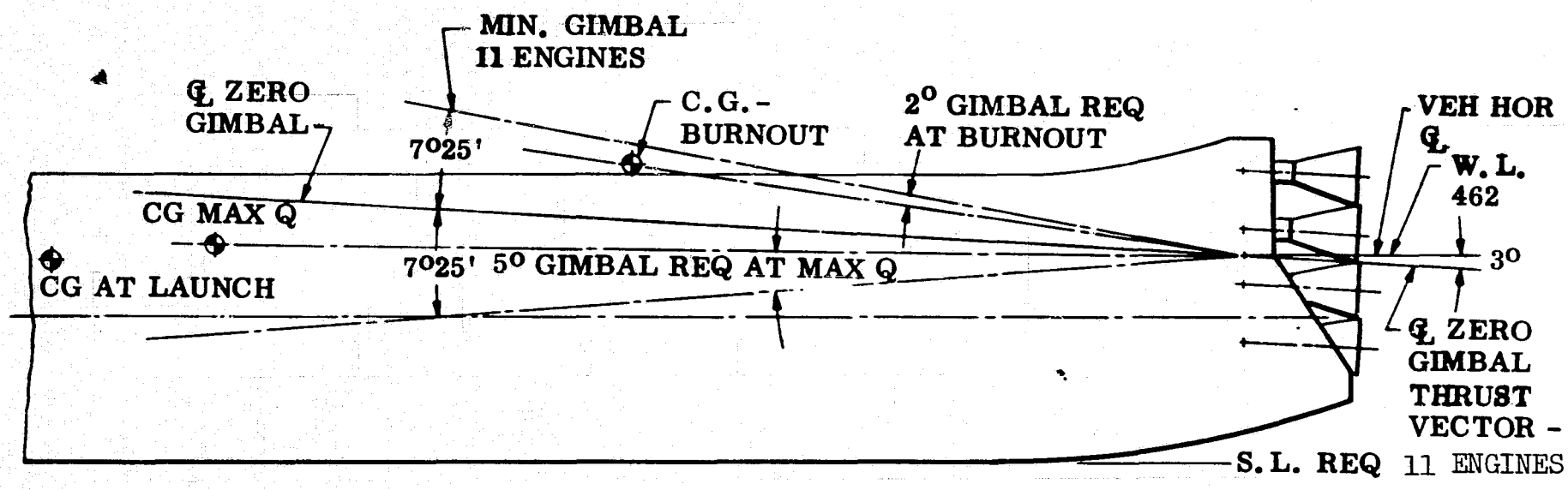

Fig. 2.3-7 Booster Minimum Gimbal Angle Requirement, Two-Stage System

Table 2.3-3

THRUST VECTOR CONTROL CAPABILITIES FOR VARIOUS ROCKET ENGINES

Engine	Angular Displacement Deg	Angular Velocity Deg/Sec	Angular Acceleration Rad/Sec^2
X1R129	7.0	30	30.0
J-2S	7.5	-	76.0
M-1	7.5	15	-
XLR81-BA-15	3.0	36	30.0
RL-10	4.0	-	32.9

(3.1.2.2.1.1) Module Replacement. Rapid turnaround of the Space Shuttle system requires engine refurbishment and module replacement as necessary. Requirements for these operations are discussed in Ref. 1(e), and the feasibility of the approach is described in Ref. 4.

(3.1.2.2.1.2) Engine Overhaul. The requirement for a 10-hour time between overhaul has been established to make feasible the long operating life specified for the engine in 3.1.2.3.1.

(3.1.2.2.2) Checkout Criteria. The capability for automatic checkout of the engine and its performance is cited in Refs. 1(c) and 1(e). This concept, which is being used in the C-5A malfunction detection, analysis, and recording (MADAR) subsystem is discussed in Ref. 5.

(3.1.2.3.1) Operating Life. The 50-hour total operational life (four overhauls) specified for each engine was derived from an estimate of 2000 flights during a 10-year program, which could be accomplished with seven vehicles that require 10 minutes of engine operation for each flight.

(3.1.2.3.3) Storage Life. The 10-year storage life for the engines is predicated on a 10-year program. Any longer time may result in obsolescence of the engine or the vehicle.

(3.2.1.2.1.1) Operation. Engine operational regimes are discussed in 3.1.1.1.1 and 3.1.1.2.1. In order to meet these requirements, propellants must be provided to the engine under specified conditions for the pumped operations but may be saturated liquid or mixed phase propellants for the unpumped idle mode.

(3.2.1.2.1.2) Chilldown. The turbopump must be preconditioned to propellant temperatures to prevent mixed phase propellant flow for pumped operation. However, the engine can be operated in an unpumped idle mode with the chilldown propellants.

(3.2.1.2.2.1) Helium. Helium is required for operation of engine valves and tank pressurization. These operations are described in Ref. 1(c).

(3.2.1.2.2.2) Autogenous Pressurant Requirements. The propellant tanks are pressurized with gaseous propellants, as discussed in Ref. 1(c), during engine operation.

(3.3.1.3) Engine Center of Gravity. During booster operation, the vehicle center of gravity moves markedly rearward. To minimize this change, a forward location of the engine center of gravity is desirable.

(3.3.1.5) Pressurants. Engine and propellant tank pressurants are discussed in 3.2.1.2.2.1 and 3.2.1.2.2.2.

(3.3.1.7.1) Control. The requirements for turbopump control of propellant flow are discussed in 3.1.1.2.6.

(3.3.1.7.2) Gimballed Engine. Thrust vector control requirements are discussed in 3.1.1.2.2.

(3.3.1.8) Electrical System. Instrumentation and checkout requirements for the engine are discussed in 3.1.2.2.2.

2.3.2 References

1. Space Shuttle Data, LMSC-A955317A, Sept. 12, 1969.
   a. Vol. 1 Design Integration
   b. Vol. 3 Structures, Materials, and Thermal Protection System
   c. Vol. 4 Propulsion and Propulsion Integration
   d. Vol. 5 Avionics
   e. Vol. 6 Performance and Flight Mechanics
   f. Vol. 7 Operations, Safety, and Refurbishment
   g. Vol. 8 Test and Production

2. Space Shuttle Data, Supplemental Data on Two-Stage Vehicle, LMSC-A959126, Sept. 20, 1969.

3. Engine Model Specification, Oxygen/Hydrogen Liquid-Propellant Rocket Engine, Rocketdyne Model J-2S, dated March 7, 1969.

4. LR129 Reusable Rocket Engine Diagnostics and Maintenance, Pratt & Whitney Aircraft, PDS 3237, dated May 12, 1969.

5. M. S. Edwards and A. P. Pennock, Development of C-5A Propulsion System Monitoring, J. Instrument Society of America, 15, 185 (1969)

CONTENTS

Section 3
REENTRY HEATING AND THERMAL PROTECTION

This section describes the results of parametric studies of reentry heating and thermal protection concepts. The study trades are based on an LMSC - ILRV orbiter configuration that is representative of both the upper stage of a Two-Stage or a Triamese system. The configuration is characterized by a flat bottom, constant-leading-edge sweep, delta-wing lifting body. An oblate ellipsoidal nose cap is used to minimize stagnation point heating levels.

3.1 REENTRY HEATING

Heating prediction methods used during the ILRV study and the results of two wind tunnel programs to measure heat transfer distributions on the orbiter configuration are discussed below. The orbiter thermal environment is described for several entry trajectories.

3.1.1 Heating Prediction Methods

All heating predictions were based on the 1962 Standard Atmosphere (Ref. 3-1) and Hansen's equilibrium air properties (Ref. 3-2). Progressive boundary layer transition starting at a local Reynolds number of 1 million and ending at 2 million was assumed. Table 3-1 summarizes the heating prediction methods used during this study. The methods are discussed below according to vehicle location.

3.1.1.1 Nose and Leading Edges. Nose stagnation point heating rates were computed by the method of Fay and Riddell (Ref. 3-3) with the velocity gradient based on the experimental data of Boison and Curtiss (Ref. 3-4). These data indicate that the effective radius for the spacecraft ellipsoidal nose with a 3.0-ft semimajor axis and 1.5-ft semiminor axis is 5.0-ft; i.e., the stagnation point heating is identical to that on a 5.0-ft

radius sphere. Body and fin leading edge heating rates were computed by the method of Fay and Riddell, modified for two-dimensional flow. Fin leading edge heating rates were increased by 20 percent, based on wind tunnel heating data discussed below. Leading edge boundary layer transition was assumed to occur when the freestream Reynolds number based on diameter equals 800,000, a criterion proposed by Bushnell (Ref. 3-5). Stagnation line turbulent flow heating rates were computed by the method of Beckwith and Gallagher (Ref. 3-6). Leading edge transition occurs late in the entry trajectory, so turbulent heating rates are considerably lower than peak laminar values.

3.1.1.2 Lower Surface. Heating rates in the nose region ($S/R_n<5$) were based on the blunt delta wing laminar heating distributions presented in Ref. 3-7. Aft of five nose radii from the stagnation point, the lower surface flow properties were based on oblique shock theory and heating rates were computed by two-dimensional flat plate theory empirically modified to account for outflow. In Fig. 3-1, the outflow correction factors for laminar and turbulent flow are plotted versus the streamline divergence parameter $\sqrt{\text{TAN}\,\alpha_L/\text{TAN}\,\epsilon}$ (Ref. 3-8). The laminar flow curve is based on correlation of lower centerline heat transfer data from several wind tunnel models with sharp or slightly blunted nose and leading edges. With increased bluntness the heating rates decrease; consequently, application of these data to the spacecraft entry heating predictions is expected to yield conservative results.

Table 3-1

AERODYNAMIC HEATING PREDICTION SUMMARY

Location	Theory	Comments
Stagnation point	Fay and Riddell	Experimental velocity gradient data for ellipsoidal nose
Leading edge-laminar	Modified Fay and Riddell	Sweep independence principle, conservative for large α
Leading edge-turbulent	Beckwith and Gallagher	Transition at $Re_{\infty,D} = 800,000$
Lower surface-laminar	Reference Enthalpy	Tangent wedge flow properties Empirical outflow correction Experimental spanwise distribution
Lower surface-turbulent	Rho-Mu	Boundary layer origin at start of transition
Upper surface/side panel	Reference Enthalpy and Rho-Mu	Experimental pressure coefficient Empirical boundary layer origin

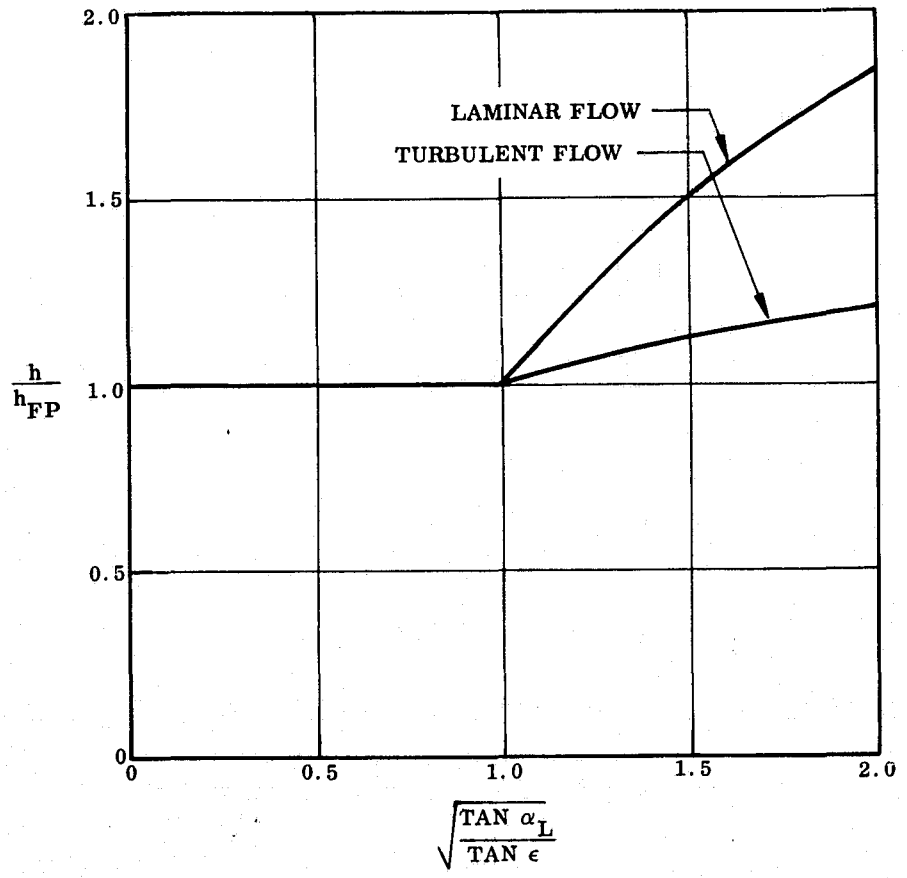

Fig. 3-1 Outflow Correction Factor for Delta Wing Lower Centerline Heating

The data indicate that two-dimensional flat plate heating theory must be modified to account for outflow when the local angle of attack exceeds the platform semiapex angle. For turbulent flow, an outflow correction factor is estimated from the laminar experimental results as follows:

From streamline divergence theory (Ref. 3-8),

$$\left(\frac{h}{h_{FP}}\right)_{LAM} = \sqrt{1 + 2j}$$

and

$$\left(\frac{h}{h_{FP}}\right)_{TURB} = \sqrt[5]{1 + \frac{5}{4}j}$$

where j is the exponent in the equation for the initial shape of the inviscid streamlines on the lower centerline, i.e.

$$Y \propto X^{j}$$

Since j is independent of the state of the boundary layer, these equations can be combined to yield the turbulent flow outflow correction factor in terms of the laminar value as follows:

$$\left(\frac{h}{h_{FP}}\right)_{TURB} = \sqrt[5]{\frac{3}{8} + \frac{5}{8}\left(\frac{h}{h_{FP}}\right)^2_{LAM}}$$

As indicated in Fig. 3-2, the turbulent flow correction factor is considerably smaller than the laminar value. The outflow factors are applied to two-dimentional flat plate heating rates computed by Eckert's reference enthalpy method (Ref. 3-9) for laminar flow and by Hanks' rho-mu method (Ref. 3-10) for turbulent flow.

3.1.1.3 Upper Surface. Heating rates on the body side panels were based on a procedure developed in analysis of wind tunnel data from several lifting entry spacecraft configurations. The heating distributions are computed by two-dimensional flat plate theory with local flow properties based on an isentropic expansion from the leading edge stagnation line to the local pressure. The empirically determined characteristics dimension used to evaluate the heating theory is four times the surface distance from the leading edge stagnation line, measured normal to the leading edge.

3.1.2 Heat Transfer Test Programs

During the ILRV study, two wind-tunnel programs were conducted to measure heat transfer distributions on the orbiter configuration. One test program was conducted in the Cornell Aeronautical Laboratory 96-Inch Shock Tunnel by use of a 17.5-inch model instrumented with 48 heat transfer and 12 pressure sensors. Laminar flow data were obtained at a Mach number of 16 and unit Reynolds number per foot of 500,000. Turbulent flow data were obtained at Mach 8 and unit Reynolds numbers per foot of 20 and 50 million. The second test program was conducted in the NASA-Langley Mach 8 Variable Density Hypersonic Tunnel with 13-inch plastic models used. Heat transfer distributions were obtained by the temperature sensitive coating technique with Tempilaq as the surface temperature indicator. Tests were conducted at a Mach number of 8 and unit Reynolds numbers per foot ranging from 1 to 10 million.

Analysis of the data from these tests is in process. Preliminary correlations indicate that the methods used to predict entry heating rates are generally conservative and no modifications to the heat shield material selections are required. The test data and correlations have been transmitted to the responsible NASA personnel.

3.1.3 Reentry Thermal Environment

Reentry temperature-time histories are shown in Figs. 3-2 through 3-4 for various orbiter locations. The entry trajectory is based on a wing loading of 50 lb/ft^2, initial entry angle of -1.0 deg, constant angle of attack of 25 deg, and peak lower surface temperature of 2200°F. The resulting aerodynamic crossrange is 1606 nm.

Figure 3-2 shows temperature histories for the nose stagnation point and the fin and body lead edge stagnation lines. The peak stagnation point temperature is 2730°F. Peak temperatures on the fin and body leading edges are 2200°F and 2070°F, respectively. Lower centerline temperature histories at 25, 50, 75, and 100 percent chord are shown in Fig. 3-3. Peak temperatures are 2120, 2190, 1890, and 1730°F, respectively. The change in slope of the temperature histories reflects the assumption of gradual boundary layer transition, starting at a local Reynolds number of 1 million and ending at 2 million. Figure 3-4 shows temperature histories at four upper surface locations. A sketch of the vehicle cross-section is included to show the locations analyzed. Peak upper surface temperatures range from 600 to 1000°F.

Additional heating analyses have been performed for 35- and 45-deg angle-of-attack entry trajectories. These trajectories are also temperature constrained, with bank angle modulated to maintain a constant lower surface maximum temperature of 2200°F during periods of high heating. The resulting crossrange is 460 nm for α = 45 deg and 840 nm for α = 35 deg. Figure 3-5 shows the effect of crossrange on peak surface temperature at six vehicle locations, based on calculations for the three trajectories. Entering at large angle of attack (angle of attack increases with decrease in crossrange) results

in a reduction in peak temperature for the nose cap, the fin leading edge, and all upper surface locations. The body leading edge and most lower surface locations experience an increase in peak temperature as the angle of attack is increased, although the peak temperature is 2200°F for all three trajectories.

Table 3-2 shows the percentage of orbiter surface area that experiences various peak temperature levels for crossranges of 0,500, 1000 and 1500 nm. The three constant angle-of-attack entry trajectories discussed above were used to generate these data. With the exception of the nose cap, all surfaces experience temperatures between 500 and 2200°F.

Table 3-2

PERCENTAGE OF ORBITER SURFACE AREA FOR VARIOUS TEMPERATURE RANGES

Temperature Range (°F)	Cross Range (nm)			
	0	500	1000	1500
Below 200	0	0	0	0
200 to 500	0	0	0	0
500 to 800	34	33	33	32
800 to 1500	11	12	13	13
1500 to 2000	25	27	28	30
2000 to 2200	30	28	26	25
2200 to 2500	0.3	0.4	0.4	0.4
2500 to 3000	0	0.1	0.1	0.1
Over 3000	0	0	0	0

The thermal environment associated with the orbiter unbanked entry at $C_{L\ MAX}$ (α = 55 deg) has also been evaluated. This trajectory involves a reentry time of 1950 sec from 400,000 ft to touchdown, generating a 67 nm crossrange, compared to 3150 sec for the 25-deg angle-of-attack trajectory, which generates 1606 nm crossrange.

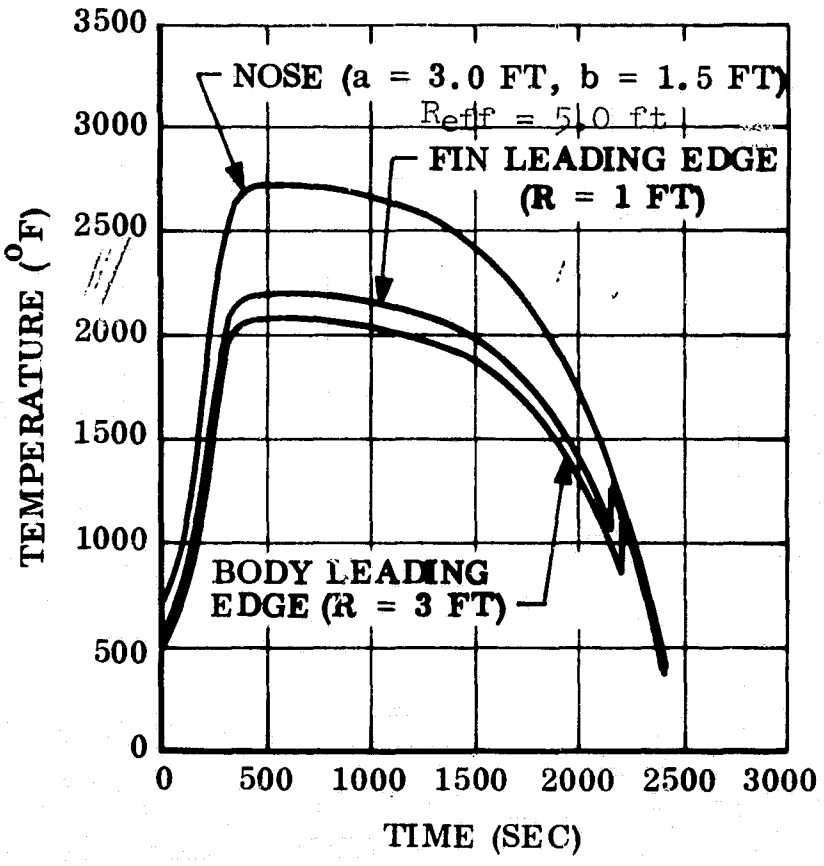

Fig. 3-2 Nose and Leading Edge Temperature Histories for Entry at α = 25 Deg

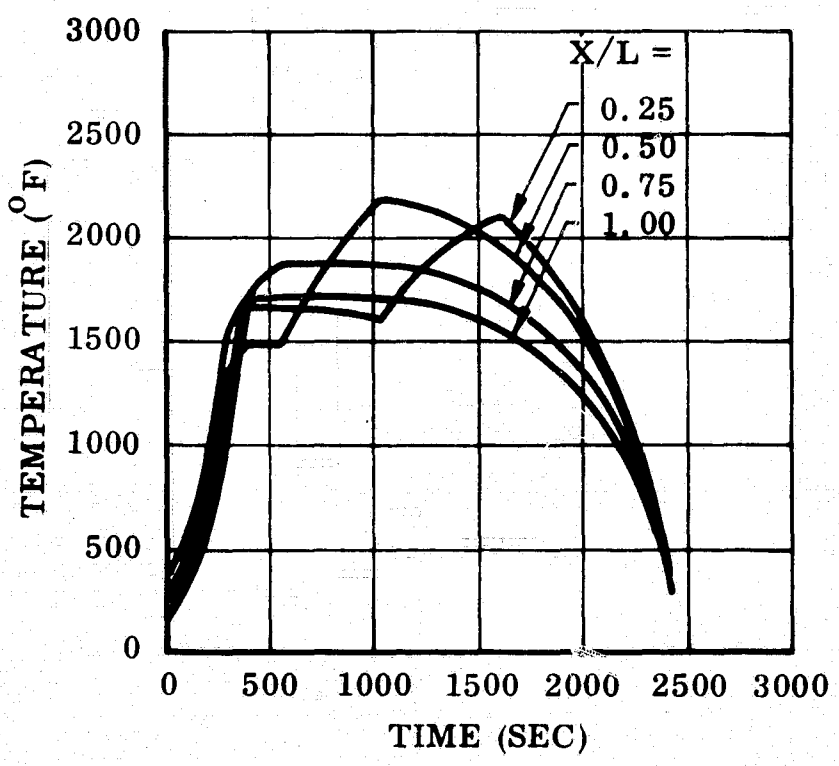

Fig. 3-3 Lower Centerline Temperature Histories for Entry at α = 25 Deg

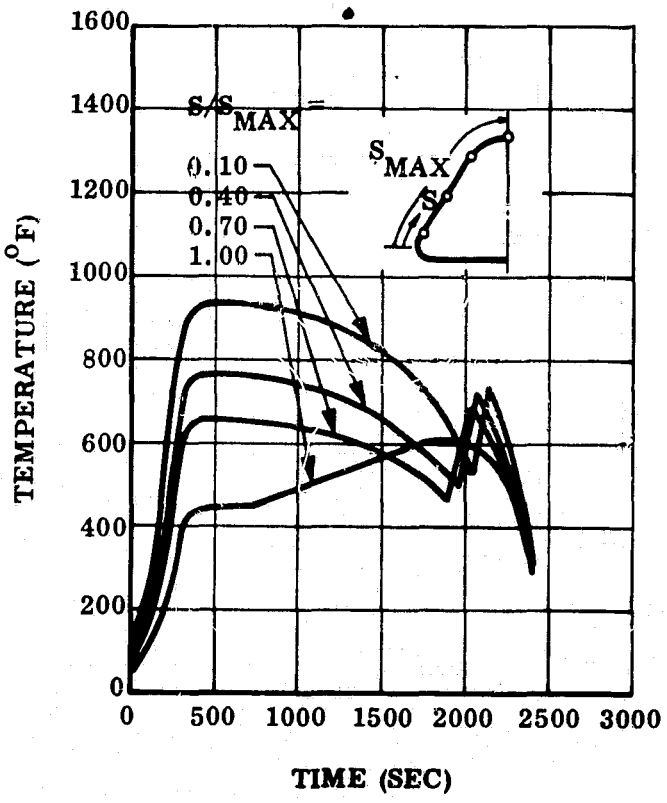

Fig. 3-4 Upper Surface Temperature Histories at 50 Percent Chord for Entry at α=25 Deg

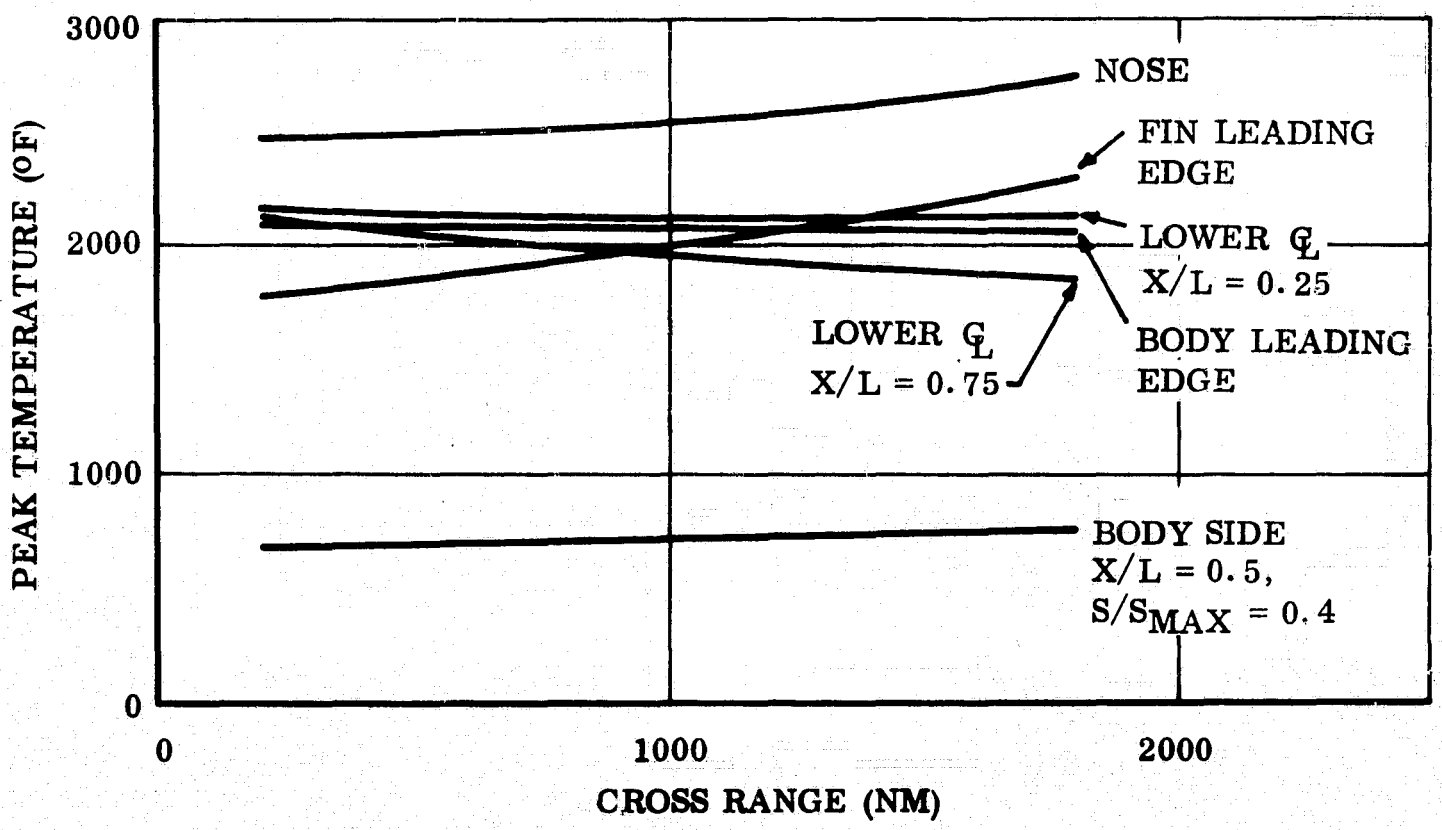

Fig. 3-5 Effect of Crossrange on Peak Surface Temperature

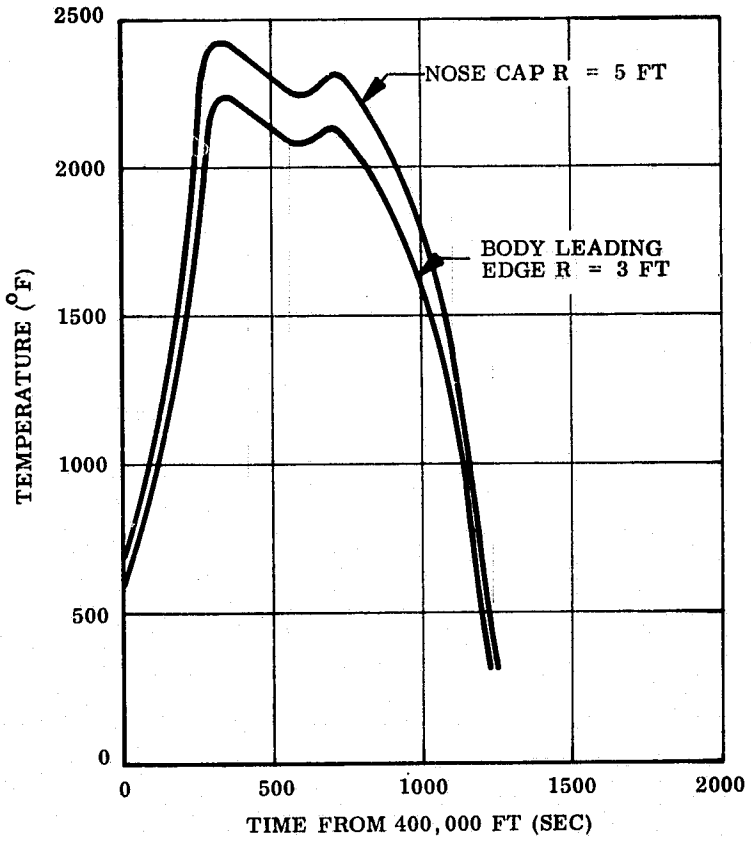

Fig. 3-6 Nose and Leading Edge Temperature Histories for Entry at α = 55 Deg

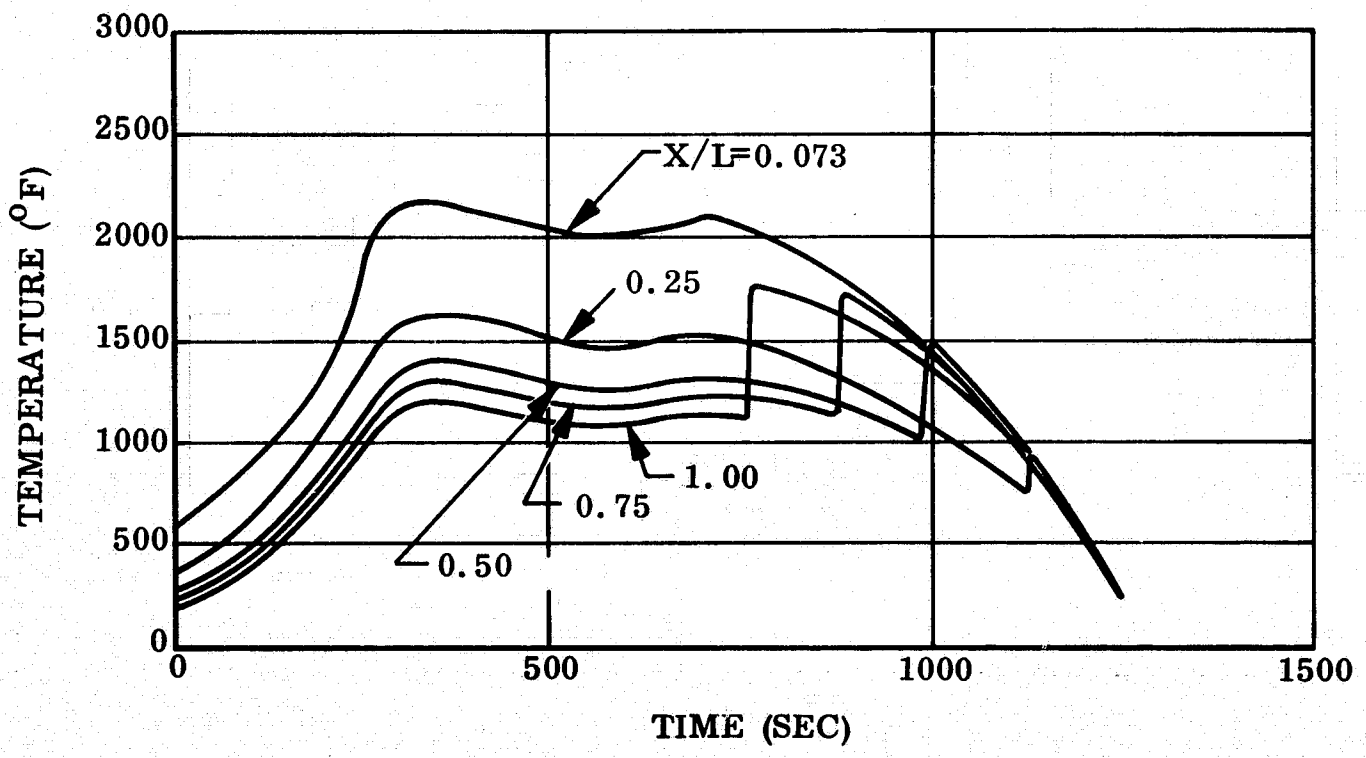

Fig. 3-7 Lower Centerline Temperature Histories for Entry at α = 55 Deg

Temperature histories for the nose cap and leading edge are shown in Fig. 3-6. Peak temperatures of 2400°F and 2225°F are experienced by the nose cap and leading edge, respectively. To constrain the maximum temperature on the lower surface to 2200°F the first 12 ft of the vehicle requires a heat shield material capable of temperatures from 2200°F to 2400°F. Fig. 3-7 shows temperature histories for five lower surface locations. The abrupt increases in temperature indicate transition from laminar to turbulent flow. For entry at $C_{L\ MAX}$, peak temperatures generally result from laminar heating.

3.2 THERMAL PROTECTION SYSTEM MATERIALS

3.2.1 Summary

The leading candidate materials for heat shield and thermal protection applications are as follows:

- Metallic plus insulation
- Rigid insulation
- Ablators

The metallic heat shields and LI-1500 lightweight rigid insulation are leading candidates for thermal protection. A Fiberglas-reinforced silicone elastomer ablator is considered as an alternate system. However, ablators undergo mass losses and are not compatible with fully reusable vehicles.

The materials and predicted temperatures used for heat shield weight estimates are summarized in Table 3-3 for various areas of the Two-Stage and Triamese vehicles. The selected materials and other candidates are discussed in the following sections.

As indicated in Table 3-3, TD-NiCr is being considered for applications to 2200°F. While TD-NiCr has a short-time capability to 2400°F, Cb-752 will be considered for ranges from 2200 to 2500°F for prolonged temperature designs.

Table 3-3

MATERIALS AND PREDICTED TEMPERATURES

Two-Stage

Surface	Orbiter			Booster		
	Forward	Center	Aft	Forward	Center	Aft
Body Upper Heat Shield	700 to 1100 Rene' 41	600 to 1000 Rene' 41	500 to 1000 Rene' 41	650 Ti	600 Ti	500 Ti
Body Lower Heat Shield	2000 to 2200 TD-NiCr	2000 to 2200 TD-NiCr	1800 to 2000 TD-NiCr	1200 Rene' 41	1000 Rene' 41	800 Rene' 41
Nose	2750 Ta-10W	–	–	1450 Rene' 41	–	–
Fin Leading Edge	–	–	2200 TD-NiCr	–	–	1650 Rene' 41
Wing/Body Leading Edge	–	2080 TD-NiCr	2080 TD-NiCr	–	1650 Rene' 41	1650 Rene' 41
Wing Upper Heat Shield	–	–	–	650 Ti	600 Ti	550 Ti
Wing Lower Heat Shield	–	–	–	1250 Rene' 41	1200 Rene' 41	1100 Rene' 41

Triamese

Surface	Orbiter			Booster		
	Forward	Center	Aft	Forward	Center	Aft
Body Upper Heat Shield	700 to 1100 Rene' 41	600 to 1000 Rene' 41	500 to 1000 Rene' 41	650 Ti	650 Ti	500 Ti
Body Lower Heat Shield	2000 to 2200 TD-NiCr	2000 to 2200 TD-NiCr	1800 to 2000 TD-NiCr	1250 Rene' 41	1200 Rene' 41	1100 Rene' 41
Nose	2750 Ta-10W	–	–	1450 Rene' 41	–	–
Fin Leading Edge	–	–	2200 TD-NiCr	–	–	1650 Rene' 41
Wing/Body Leading Edge	–	2080 TD-NiCr	2080 TD-NiCr	–	1650 Rene' 41	1650 Rene' 41
Wing Upper Heat Shield	–	–	–	650 Ti	600 Ti	550 Ti
Wing Lower Heat Shield	–	–	–	1250 Rene' 41	1200 Rene' 41	1100 Rene' 41

Note: 1. Cb-752, 2200°F to 2500°F (if required)
2. LI-1500 interchangeable with metallic heat shields
3. Ablator – backup heat shield

3.2.2 Metallic Materials

Selection of a material or material system is determined by the strength, mechanical and metallurgical stability,and oxidation resistance. For this survey, candidate materials were classified into four basic groups with respect to their maximum long-time service temperature, as follows:

- Service up to 1000°F
- From 1000° to 2000°F
- From 2000° to 2500°F
- Above 2500°F

Table 3-4 is a compilation of selected candidate alloys, based on an analysis of availablility, mechanical and physical properties, and their maximum structural utilization temperature. Illustrated in Table 3-5 are merit indices devised to relate materials to various design characteristics and to provide an efficient index for materials comparison. Data included in preparation of these indexes include factors listed below:

- Structural stability during cyclic exposure ($\rho E_c^{1/2}$)
- Fabricability
- Physical properties (α, K, C_p, and emissivity)
- Mechanical properties (F_{tu}/ρ , F_{cy}/ρ , and creep)
- t_m - material practical minimum gage thickness
- Oxidation characteristics
- Metallurgical stability during cyclic environment

Table 3-4

CANDIDATE HEAT SHIELD METALS

Base Metal	Melting Point (°F)	Alloy Designation	Max. Structural Utilization Temperature (°F)
Light Metals			
Aluminum	1200	2219-T81 6061-T6 7075-T6	300 250
Titanium	3100	8Al-1 Mo-1V 6Al-4V 5Al-2, 5Sn	600
Superalloys			
Nickel base	2650	Inconel 718 Inco 625 Rene' 41	1400 1400 1600
Dispersion strengthened	2650	TD-NiCr TD-Ni	2200
Cobalt base	2700	Haynes 25 (L-605)	1800
Refractory Alloy			
Tantalum	5425	90Ta-10W	3100
Molybdenum	4750	TZM	3100
Columbium	4380	Cb752	2700
Tungsten	6100	W-2% ThO_2	3200

Table 3-5

MERIT INDEXES FOR CANDIDATE MATERIALS

Temp. Range	Vehicle Structural Application	Candidate Material (1)	Physical Properties (3) P S G E	Tensile Properties (3) P S G E	Creep Resistance (2)(3) P S G E	Formability (3) P S G E	Weldability (3) P S G E	Oxidation Resistance (3) P S G E	Leading Candidate Materials	Remarks
-421° – 1000°F	Wing, tanks, body structure	2219-T81	———	———	———	———	———	———	*2219-T81	Good fabricability and strength
		6061-T6	———	———	———	———	———	———		Good weldability, moderate strength
		7075-T6	———	———	———	———	—	———	*7075-T6	High strength, welding not practical
		Be 38A1	———	———	———	—	NA	—		Not weldable
		AMS 7902	———	———	———	—	NA	—		
		8A1-1Mo-1V	———	———	———	———	———	———	8A1-1Mo-1V	Good strength and fabricability
		6A1-4V	———	———	———	———	———	———		Good strength and fabricability
		5A1-2.5Sn	———	———	———	———	———	———		Low strength, good fabricability
1000° – 2000°F	Upper surface primary and secondary structure heat shield	Cobalt base Alloy: Haynes 25	—	———	———	———	—	———	*Haynes 25	Annealed material with moderate tensile properties, good oxidation resistance to 1600°F
		Nickel base Alloy: Inco 625 (1400°F)	—	———	———	———	—	———	*Inco 625	Matrix strengthened alloy with moderate tensile properties, metallurgically unstable above 1400°F
		Inco 718 (1400°F)	—	———	———	———	———	———		Age hardenable alloy with high tensile properties, moderate creep resistance
		Hastelloy X	—	—	———	———	———	———		Superior oxidation resistance to 2000°F
		Rene 41 (ann.) (1600°F)	—	———	———	—	—	———	*Rene 41	Avg weldability, subject to embrittlement and alloy depletion above 1600°F
		TD Nickel	—	—	—	—	—	—		Not competitive with mechanical properties of other superalloys
		TD NiC✓	—	———	—	—	—	———	*TD NiC✓	Candidate uncoated material for application to 2200°F

Notes: (1) Maximum structural temperature limit

(2) Based on 0.5 percent creep at specified temperature

(3) Rating legend is as follows:

E – Excellent
G – Good
S – Satisfactory
P – Poor

NA – not applicable

Table 3-5 (Cont)

Temp. Range	Vehicle Structural Application	Candidate Material (1)	Physical Properties (3) P S G E	Tensile Properties (3) P S G E	Creep Resistance (2)(3) P S G E	Formability (3) P S G E	Weldability (3) P S G E	Oxidation Resistance (3) P S G E	Leading Candidate Materials	Remarks
2000° – 2500°F	Lower surface leading edge, and heat shield	Chrome 30					Not Practical			Extremely brittle material at room temperature
		TD Nickel								Not to be used as primary structural application, not competitive with Cb alloys
		TD NiCr (2200°F)							*TD NiCr	Candidate uncoated material for application to 2200°F
		Columbium (4) Alloy								
		D-43								Poor weldability
		B-66								Superior density-compensated strength values; poor formability and weldability properties
		FS-85								High density
		C-129Y								Except for lower creep resistance, similar to Cb 752
		Cb-752							*Cb-752	Moderately high mechanical properties
2500° – 3500°F		Tantalum (4) Alloy								
		90Ta-10W							*90Ta-10W	Moderate mechanical properties, very good with respect to fabricability
		T-222								High mechanical properties, mill rolling problems
		Molybdenum TZM					NA			
3500° – 4900°F	Nose cap	Tungsten-Thoria			NA		NA		*Tungsten-Thoria	Tested in reentry profile
		Tungsten					(4)			Limited by oxidation protective system
		Zirconia Rod								Tested in reentry profile

Notes: (1) Maximum structural temperature limit

(2) Based on 0.5 percent creep at specified temperature

(3) Rating legend is as follows:
E – Excellent
G – Good
S – Satisfactory
P – Poor

(4) With oxidation protective coating
NA – Not applicable

3.2.2.1 Titanium Alloy. Fig. 3-8 through 3-11 show candidate titanium alloy capability vs temperature compared with aluminum. Titanium alloy 8Al-1Mo-1V was selected for applications up to 600°F because of its excellent response to fabricability, high strength, and extensive history of use in manufacturing.

3.2.2.2 Superalloys. The term superalloy usually defines the nickel, cobalt, and iron base alloys that are intended for structural use in the temperature range of 1000 to 2000°F. They have more oxidation resistance than stainless steels and display considerably more strength above 1000°F. Generally, the cobalt-base alloys are more chemically and metallurgically stable at higher temperatures than the nickel-base alloys. Most superalloys display good weldability with the exception of the thoria dispersed strengthened alloys. Therefore, the metallurgical and chemical stability must be considered in determining the relative merits of the candidate alloys for this program. Figures 3-12 through 3-14 show temperature-property data.

The superalloys are oxidation resistant but will oxidize at high temperatures. The oxidation behavior of a metal or alloy depends not only on the composition of the reactants and environment, but also on the internal and surface structure, the state of stress, and geometry of the part. The process of oxidation is also sensitive to velocity, density and composition, and flow pattern of the oxidizing environment. Alloys designed for strength may not have maximum oxidation resistance. When maximum strength is desired, protective coatings should be considered. Usually a light surface oxide is desirable for high emittance; however, intergranular oxidation in small amounts can be a serious problem on thin sections. It not only reduces the cross-section, but can act as a notch in notch sensitive materials. Of the superalloys, the precipitation hardenable nickel base alloys, such as Rene' 41, are the most susceptible to intergranular oxide penetration. As previously mentioned, stress also affects the rate of oxidation. It appears that oxidation proceeds at a constant rate with increasing stress until a threshold level is reached, where oxidation then proceeds more rapidly. Static oxidation behavior at one atmosphere is used for initial

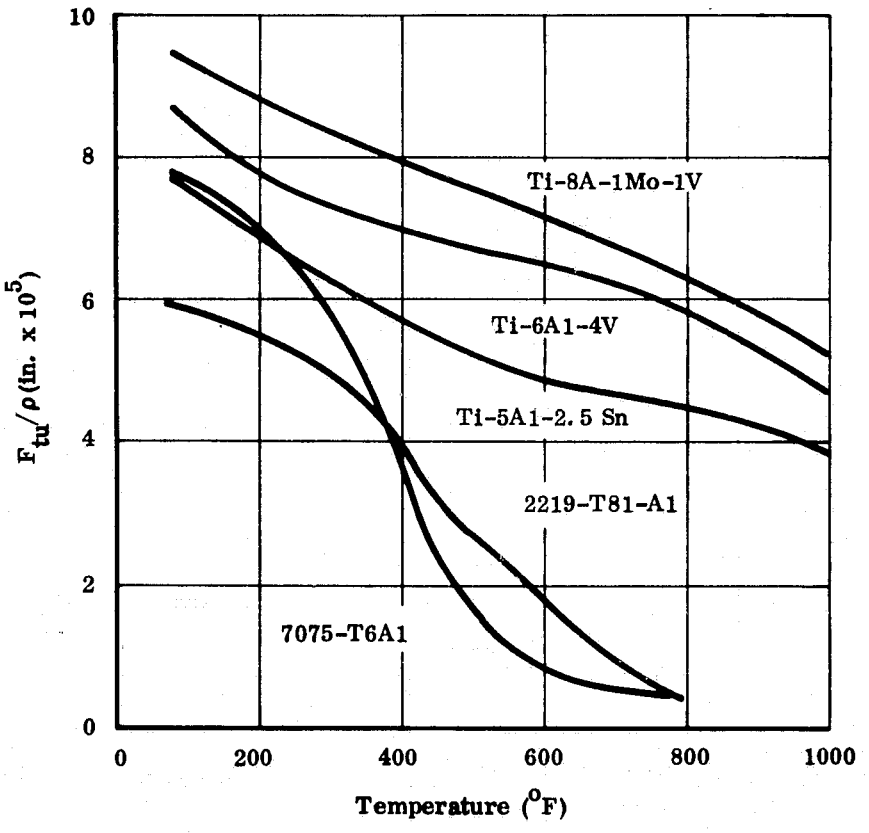

Fig. 3-8 Density Compensated Ultimate Stress vs Temperature - Aluminum and Titanium Alloys

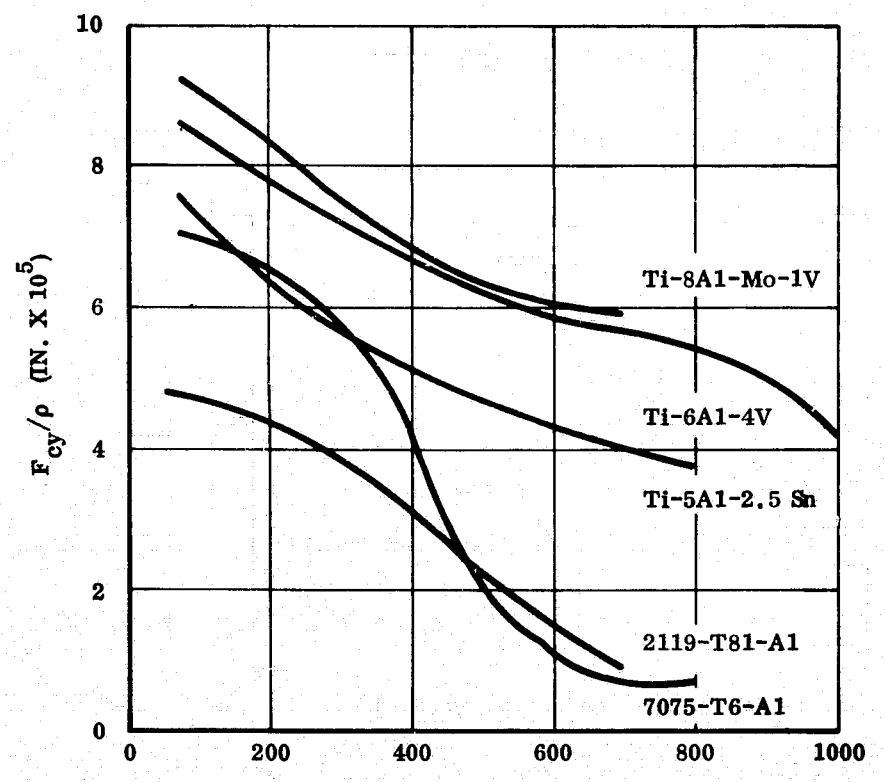

Fig. 3-9 Density Compensated Compressive Yield Stress vs Temperature - Aluminum and Titanium Alloys

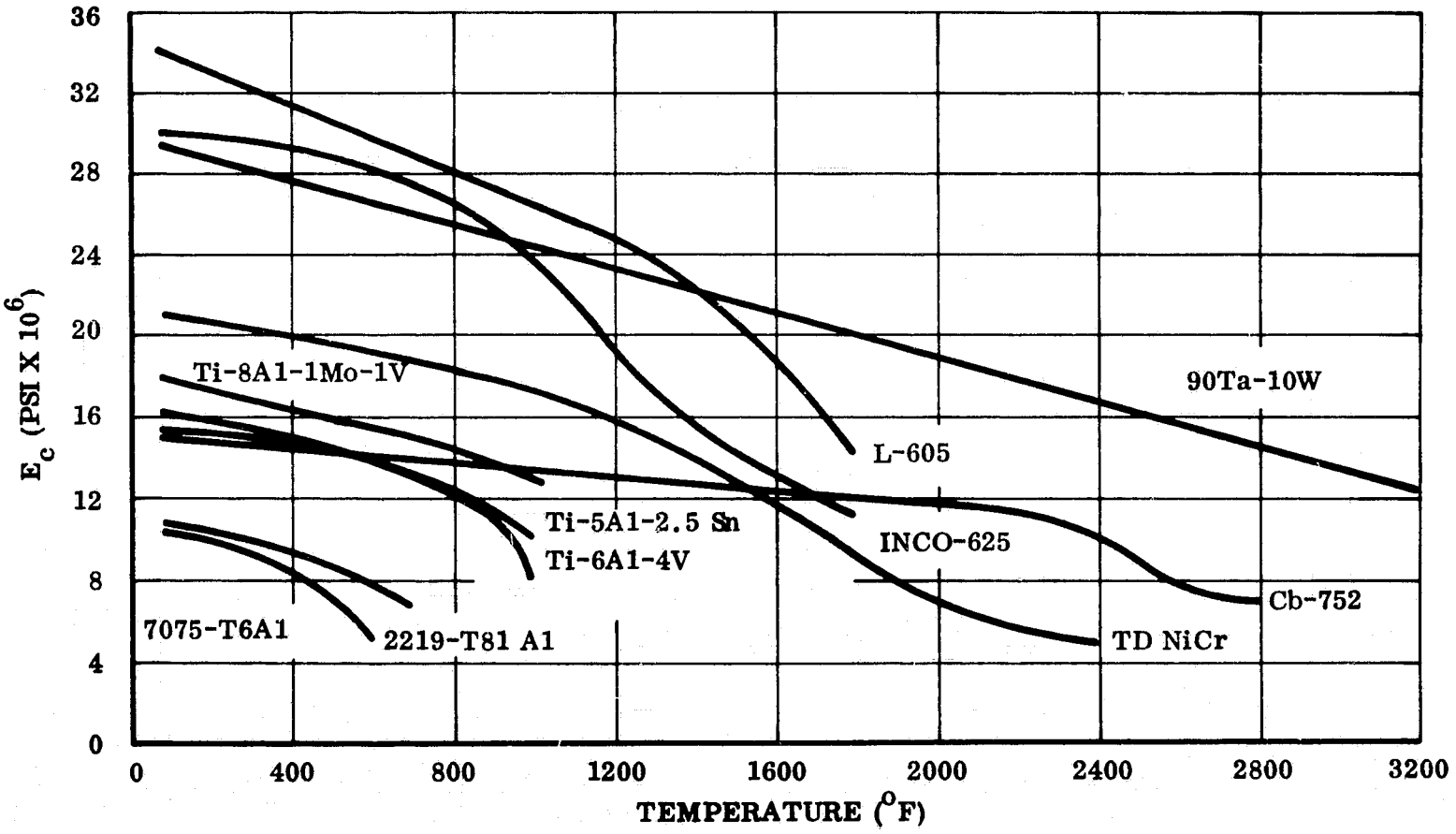

Fig. 3-10 Compressive Modulus of Elasticity vs Temperature of Candidate Materials

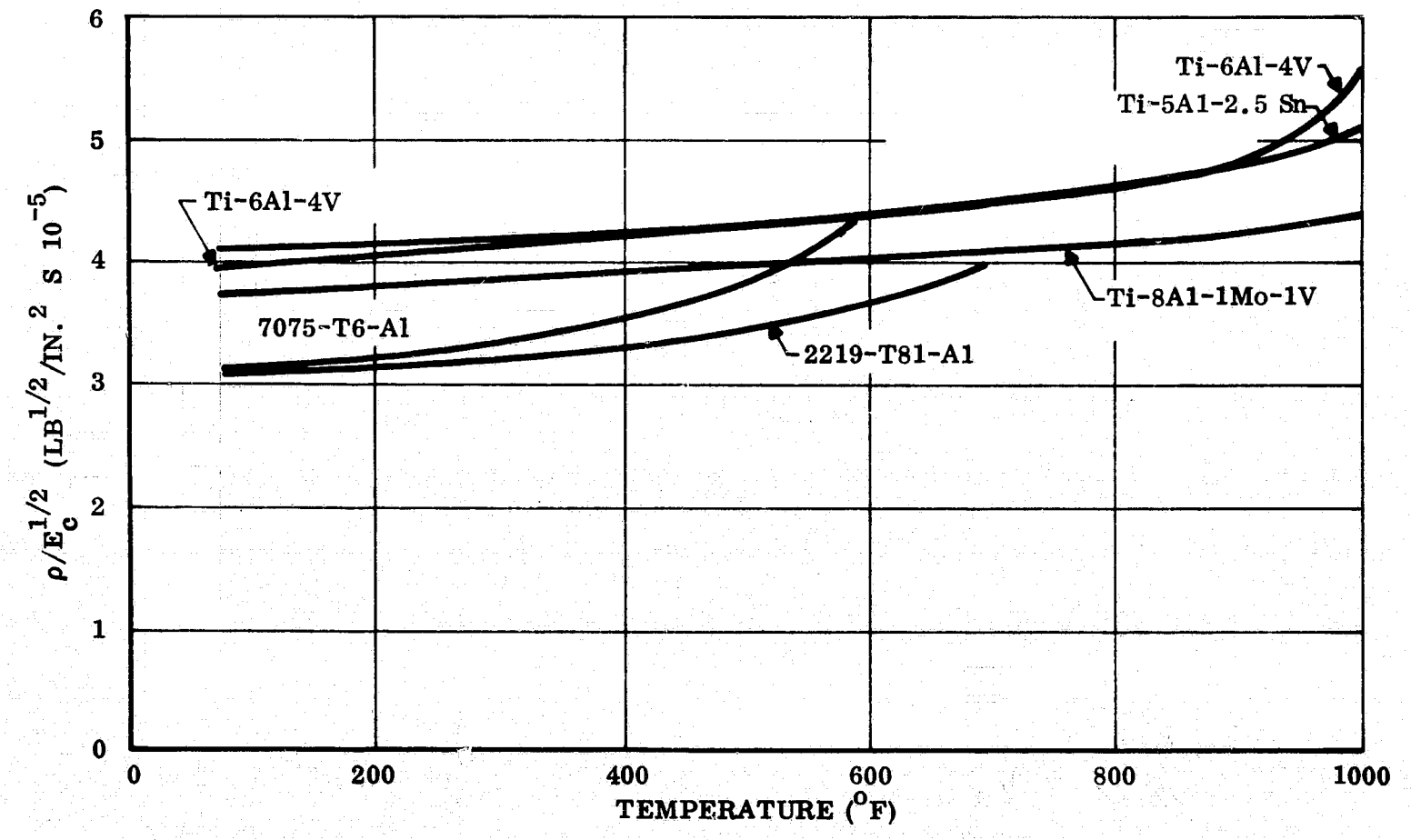

Fig. 3-11 Structural Stability Comparison of Aluminum and Titanium Alloys

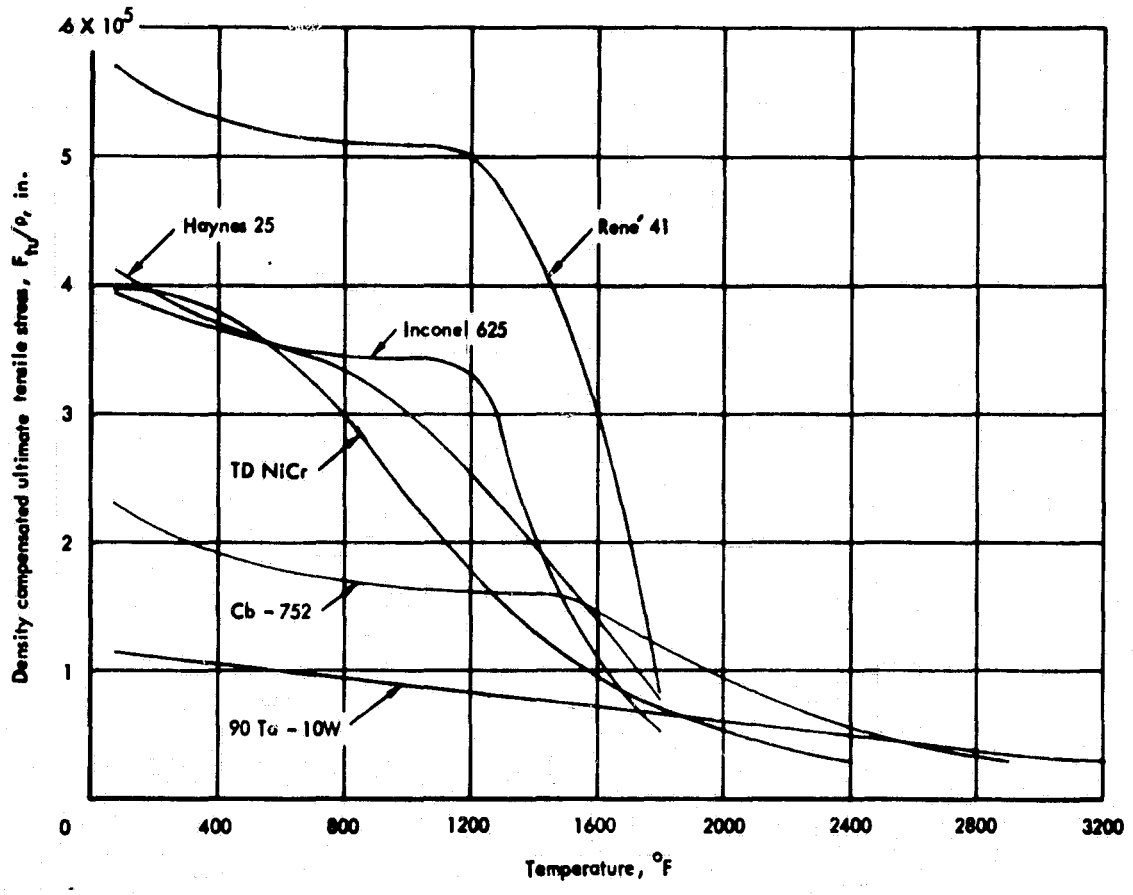

Fig. 3-12 **Density Compensated Ultimate Tensile Stress vs Temperature of Candidate High Temperature Materials**

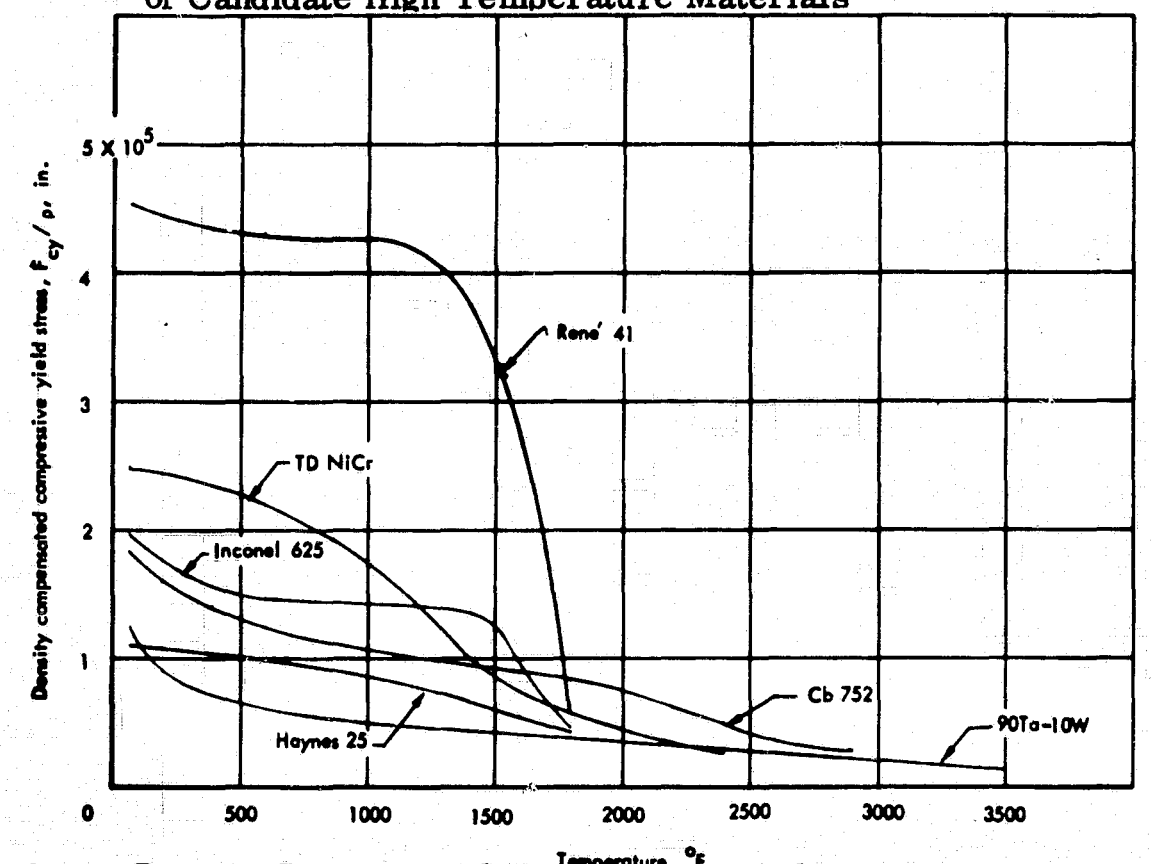

Fig. 3-13 **Density Compensated Compressive Yield Stress vs Temperature of Candidate High Temperature Materials**

alloy comparison as illustrated in Fig. 3-15. Depth of penetration per side for the candidate superalloys is based on assumed (1) uniform oxide attack, (2) depth of penetration (extrapolated from current data) is uniform and linear with respect to time and temperature to the extrapolated points, and (3) no stress. These published data have been substantiated by static thermal stability tests conducted in the NASA Hypersonic Wing Study*.

Inconel 625. Inconel 625 nickel-base alloy was evaluated for temperatures up to 1400°F (heat shield 1800°F) because of its excellent combination of desirable properties and oxidation resistance. Haynes alloy, H.S. 25 (L605), is considered a backup rather than primary material choice because of higher weight as compared to Inco-625. However, Alloy L605 is superior in thermal and metallurgical stability and can be used to upgrade the system to a maximum service temperature of 1600°F (1800°F for heat shields).

TD-NiCr. The thoria-dispersed strengthened alloy, TD-NiCr, was selected for application to heat shields and leading edge designs up to 2200°F. TD-NiCr is a nickel-chromium base alloy strengthened by an ultrafine and a highly uniform dispersion of thoria (ThO_2) that has outstanding oxidation resistance, structural stability, and moderate strength up to 2400°F. This alloy was primarily developed for long-time service in severe applications at temperature ranges bridging that served by superalloys and coated refractory metals. These outstanding properties, supported by screening tests performed in the NASA Hypersonic Wing Program, make it a distinct choice for heat shields and leading edge structure. Table 3-6 summarizes the advantages and disadvantages of TD-NiCr.

---

*Hypersonic Cruise Vehicle Wing Structure Evaluation, Contract No. NAS1-7573, Lockheed Missiles & Space Company, Sunnyvale, California

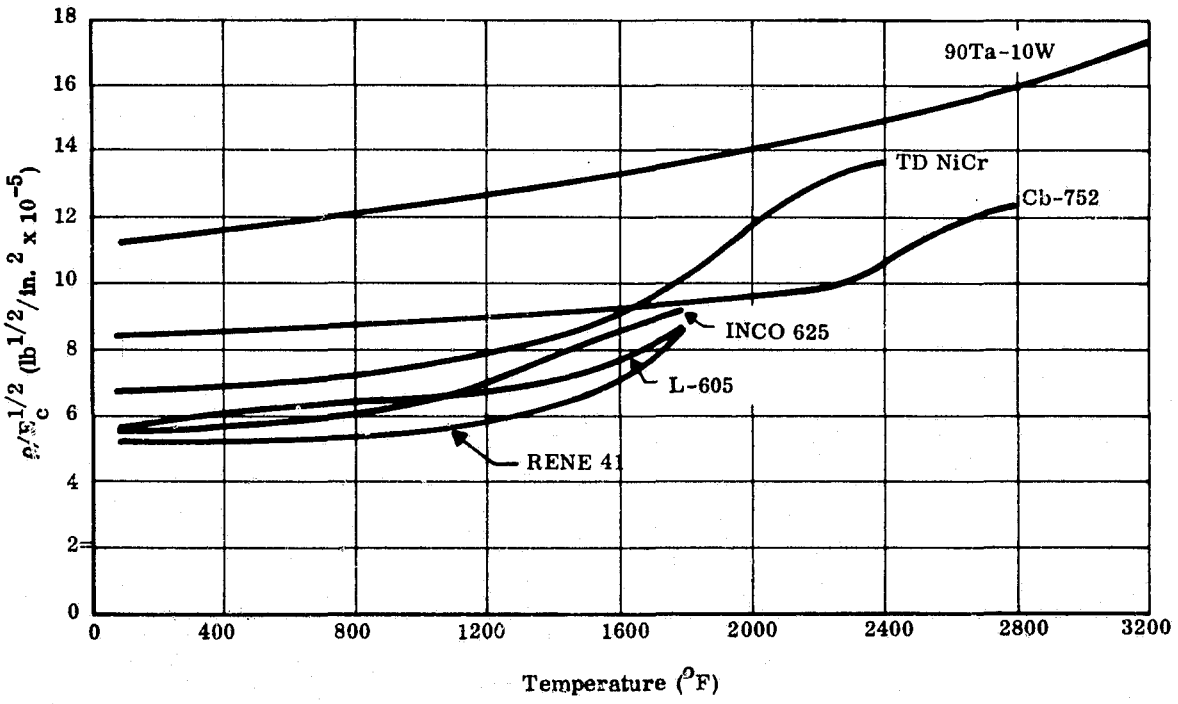

Fig. 3-14 Structural Stability Comparison of Candidate High Temperature Materials

REF: DMIC REPORT 153 PHYSICAL METALLURGY OF NICKEL BASE SUPERALLOYS
DMIC REPORT 214 OXIDATION OF NICKEL- AND COLBALT-BASE SUPERALLOYS

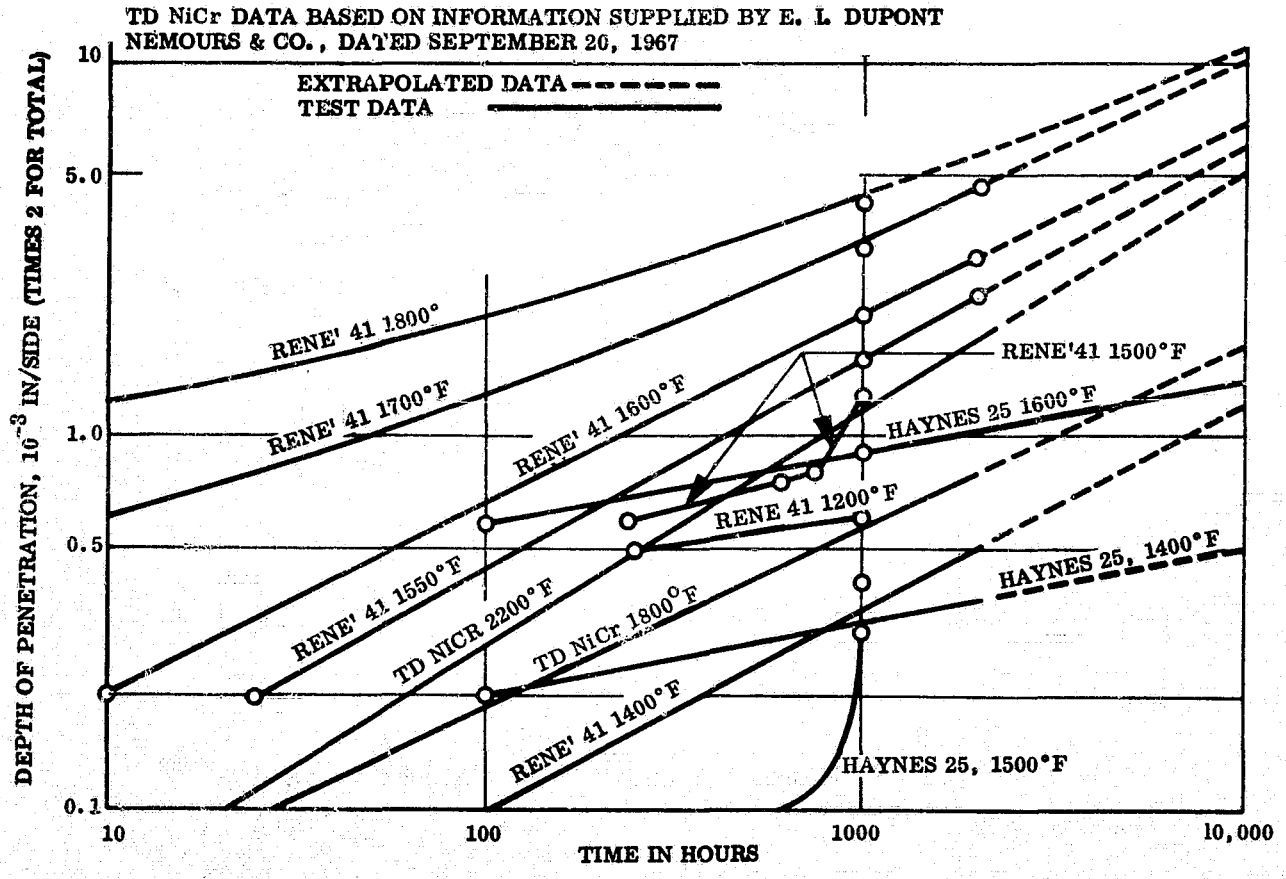

Fig. 3-15 Depth of Oxidation vs Temperature for Rene' 41, TD NiCr and HS 25

Table 3-6

TD-NiCr MATERIAL

Advantages	Disadvantages
No oxidation-protective coating	Limited availability
Good RT ductility	Limited to 2200°F (short time to 2400°F)
Good high-temperature strength	Limited elevated temperature ductility
Satisfactory creep resistance	Material property data shortage
No RT property degradation after exposure	Flatness problems (honeycomb face sheet applications)
Satisfactory fastening	Low welding allowables
Mechanical	
Brazing	

3.2.2.3 Refractory Metals. The increasing demand for structural materials capable of operating at temperatures higher than the superalloys requires consideration of refractory base materials.

Columbium. Columbium possesses several outstanding properties that make it attractive for high-temperature structural applications. The metal and most of its alloys possess excellent fabricability,and its density is less than most of the refractory materials. However, the use of columbium at temperatures greater than 1000°F requires the use of an oxidation protective system, since the oxide of columbium is nonprotective.

Oxidation of Columbium. Unprotected columbium reacts with oxygen to form a nonadherent oxide at a rate dependent on alloy composition, temperature, and environment. At temperatures greater than 2700°F, the rate is apparently great enough to produce an exothermic reaction, that is, self-sustaining. This pressure and temperature dependent phenomenon is called "autoignition." At lower temperatures, the diffusion of oxygen causes embrittlement of the substrate.

Columbium retains useful strength to temperatures approaching 3000°F. Consideration of the apparent autoignition restricts its maximum useful temperature to 2700°F. Reuse of coated columbium should be considered to be 2500°F maximum.

Coating Systems for Columbium. Two fused slurry coating systems R512A (Si-20Cr) and R512E (Si-20Cr-20Fe) developed by Sylvania High Temperature Composites Laboratory promise to be the best coatings developed to date for columbium. The coatings, basically brazing alloys, are extremely chemically aggressive in the molten phase and have a great affinity to wet areas of limited access, such as fayed surface. Figure 3-16 illustrates the predicted coating life of the Cb-752/R512E system under cyclic exposures. These data represent a composite of tests performed at Lockheed and those reported by the supplier.

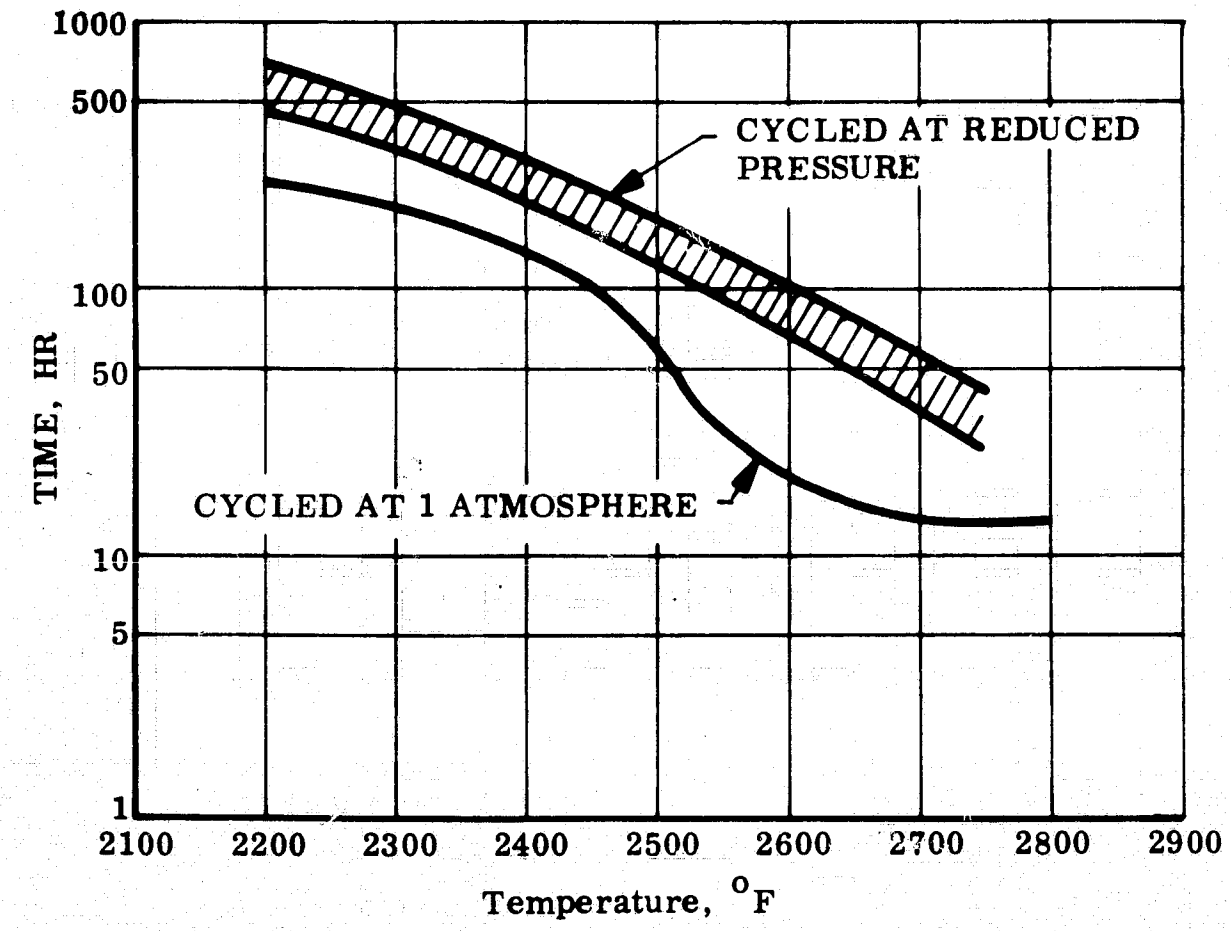

Fig. 3-16 **R-512 Coating Life – Cb 752**

Tantalum. Tantalum offers the greatest temperature range of structural usefulness of any metal, with its high melting point, retention of ductility at low temperatures, and excellent fabricability. Its greatest potential as a structural material lies in the temperature range greater than that served by columbium.

Oxidation of Tantalum. Like columbium, unprotected tantalum oxidizes at a high rate when exposed to temperatures over 1000°F. At some high, and as yet undefined temperature (T > 3000°F), autoignition can occur. For this reason, a protective coating system must be employed when service temperatures exceed 1000°F in oxidizing environments.

Protective Coating Systems for Tantalum. At the present time, only two coating systems appear to be practical to protect tantalum at 3000°F. One is Sylcor R512C coating (Si-20Ti-10Mo), and the other is the more conventional R505 (Sn-25Al) coating. Previous experience with a third coating system, the modified boundary layer disilicide over a tantalum substrate, has indicated that more development work is required before it is practical to coat complex shaped hardware.

Tungsten. Tungsten is a candidate material for ultrahigh temperature application. If used in a materials system employing a silicide protective coating, maximum service temperatures under oxidizing environments are limited to 3200°F because of coating limitations. The possible use of this material as an uncoated nose cap is practical because of the mode of oxidation at ultrahigh temperatures; however, the optimum potential of this candidate system has not been fully investigated nor considered in this survey.

3.2.3 Metallic Materials Selection

The candidate alloys are being reviewed for heat shield application by parametric analysis, prior test evaluations, and current Lockheed/NASA testing.

3.2.3.1 Selection of 1600°F Superalloys. For evaluation of 1600°F structures, Rene' 41 was selected because of its excellent high-temperature strength, acceptable fabricability, and acceptable resistance to oxidation. However, additional material weight may have to be considered because of oxidation for the operational temperatures and flight times for this program. There are two recommended heat treatments for Rene' 41 alloy sheet. One yields maximum creep properties (2150°F solution anneal followed by a 1650°F age cycle), and another determines the maximum elevated temperature tensile properties (1950°F solution anneal plus a 1400°F age cycles).

Haynes 25 cobalt base alloy has been selected as a backup material because of its excellent combination of ductility, oxidation resistance, and other desirable properties.

The thoria-dispersed strengthened alloy, TD-NiCr, was selected for application to heat shields and leading-edge designs from 1600 to 2200°F. TD-NiCr has outstanding oxidation resistance, structural stability, and moderate strength up to 2400°F.

3.2.3.2 Selection of Refractory Alloy Materials Systems. For prolonged service from 200 to 2500°F, the Cb-752/R512E materials system is the leading candidate because of its superior overall properties, previous manufacturing experience, and available design data. Coating life for this material was shown in Fig. 3-16. For service from 2500°F to 3000°F, the 90 Tz-10W/R512C material system was selected because of high reliability and previous manufacturing experience with it. As a backup porous-metal concept, a 90Ta-10W/R505 system was evaluated.

3.2.3.3 Material Cost. Cost-effectiveness studies have not been finalized for the various materials. Some recent Lockheed experience in actual purchases of superalloy and refractory metals is shown in Fig. 3-17 as a function of material thickness.

The lower materials cost of TD-NiCr, compared to the cost of Cb-752, is significant, particularly since an oxidation-protection coating is not required

for the TD-NiCr. For usage of temperatures below 1800°F, the competitive price of the more efficient Rene' 41, compared to that of the H.S. 25, is of interest.

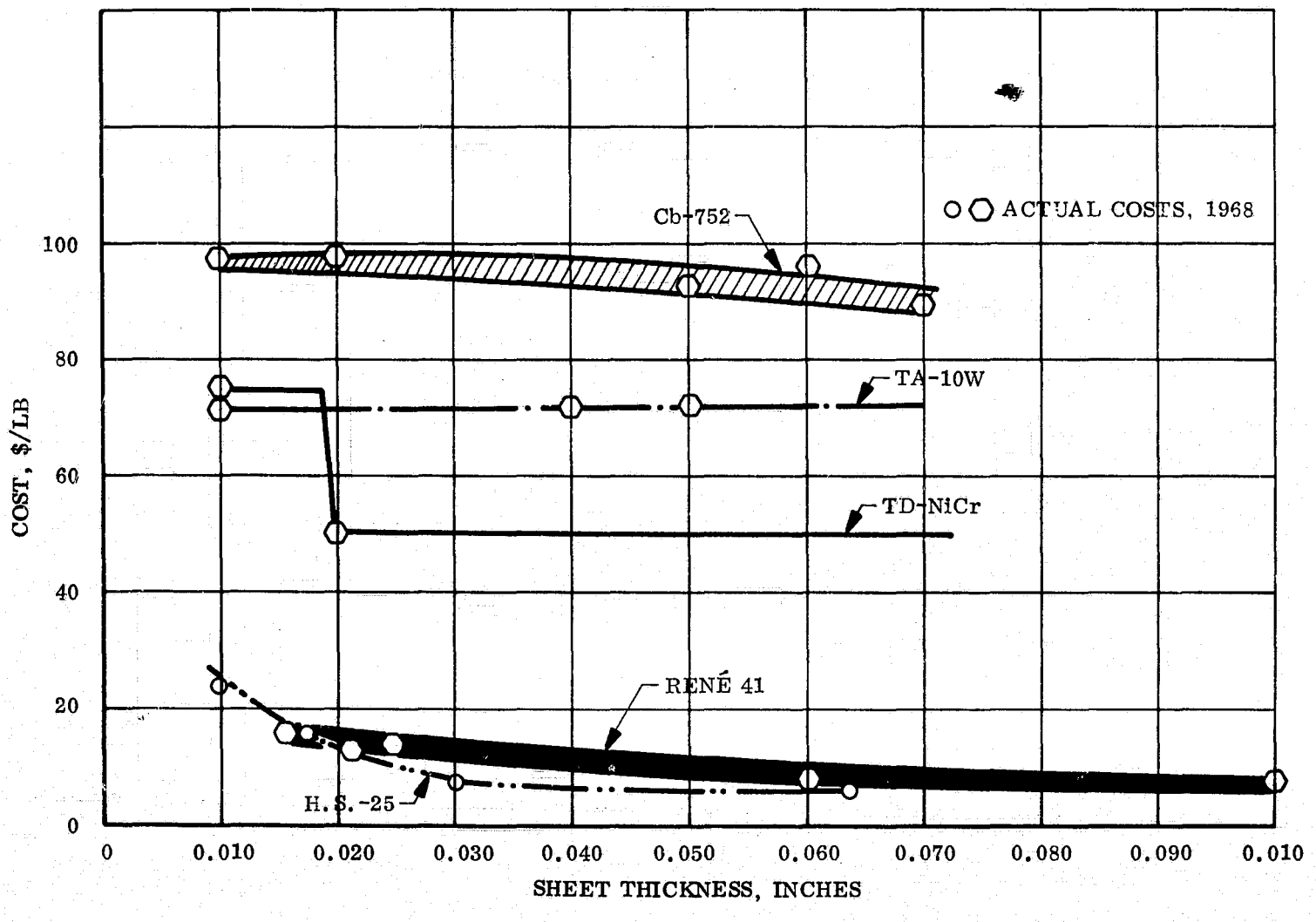

Fig. 3-17 Material Costs vs Thickness

3.2.4 Material Minimum Gage Requirements

Minimum gage for fabrication of acceptable structural elements, sheet thickness availability, and sheet thickness variation will be considered in the structural concept optimization. Table 3-7 presents minimum metallic thicknesses for specific concepts.

Table 3-7

MINIMUM GAGE CRITERIA

Material Alloy Designation	Structural Configuration: Single Corrugation	Corrugation-Stiffened: Skin	Corrugation-Stiffened: Corrugation	Integrally Stiffened	Honeycomb Sandwich: Skin	Honeycomb Sandwich: Core	Frame Bulkhead Application
Aluminum 2219T81	0.016	0.016	0.012	0.016(a)	0.012	0.0007(b)	0.020
Beryllium AMS7902	0.016			0.016			0.020
Titanium Ti 8A1-1Mo-1V	0.016	0.016	0.012	0.016	0.010	0.002(c)	0.020
Inconel 718	0.016(d)	0.016(d)	0.012(d)	(e)	0.012(d)	0.002	0.020
René 41	0.010	0.010	0.010	0.020	0.010	0.002	0.020
Inconel 625	0.010	0.010	0.010	(e)	0.008	0.002	0.012
TD-NiCr	0.010	0.010	0.010	(e)	0.010		0.012
Haynes 25, L605	0.010	0.010	0.010	(e)	0.008	0.002	0.012
Columbium Cb 752-R512E		0.012	0.012(f)	0.012			0.016
Tantalum 90Ta-10W(g)				0.012			0.016

(a) Minimum selected on basis of manufacturing considerations
(b) Core material: 5052 aluminum alloy
(c) Core material: polyimide (1.2 lb/ft^2)
(d) Gases selected because of distortion due to heat treatment of thinner gages
(e) Not considered because of serious manufacturing problems (warpage, distortion, extremely difficult chemically to mill)
(f) Poor structural resistance welds: projected application of solid-state, roll diffusion, bonded technique method
(g) For strength requirements: T-222 Tantalum alloy

3.2.5 Insulation Materials for Metallic Heat Shields

Insulation is required as a part of the thermal protection system with metallic heat shields. Several insulation materials were considered; however, there were three leading candidates. These are low-density, fibrous, silica materials, such as microquartz, dynaquartz and dynaflex. Characteristics of leading candidate insulation materials are as follows:

Insulation	Density (lb/ft^3)	Maximum Utilization Temperature (°F)
Microquartz	3.5 (3.0 nominal)	1600
Dynaquartz	4.5	2750
Dynaflex	6.0	2800

Selection criteria for insulation materials include temperature limit, thermal conductivity, weight, shrinkage, reliability, fabricability, and availability. A limitation of dynaquartz is brittleness leading to a tendency to break up under vibration loads.

3.2.6 Thermodynamic Properties

Figures 3-18 through 3-20 present some pertinent thermodynamic characteristics of the candidate materials.

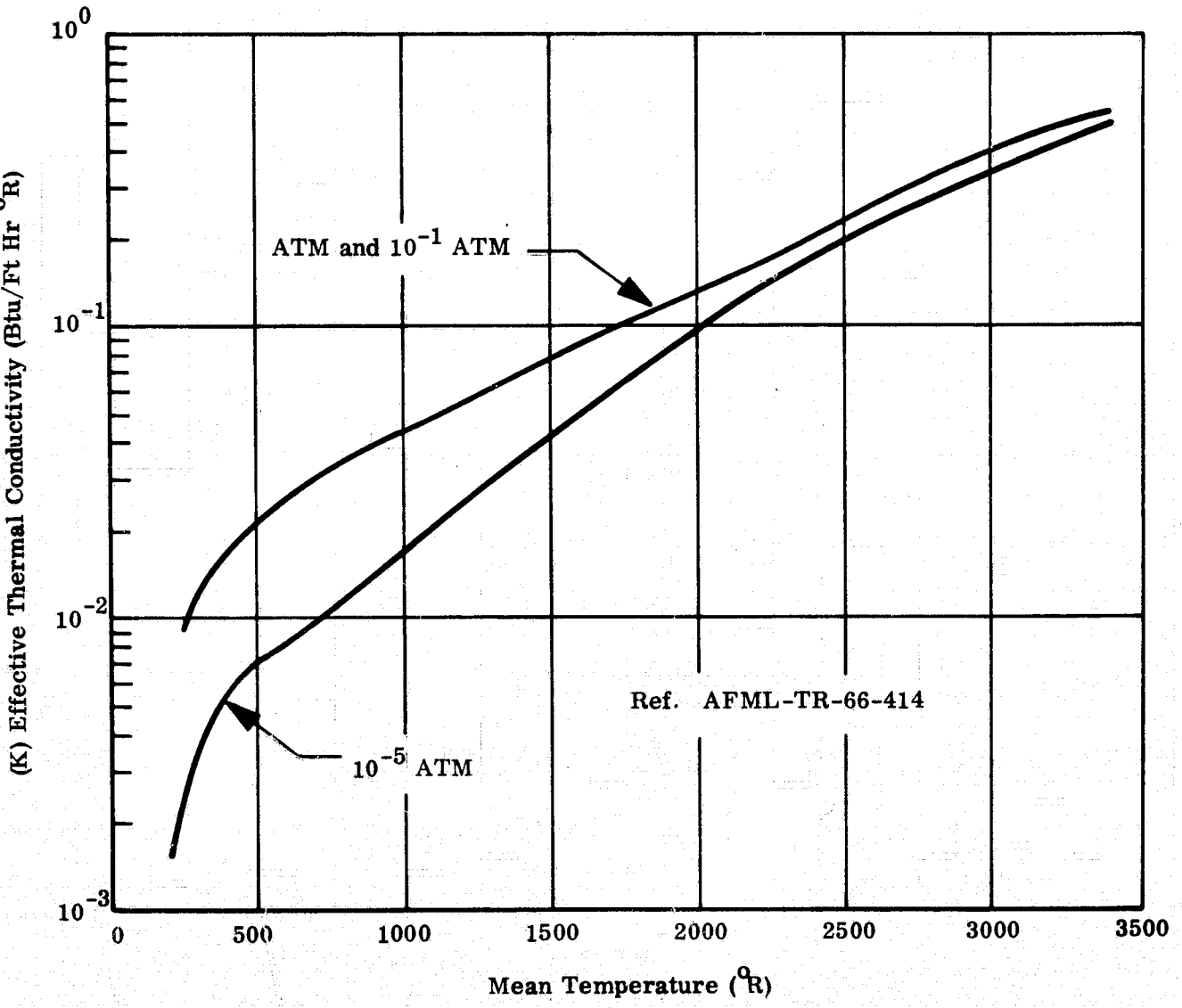

Fig. 3-18 Effective Thermal Conductivity vs Temperature - Dynaflex in Air at Various Pressures

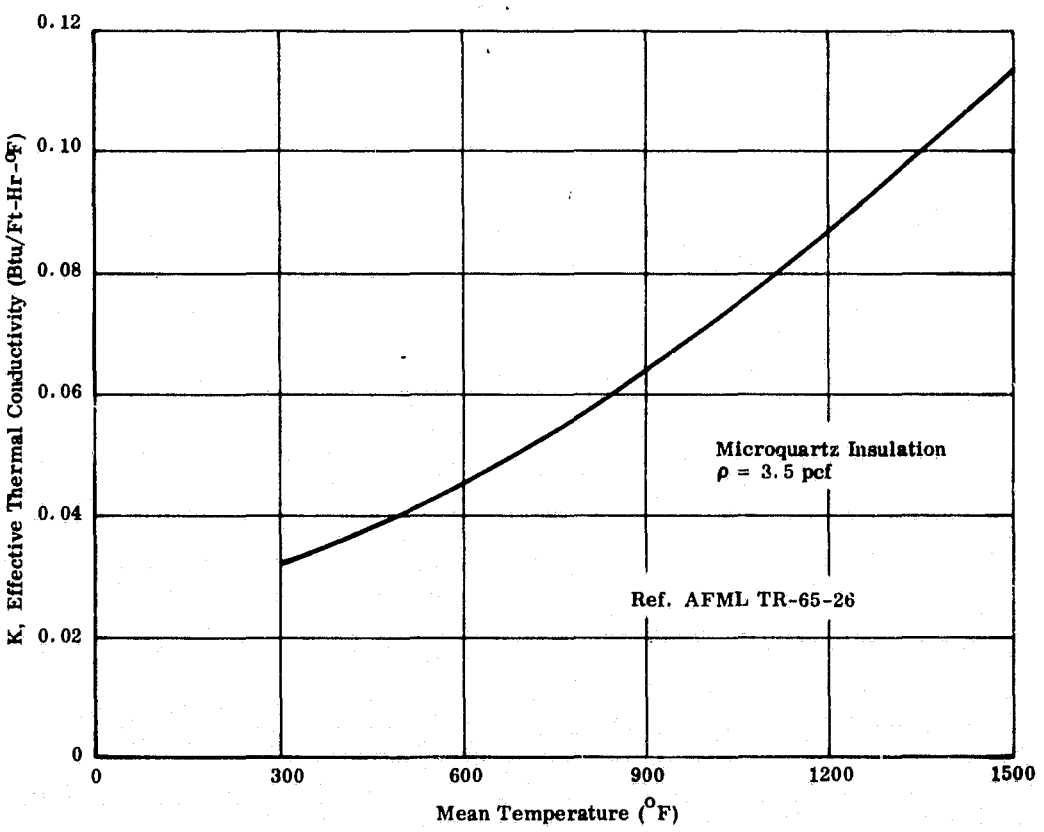

Fig. 3-19 Effective Thermal Conductivity vs Temperature of Microquartz

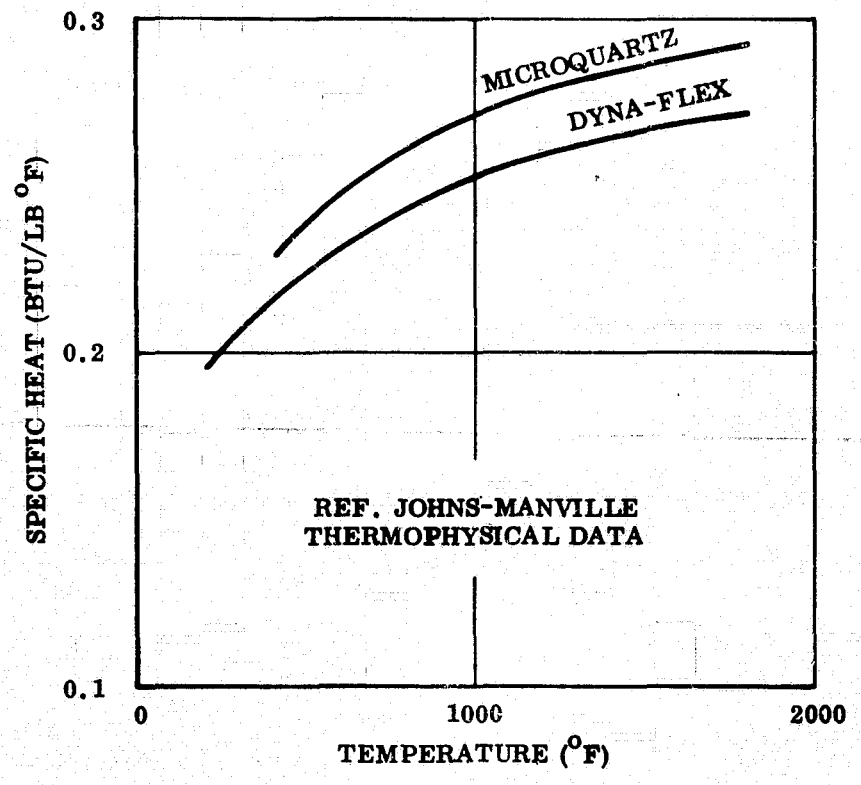

Fig. 3-20 Specific Heat of Microquartz and Dynaflex

3.2.7 LI-1500 Lightweight Insulation Development

During the past several years, the Lockheed Materials Sciences Laboratory has been working on material systems applicable to reentry vehicles. One of the major developmental efforts has been focused on LI-1500 - an advanced, reusable, rigidized, lightweight insulation heat shield for application to a lifting reentry vehicle. This is a light-weight insulation with a density range of 12 to 15 lb/ft^3. It is an all-silica system consisting of randomly oriented quartz fibers inorganically bonded and sintered at high temperatures. The system has a surface temperature capability in excess of $2500^{\circ}F$ for long periods of time without surface melting or material removal. It is being considered for application over the major portion of a lifting reentry vehicle in the areas where the heating rate is 40 Btu/ft^2-sec or less.

A material process undergoing development is expected to provide LI-1500 with uniform material properties along with a compatible surface coating to increase the emissivity and harden the surface for handling purposes. Panels up to 15 x 20 x 4 in. have been fabricated; however, larger size panels are limited only processing facilities. LI-1500 is easily cut and machined with conventional tools.

Results of the material development efforts, elemental tests, and fabrication feasibility studies indicate that this material system has significant potential merit in weight, cost savings, and design simplification for spacecraft application relative to existing or proposed ablator or metallic re-radiative heat-shield materials.

Table 3-8 summarizes the composition, application, and manufacturing parameters. The development approach, testing, preliminary design data, and conclusions pertaining to LI-1500 material system development are discussed in the following paragraphs.

Table 3-8

LIGHTWEIGHT INSULATION

Composition

Quartz fibers/SiO_2

Density $\approx$ 12 to 15 lb/ft^3

Rigid, high strength

Application

Lifting reentry ($q < 30$ Btu/ft)

Reusable (noncharring or ablating)

Higher temperature capability with refractory fibers

Producibility

Repeatable mechanical and physical properties

Good fabrication and machinability

Size: Current· future-unlimited 15 x 20 x 4 in.

3.2.7.1 LI-1500 Development Approach. Figure 3-21 shows the developmental approach of LI-1500, starting with the material development, establishing basic material properties from elemental tests, establishing design requirements and criteria from structural/thermal panels, and eventually qualifying the thermal protection system and compatibility with other systems through through system tests.

3.2.7.2 LI-1500 Testing. Considerable elemental testing has been performed on LI-1500 material. Table 3-9 presents a summary of the types of tests performed, including simulated ascent, orbital, and reentry flight phases. Tests on LI-1500 material conducted prior to mid-1968 have been reported*.

* Lockheed Missiles & Space Company, "Lightweight Insulation (LI-15) Test summary," LMSC-685434, Sunnyvale, Calif., 22 Apr 1968

Table 3-10 presents a summary of some recent tests and indicates the testing agency.

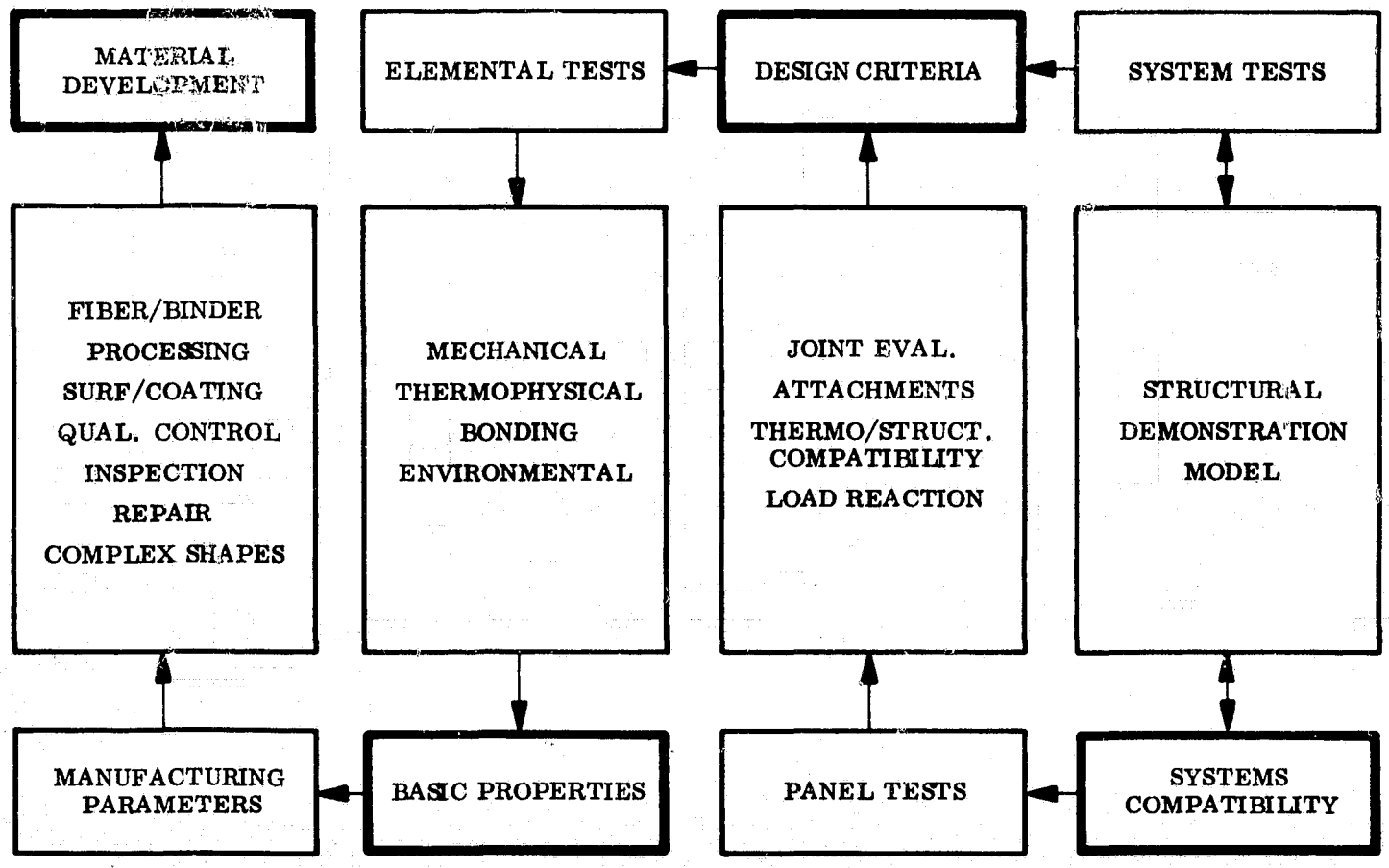

Fig. 3-21 LI-1500 Approach

Pacemaker Test. Two panels of LI-1500 (11 x 5 x 0.4 in.) were flown on the NASA Pacemaker reentry test vehicle in June 1968. Table 3-11 and Figs. 3-22 through 3-24 show a summary of the flight, trajectory data, and the specimens before and after the flight. As can be seen in Fig. 3-24, the LI-1500 material survived the flight and recovery operation without material degradation.

Table 3-9

TEST SUMMARY

- Tension
- Compression
- Bending
- Shear
- Rapid decompression
- Cold soak
- Transmissibility
- Coefficient of expansion
- Conductivity
- Specific heat
- Reentry heating
  - Radiant
  - Convective
- Vacuum
- Acoustic

Table 3-10

RECENT TESTS

Test Description	Test Location	Results	Remarks
Compression	LMSC	50 to 100 psi	Dependent on density
Shear	AFFDL LMSC	15 to 45 psi	Dependent on density
Radiant heat and acoustic	AFFDL	10 cycles at max surface temperature of 2300°F 20 min. at 156, 162, and 168 db Sweep from 150 to 1100 cps	Radiant heat – no cracking or shrinkage Acoustic – bond failure at 168 db
Acoustic and Radiant heat	AFFDL	165 db for 5 min random 50 cycles at 2500°F 1 cycle each from 2600°F to 3100°F	Acoustic – survived Radiant heat – surface cracking on first test – no shrinkage
Acoustic	LMSC	10 min at 150, 156, and 163 db 5 min at 161 – random	Survived Survived – after 2500°F Thermal cycle
Radiant heat	LMSC	2500°F thermal pulse	Surface coating development and material qualification
Strain Compatibility (AL-Ti/LI-15)	LMSC	Al at R.T. – 63,000 psi Ti at R.T. – 119,000 psi Ti at 600°F – 80,000 psi	No failure in LI-15

Table 3-11

PACEMAKER SUMMARY

NASA Reentry test vehicle

Honest John/Nike Missile

Flight date - 20 June 1968

Materials tested

AVCO Mod 5 at 30 lb/ft^3

Foam Teflon at 20-25 lb/ft^3

LI-15 at 15 lb/ft^3

Reentry environment (predicted based on ϵ = .8)

Maximum surface temperatures = 2300°F

Total heat = 650 Btu/ft^2

3 sec > 2250°F

3.2.7.3 Preliminary Design Data. Summarized in Table 3-12 are the test results on LI-1500 material, which may be used as preliminary design data. These data are representative of LI-1500 material with a density of 15 lb/ft^3. The mechanical properties vary significantly with density.

3.2.7.4 Conclusions. Results of the LI-1500 material development effort and tests and the material fabrication characteristics indicate that this material system has significant potential merit in weight, cost savings, and design simplification relative to existing metallic reradiative heat shields or ablative systems for reentry spacecraft application. The successful development and qualification of this material system would represent a significant technological breakthrough in heat-shield systems.

3.2.8 Ablator Material Candidates

The thermal environment for lifting entry trajectories suggests ablators with the following characteristics:

- Low density
- Small char formation with high char strength
- Minimum char recession (spallation or oxidation)
- Low thermal conductivity to limit heat conducted to substructure

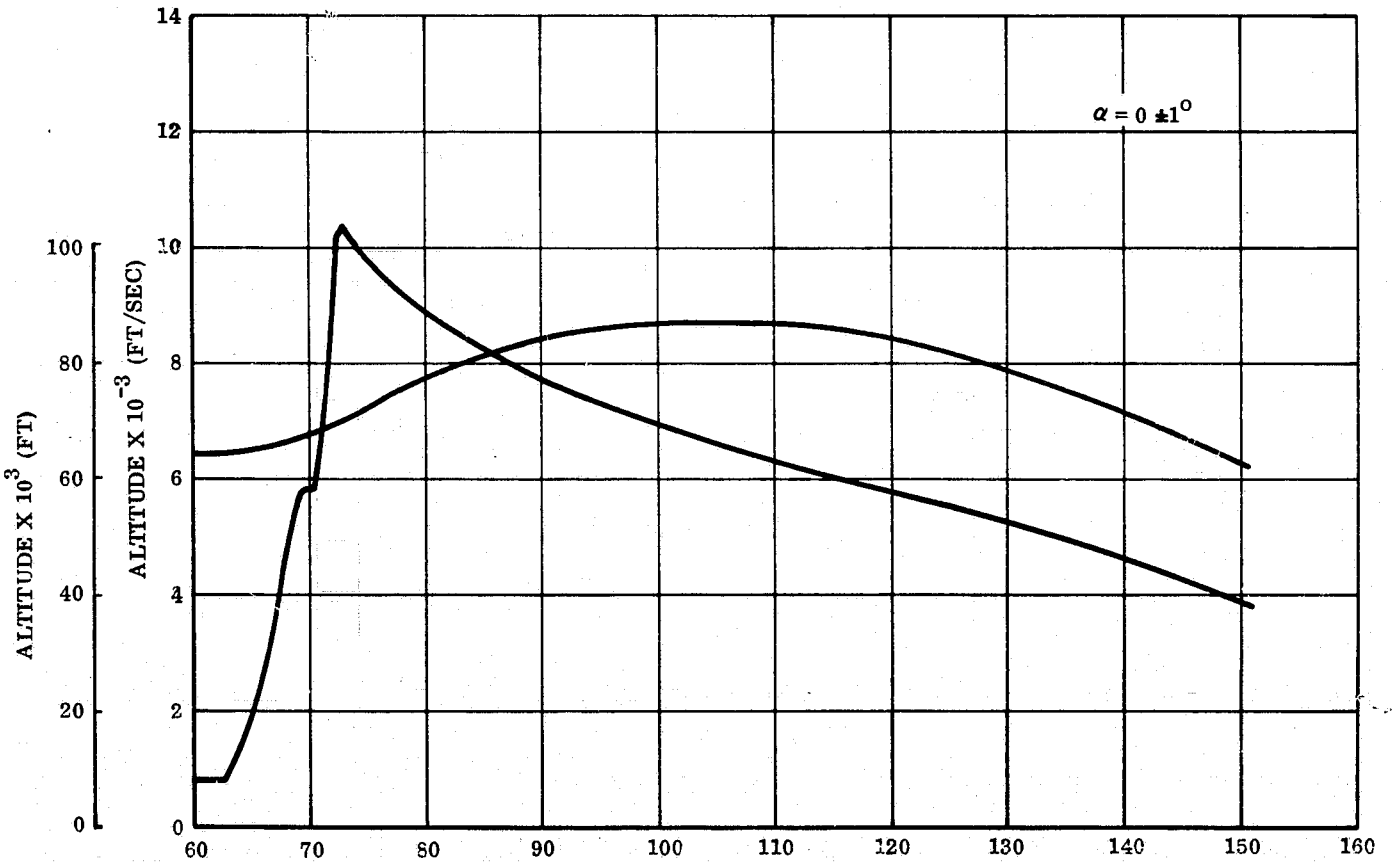

Fig. 3-22 Pacemaker Velocity/Altitude Histories

The prime consideration for these long entry time environments is the thickness of char formed and the mount lost through chemical oxidation and mechanical erosion. Thick char layers formed during long entry time, low heat rate environments experience thermal stresses that could cause spallation and precipitate mechanical erosion. The material system to be chosen must have char layers that resist spallation and exhibit good resistance to oxidation. Current methods to reduce char erosion have glass fiber added to the basic silicone material or a phenolic Fiberglas honeycomb encasing the basic silicone material.

Candidate materials are listed in Table 3-13. Since none have been exposed to the long time heating projected for a typical shuttle vehicle entry, a combination of analysis and subscale screening tests are required to arrive at the final candidates and specific section weight requirements for design

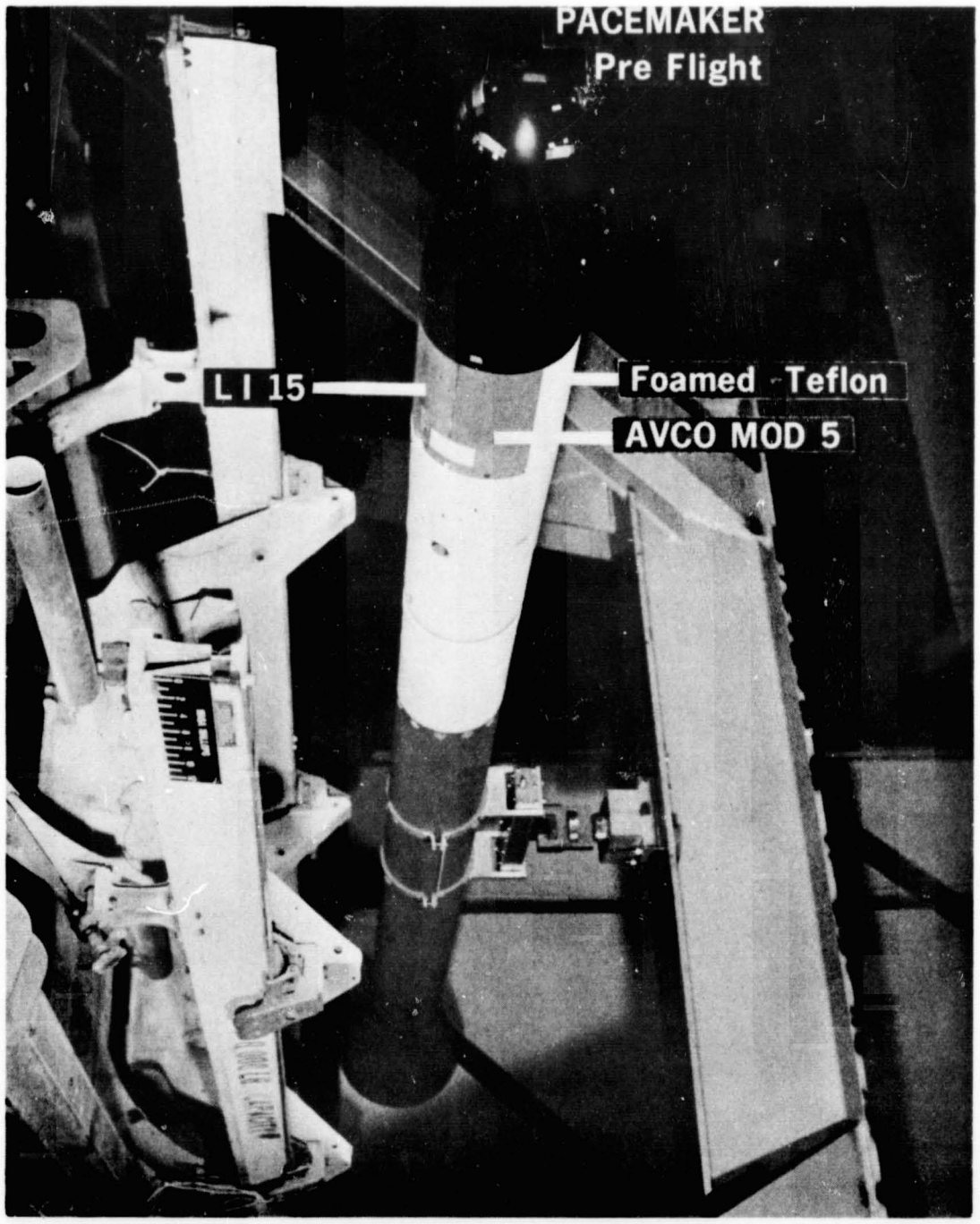

Fig. 3-23 Pacemaker - Preflight

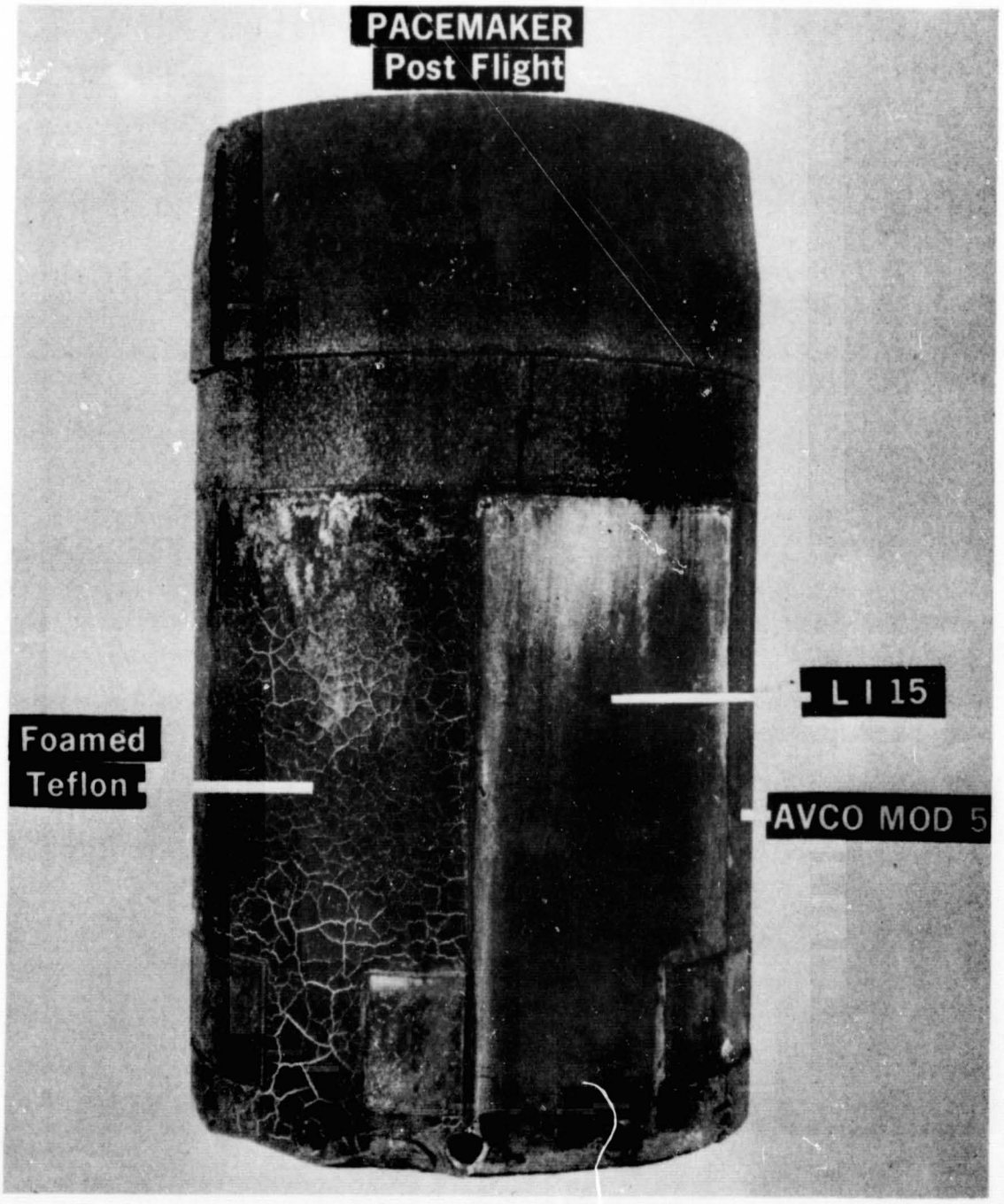

Fig. 3-24 Pacemaker - Postflight

Table 3-12

LI-1500 TEST DATA SUMMARY

Description of Test	No. of Tests	Results	Remarks	Location of Test
MECHANICAL				
Tensile	36	90 to 110 psi	Conducted in 1966	LMSC
Compression	22	90 to 110 psi	Conducted in 1966	LMSC
Flexure	17	166 psi	Average value	LMSC
Modulus-Tensile	36	1.0 to 3.0 x 10^4 psi	Conducted in 1966	LMSC
Modulus-Compression	22	0.5 to 1.0 x 10^4 psi	Conducted in 1966	LMSC
Modulus-Flexure	17	3.35 x 10^4 psi	Average value	LMSC
PHYSICAL				
Density		15 lb/ft^3	Average density	LMSC
Coefficient of Expansion	1	3 x 10^{-7} in./in. ^oF		LMSC
Conductivity	1		Actual data to 700^oF	SoRI
Specific Heat	1	0.28 Btu/lb^oF	Actual data to 1800^oF	LMSC
Emittance		0.6 to 0.8	Varies with coating	
Transmissibility	4		Varies with thickness and coating	LMSC
ENVIRONMENTAL				
Cold Soak	1	-350^oF for 4 hr	Survived	LMSC
Decompression	1	40 psig in 40 sec	Survived	LMSC
Vacuum	1	7 mm Hg and 2000^oF for 1 hr	Survived	LMSC
Acoustic Reentry Heating	5	168 db for 15 min	Both virgin and thermally cycled	LMSC, AFFDL
Radiant	4	48,000 Btu/ft^2 (max.)	Survived	LMSC, AFFDL

Table 3-13

CANDIDATE MATERIAL SYSTEMS

Material	Potentials of Material for Orbiter Vehicle Application	State-of-the Art Materials
Silicone Elastomers	Good oxidation and erosion resistance of high and low density systems	Yes
Carbon Phenolic	Good erosion resistance	Yes
Refrasil Phenolic	Better erosion resistance than carbon phenolic because of silica, which forms a melt layer in the system.	Yes
Polyurethane	Low density and conductivity, poor erosion resistance, not suitable for orbiter vehicle application	Yes
Nylon-Phenolic	High density, poor erosion resistance, not suitable for orbiter vehicle application	Yes
Nomex-Gelatin	Low density	No

entry conditions. Lockheed experience from the ENCAP program (Refs. 3-11 and 3-12), where state-of-the-art material screening tests were conducted to select a material that could be fabricated into a flexible heat shield, provides a sound basis for an unbiased screening evaluation of candidate state-of-the-art materials.

Computer programs that predict mechanical and chemical erosion for coupled thermal and structural environments have been developed during the Advanced Ballistics Reentry Environment Studies (ABRES). Originally developed for high-density carbon materials, these programs have been modified to accomodate low-density silicone materials based on existing basic properties and performance data.

Specific silicone materials developed for recent programs or advanced in the literature are listed in Table 3-14. For silicone materials with densities from 32 to 45 lb/ft^3, most manufacturer's tests have indicated low char erosion for heat rates less than 100 Btu/ft^2-sec. Data are available for sustained low heat rates resulting in high heat loads (30,000 Btu/ft^2). The potential of these materials is illustrated by the PRIME flight test results, where a 32 lb/ft^3 silicone elastomer material, ESA3560 HF, formed approximately 0.60 in. of char with a loss of 0.060 in. by erosion. The total heat experienced at this location was about 30,000 Btu/ft^2, with a maximum heat rate of 100 Btu/ft^2-sec. The panel baseline material system for the orbiter presented in Table 3-15 was evaluated or reported in the following section.

3.3 THERMAL STRUCTURAL CONCEPTS

Both booster and orbital stages of the Space Shuttle are of state-of-the-art aluminum primary structure. Any of three thermal protection systems listed below can be employed interchangeably for the primary structure:

- Metallic heat shields with internal insulation
- LI-1500 rigid insulation on the external surface
- Ablation heat shields (backup)

Table 3-14

STATE-OF-THE-ART SILICONE BASED MATERIALS

Density lb /ft^3	Material	Manufacturer	Program/ Reference	Comments
28	MA25S	Martin-Marietta	X-15A-2	Heat rates 0-7Btu /ft^2-sec sprayable, room temperature cure
32	ESA3560HF in honeycomb	Martin-Marietta	PRIME	Heat rates 7-125Btu/ft^2-sec showed low char erosion in flight test and plasma tests
55	ESA5500HF in honeycomb	Martin-Marietta	PRIME	Heat rates 125-200Btu/ft^2-sec
55	D-C 325 in honeycomb	Dow Corning (McDonnell-Douglas)	Gemini	Heat rates 100-300 Btu/ft^2-sec plasma tests indicate negligible erosion for $\dot{q}$ <90Btu /ft^2 sec, low total heats
40	TBS 757	General Electric	-	Material chosen for modification during ENCAP program molded without honeycomb matrix - range of densities are available
20-80	ESM 10XX	General Electric	-	G. E. claims good erosion resistance for lifting entry environments, without honeycomb reinforcement matrix. Range of densities available.

Table 3-15

BASELINE MATERIAL SYSTEMS

Location	Baseline	Alternatives
Panels	20 lb/ft^3 Silicone Elastomer	Higher density silicone ablators
Leading Edge	Refrasil Phenolic	Carbon phenolic medium to high density silicone ablators

The preferred metallic heat shield is a large corrugated panel with multiple clip supports. Discussion of these and other systems follow.

3.3.1 Candidate Thermal Structural Concepts

Various thermal protection systems that were investigated are shown in Fig. 3-25. Both passive and active systems were studied. Passive systems provide sufficient thermal insulation to limit the maximum structure temperature to an acceptable value. The following passive system concepts were evaluated:

- Felt-like high-temperature insulations, such as dynaflex and microquarts in conjunction with metallic heat shields
- A Lockheed-developed lightweight rigid silica insulation, designated LI-1500
- A fiberglas-reinforced sillcone elastomeric ablator (ρ = 20 lb/ft^3)

As shown on Fig. 3-25, the LI-1500 and metallic heat shield concepts were also evaluated in conjunction with a closed-loop active cooling system. In all cases, the spacecraft internal structure was assumed to have a design maximum temperature of 150°F. Heating calculations are based on the L/D = 2 spacecraft and maximum cross-range entry trajectory.

Recent studies indicate that large corrugated heat shields with multiple clip supports are lighter in weight than post-supported integrally stiffened heat shields. The corrugated heat shield shown in Fig. 3-26 is mounted with a multiple-clip arrangement through a glass rock insulator to the primary aluminum structure. Corrugation amplitude is one-tenth the corrugation pitch with a flat provided between corrugation arcs to enable attachment of the continuous support clip. Mechanical fasteners and resistance spot welding are used to attach respectively the TD-NiCR and Rene' 41 corrugated heat shields. Blanket type insulation (dynaflex and microquartz) is packaged between the corrugation shield and the structural panel.

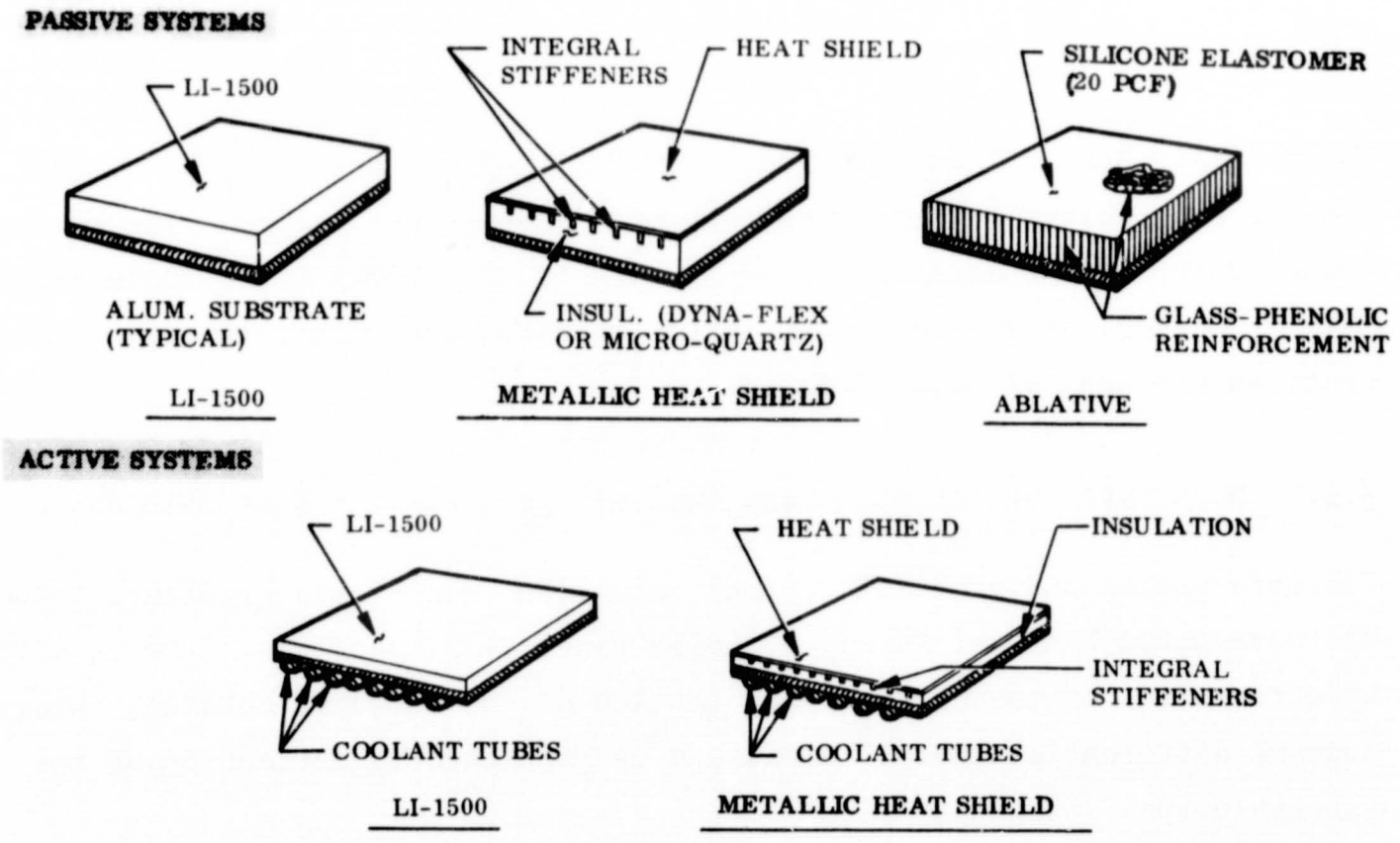

Fig. 3-25 Passive and Active Thermal-Structural Concepts

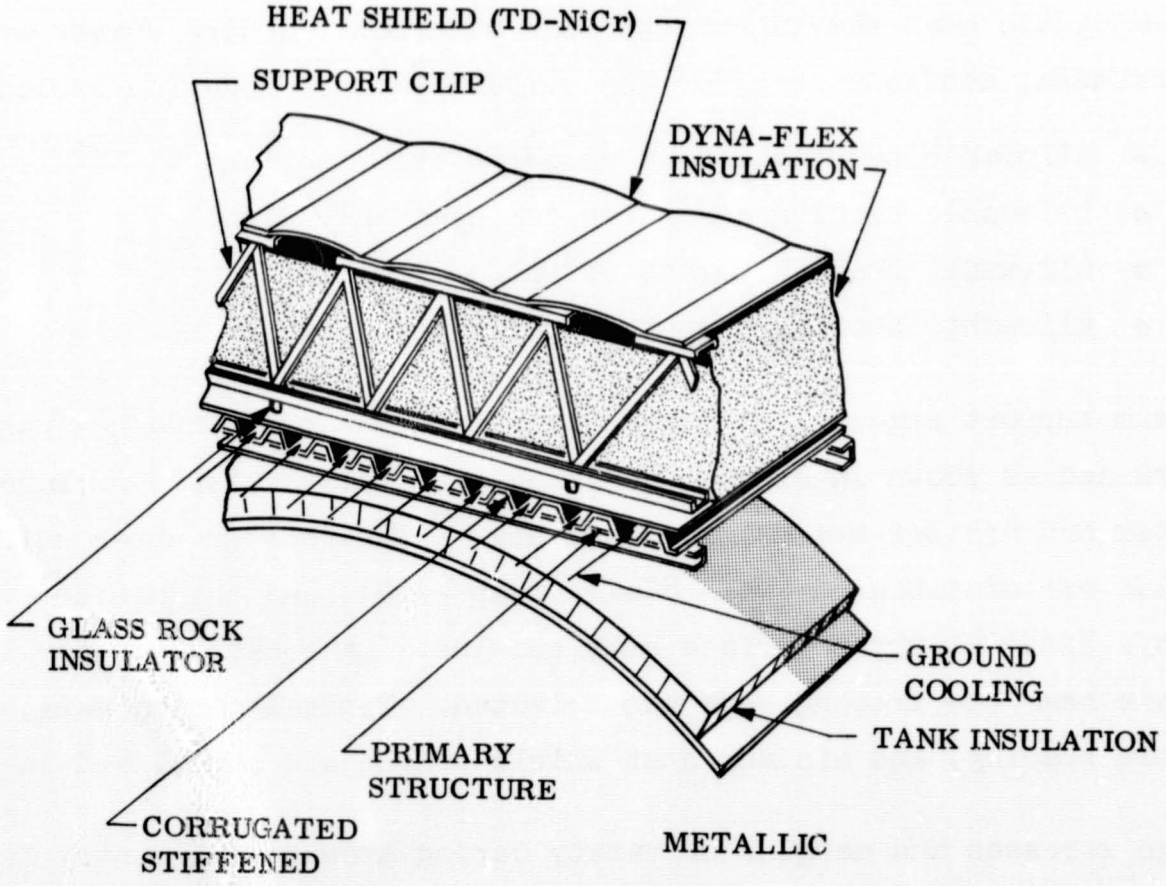

Fig. 3-26 Metallic Heat Shield

The metallic heat shield arrangement of Fig. 3-26 is applicable for both booster and orbiter for the Two-Stage and Triamese approaches. The basic change with vehicle application is the use of the proper heat-shield materials. However, as insulation thickness changes, other support clip configurations are used if more efficient.

3.3.2 Structural Optimization and Analysis for Metallic Heat Shields

Circumferential differential thermal expansion fromthermal gradients between the corrugated heat shield and phenolic panel fairing of Fig. 3-26 is allowed by deformation of the circular-arc portion of the corrugation skin. Longitudinal differential thermal expansion is permitted by deflection of the support clips.

Closed form optimization equations were developed for the circular-arc corrugation heat shield subjected to uniaxial bending. For rapid evaluation of the candidate heat shield concepts and materials, design curves were constructed. For example, design curves for the circular-arc corrugation include:

- Allowable bending moment vs corrugation thickness
- Allowable bending moment vs corrugation radius
- Allowable bending moment vs width of flats
- Allowable bending moment vs corrugation pitch

Optimum support spacing for the multi-supported corrugated heat shields was determined as shown in Figs. 3-27 and 3-28 for the lower surface of the booster and orbiter stages, respectively. (The booster upper surface heat shields are of titanium (Ti - 8 al - 1 Mo - 1V), and the orbiter vehicle employs Rene' 41 upper surface heat shields.) A location on the lower surface near the leading edge was selected. Typical design data, optimum support spacing, and minimum heat shield weight are summarized in Table 3-16.

Design stresses and margins of safety during ascent and reentry are summarized in Table 3-17 for lower surface booster and orbiter heat shields. The most critical loading conditions occur at maximum αq during ascent and at maximum heating during reentry.

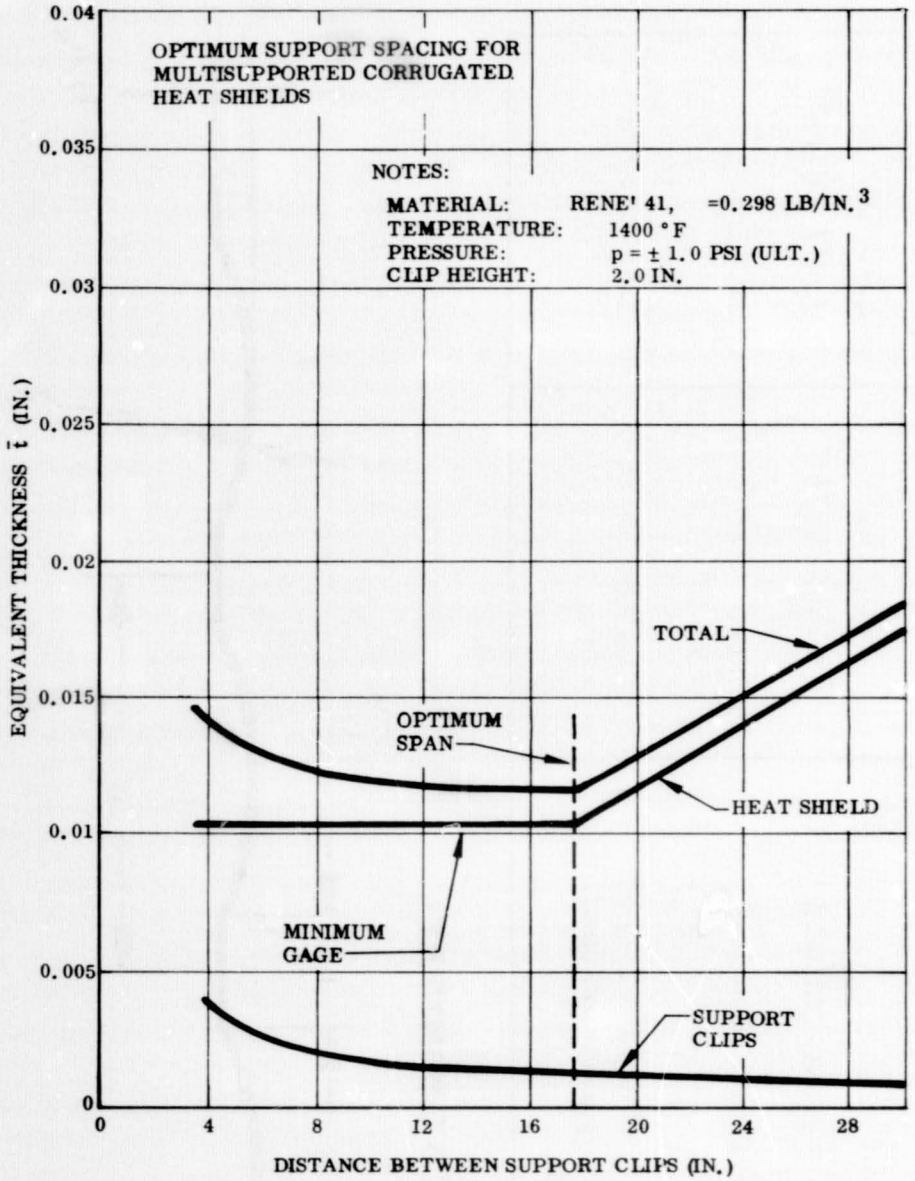

Fig 3-27 Booster Heat Shield Optimization, 1400° F Location

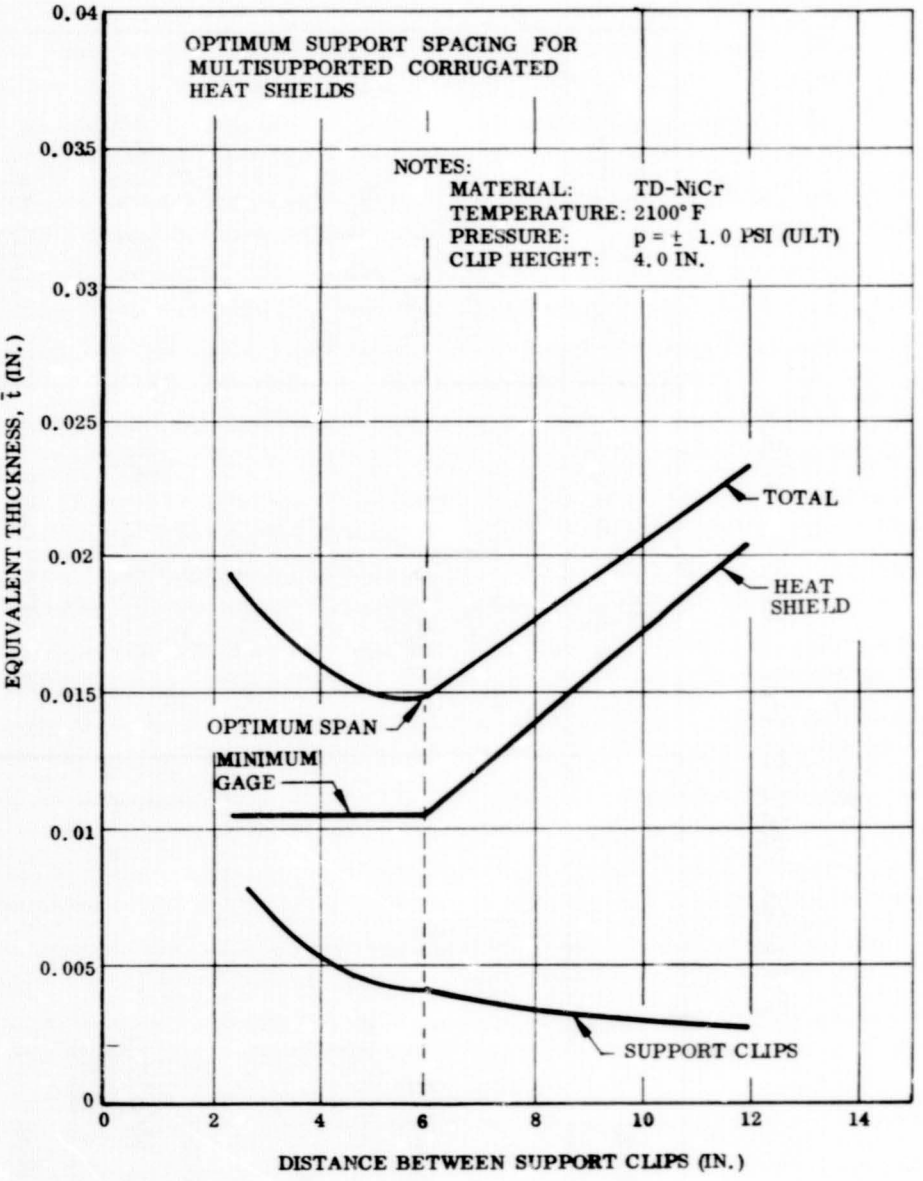

Fig. 3-28 Orbiter Heat Shield Optimization, 2100° F. Location

Table 3-16

TYPICAL HEAT SHIELD DESIGN DATA

Item	Booster Lower Surface	Orbiter Lower Surface
Material	Rene' 41	TD-NiCr
Temperature, T	1400°F	2100°F
Pressure, Δp (ULT.)	±1.0 psi	±1.0 psi
Clip Data		
Height, h	2.0 in.	4.0 in.
Thickness, tc	0.014 in.	0.011 in.
Weight, W/clip	0.057 lb/ft^2	0.189 lb/ft^2
Heat Shield Data		
Skin thickness, t	0.010 in.	0.010 in.
Radius, R	0.83 in.	1.05 in.
Flat width, bf	0.28 in.	0.36 in.
Pitch, bs	1.10 in.	1.40 in.
Weight, W/heat shield	0.442 lb/ft^2	0.487 lb/ft^2
Optimum Support Spacing	17.6 in.	6.0 in.
Total unit weight of heat shield, clip, and oxidation allowance	0.499 lb/ft^2	0.687 lb/ft^2

HEAT SHIELD GEOMETRY:

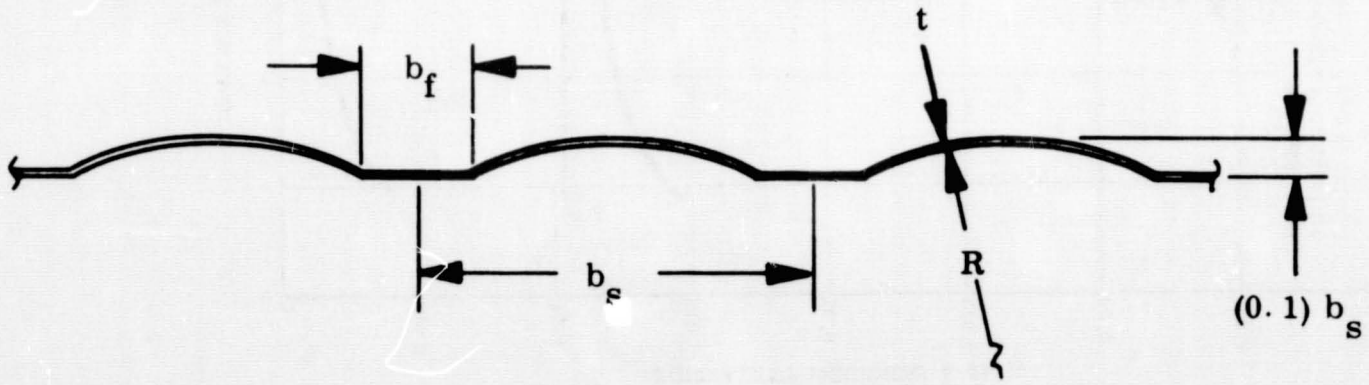

Table 3-17

TYPICAL HEAT SHIELD DESIGN STRESSES
AND MARGINS OF SAFETY

Item	T, (°F)	Δp, (psi)	f, (psi)	Fc,cr, (psi)	M.S.
Booster Lower Surface at ℄					
Ascent Trajectory t = 70 sec (max$q\alpha$)	200	±0.96	81,700	91,500	0.12
Reentry Trajectory Assumed	1400	±1.0	85,200	85,200	0
Orbiter Lower Surface					
Ascent Trajectory t = 70 sec (max$q\alpha$)	200	±2.3	18,600	39,400	1.11
Reentry Trajectory					
t = 1000 sec	2100	±1.0	8,100	8,100	0
t = 2000 sec	1300	±2.0	16,200	24,000	0.48

List of Symbols

T = Temperature of external surface
Δp = Differential pressure acting on neat shield (ultimate)
f = Applied bending stress due to pressure
Fc,cr = Allowable bending stress of corrugation
M.S. = Margin of safety of corrugation

3.3.3 Metallic Heat Shield Attachment Concepts

The fundamental methods of heat shield attachment considered were as follows:

- Removable heat shield
- Removable subpanel
- Removable primary structure panel

Application of each attachment method are shown in Figs. 3-29 through 3-32. Details of each attachment method are dependent on the following:

- Type of primary structure
  Integral load-carrying cryogenic tanks
  Nonintegral cryogenic tanks
- Arrangement of primary structural rings and stiffeners
  Internal rings and stiffeners
  External rings and stiffeners
  External rings and internal stiffeners
  Internal rings and external stiffeners

Functional design requirements for the thermal protection system were as follows:

- Heat shield refurbishment, if necessary
- Periodic inspection and repair of vehicle primary structure
- Periodic inspection and repair of cryogenic tankage
- Removal of nonintegral cryogenic tankage for repair and replacement

An application of the removable heat shield concept to nonintegral tankage and internal rings is shown in Fig. 3-29. An access hole is provided for removal of heat shield clip fasteners. The access hole is covered by an expendable snap-in button designed for positive retention. A phenolic glass fabric membrane spanning between frames may be needed to provide a passageway for ground cooling. Since the heat shield is attached directly to the primary structure, no subpanel is required. Because of the large number of heat shield clip fasteners, complete inspection of the vehicle primary structure is difficult.

REMOVABLE HEAT SHIELD

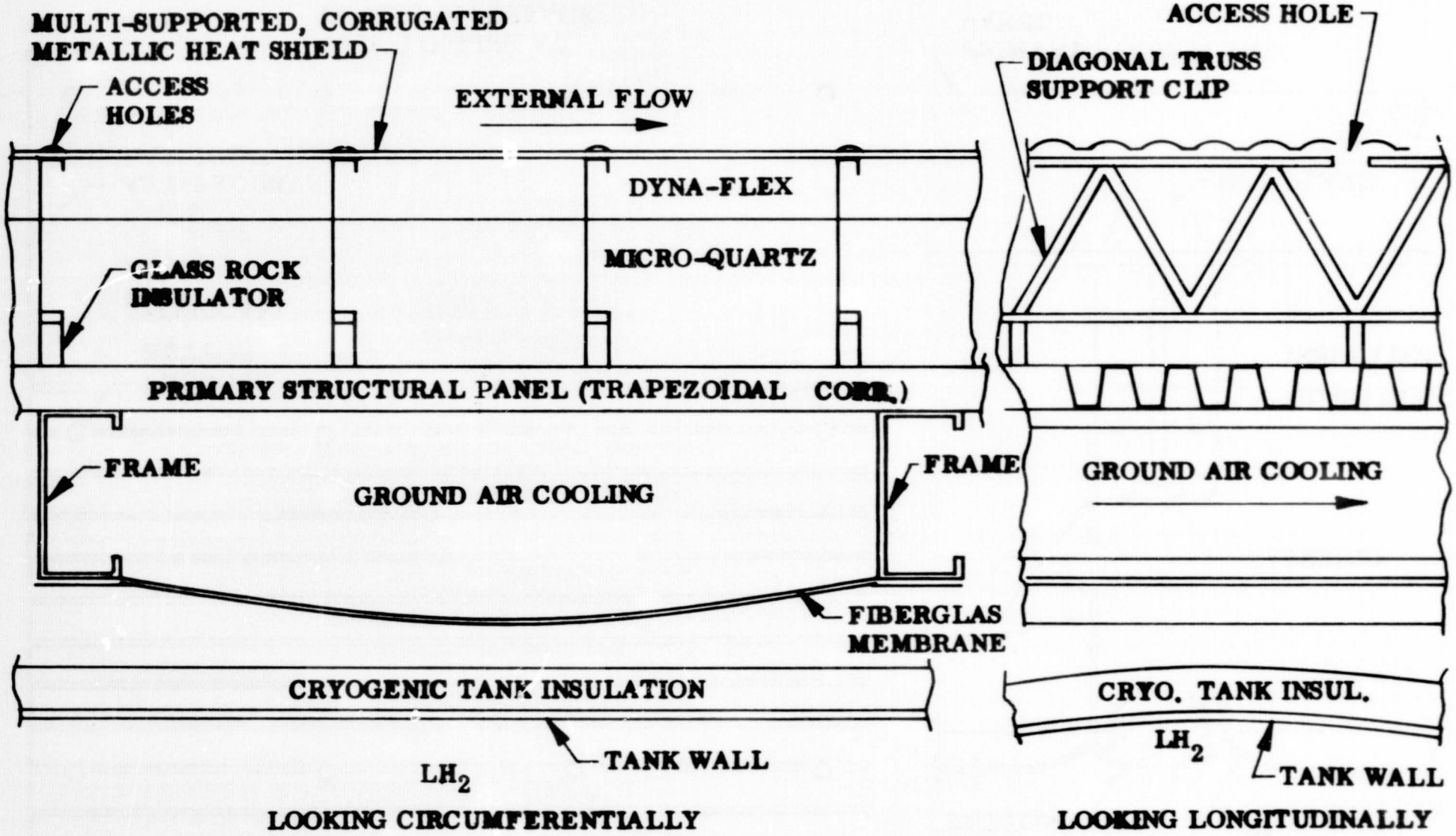

Fig. 3-29 Thermal Protection System-Orbiter Stage, Lower Surface, Nonintegral Tankage (Sheet 1 of 2)

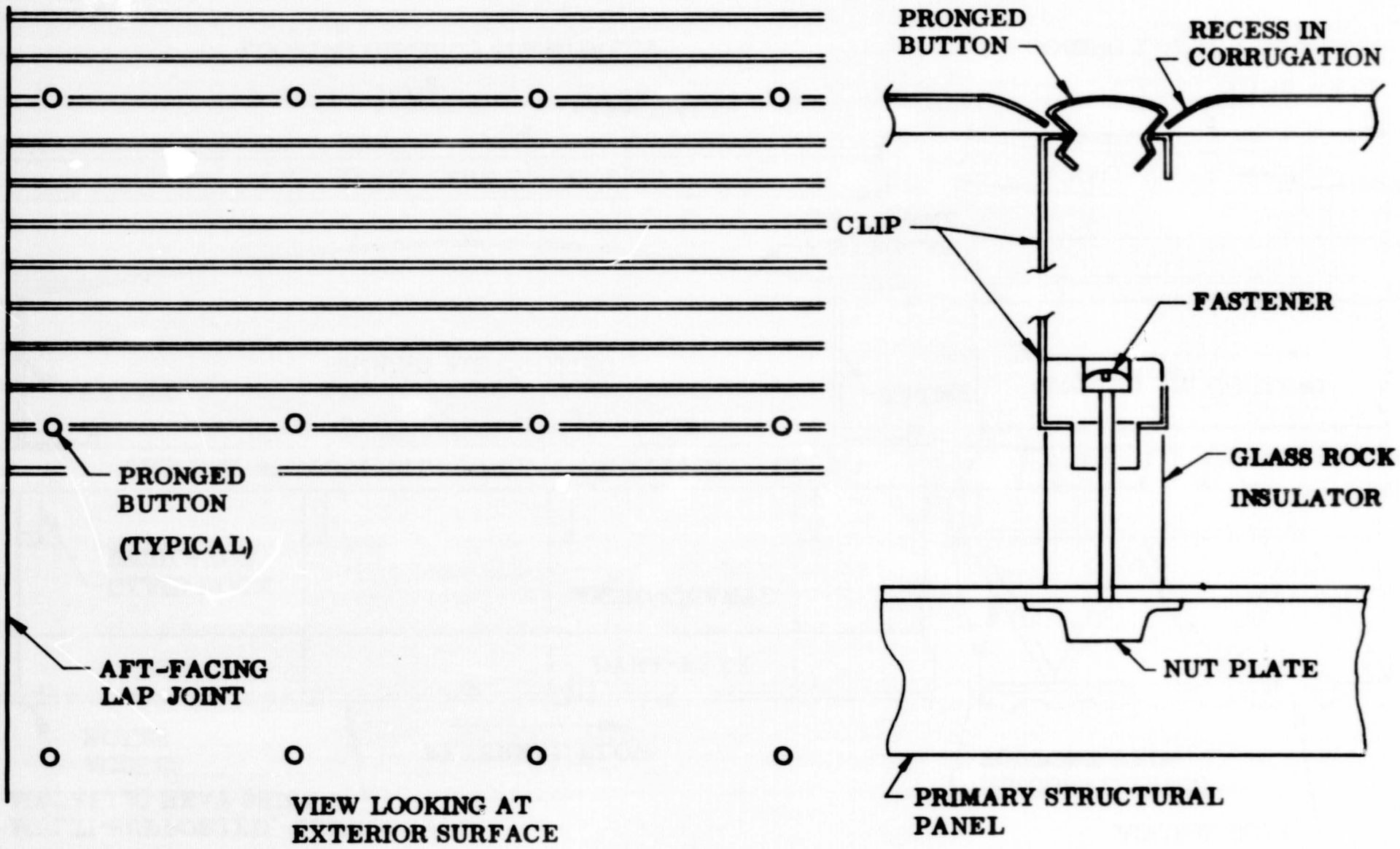

Fig. 3-29 Thermal Protection System-Orbiter Stage, Lower Surface, Nonintegral Tankage (Sheet 2 of 2)

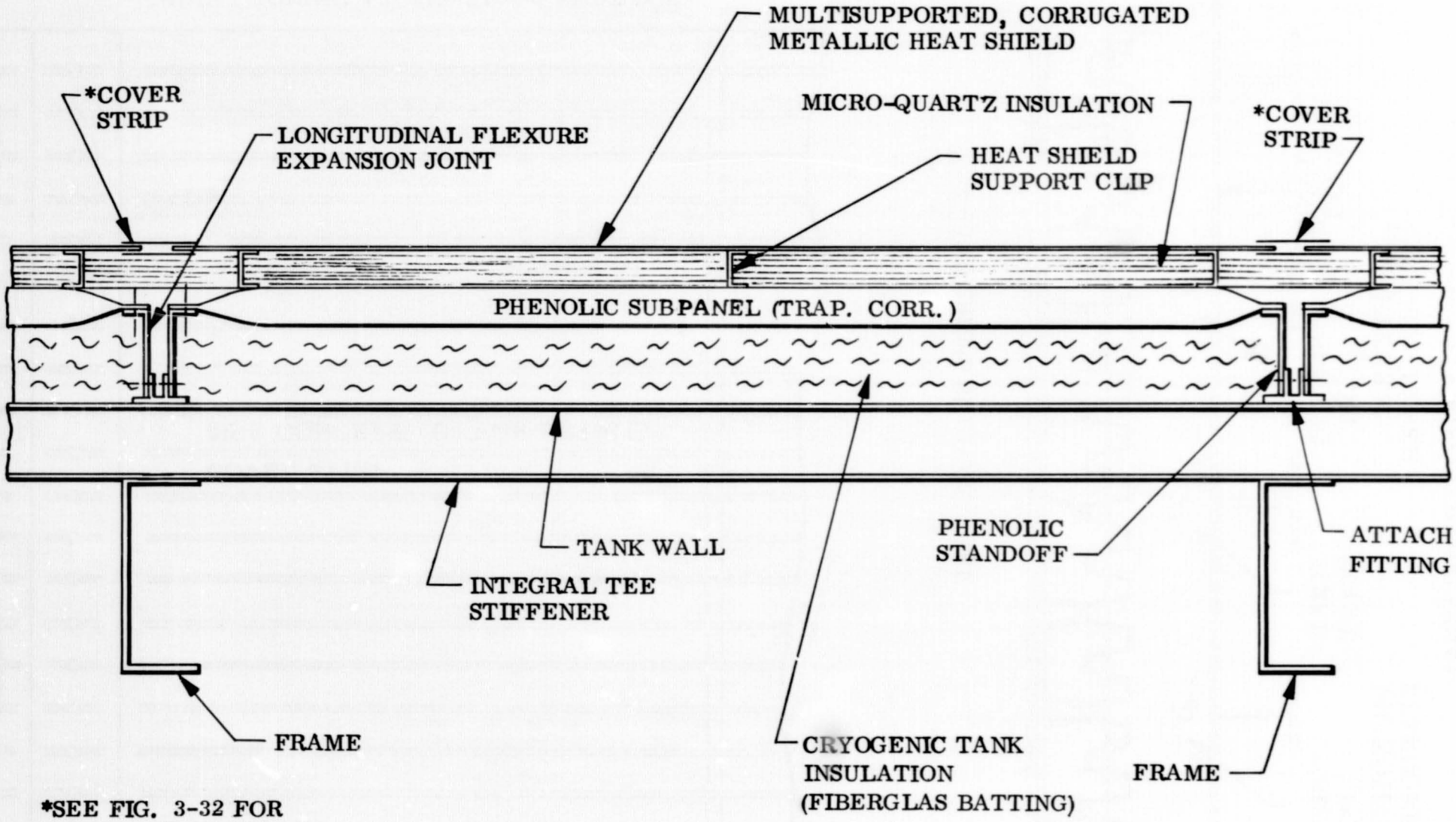

Fig. 3-30 Thermal Protection System - Booster Stage, Lower Surface, Integral Tankage (Sheet 1 of 2)

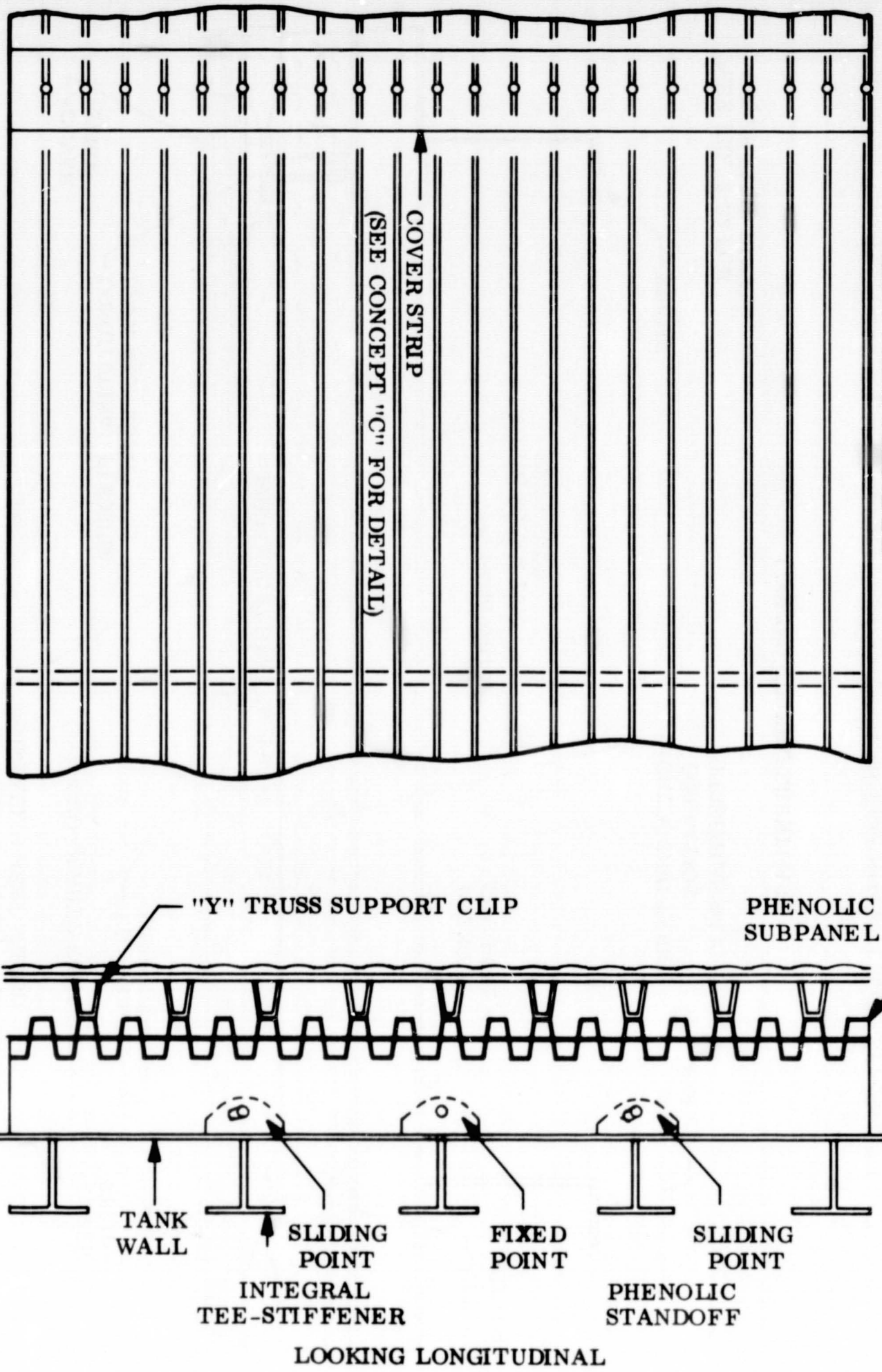

Fig. 3-30 Thermal Protection System - Booster Stage, Lower Surface, Integral Tankage (Sheet 2 of 2)

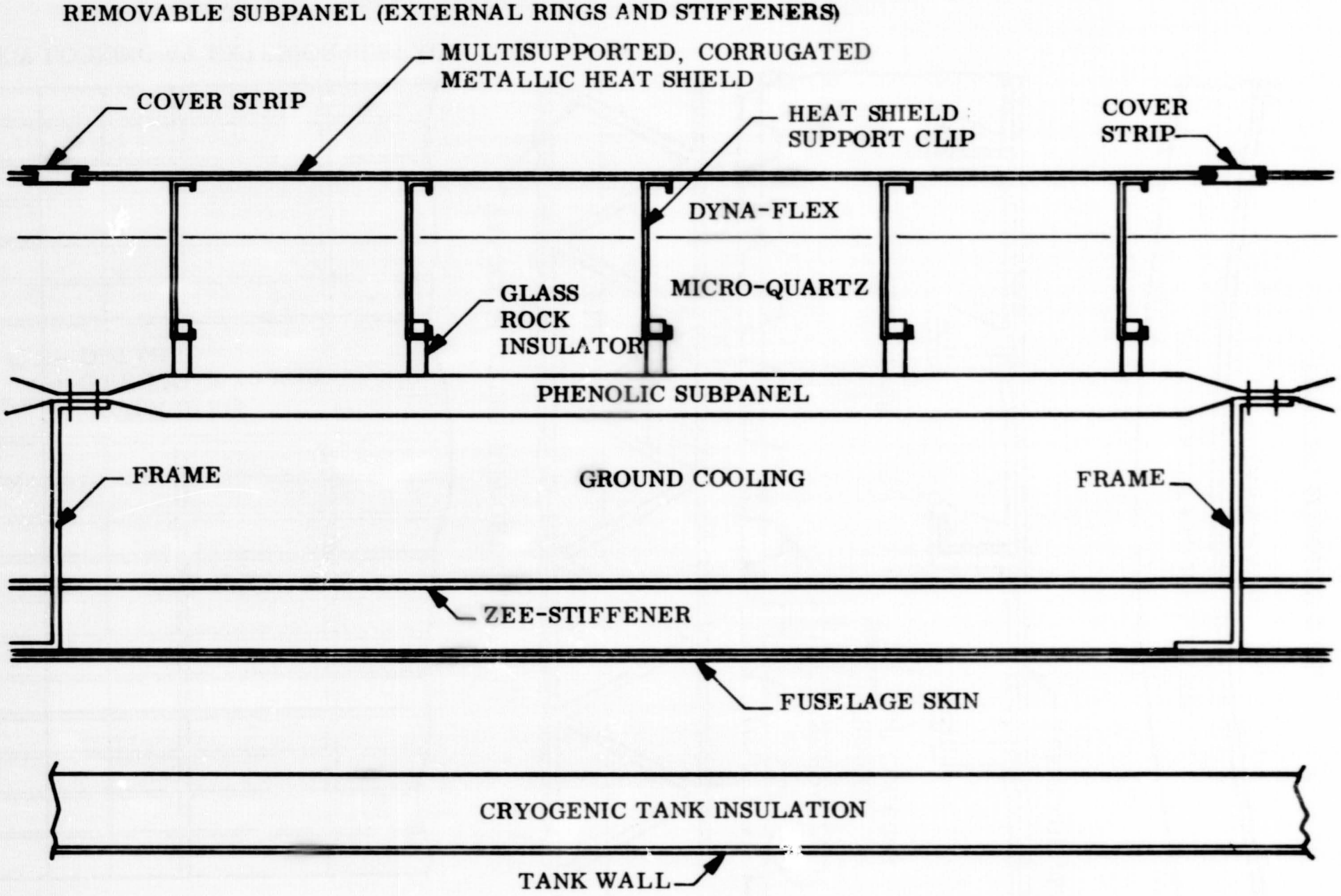

Fig. 3-31 Thermal Protection System - Orbiter Stage, Nonintegral Tankage, Removable Tanks (Sheet 1 of 2)

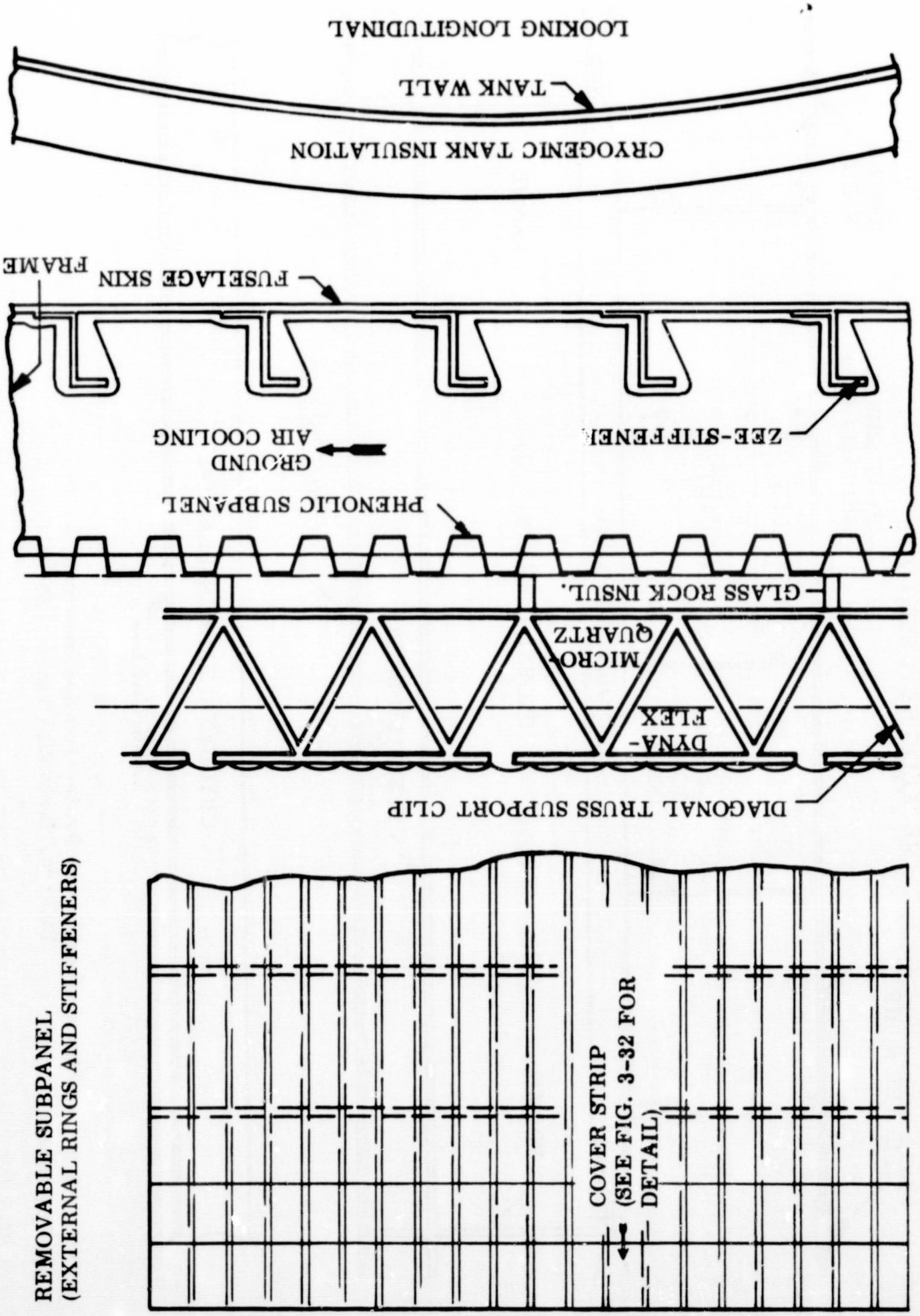

Fig 3-31 Thermal Protection System - Orbiter Stage, Nonintegral Tankage, Removable Tanks (Sheet 2 of 2)

REMOVABLE PRIMARY STRUCTURE PANEL

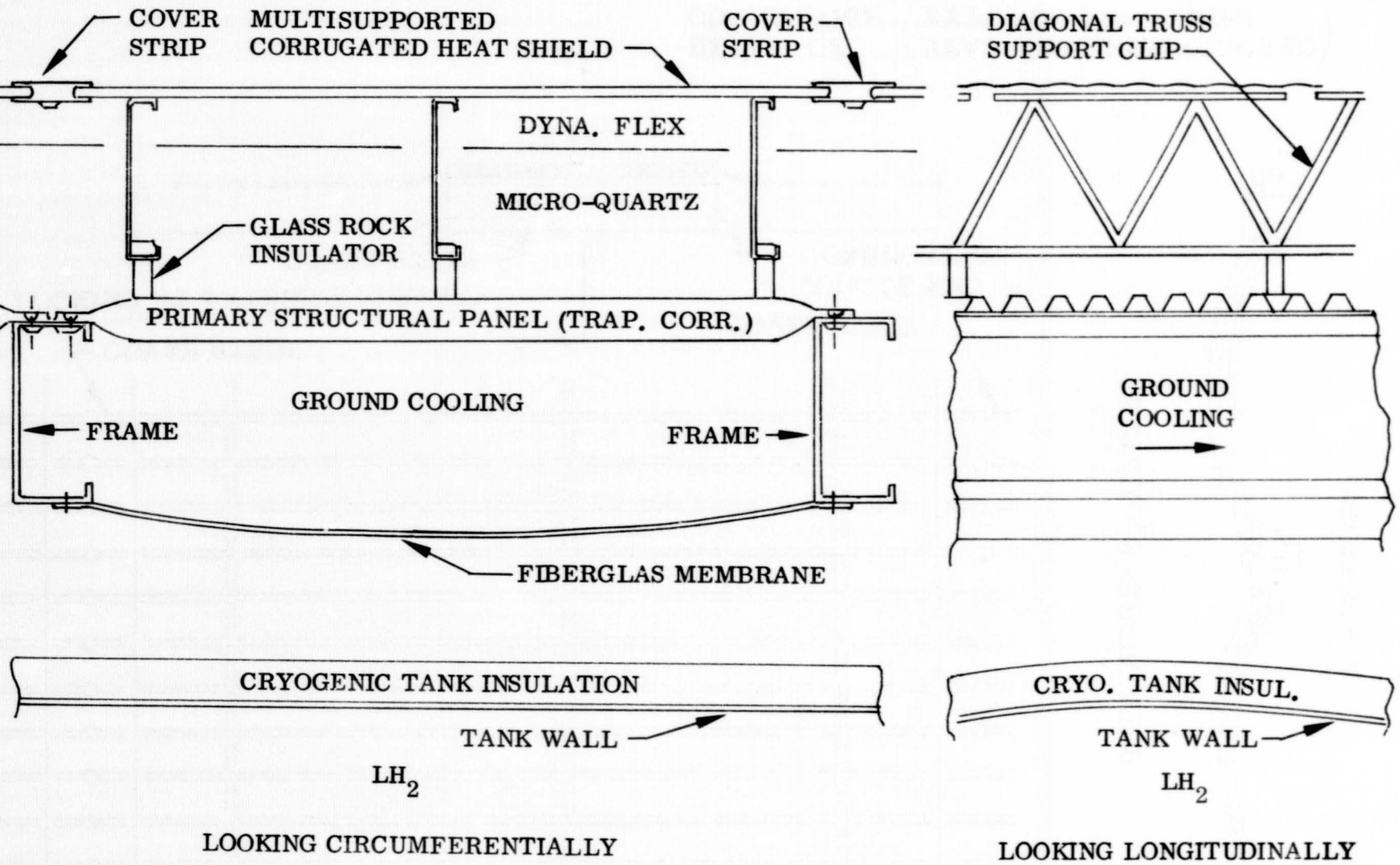

Fig 3-32 Thermal Protection System - Orbiter Stage, Lower Surface Nonintegral Tankage (Sheet 1 of 2)

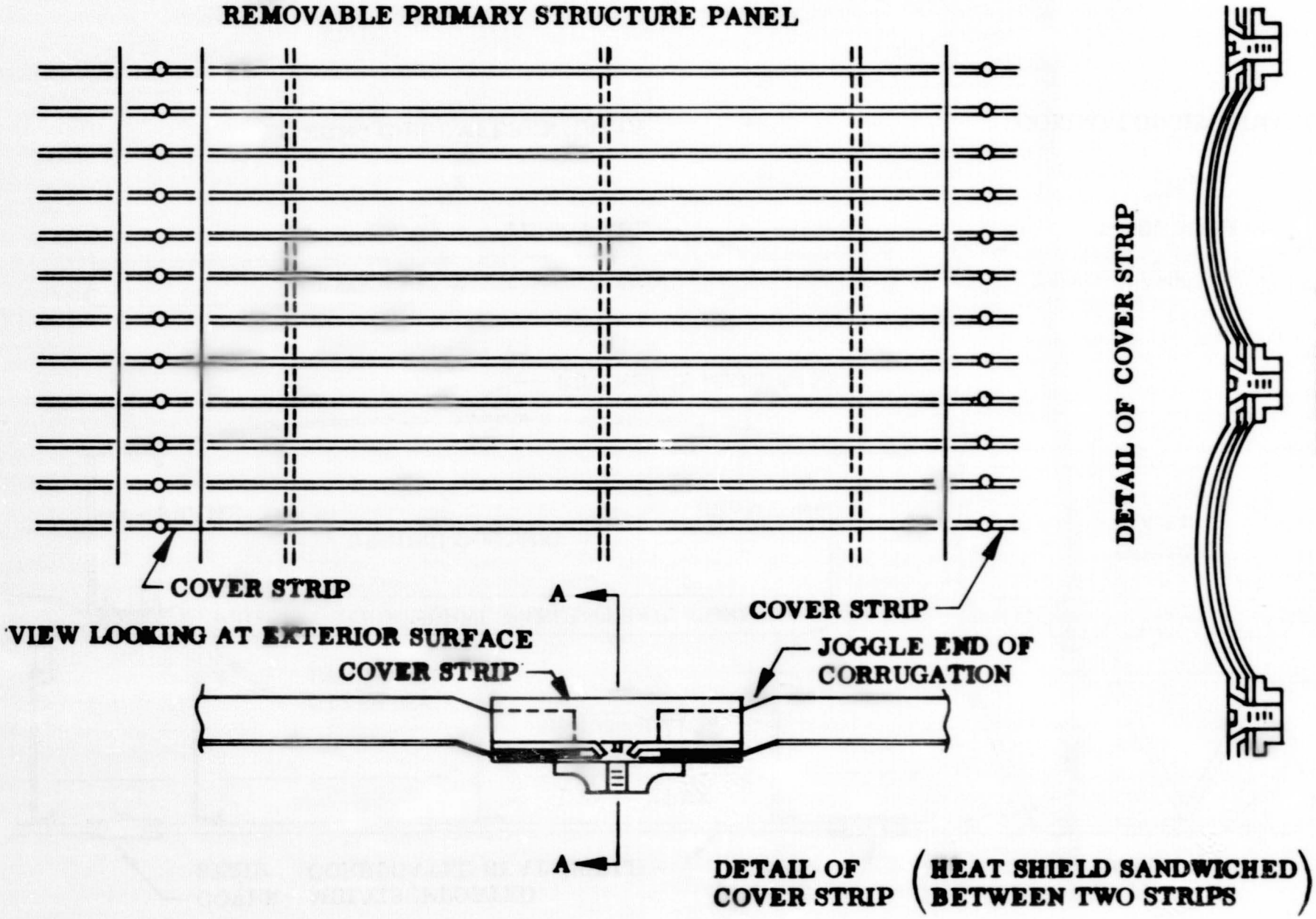

Fig 3-32 Thermal Protection System - Orbiter Stage, Lower Surface, Nonintegral Tankage. (Sheet 2 of 2)

Also, because of continuous, nonremovable primary structure panels, a splice around the entire circumference of the vehicle must be considered for removal of the cryogenic tankage.

An application of the removable subpanel heat shield attachment concept to integral cryogenic tanks with internal rings and stiffeners is shown in Fig. 3-30. A cover strip between adjacent heat shields provides access to the subpanel fasteners. Heat shorts to the cryogenic tankage are minimized by widely space phenolic standoffs. Fixed and sliding attachment points allow for thermal movement in the circumferential direction between the standoff and cryogenic tankage. The standoff permits flexure to accommodate similar relative thermal movement in the longitudinal direction.

Additional applications of the removable subpanel heat shield attachment concept to nonintegral cryogenic tankage and external rings is shown in Figs. 3-31 and 3-32. The external rings can be spliced to allow removal of cryogenic tankage for repair and replacement. The phenolic subpanel is mechanically attached to the external rings, leaving an air passageway for ground air cooling.

An application of the removable primary structure panel heat shield attachment concept is shown in Fig. 3-32. This attachment method is suitable only for nonintegral cryogenic tankage. A cover strip between adjacent heat shields provides access to the primary structural panel fasteners. Closeouts, fasteners, and lack of longitudinal continuity increase the weight of the primary structural panel. In other respects, Figs. 3-31 and 3-32 are similar.

3.3.4 LI-1500 Rigid Insulation Application

LI-1500 material is being considered as the outer surface thermal protection system for vehicle areas where the heating rates are less than 40 Btu/ft^2-sec. Figure 3-33 illustrates the application of the LI-1500 material.

The structural arrangement is designed so that the LI-1500 material protects the primary load-carrying structure and is only subjected to the LI-1500 inertial loads and to air loads. The rigid heat shield is bonded to the primary structure, which also serves as a passageway for ground cooling air, if required. Since the LI-1500 material has a very low thermal coefficient expansion, minimum external expansion joints are necessary.

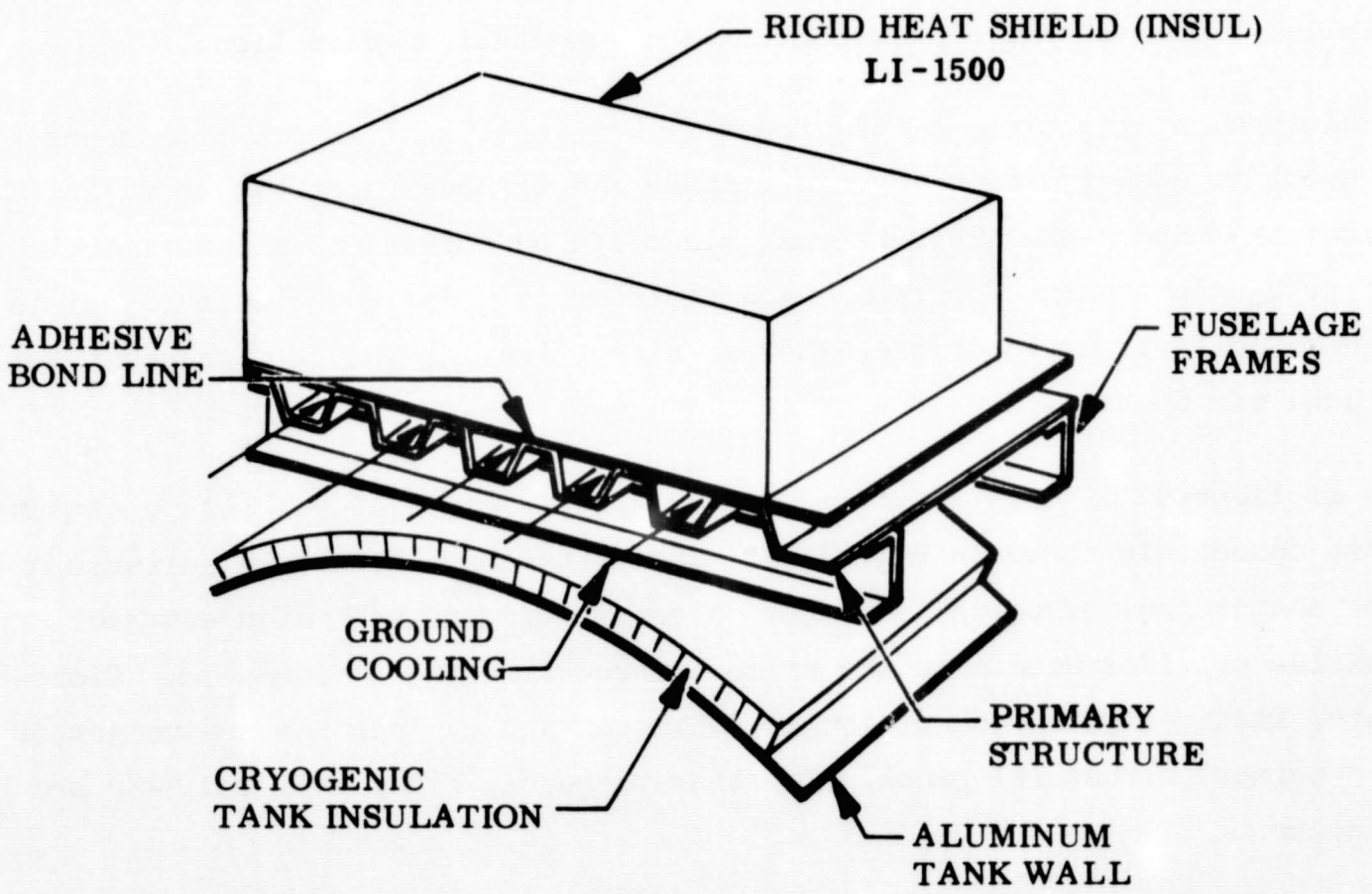

Fig. 3-33 Application of LI-1500 Material

3.3.5 Thermal Protection System Weights

Metallic thermal protection system weights summarized in Table 3-18 include upper and lower surfaces of the orbiter, booster fuselage, and booster wing. Booster wing thermal protection system weights are presented for aluminum primary structure at 200°F and titanium primary structure at 600°F. The thermal protection system weights include metallic heat shield, support clips, fasteners, glass rock insulator, insulation, packaging, subpanel, and stand-off. The dynaflex and microquartz insulation is packaged in a 0.002-in. Hastelloy X-750 foil to prevent absorption of moisture.

3.4 PASSIVE AND ACTIVE COOLING THERMAL PROTECTION SYSTEMS

3.4.1 Passive

Passive thermal protection systems provide sufficient thermal insulation to limit the maximum structure temperature to an acceptable value. Since hypersonic lift-to-drag ratio is the major parameter affecting entry duration, this quantity also significantly affects passive insulation requirements. In Fig. 3-34, the required passive insulation thickness at the lower surface peak heating location versus L/D is plotted. Maximum cross-range entry (α = 15 deg) and a substrate temperature limit of 150°F are assumed. These results are representative of both rigid insulators (such as LI-1500) and fibrous insulators, since the insulating characteristics of the two concepts are similar. As shown in Figure 3-34, the required insulation thickness is extremely sensitive to hypersonic L/D with impractical values being required for the high L/D vehicles.

Because of the large passive insulation thickness required for L/D = 2, use of such a system is often considered unattractive. Figure 3-35 indicates why such excessive insulation thicknesses are required. This figure shows the temperature distribution through a 5-inch slab of insulation at two times during entry-peak heating and touchdown. At peak heating, the temperature distribution is monotonic with a maximum of about 1900°F at the outer surface. At touchdown, the outer surface temperature has decreased to

Table 3-18

TYPICAL THERMAL PROTECTION SYSTEM WEIGHTS

Item	Orbiter		Booster Fuselage	
	Upper Surface (lb/ft^2)	Lower Surface (lb/ft^2)	Upper Surface (lb/ft^2)	Lower Surface (lb/ft^2)
Metallic Heat Shield and Clips				
Heat shield	0.442	0.487	0.375	0.442
Clip	0.057	0.189	0.048	0.057
Oxidation	-	0.011	-	-
Fasteners	-	0.027	-	-
	(0.499)	(0.714)	(0.423)	(0.499)
Heat Shield Insulator				
Glass rock insulator	-	0.023	-	-
Screw and nut	-	0.038	-	-
		(0.061)		
Insulation				
Dynaflex	-	0.625	-	-
Microquartz	0.750	0.938	0.250	0.438
Packaging	0.202	0.316	0.183	0.190
	(0.952)	(1.879)	(0.433)	(0.628)
Subpanel*				
Subpanel	0.400	0.400	0.400	0.400
Close-out and fasteners	0.040	0.040	0.040	0.040
Stand-off	-	-	0.084	0.084
	(0.440)	(0.440)	(0.524)	(0.524)
TOTAL WEIGHT	1.891	3.094	1.380	1.651

*Orbiter--ram and ground cooling
Booster--minimizes heat shorts

Table 3-18 (Cont'd)

	Booster Wing Aluminum Primary Structure		Booster Wing Titanium Primary Structure	
	Upper Surface (lb/ft^2)	Lower Surface (lb/ft^2)	Upper Surface (lb/ft^2)	Lower Surface (lb/ft^2)
Metallic Heat Shield and Clips				
Heat shield	0.375	0.442	0.375	0.442
Clip	0.048	0.057	0.048	0.057
Oxidation	-	-	-	-
Fasteners	-	-	-	-
	(0.423)	(0.499)	(0.423)	(0.499)
Heat Shield Attachment				
Glass rock insulator	-	-	-	-
Screw and nut	-	-	-	-
Insulation				
Dynaflex	-	-	-	-
Microquartz	0.250	0.438	0.125	0.175
Packaging	0.183	0.190	0.178	0.180
	(0.433)	(0.628)	(0.303)	(0.355)
Subpanel (Ram and Ground Cooling				
Subpanel	-	-	-	-
Closeout and fasteners	-	-	-	-
Standoff	-	-	-	-
TOTAL WEIGHT	0.856	1.127	0.726	0.854

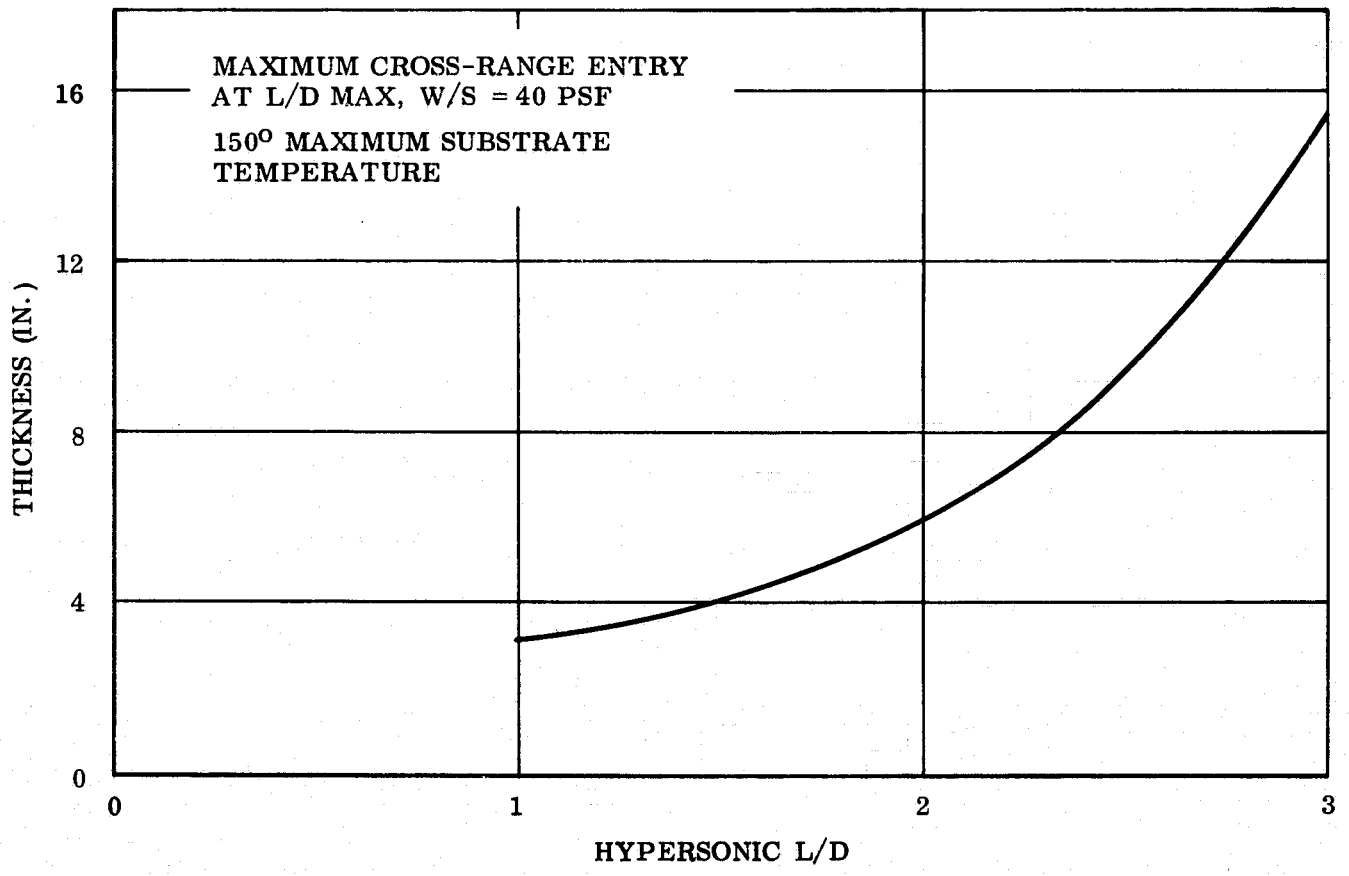

Fig 3-34 Passive Insulation Thickness vs Hypersonic L/D

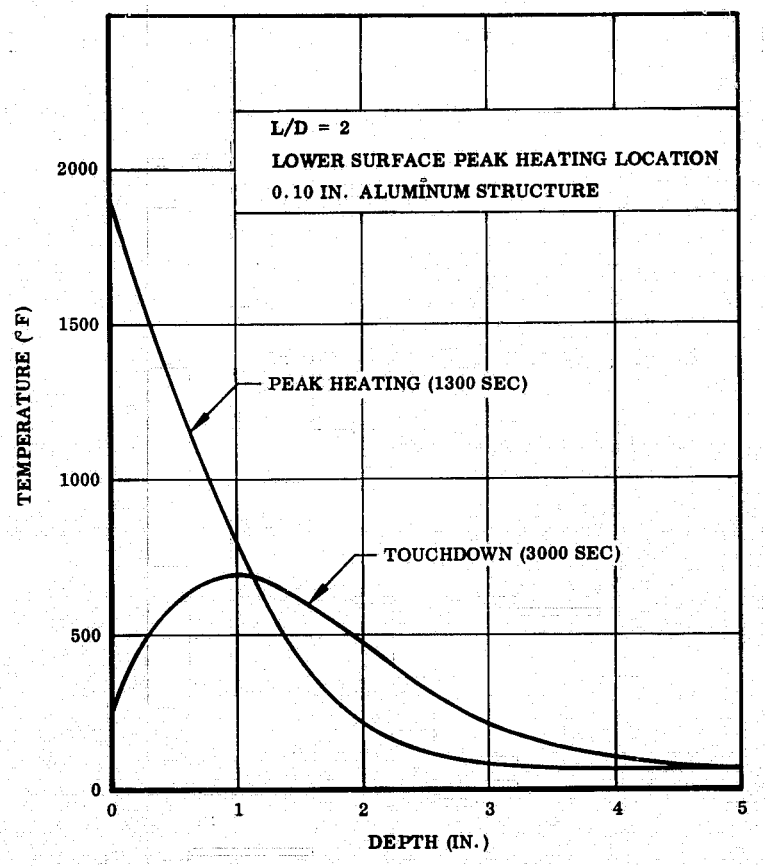

Fig. 3-35 Temperature Distribution Through 5-Inch Passive Insulation

approximately 250°F as a result of radiative cooling and also convective cooling during low speed flight. Figure 3-36 shows the temperature response of the aluminum structure for three insulation thicknesses. Because of the energy stored in the insulation during entry, the structure temperature continues to rise following touchdown and, depending on the particular thickness, reaches a maximum value 2 to 4 hours after touchdown. The results shown in Figs. 3-35 and 3-36 indicate that the large required thicknesses of insulation do not arise from aerodynamic heating during flight but from a post-touchdown heating of the structure on the ground.

Because of the large potential savings in insulation weight, two approaches were considered to alleviate the effects of post-touchdown heating. These are (1) use of either ram air or engine bleed air for cooling during low-speed flight and (2) use of a ground cooling cart after landing. Previous analyses have shown the use of ram air to be superior to engine bleed air because of the large weight penalty required by the bleed air heat exchanger and expansion turbine. Figure 3-37 shows the effect of ram air cooling on structural temperature based on a conservative heat transfer coefficient of 5 Btu/ft^2-hr-°F. Air cooling is assumed to be initiated at M = 0.8 and to be continued to touchdown. By comparing Figs. 3-36 and 3-37, it is seen that use of ram air has only a slight effect on the insulation thickness required to limit the structure to 150°F. A considerably larger effect is shown in Fig. 3-38, wherein ram air cooling is combined with use of ground cooling initiated 10 minutes after touchdown. For the lower surface location, the combined effect of both ram air and ground cooling is seen to reduce the required insulation thickness from 5.7 in. to 3.1 in.

Additional studies conducted at Lockheed show comparable reductions in passive insulation thicknesses for various vehicle locations and entry modes, using ram air/ground cart cooling. In general, insulation unit weight reductions between 45 and 65 percent result, compared to the no cooling values.

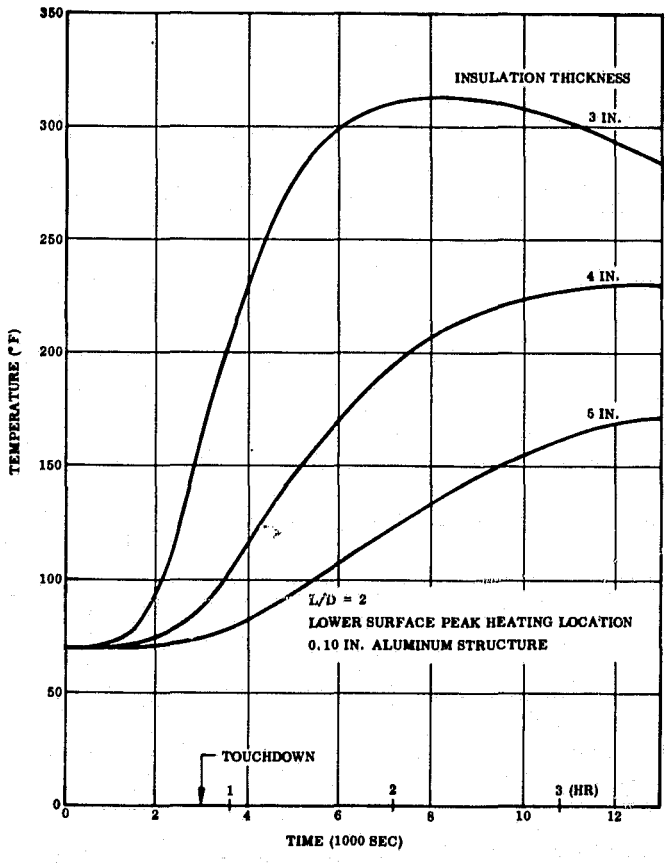

Fig. 3-36 Structure Temperature Histories for Three Insulation Thicknesses

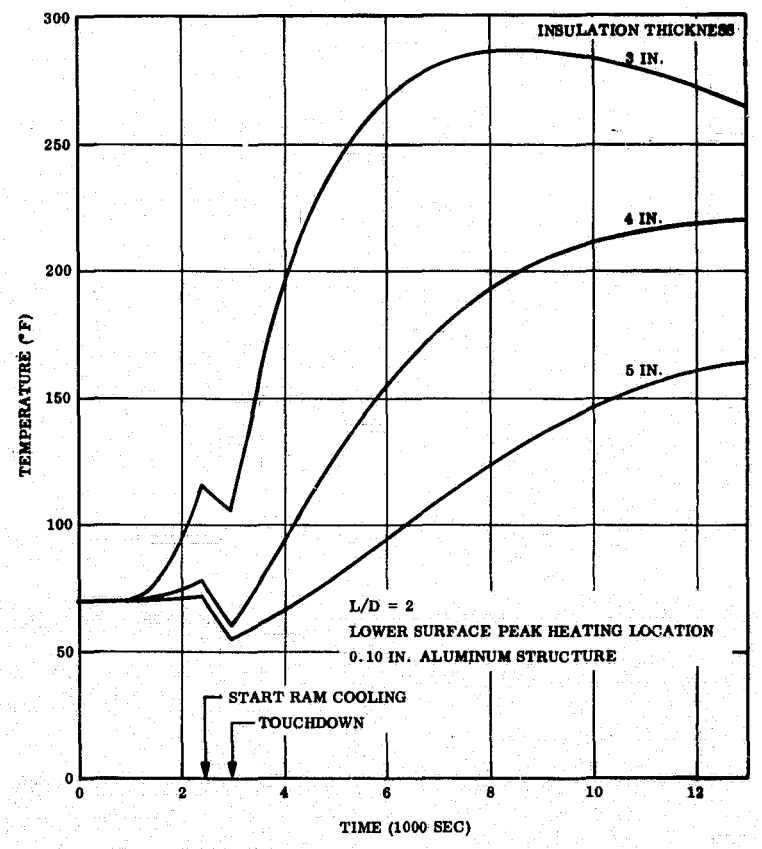

Fig. 3-37 Structure Temperature Histories for Three Insulation Thicknesses (Based on Ram Air Cooling)

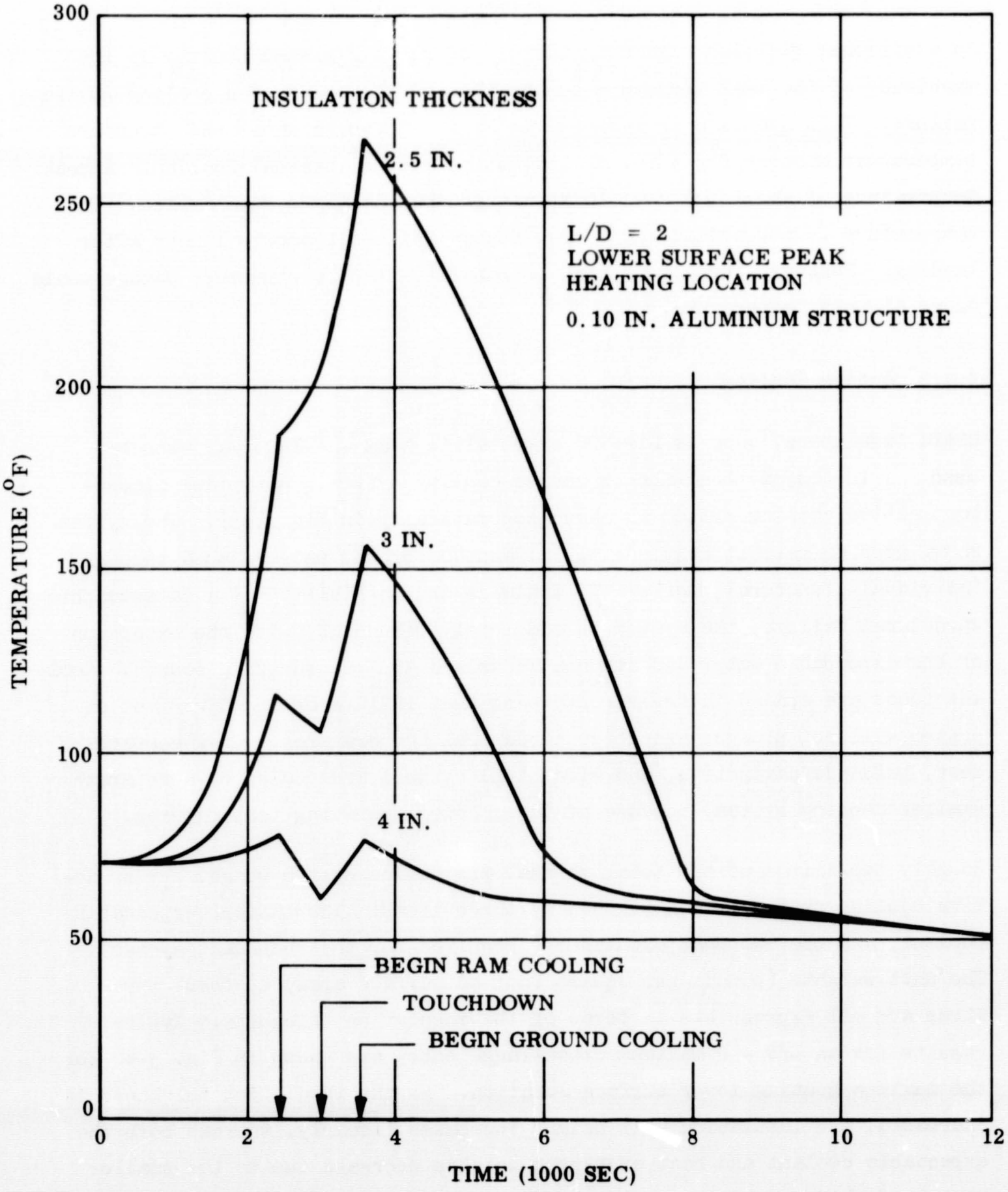

Fig. 3-38 Structure Temperature Histories for Three Insulation Thicknesses (Based on Ram and Ground Air Cooling)

An additional question regarding the use of ram air/ground cooling is the magnitude of the peak structure temperature in the event of a cooling system failure. This question is answered in Fig. 3-36, which shows the structure temperature history for 3 in. of insulation and no internal cooling. A peak temperature of about 300°F would result if the cooling system failed. This temperature is not considered a crew hazard, since it occurs 1 hour after landing. Further, there is a high probability that no structure damage would occur at this temperature.

3.4.2 Active Cooling

Rigid insulators, such as LI-1500 or metallic heat shields, may also be used in conjunction with an active cooling system. A typical closed-loop active cooling system is shown schematically in Fig. 3-39. The system shown uses 60 percent ethylene glycol and 40 percent water pumped through individual structural panels. To minimize the possibility of a catastrophic structural failure, the system is completely redundant, with the exception of the expendable water and ammonia tanks and the pressurizing source. Coolant tubes are spaced in the structure so that failure of one distribution system will not produce excessive structural temperatures. Crew compartment, guidance/navigation, and electrical systems are cooled by a separate smaller cooling system, because of their lower operating temperatures.

Roughly two-thirds of the total thermal protection system weight for an active cooling system is contributed by three items: insulation, expendable coolant, and the two heat exchangers(required for the redundant system). The unit weights (pounds per squart foot of surface area) of these three items are all expressible in terms of the insulation thickness. Typical results for an L/D - 2 maximum cross-range entry are shown in Fig. 3-40 for the maximum heating lower surface location. As the insulation thickness is increased, the insulation unit weight increases linearly, whereas both the expendable coolant and heat exchanger weights decrease due to the smaller heat load absorbed by the cooling system. By summing these three weight items, an insulation thickness may be selected for minimum system weight.

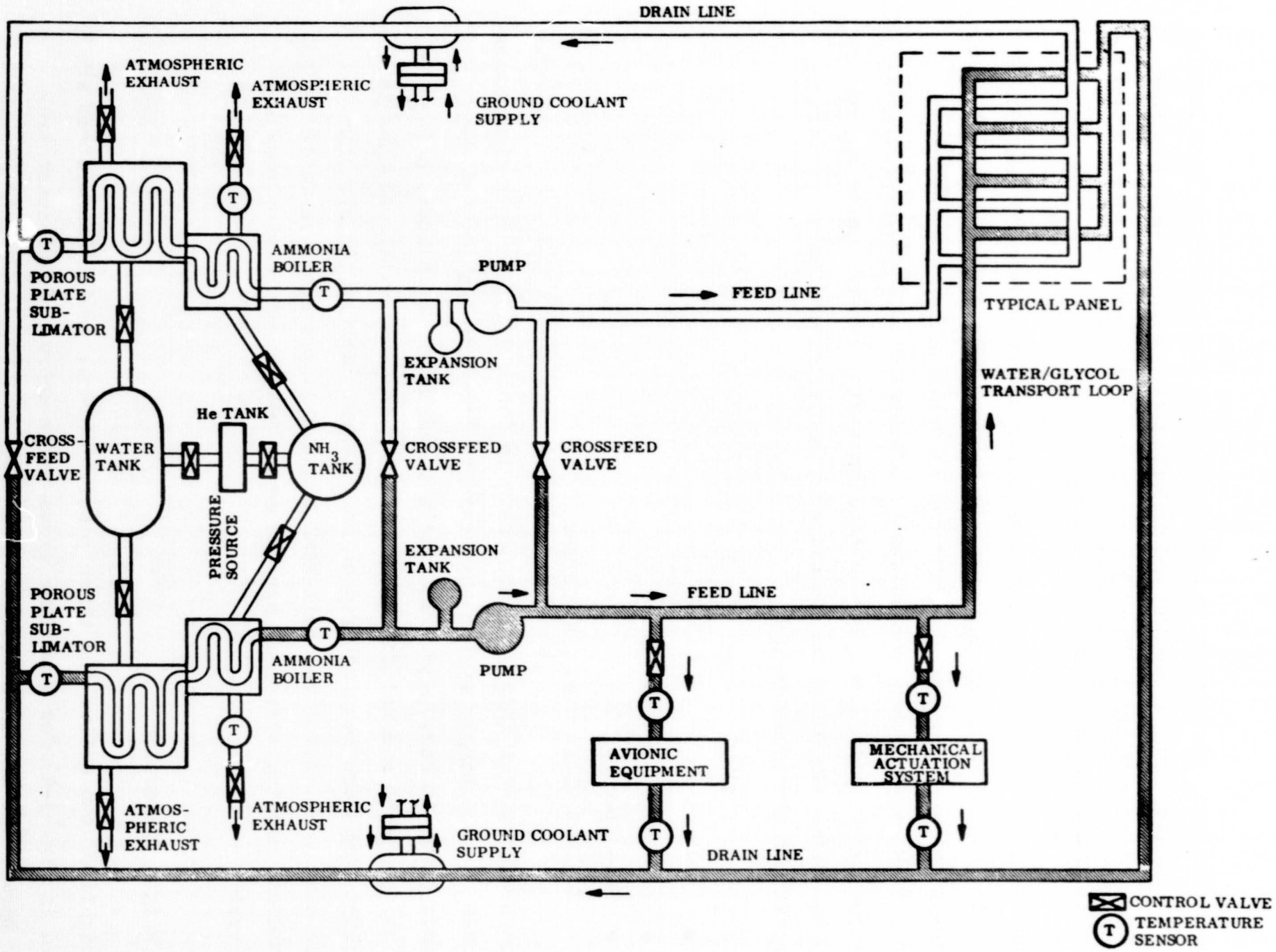

Fig. 3-39 Water/Glycol Cooling System Schematic

For the conditions represented in Fig. 3-40, this thickness is approximately 1.4 in. A similar active cooling weight optimization for a vehicle upper surface location is shown in Fig. 3-41. In this case, the insulation thickness corresponding to minimum weight is about 1 in.

Once the insulation and total coolant requirements have been determined, a large number of calculations are required to arrive at a minimu weight system. Variables requiring consideration include flow rate, tube spacing, tube diameter, flow length, pump weight system pressure drop, and power supply. For LI-1500 material, typical active cooling sizing results based on use of LI-1500 are tabulated below for an L/D = 2, 50 psf wing loading vehicle entering at maximum cross-range.

- Panel size, 3 x 6 ft
- Flow length, 3-ft
- Tube diameter, 0.1-in.
- Tube spacing, 1-in.
- Coolant flow rate, 180 lb/sec

A weight breakdown for this systemis shown in Table 3-19 for both the redundant system and the single system that results from eliminating the dual components shown in Fig. 3-39. The coolant weight shown includes a 20-percent contingency to account for residual and carry-over water and ammonia. The coolant tubes are manufactured as an integral part of the aluminum airframe structure, using the roll-bond technique. As shown in Table 3-19, the redudnant cooling system is approxi mately 20 percent heavier than the single system.

3.4.3 Weight Comparison

Unit weights of two active and three passive thermal protection systems are compared in Fig. 3-42 for a maximum cross-range entry. Significant trajectory parameters are as follows:

- Orbit altitude, 100 nm
- Initial entry angle (γ_e) -1.0°
- Wing loading (W/S), 50 psf
- Entry time from 400,000 ft to touchdown, 50 min.

Unit weights shown in Fig. 3-42 for both the LI-1500 and metallic heat shield concepts are based on the utilization of ram air and ground cooling, as discussed previously. Ablative weights are based on the analysis methods discussed previously and assume a 20 lb/ft^3 partial depth silicone elastomer, including a 4 lb/ft^3 honeycomb core. An ablator bond line temperature of 600°F is assumed. The data shown are based on a spacecraft length of approximately 90 ft (surface area $\sim$ 4000 ft^2); however, the relative weights are applicable to larger vehicles, since all the systems are sized on the basis of one lower and one upper surface insulation (or ablator) thickness.

The maximum cross-range thermal protection system weight comparison (Fig. 3-42) indicates a minimum weight system results from the use of LI-1500, either passively or with active cooling. The large corrugated metallic heat shield weight is about 3% higher. Post-supported metallic heat shields are heavier, particularly with active cooling. The 20 lb/ft^3 silicone ablator provides the second highest unit weight and is also unattractive because of its replacement requirement.

Lifting entry vehicle thermal protection system weight comparisons for maximum down-range entry show that a minimum weight system, for either rigid insulators or metallic heat shields, results from the use of active cooling. For example, on the Lockheed/AFFDL FDL-5 high L/D entry vehicle with metallic heat shield, the average unit weight is 4.8 lb/ft^2 for passive cooling and 4.1 lb/ft^2 for active cooling. This information, entry trajectory, and associated characteristics have been discussed extensively in the literature. Minimum thermal protection system weight with active cooling results from the greater time required for maximum down-range entry. For example, the trajectory used for the above comparison required about 6000 seconds total entry time (400,000 ft to touchdown).

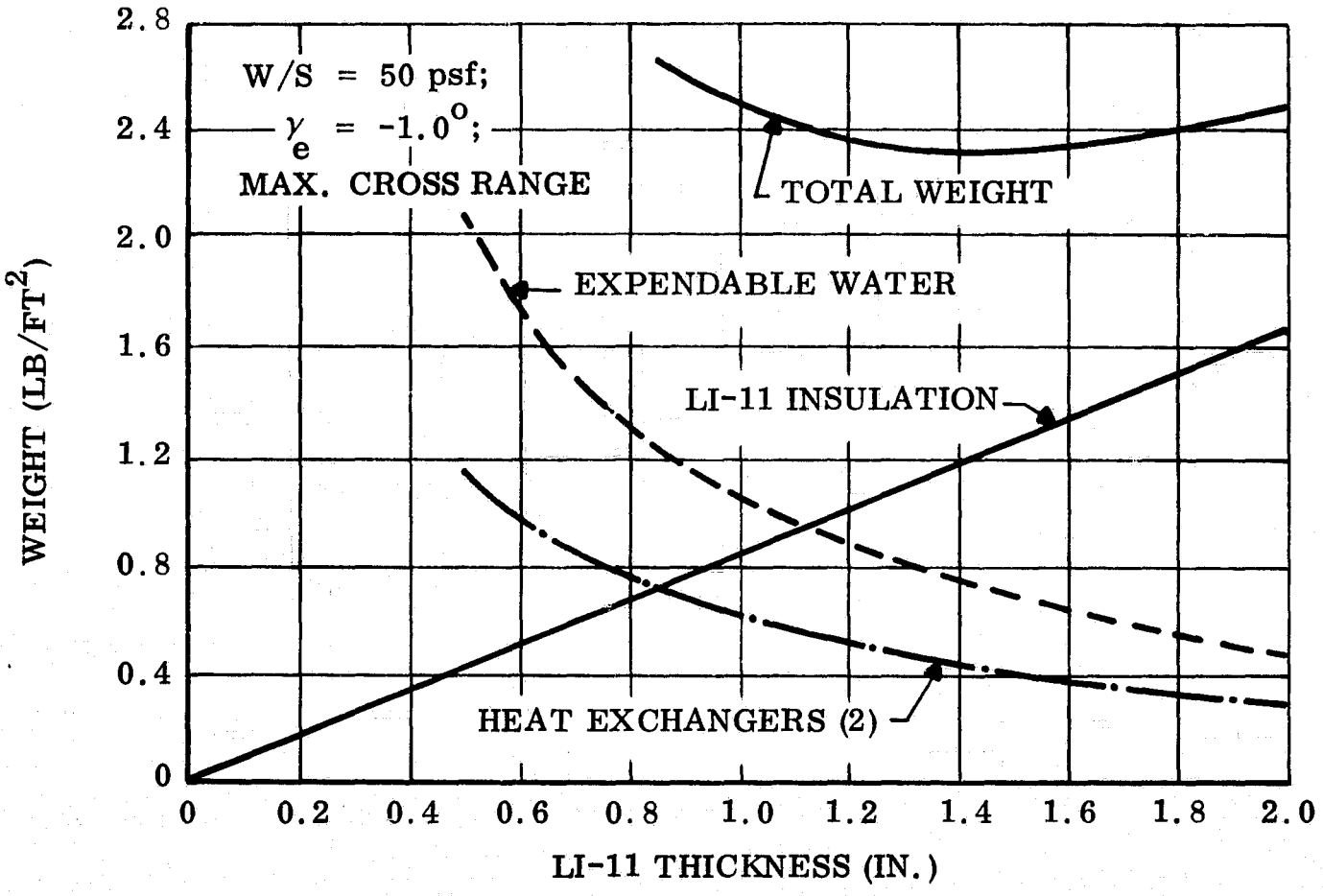

Fig. 3-40 Active Cooling Optimization - L/D = 2.0 Lower Surface

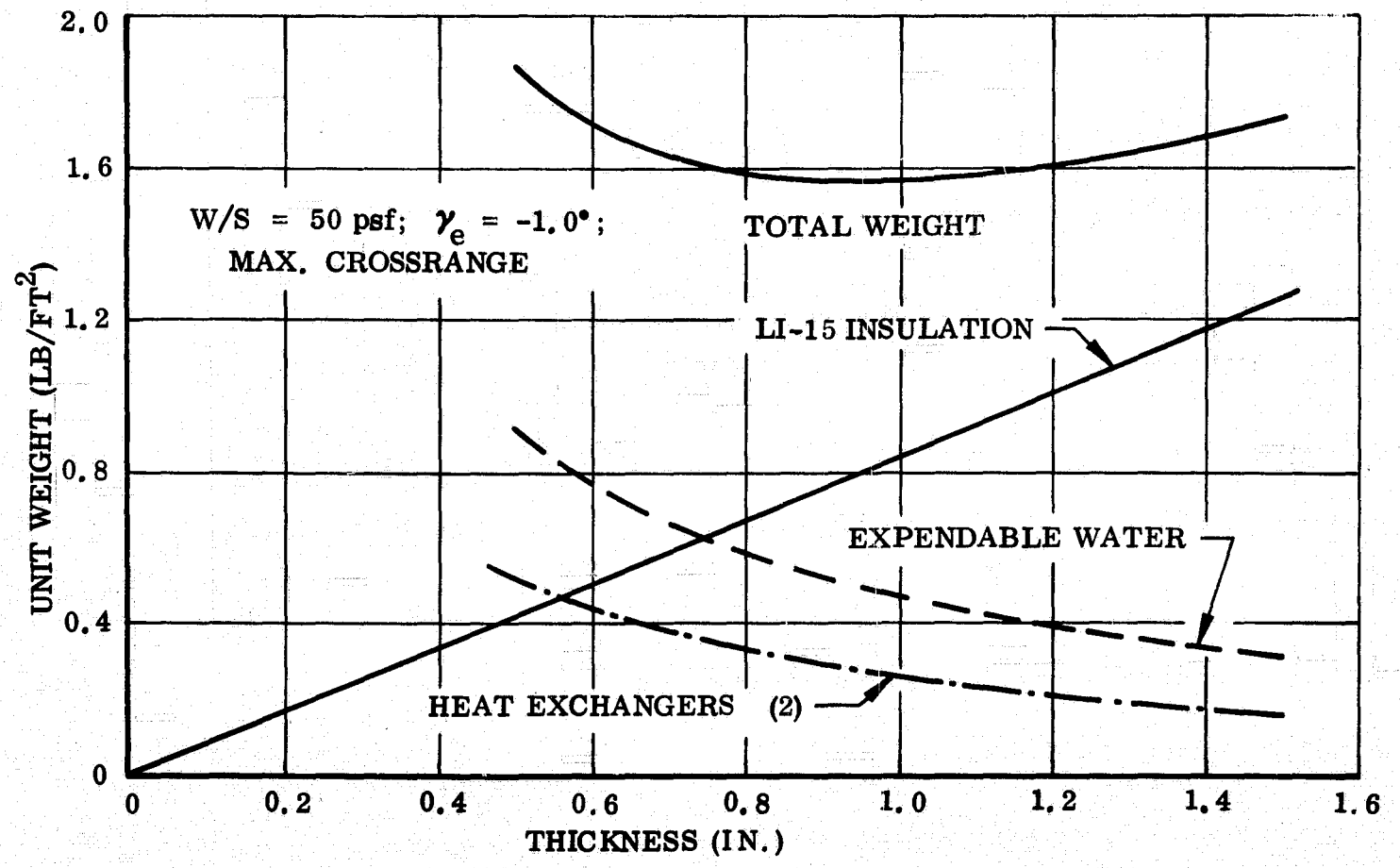

Fig. 3-41 Active Cooling Optimization - L/D = 2.0, Upper Surface

Table 3-19

WEIGHT SUMMARY - LI-1500 ACTIVE SYSTEM

	Weight-(lb) Single	Redundant
Lower surface, LI-1500 (1.4 in.)*	2500	2500
Upper surface, LI-1500 (1.0 in.)*	2250	2250
Expendable coolant (20% contingency)	2227	2227
Heat exchanger	773	1546
Glycol (panel, feed and drain, and supply)	1050	1900
Batteries	399	683
Feed and drain hardware	119	238
H_2O tank and pumping	110	110
Misc. (pumps, accumulators and hdwe)	35	64
Total (lb)	9463	11518
Unit weight (lb/ft^2)	2.56	3.12

*Includes 0.020 in. cr coating at 60 lb/ft^3

3.4.4 Recommendations

Thermal protection system weight comparisons indicate the following:

- For maximum cross-range entry:

  Use of rigid insulators, typified by LI-1500, results in minimum weight when used passively or with active cooling.

  Metallic heat shield concepts are competitive, except with active cooling.

- For maximum down-range entry:

  Active cooling compared to passive results in minimum weight.

Regardless of the reentry mode, use of active cooling is believed to introduce serious reliability problems. For example, the aerodynamically heated surface area of current ILRV configurations can be as large as 20,000 ft^2. For optimum panel and tube spacing, this heated area requires approximately 50,000 individual tubes and twice as many connections. The curve shown in Fig. 3-43 illustrates the resulting maximum structure temperature versus insulation thickness for no structural cooling. These results are valid for either LI-1500 or the metallic heat shield concept with entry at maximum cross range. Active cooling insulation thicknesses that provide minimum system weight generally vary between 1 and 1.5 in. for windward vehicle locations. Should a cooling system failure occur prior to or early in the entry maneuver, the aluminum structure could seriously overheat, as shown in Fig. 3-43.

An additional factor concerning active cooling systems is that, while these systems provide minimum weight for maximum down-range entry, this benefit is somewhat misleading in that a slight delay in deorbit time will shift the entire footprint down range. Therefore, it is somewhat questionable to select the thermal protection system based on maximum down-range entry.

On the basis of the above considerations, it is recommended that active cooling thermal protection systems not be considered for use on the Space Shuttle.

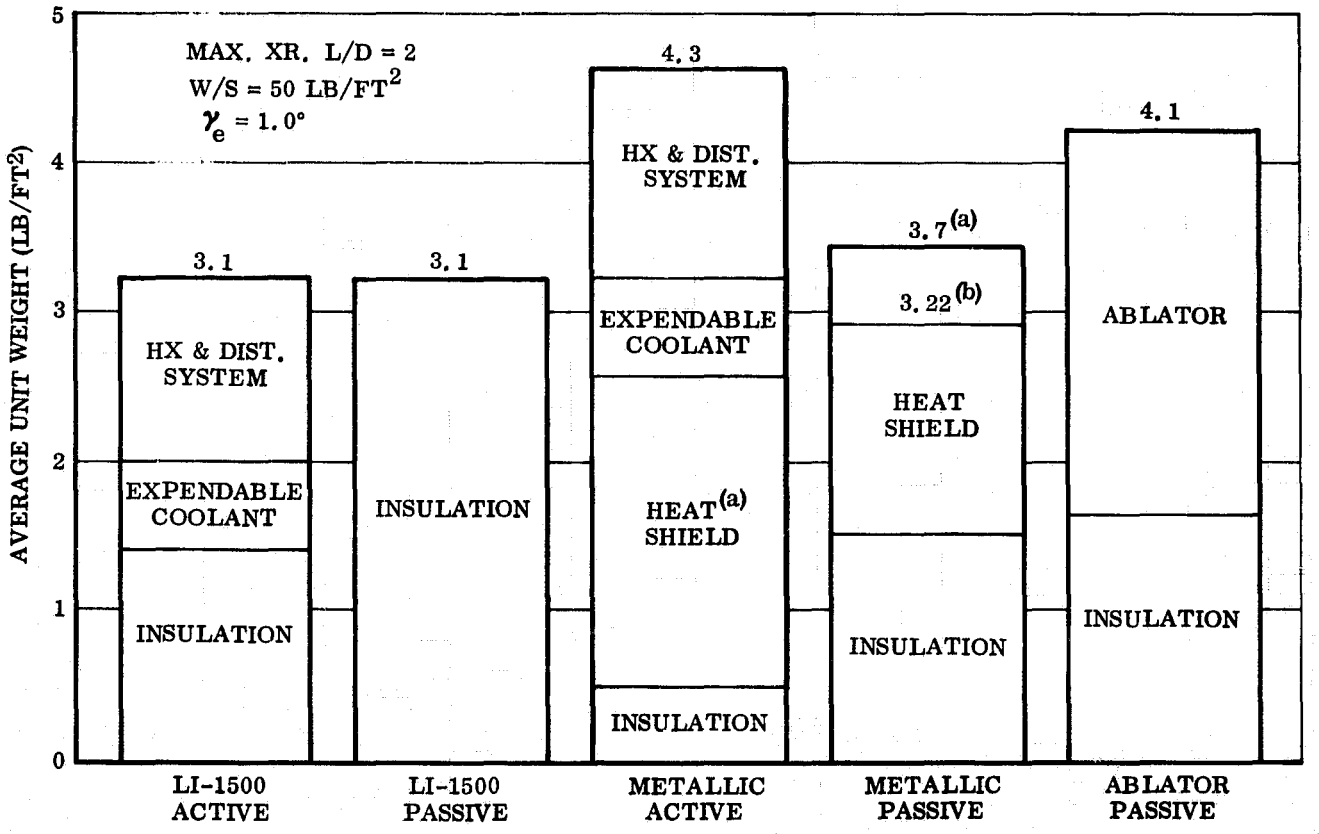

(a) WEIGHT FOR POSTSUPPORTED HEAT SHIELD.

(b) WEIGHT FOR LARGE CORRUGATED HEAT SHIELD.

Fig. 3-42 Thermal Protection System Comparison

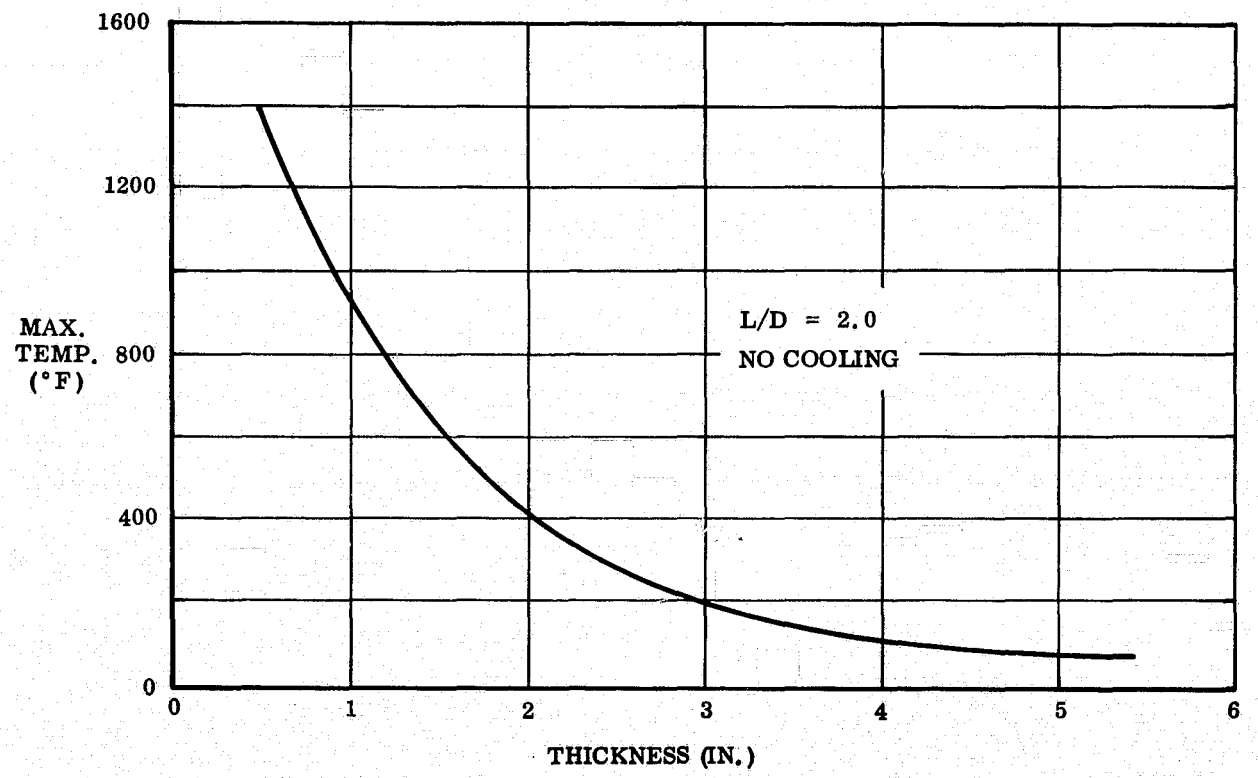

Fig. 3-43 Maximum Substrate Temperature vs LI-1500 Thickness

3.5 PARAMETRIC STUDIES

Lifting entry vehicle aerodynamic heating levels and their impact on thermal protection system selection are influenced by a large number of parameters. These may be broadly classified as follows:

Heating parameters:

- Heating prediction methods
- Inviscid flow field prediction methods
- Boundary layer transition

Vehicle parameters:

- Geometry
- Weight
- Aerodynamic coefficients
- Surface characteristics (roughness, emittance, etc.)

Trajectory parameters:

- Orbit characteristics
- Initial entry conditions
- Entry footprint requirements (vehicle attitude)

For a given vehicle geometry, it is convenient to prepare a series of curves that establish the reentry heating boundaries for given temperature limits and vehicle attitudes. Such curves define the allowable entry corridor available for maneuvering and are also useful for illustrating parametric study results.

3.5.1 Entry Heating Boundaries

Minimum flight altitudes based on lower surface temperature limits of 2100, 2300, and 2500°F are shown in Figs. 3-44, 3-45, and 3-46, respectively. These curves are based on radiation equilibrium conditions and exclude the first 5 ft aft of the stagnation point, where use of a material with higher temperature capability is assumed. The configuration assumed to generate the minimum altitudes is a slab delta wing with 78-deg sweep.

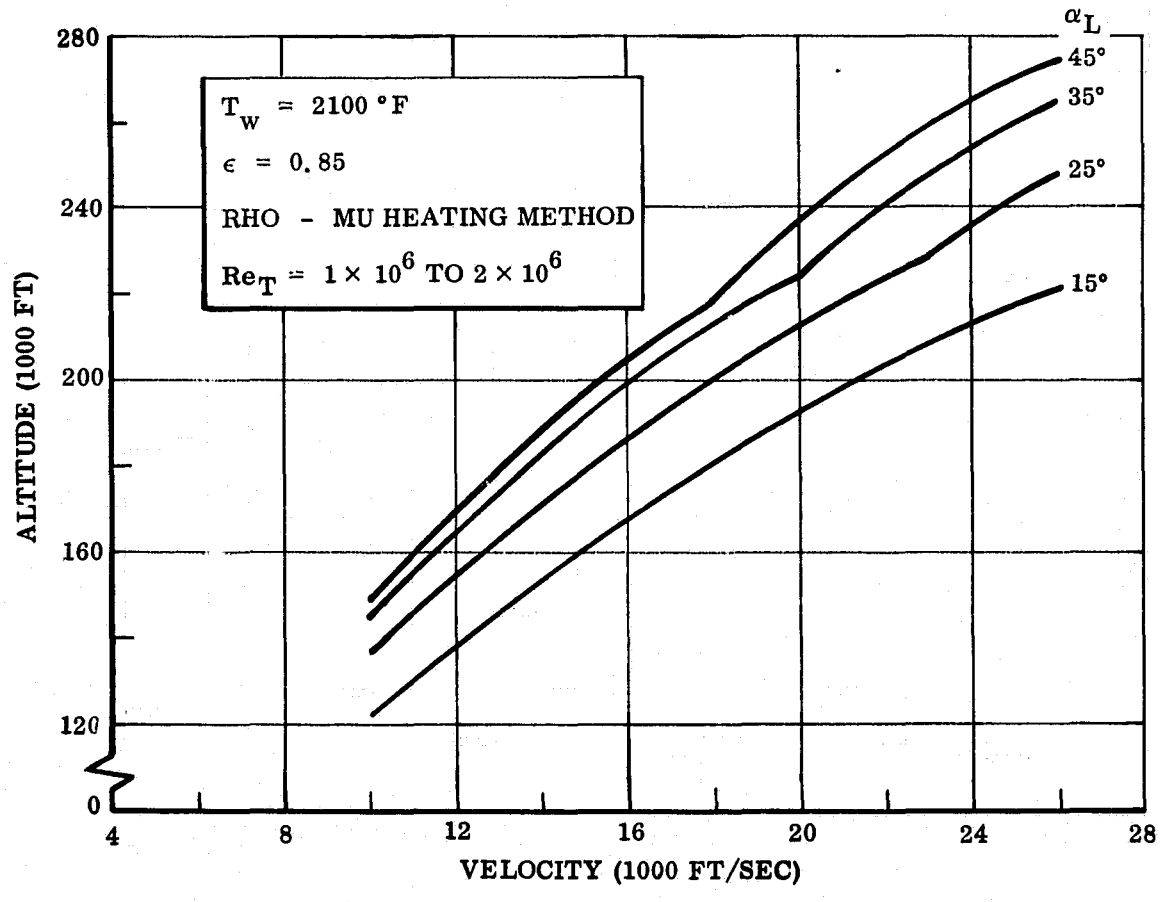

Fig. 3-44 Minimum Altitude Based on Lower Surface Heating Constraints, T_W = 2100° F

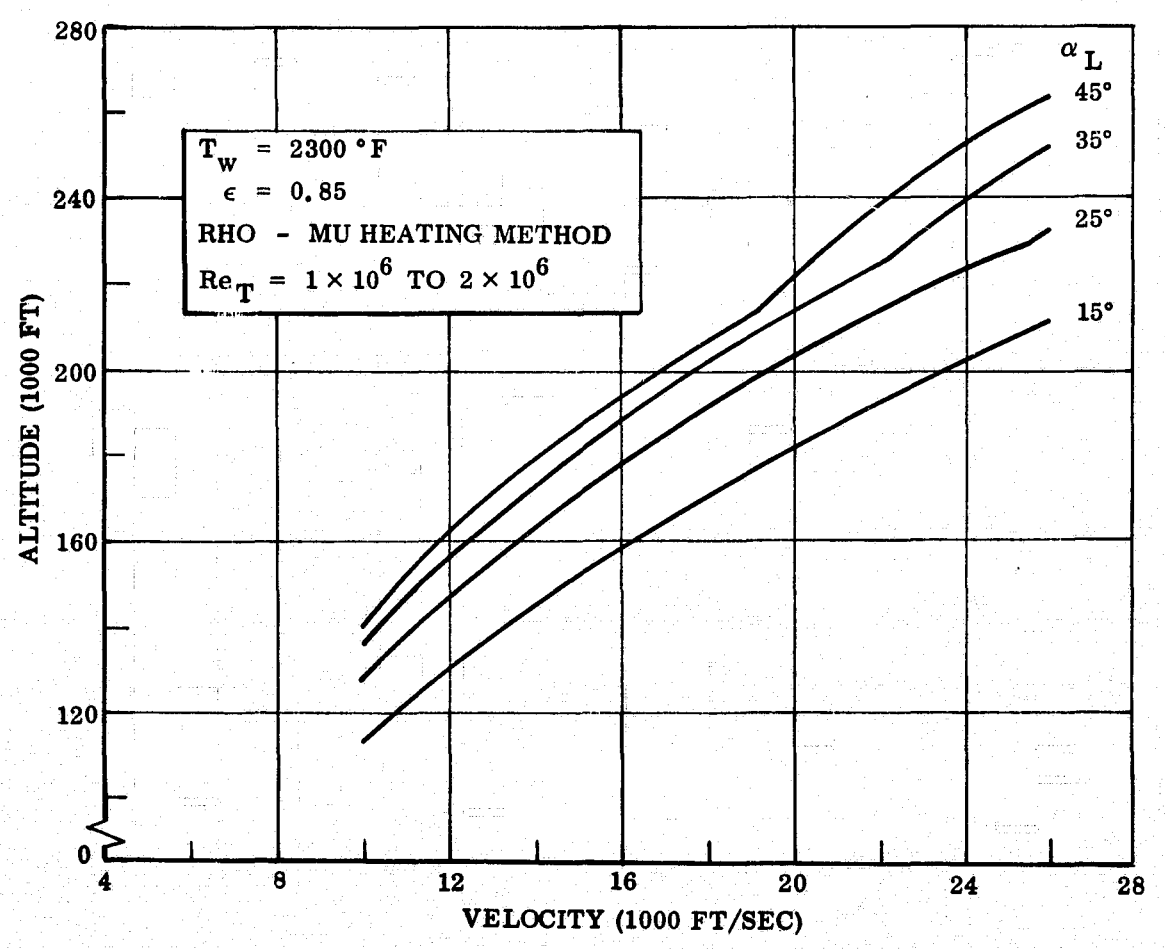

Fig. 3-45 Minimum Altitudes Based on Lower Surface Heating Constraints, T_W = 2300°F

At the higher velocities, the altitude limits are determined by laminar heating at the start of the lower surface heat shield (X = 5 ft). At lower velocities the altitude limits are determined by turbulent heating at the location of boundary layer transition on the forward ramp. The heating boundaries are shown as a function of forward ramp local angle of attack (α_L) which is equal to vehicle angle of attack plus the ramp angle. By superimposing unbanked equilibrium glide entry profiles on these heating boundary curves, a direction measure of the allowable bank angle may be obtained for various angles of attack and velocities. Entry performance studies may then be conducted, with the resulting allowable bank angle variation used to determine maximum cross range for a given temperature level. Results of such studies are presented in the following paragraphs.

3.5.2 Reentry Corridor

Figure 3-47 is an altitude-velocity plot illustrating the wings-level entry profile for a planform loading of 50 lb/ft^2. The lower surface heating boundary for a temperature of 2200°F is also shown. Both curves assume a vehicle angle of attack of 35 deg. The minimum altitude difference between the two curves is defined as the entry corridor (ΔH) and is a measure of the altitude available for cross-range maneuvering, since achieving cross-range requires banking the vehicle which, in turn, lowers the equilibrium altitude. The velocity at which the corridor occurs depends on the heating boundary temperature limit and on the type of boundary layer flow; for laminar flow, ΔH occurs at approximately 21,000 fps whereas for turbulent flow, ΔH occurs at about 18,000 fps.

By varying the vehicle angle of attack, wing loading, and heating boundary temperature, a series of curves similar to Figure 3-47 may be generated. For a given wing loading, the corridor may then be plotted as a function of vehicle angle of attack for various temperatures. A typical plot is shown in Figure 3-48 for W/S = 50 lb/ft^2. The curves for different heating boundary temperatures (2100 to 2500°F) are denoted by the velocity at which the corridor

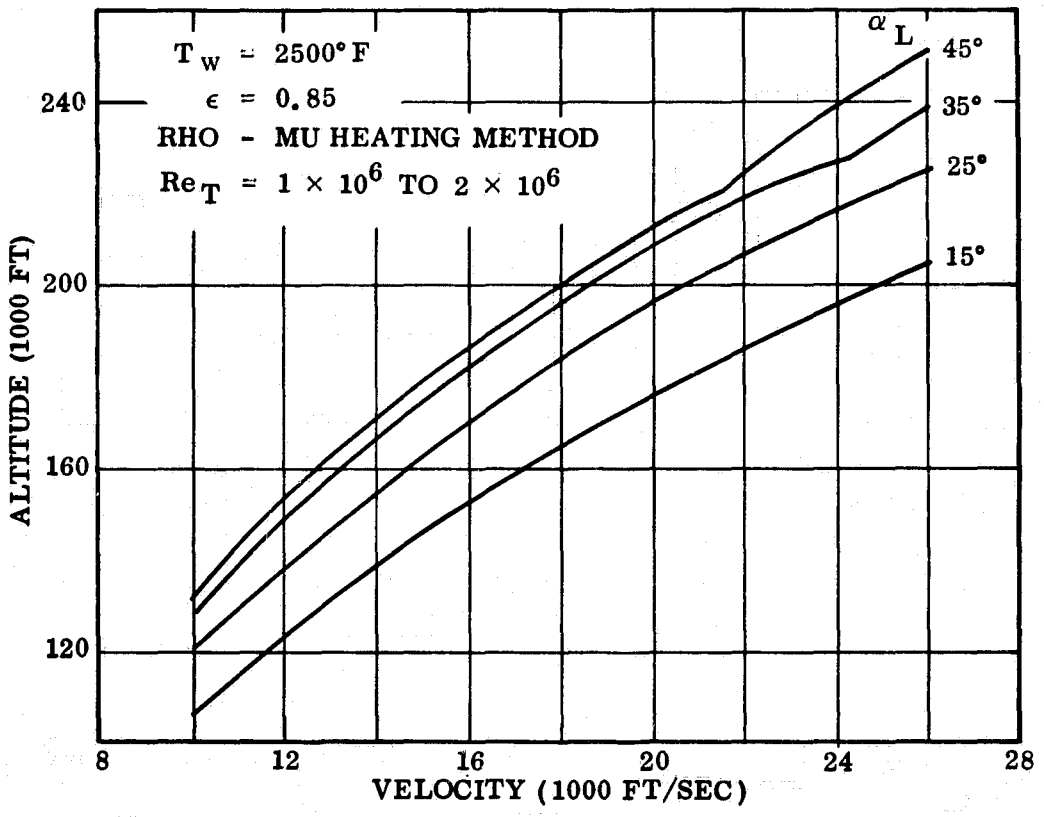

Fig. 3-46 Minimum Altitudes Based on Lower Surface Heating Constraints, T_W = 2500°F

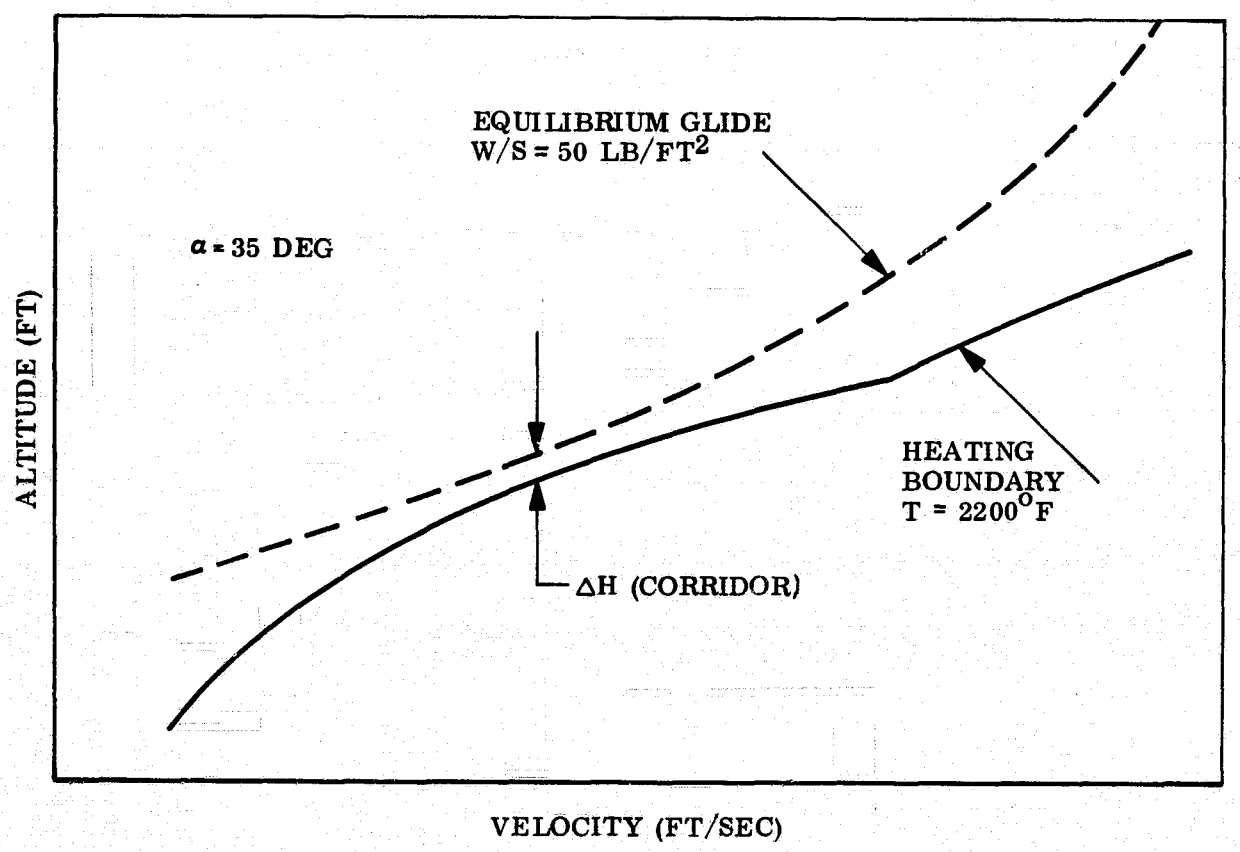

Fig. 3-47 Unbanked Entry Profile and Heating Boundary

occurs. From the data of Figure 3-48, vehicle angles of attack may be selected to result in maximum corridor for each temperature. For example, with a temperature boundary of 2100°F, an angle of attack of 25 provides the maximum ΔH. For 2500°F, an angle of attack of 45 deg is optimum. For a range of wing loadings between 30 and 80 lb/ft^2, the angle of attack for maximum corridor is independent of wing loading, since varying the wing loading displaces the curves of Figure 3-48 in the vertical direction only.

Figure 3-49 shows the altitude corridor versus wing loading with heating boundary temperature as a parameter. As discussed above, each temperature curve corresponds to a particular angle of attack. Several important points may be drawn from this figure. First, for a heat shield temperature limit of 2100°F, the vehicle wing loading cannot exceed 50 lb/ft^2 whereas a design limit of 2200°F allows wing loadings up to approximately 65 lb/ft^2. In other words, changing the heat shield allowable temperature by only 100°F, permits the wing loading to be increased by about 15 lb/ft^2. In general, low wing loadings are undesirable because of the increase in vehicle length and, in turn, launch weight, which results for a given basic configuration.

Figure 3-49 also illustrates wing loading limits for various corridor altitudes. In effect, the corridor may be considered as an altitude margin or design tolerance. For a corridor of 20,000 ft and a heat shield temperature limit of 2200°F (the assumed limit of TD-NiCr), a wing loading less than 25 lb/ft^2 is required. Considering various sources of altitude error during entry such as guidance and control, initial entry conditions, atmospheric dispersions, and required tolerance for uncertainties in aerodynamic heating prediction, an altitude margin of 20,000 ft is probably required. These considerations lead to the conclusion that a lower surface heat shield temperature capability of about 2500°F is most desirable to allow flexibility in wing loading and also altitude margin.

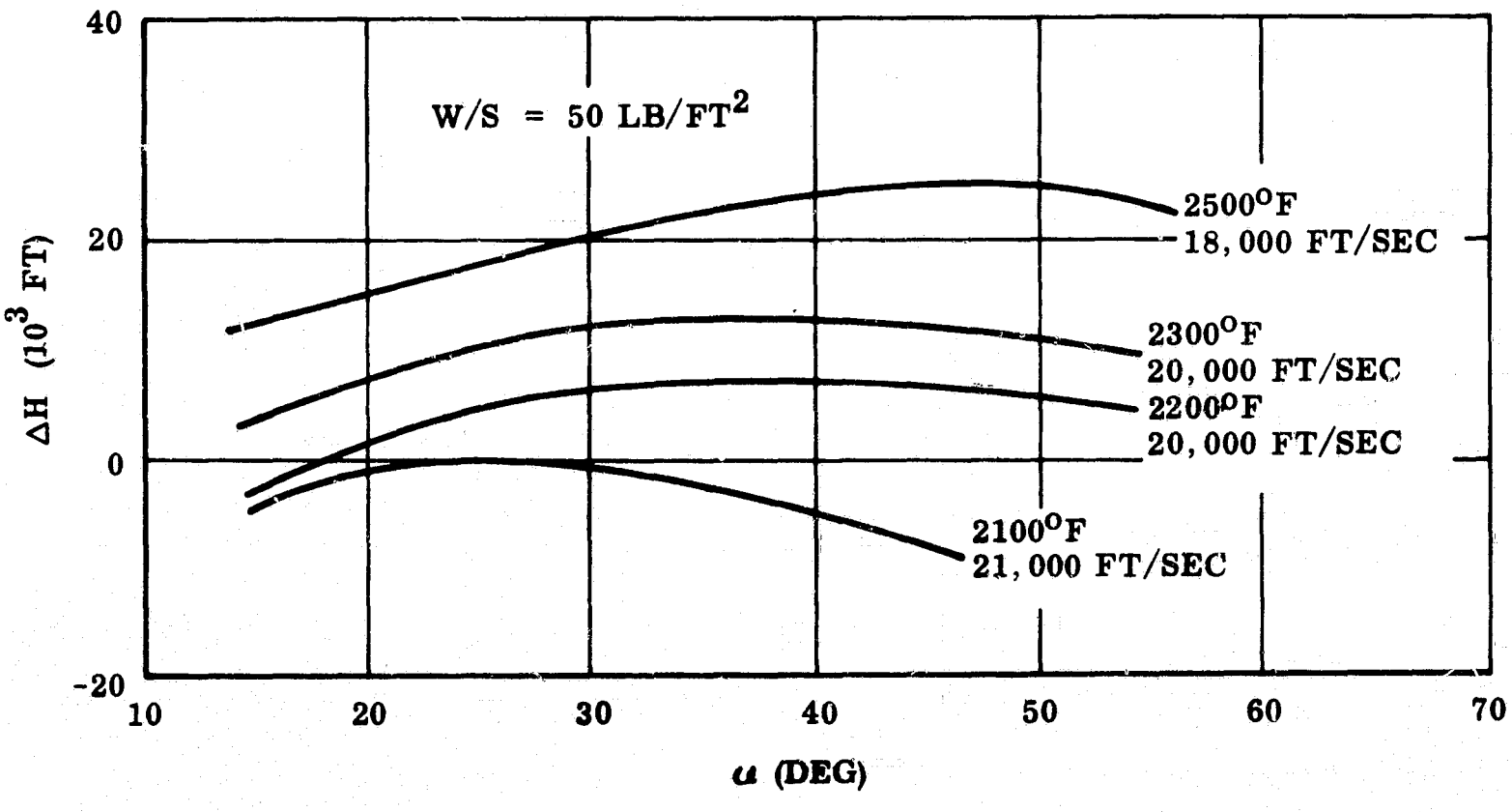

Fig. 3-48 Corridor vs Angle of Attack

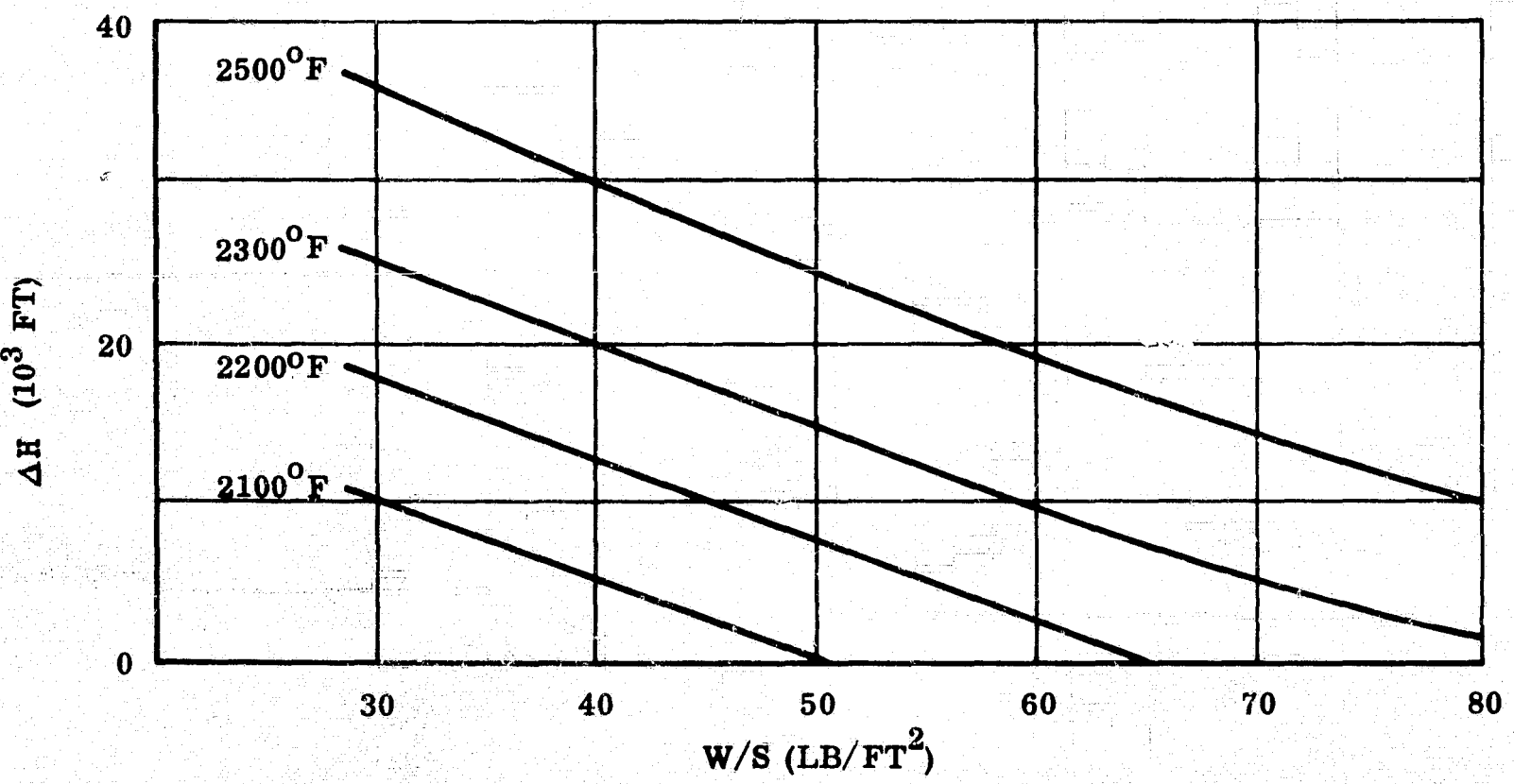

Fig. 3-49 Corridor vs Wing Loading

3.5.3 Heating Parameters

The effect of aerodynamic heating uncertainties on the lower surface heating boundaries is illustrated in Figures 3-50 and 3-51. These figures show how the heating boundaries presented in par. 3.5.1 would change, dependent on the assumptions made regarding turbulent heating theory, surface emittance, flow field, and transition criteria. For example, at 18,000 ft/sec and a local angle of attack of 20 deg, the heating boundary would increase by 11,700 ft if the reference enthalpy method had been selected as the basic turbulent heat transfer theory instead of the rho-mu method. The assumptions regarding flow field and heating theory have a significant influence on heat shield material selection and vehicle performance. The uncertainties regarding surface emittance and flow field can be reduced by test and analysis, but the appropriate heating theory and transition criteria can only be established through a flight test program.

3.5.4 Vehicle Parameters

The effect of wing loading on the reentry corridor is discussed in par. 3.5.2. From equilibrium glide relations, it can be shown that the absolute surface temperature varies with wing loading to the 1/8 power for laminar flow and to the 1/5 power for turbulent flow. Figure 3-52 shows the effect of wing loading on surface temperatures at several locations on the orbiter, based on a wings-level equilibrium glide at a velocity of 20,000 ft/sec and vehicle angle of attack of 25 deg. At the leading edge stagnation line, the unit heat shield weight increases by 0.10 lb/ft^2 per 10 psf increase in wing loading for the LI-1500 system. The corresponding value is 0.04 lb/ft^2 for the metallic heat shield with dynaflex/microquartz insulation.

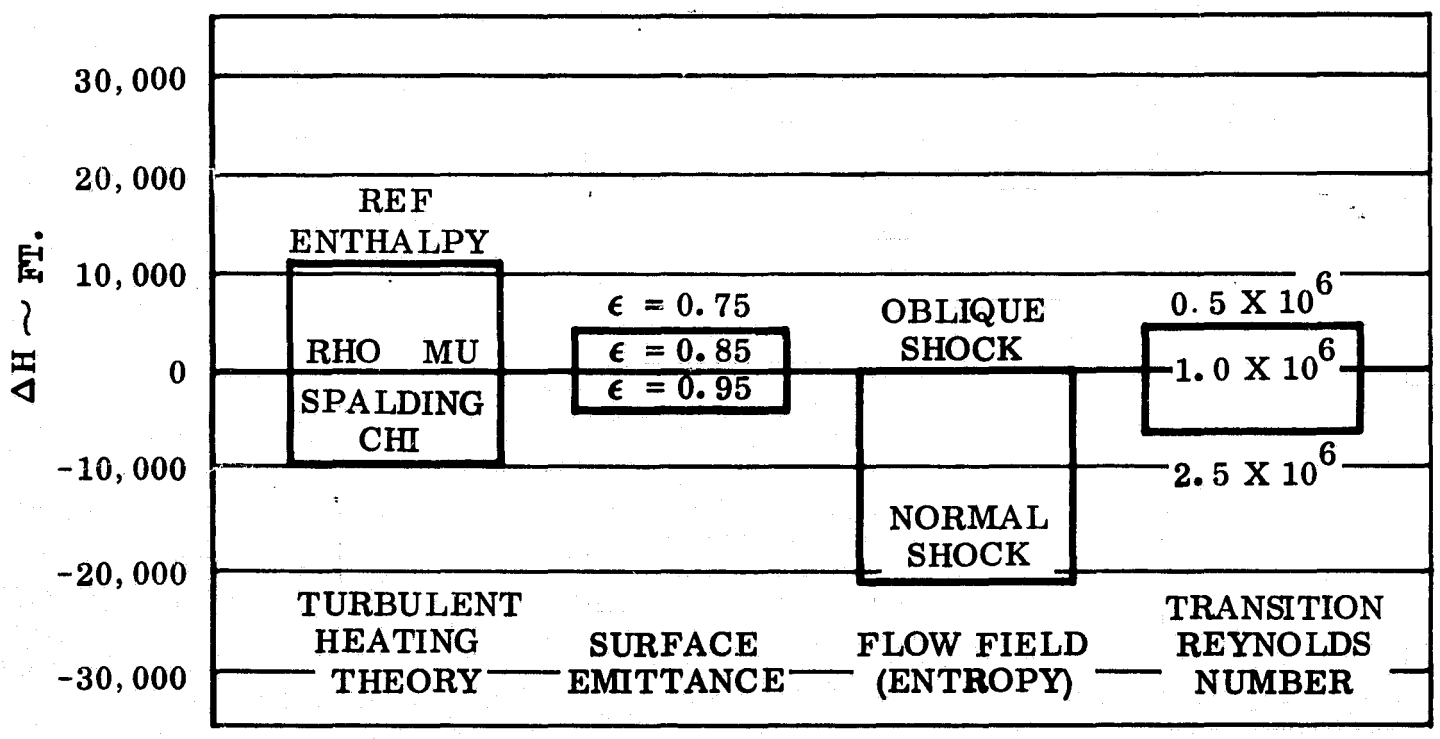

Fig. 3-50 Altitude Sensitivity to Heating Parameters (V_∞ = 18,000 fps, α_L = 20 deg)

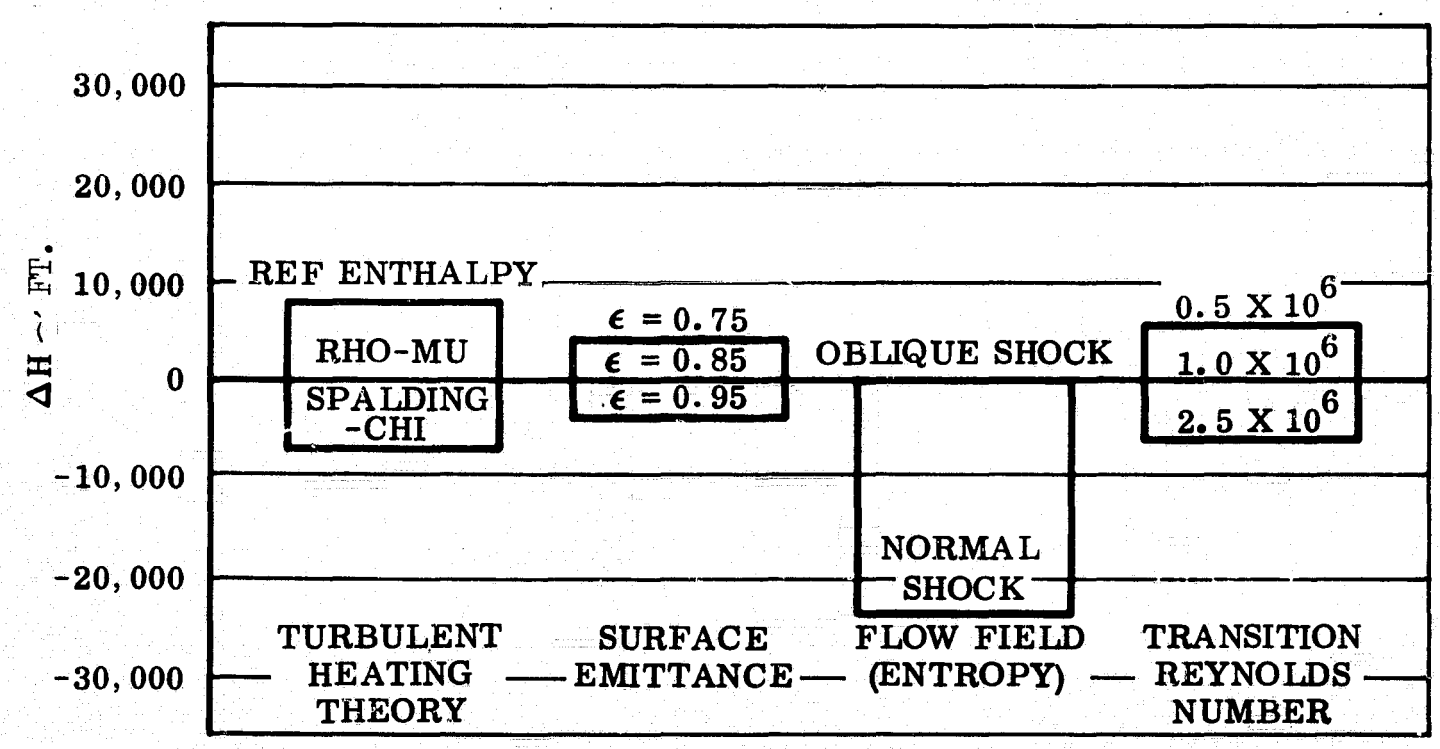

Fig. 3-51 Altitude Sensitivity to Heating Parameters (V_∞ = 18,000 fps, α_L = 40 deg)

Figure 3-53 shows the effect of angle of attack on surface temperatures at several locations on the orbiter. All calculations were based on wings-level equilibrium glide at a velocity of 20,000 ft/sec and wing loading of 50 lb/ft^2. A significant reduction in nose cap temperature results from increasing the angle of attack. Although not shown in Figure 3-53, temperatures at all leeward surface locations and the fin leading edges are also reduced. The body leading edge temperature remains nearly constant, whereas the lower surface temperatures increase slightly with increasing angle of attack.

3.5.5 Trajectory Parameters

From a heating standpoint, the most significant trajectory parameters are the initial entry conditions and the cross range requirements. The initial entry conditions determine the altitude and velocity at pullup, which is generally the peak laminar heating point for lifting entry spacecraft. To achieve large cross range, the spacecraft must enter at relatively small angle of attack to increase the L/D. This, coupled with the decrease in vertical lift coefficient due to banking, results in lower flight altitudes and therefore sizable heating increases on the nose cap, fin leading edge, and leeward surfaces. The increase in peak temperature can be minimized by modulating bank angle during entry so that the bank angle is small during peak heating. The trajectories discussed in par. 3.1 use bank angle modulation to maintain a constant 2200°F lower surface temperature during periods of high heating.

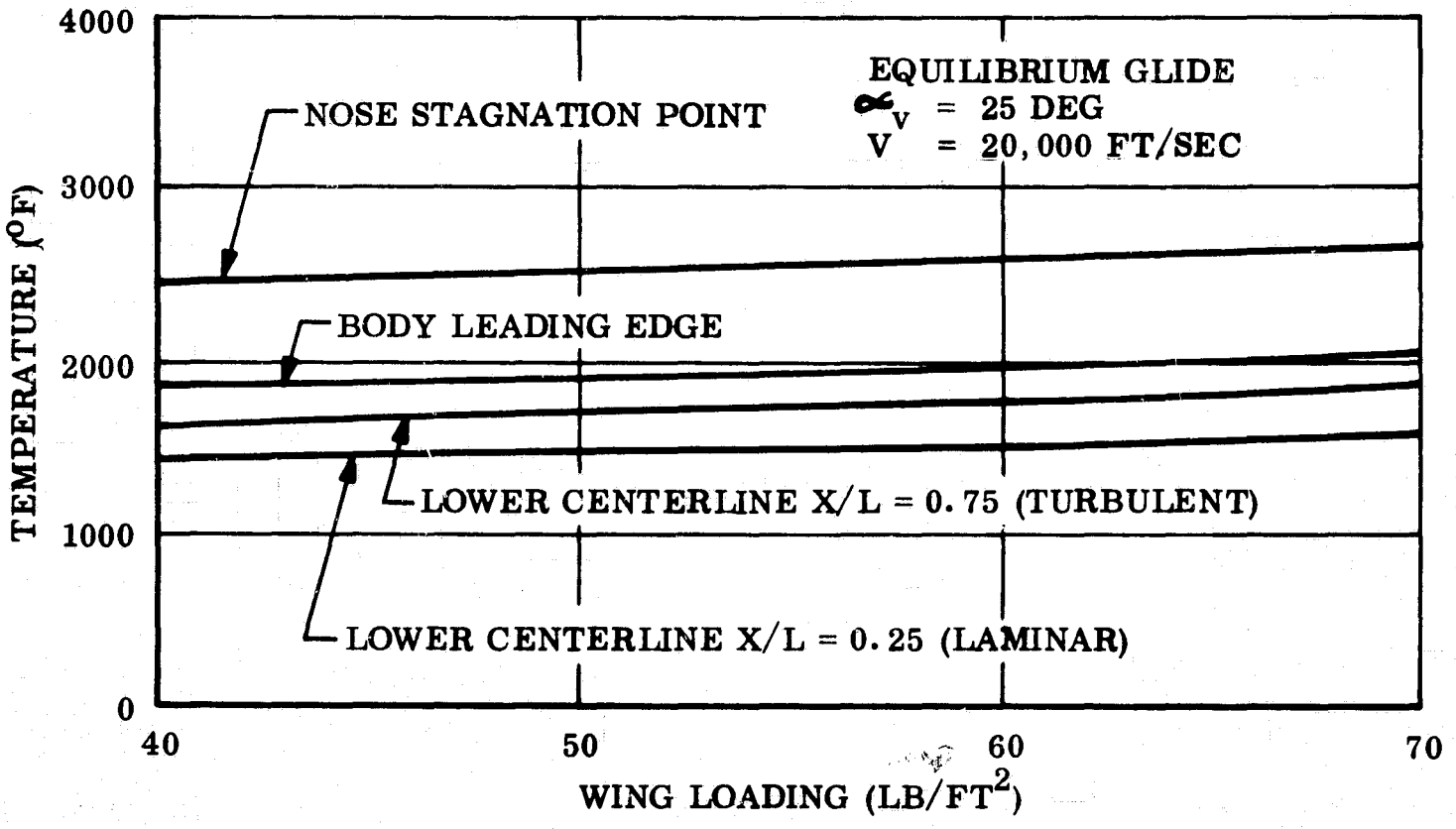

Fig. 3-52 Effect of Wing Loading on Surface Temperature

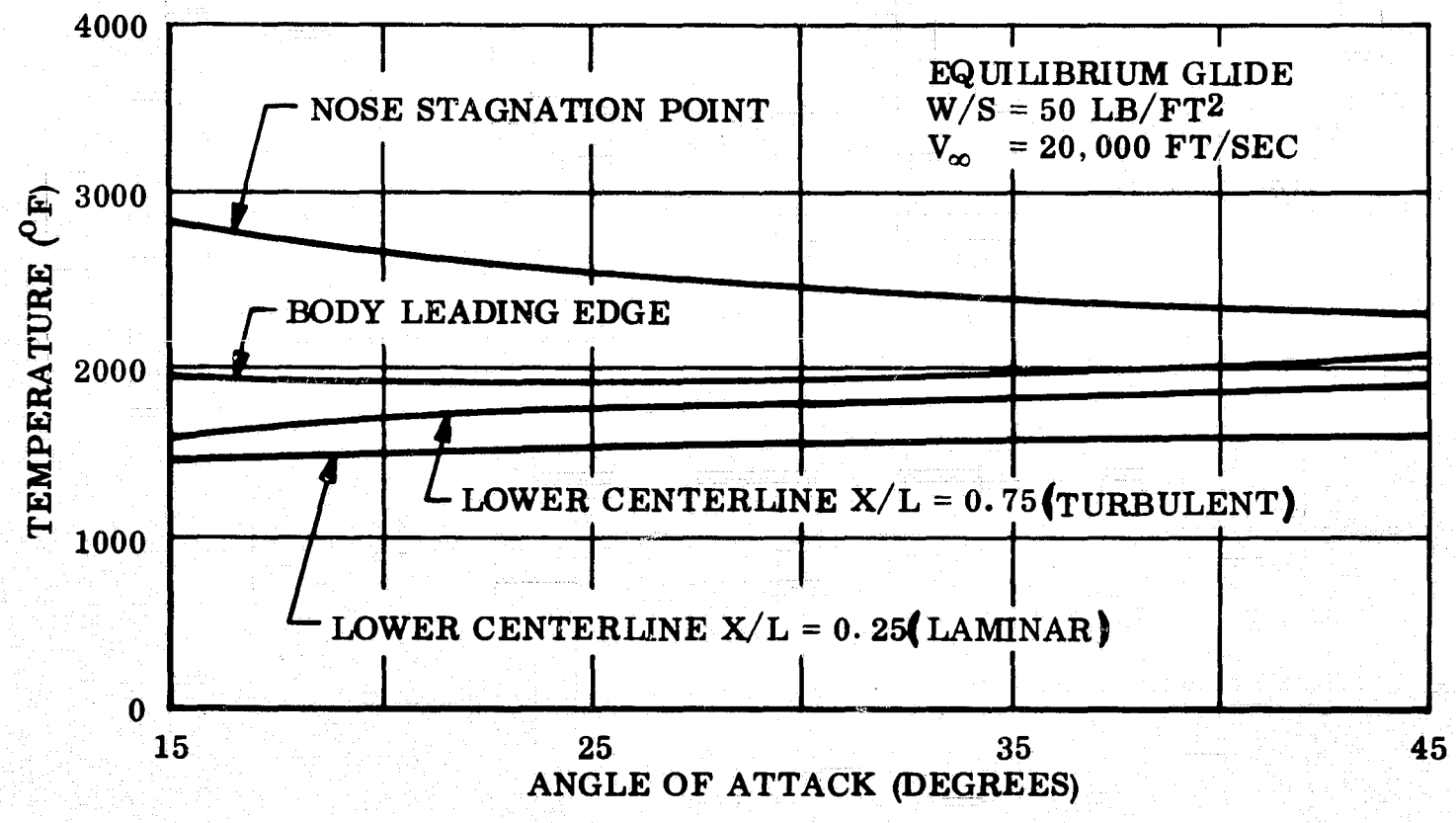

Fig. 3-53 Effect of Angle of Attack on Surface Temperature

Figure 3-54 shows the effect of cross range on peak surface temperature at six locations on the orbiter, based on the temperature constrained trajectories discussed in par. 3.1. As noted previously, large cross range results in higher temperatures on the nose cap, fin leading edge, and leeward surfaces. Table 3-2 shows the percentage of surface area that experiences various peak temperature levels for cross ranges of 0, 500, 1000, and 1500 nm. This table shows that the impact of cross range on heat shield material selection is small, primarily as a result of modulating bank angle during peak heating to avoid excessive temperature.

Although cross range has little effect on heat shield material selection, it has a large effect on insulation weight. This is due primarily to the increased entry time (i.e., total heat input) associated with increasing cross range. Figure 3-55 shows how total heat input at six locations on the orbiter varies with cross range. Figures 3-56 and 3-57 show the variation of heat shield unit weight with cross range for the LI-1500 and metallic heat shield concepts. Pertinent assumptions used to generate these data are listed on the figures. The heat shield requirements are based on temperature-constrained entry trajectories with maximum lower surface temperatures of 2200°F. Heat shield weights for the LI-1500 system increase more rapidly with cross-range, because the metallic system uses lighter weight insulation. For the LI-1500 system, the average unit heat shield weight increases by 0.055 lb/ft^2 per 100 nm of cross range. For the metallic system the corresponding value is 0.035.

3.6 ABLATOR EVALUATION

This discussion concerns the thermodynamic evaluation of a typical low density ablator for the lower surface of the orbiter vehicle. The chosen material

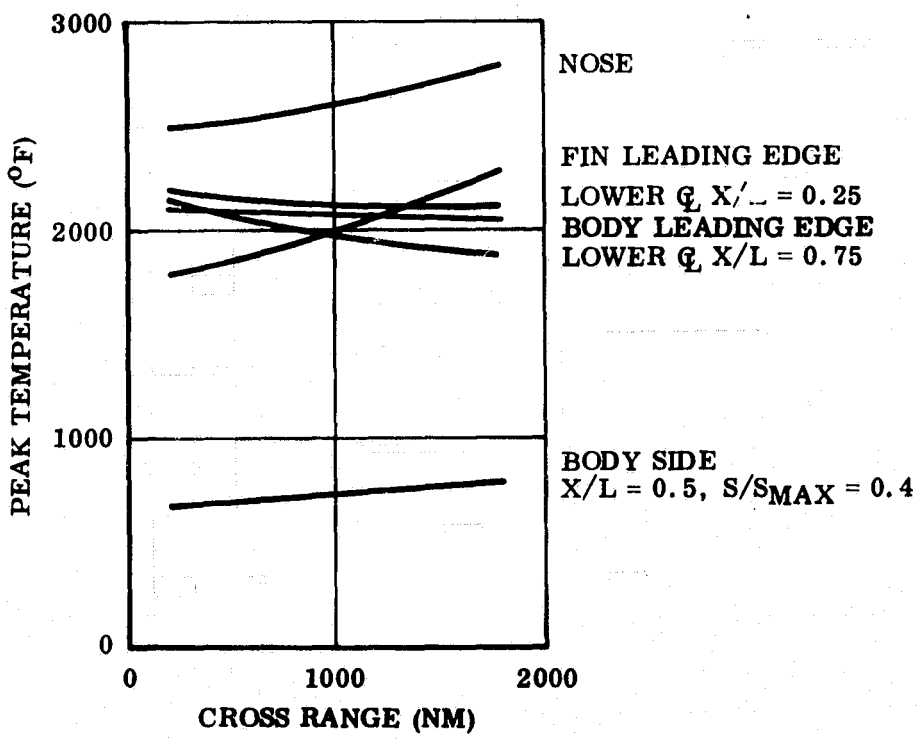

Fig. 3-54 Effect of Cross Range on Peak Surface Temperature

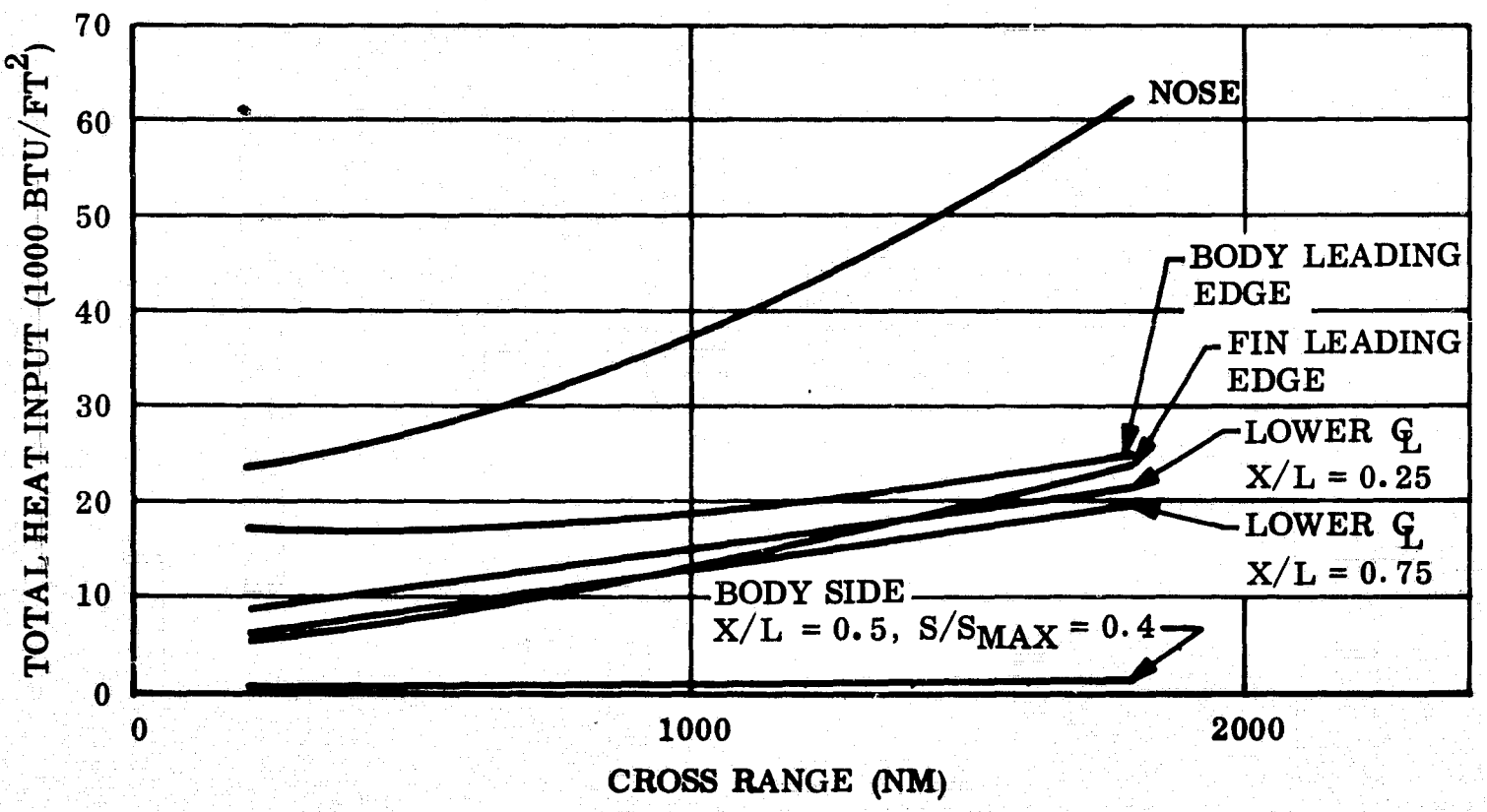

Fig. 3-55 Effect of Cross Range on Total Heat Input

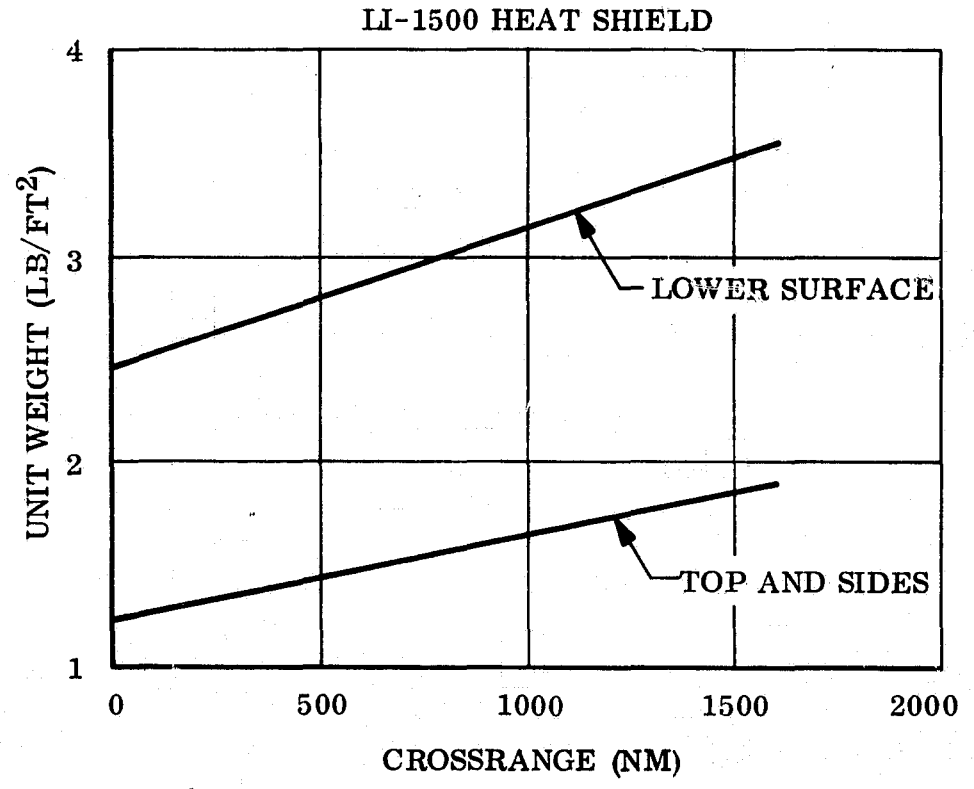

- o 2200°F MAXIMUM SURFACE TEMPERATURE
- o 200°F MAXIMUM STRUCTURE TEMPERATURE
- o INCLUDES 0.25 LB/FT^2 FOR AIR COOLING DUCTS
- o RAM AIR AND GROUND AIR COOLING
- o LI-1500 DENSITY OF 12 LB/FT^3

Fig. 3-56 Variation of LI-1500 Heat Shield Weight With Cross Range

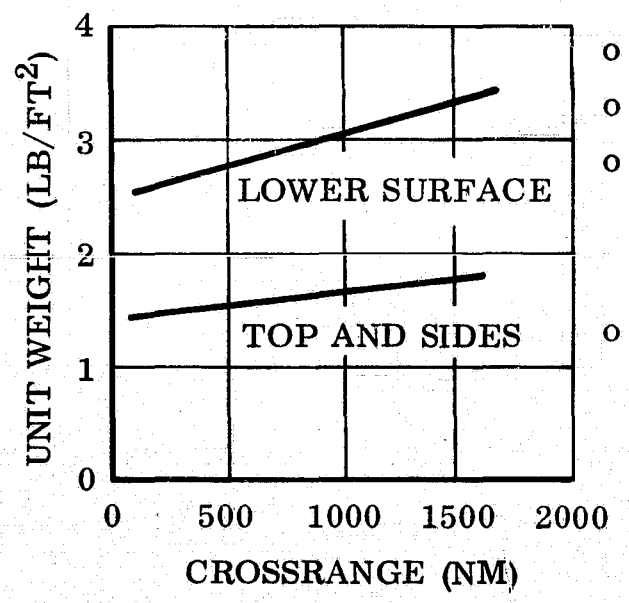

- o 2200°F MAXIMUM SURFACE TEMPERATURE
- o 200°F MAXIMUM STRUCTURE TEMPERATURE
- o CLIP SUPPORTED METALLIC HEAT SHIELD LOWER SURFACE TD-NI-CR–1.53 LB/FT^2 TOP AND SIDES RENE'41–1.14 LB/FT^2 INCLUDES SUPPORTS, PACKAGING AND SUBPANEL
- o RAM AIR AND GROUND AIR COOLING

Fig. 3-57 Variation of Metallic Heat Shield Weight With Cross Range

is a silicone elastometer with a density of 20 lb/ft^3 (a modified form of General Electric TBS 757, consisting of TBS 757A, RTV 665A Silica Eccosphers, and TBS 757B (catalyst)), reinforced by a phenolic fiberglas honeycomb to inhibit char removal. This particular version of TBS-757 was extensively tested (thermogravmetric analysis (T.G.A.) and plasma jet tests) by Lockheed during the ENCAP study (Ref. 3-11). Because of the relatively mild thermal environment associated with the top and sides of the orbiter, the ablator was evaluated only for the lower surface.

The interaction of a charring ablative material with the external thermodynamic environment represents a complex problem. The formulation of a physical model on which to base a performance analysis of a consumable material requires a rigorous accounting of all energy transfer and physical chemical change processes. A theory describing this model was formulated at Lockheed for nylon-phenolic (Ref. 3-13). Figure 3-58 outlines the energy exchange processes for a typical charring ablator. The model includes (1) convective heat transfer at the surface and energy blockage due to outgassing of the charring material; (2) depolymerication of the virgin material in depth; (3) conversion of the charred material to complex gaseous products that diffuse to the surface, providing energy absorption by sensible enthalpy charge and by chemical cracking; (4) energy conduction through the charred and uncharred material; and (5) erosion of the char layer by oxidation and mechanical forces. Figure 3-59 illustrates the temperature and density variation through a typical charred ablator.

This physical model for a depolymerizing material has been incorporated into a one-dimensional heat conduction equation, and a numerical solution was programmed for the Univac 1108. (Ref. 3-14).

The pyrolysis reaction is specified as a rate equation wherein the rate coefficient is expressed in Arnhenius form. The rate coefficient (k_o), reaction order (m), and the activation energy (E/R) for the silicone system were obtained from the T.G.A. and plasma arc tests performed during the ENCAP study.

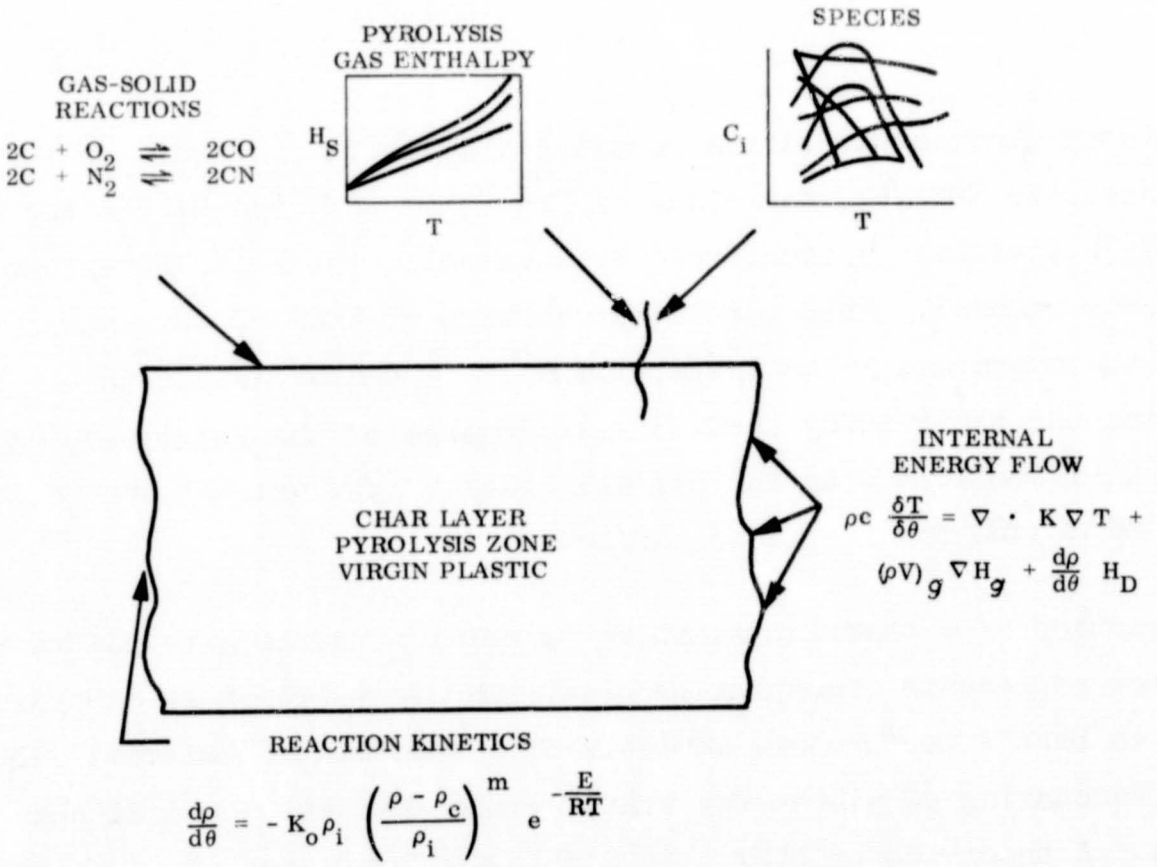

Fig. 3-58 Thermal Model of Charring Ablator

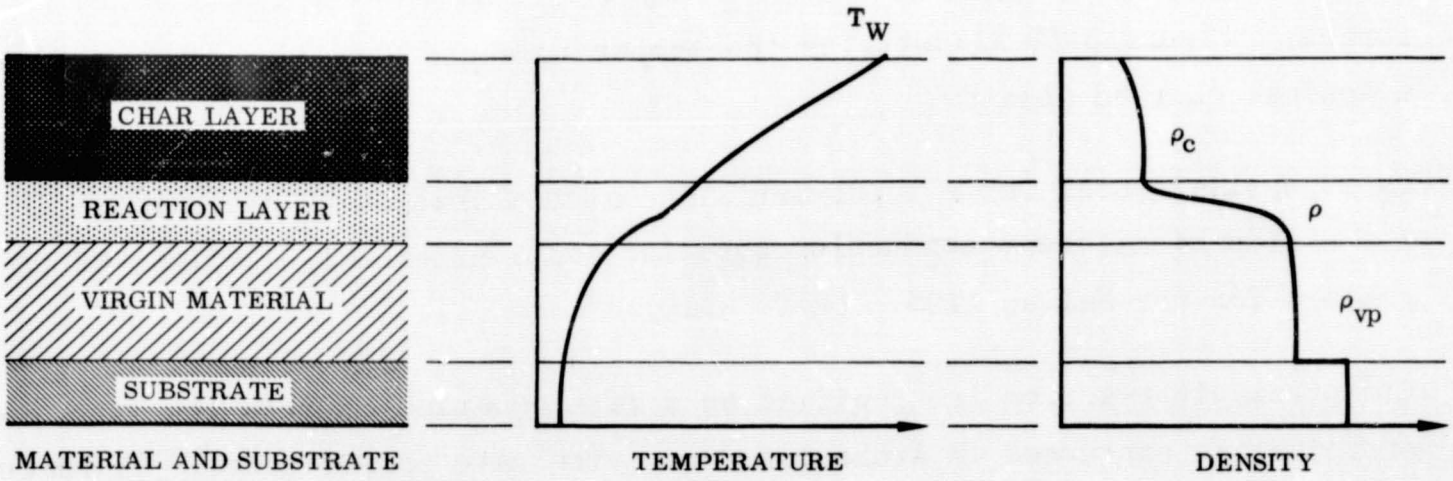

Fig. 3-59 Thermochemical Degradation of Typical Ablator

The rate equation is as follows:

$$\frac{d\rho}{d\theta} = -K_o \rho_i \left(\frac{\rho - \rho_c}{\rho_i}\right)^m e^{-\frac{E}{RT}}$$

Figure 3-60 presents the thermal conductivity (as obtained from analysis of arc-jet tests on the ENCAP study Ref. 3-11) specific heat, and emittance used in the evaluation of TBS-757. Figure 3-61 shows the gas enthalpy, corresponding to the various element species generated during pyrolysis, as a function of temperature and pressure. The enthalpy represents the energy absorption capability of the pyrolysis gases.

Table 3-20 lists the total heat load, ablator thickness, char thickness, and time to touchdown for the maximum and minimum cross-range trajectories presented in Volume I. On the basis of flight test results from the PRIME vehicle (Ref. 3-15) for a low-density silicone ablator, it was assumed that the modified TBS-757 would experience negligible surface erosion. For a maximum substructure temperature of 200°F, 2.3 in. of ablator is required for the 1600-nm cross-range trajectory and 1.2 in. for the 67-nm cross-range trajectory. (See para. 3.1.3).

The lower portion of Table 3-21 shows the unit weight for a full depth ablator and two partial depth ablators bonded to LI-1500 for intermediate bondlines of 600°F and 1000°F. The more recent polyimide adhesives (Refs. 3-15 and 3-16) appear to have bonding capability to 1000°F, whereas adhesives such as RTV-30 can withstand 600°F. The thermal protection system unit weight can be reduced by 28 percent for all cross ranges if a partial depth ablator with a 1000°F bondline and polyimide adhesive is employed. A reduction of about 14 percent in unit weight can be realized by using a partial depth ablator with a 600°F bondline. The partial depth balator system uses LI-1500 as the second part of the composite system.

3.7 CONCLUSIONS

Current technology with minimum development for thermal protection systems and available aircraft technology for primary structure can be used to obtain

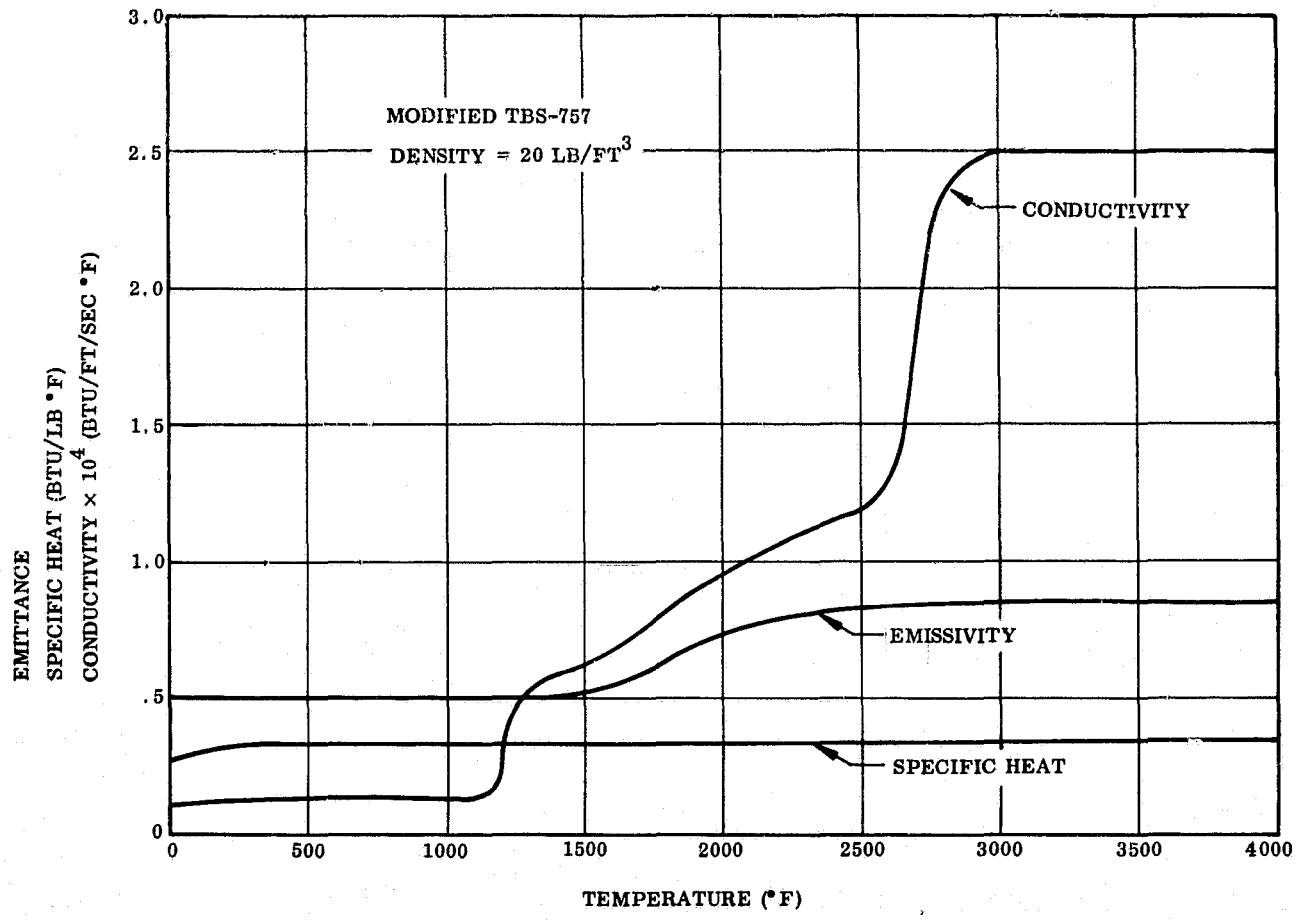

Fig. 3-60 Evaluation of TBS-757 - Temperature vs Emittance, Specific Heat, and Conductivity

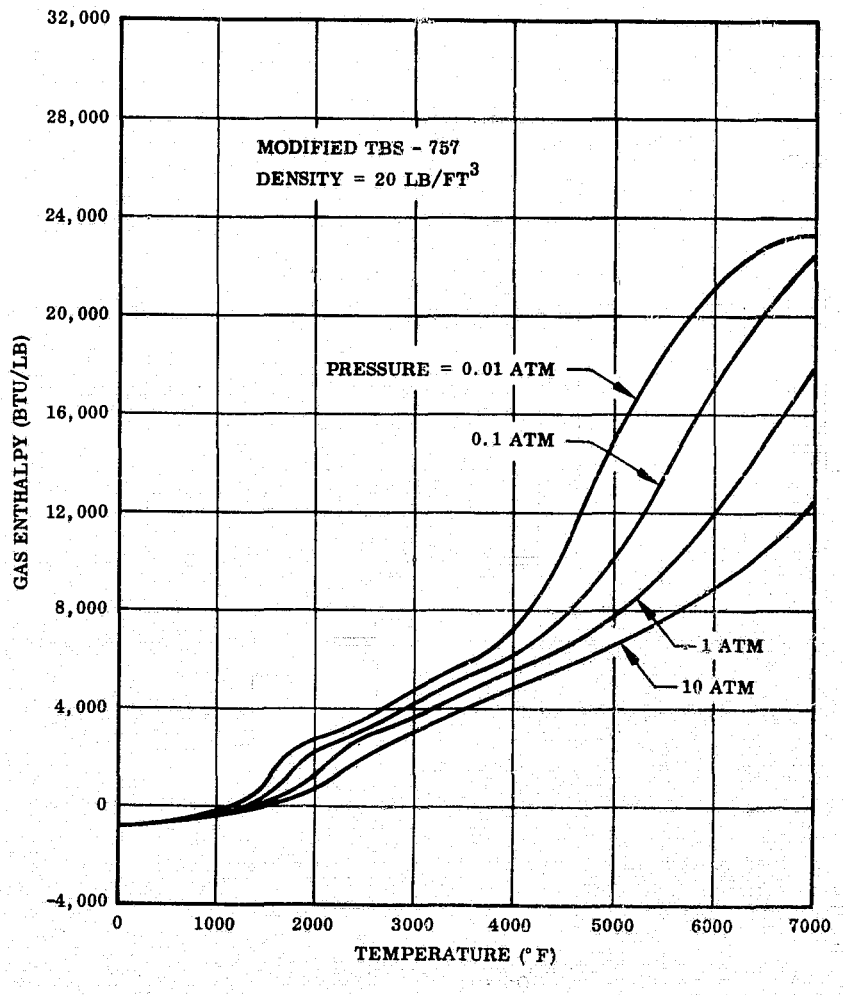

Fig. 3-61 Evaluation of TBS-757 - Temperature vs Gas Enthalpy

Table 3-21

LOWER SURFACE ABLATOR PARAMETERS

Environment Induced Parameters

Cross-Range (nm)	Q Total$_2$ (Btu/ft^2	Ablator Thickness (in.)	Char Layer Thickness (in.)	Time 400,000 ft to Touchdown (sec)
67	6,100	1.2	0.43	1950
1600	21,500	2.3	0.85	3050

Ablator Unit Weight (lb/ft^2)

Cross range (nm)	Full Depth Ablator	Partial Depth Ablator/LI-1500 600°F Bondline	Partial Depth Ablator/LI-1500 1000°F Bondline
67	2.85	2.45	2.05
1600	5.15	4.15	3.65

- 200°F aluminum substructure
- Internal ram air cooling at M_α = 0.8 and ground cart cooling at 10 min. after touchdown
- Maximum surface temperatue at 200°F
- Includes 0.25 lb/ft^2 for air cooling duct
- Includes 0.10 lb/ft^2 for adhesive
- Includes 5 lb/ft^3 phenolic honeycomb core

a Space Shuttle system, as presently defined. Also, since metallic-fibrous and rigid insulation heat shield concepts are similar in weight, the thermal protection selection has minimum impact on vehicle sizing and performance. The thermal protection selection, however, has major impact on vehicle reuse.

3.8 REFERENCES

3-1 U. S. Standard Atmosphere for 1962, U. S. Government Printing Office, December 1962

3-2 Hansen, C. F. "Approximations for the Thermodynamic and Transport Properties of High Temperature Air," NASA TR R-50, 1959

3-3 Fay, C. F. and Riddell, F. R., "Theory of Stagnation Point Heat Transfer in Dissociated Air," Journal of Aerospace Sciences, February 1958

3-4 Boison, J. C. and Curtiss, H. A., "An Experimental Investigation of Blunt Body Velocity Gradient," ARS Journal, February 1959

3-5 Bushnell, D., "Effects of Shock Impingement and Other Factors on Leading Edge Heat Transfer," NASA TN D-4543, April 1968.

3-6 Beckwith, I. and Gallagher, J., "Experimental Investigation of the Effect of Boundary Layer Transition on the Average Heat Transfer to a Yawed Cylinder in Supersonic Flow:, NACA RM 56 E09, 1956.

3-7 White, J. L., "Pressure and Heat Transfer Distributions on a Blunt 80-Deg Sweep Delta Wing at Mach Number 19 (U)", AEDC-TR-67-117, June 1967 (Conf)

3-8 Neumann, R. and Renfroe, P., "Evaluation of the Heat Transfer and Flow Fields About Highly Swept Delta Wings in Hypersonic Flow (U)," ASD-TDR-64-76, April 1964 (Conf).

3-9 Ecker, E.R.G., "Survey on Heat Transfer at High Speeds", WADCTR 54-70, April 1954

3-10 Savage, R. and Jaeck, C., "Investigation of Turbulent Heat Transfer at Hypersonic Speeds" AFFDL-TR-67-144, December 1967.

3-11 "Encapsulation and Recovery of Space Objects," AFAPL-TR-67-124 (SECRET) LMSC B118347, December 1967.

3-12 "Encap Vehicle, Vol. II, Heat Shield Material Evaluation," AFAPL-TR-68-117, January 1969.

3-13 K. M. Kratsch, L. F. Hearne, H. R. McChesnly, "Theory for the Thermophysical Performance of Charring Organic Heat-Shield Composites." LMSC-803099, October 1963.

3-14 M. G. Meyer, "Charring in Re-Inforced Plastics (Chirp)," LMSC 55-24-TSS21, November 1965.

3-15 J. W. McCown, "Review of Heat Shield Concepts for Future Reentry Spacecraft," AIAA Paper No. 68-1127, October 1968.

3-16 C. Milewski and J. D. Martra, Jr., "Advanced Heatshield Concepts for Lifting Entry Vehicles," Martin-Marietta Co., RM-316, July 1967.

3-17 Thomas, A. C., Perlbachs, A. and Nagel, A. L., "Advanced Re-entry Systems Heat Transfer Manual for Hypersonic Flight", AFFDL-TR-65-195, October 1966.

APPENDIX A

ROCKET ENGINE CRITERIA FOR A REUSABLE SPACE TRANSPORT SYSTEM

1. SCOPE

1.1 GENERAL. This document establishes Rocket Engine Criteria including performance and design requirements for a reusable, man-rated rocket engine. The intended application for this rocket engine is to satisfy primary propulsion requirements for integrated launch and reentry operation of a reusable space transport system.

1.2 FUNCTION. This rocket engine shall use hydrogen and oxygen as propellants and shall have the following salient features:

a. The engine shall conform to an envelope prescribed in this specification and shall be capable of being used for a multi-engine installation on an interchangeable basis.

b. The engine shall have a single thrust chamber capable of efficient operation from sea level to vacuum altitudes and shall be compatible with vehicle thrust vector control criteria.

c. The engine shall upon command, operate in a normal (full thrust), throttled, or emergency mode.

d. The engine shall be capable of safe shutdown from any operational mode or malfunction situation.

e. The engine shall have a multiple restart capability at any altitude or attitude condition after proper pre-conditioning.

f. The engine shall be dynamically stable throughout the specified mixture ratio and will provide a mixture ratio control system for vehicle propellant management.

g. The engine shall be provided with a checkout and malfunction detection system.

h. The engine upon replacement, repair or overhaul of components shall be capable of reuse without limitation within the original design and performance envelope.

2. APPLICABLE DOCUMENTS - The following applicable documents, of the exact issue shown, form a part of this specification to the extent specified herein. In the event of conflict between documents referenced here and other detailed contents of Sections 3, 4 and 5, the detailed requirements of Sections 3, 4 and 5 shall be considered superseding requirements.

SPECIFICATIONS

Military

MIL-P-25508D 16 March 1962	Propellants, Liquid Oxygen
MIL-P-27201 21 May 1959	Propellants, Liquid Hydrogen

3. REQUIREMENTS

3.1 PERFORMANCE. The engine shall perform within the specified operational limits during and after exposure to the environmental conditions and load factors specified herein.

3.1.1 Functional Characteristics. The function of the engine shall be to provide propulsive force for vehicle launch, orbital insertion, rendezvous, space maneuvers, and reentry.

3.1.1.1 Primary Performance Characteristics. The engine shall have the following sea level to vacuum performance characteristics when supplied with propellants specified in 3.3.1.4 at pressures and temperatures specified in 3.2.1.2.1.1, electrical power as specified in 3.2.1.3.1.1, and helium or pressurizing gases as specified in 3.3.1.5.

3.1.1.1.1 Thrust. The engine shall be capable of providing thrust as specified below.

3.1.1.1.1.1 Normal Rating. The normal rating shall provide 400,000 pounds of thrust $\pm$ 3.0 percent (3σ) pounds at sea level over the mixture ratio range from 6.5:1 to 7.5:1. The engine shall have unlimited reuse under this condition.

3.1.1.1.1.2 Throttled Ratings. Throttled ratings shall extend from 10 to 100 percent of the normal rating over the mixture ratio range of 6:5:1 to 7.5:1. The engine shall have unlimited reuse under this condition.

3.1.1.1.1.3 Emergency Rating. The emergency rating shall provide 115 percent of normal rated thrust at a mixture ratio to be specified. The engine shall be capable of reuse without overhaul after operation at this condition.

3.1.1.1.1.4 Unpumped Idle Rating. The engine shall be capable of operating in an unpumped idle mode during chilldown. After chilldown, transient times to pumped ratings shall be minimal. The engine shall have unlimited reuse under this condition.

3.1.1.1.2 Specific Impulse. The engine minimum specific impulse shall be as follows:

DELIVERED SPECIFIC IMPULSE
LBF-SEC/LBM
MIXTURE RATIO - 7: 1

Vehicle / Engine Operation	Booster		Orbiter	
	Sea Level	Altitude	Sea Level	Altitude
a. Bell Engine				
100% normal rating	388	428	379	454
115% normal rating				
10% normal rating	380	420	371	445
unpumped idle	-	380	-	380
b. Aerospike Engine				
100% normal rating	375	453	375	453
115% normal rating				
10% normal rating	370	445	370	445
unpumped idle	-	320	-	320

3.1.1.2 Secondary Performance Characteristics.

3.1.1.2.1 Duty Cycle. Each duty cycle shall consist of the following:

a. Booster - Sea level start, up to 200 seconds of continuous burn from normal rated thrust at sea level including continuous throttling to 10 percent of normal rated thrust prior to staging, and command shutdown.

b. Orbiter - After staging, up to 300 seconds of continuous burn from normal rated thrust at vacuum including continuous throttling to 10 percent of normal rated thrust prior to injection into orbit and command shutdown.

- Altitude restarts in any operating mode followed by varying burn time intervals, accumulating as much as 300 seconds total operation.

- Up to 30 days of orbital coast between any shutdown and a subsequent restart.

- Restart for retro/deorbit in any operating mode with up to 125 seconds of burn time followed by command shutdown.

3.1.1.2.1.1 Starting. The engine shall be capable of unlimited starts and restarts at sea level and altitude under conditions specified in 3.1.2.4 when supplied with saturated or mixed phase propellants.

3.1.1.2.1.2 Shutdown. The engine shall be capable of being shutdown automatically in a safe positive manner either by command signal from the vehicle or by engine initiated command signal as a result of self-detected and analyzed malfunction condition.

3.1.1.2.2 Thrust Vector Control. The engine shall be capable of providing thrust vector control equivalent to ± 7.5 deg conical pattern around the engine longitudinal center line with an angular rate of (to be determined) deg/sec and an angular acceleration of (to be determined) rad/sec^2.

3.1.1.2.3 Attitude. The engine shall be capable of operation in any attitude when supplied with specified propelants at specified pump inlet pressures and temperatures.

3.1.1.2.4 Thrust Transients. The times required for thrust buildup or shutdown to reach various engine operational rating shall be as follows: Times are based on specified propellants at specified pump inlet conditions and preconditioning temperatures.

3.1.1.2.4.1 Start Signal to 100% Normal Rating. Five seconds permitted.

3.1.1.2.4.2 Start Signal to Pumped Idle Rating (10%). Four seconds permitted.

3.1.1.2.4.3 Pumped Idle to 100% Normal Rating. Two seconds permitted.

3.1.1.2.4.4 100% Normal Rating to Zero Thrust. Five seconds permitted.

3.1.1.2.4.5 Maximum Thrust Rise Rate. The maximum thrust rise rate shall not exceed (to be determined).

3.1.1.2.5 Combustion Stability. The engine shall be controlled to operate as specified herein in such a manner as to prevent or suppress damaging or destructive combustion instability.

3.1.1.2.6 Mixture Ratio Control. The engine mixture ratio shall be capable of being controlled over an oxidizer to fuel weight flow rate ratio range of 6.5 to 7.5 between 10 percent and 100 percent of normal rated thrust either by command signal from the vehicle or by engine initiated signal to satisfy propellant utilization requirements.

3.1.1.2.7 Transient Pre- and Post-Propellant Flows. The engine pre- and post non-impulse propellant flows shall be minimized and repeatable within _____ (limits to be determined).

3.1.1.2.8 Propellant Dump. Requirement for propellant dump through the engine without ignition shall be determined.

3.1.1.2.9 External Leakage. The engine shall not leak externally except through drain connections as specifically provided by the engine manufacturer and accepted by the Vehicle Contractor/Procurement Agency.

3.1.2 Operability.

3.1.2.1 Reliability. The reliability design requirement for the engine shall be determined, at the performance ratings specified in 3.1.1.1 for the duty cycle specified in 3.1.1.2.1 throughout the useful life of the engine specified in 3.1.2.3.1.

3.1.2.2 Maintainability.

3.1.2.2.1 Maintenance and Repair Cycle.

3.1.2.2.1.1 Module Replacement. For minor engine repair, individual components or modules (to be defined) shall be capable of field replacement without necessitating a refire test of the engine.

3.1.2.2.1.2 Engine Overhaul. The engine shall be capable of overhaul to a "like-new" condition after each 10 hours of operating time until expiration of total useful life as specified in 3.1.2.3.1.

3.1.2.2.2 Checkout Criteria.

On an automatic basis as well as on vehicle command, the engine will determine and report its operational readiness for flight, will monitor, record and report its performance and determine and signal malfunction conditions by assessing proper performance and operational parameters. The reporting sequence on any parameter shall be capable of being altered as required on vehicle command.

3.1.2.3 Useful Life. The useful life of the engine shall be as noted in the following sections.

3.1.2.3.1 Operating Life. The operating life shall be not less than 50 hours (from receipt by procuring agency to scrap) based on accomplishing periodic overhaul at intervals of not less than 10 hours of operating time.

3.1.2.3.2 Orbital Life. The orbital life shall not exceed a maximum of 30 days nonoperating time during any one mission.

3.1.2.3.3 Storage Life. The storage life shall not be less than 10 years from receipt by procuring agency until refurbishment.

3.1.2.4 Environmental. The engine shall be subject to and capable of withstanding the following environmental requirements.

Environment	Non-Operational						Operational	
	Storage	Transport Ground/ Air	Launch(3) Readiness	Orbital(3) Coast	Reentry(3)	Return(3) Flight	T/O and Ascent	Orbital
Temperature	-20°F to +140°F	-20°F to +140°F						
Pressure	SL	SL	SL	Vacuum	Vacuum	Vacuum to SL	SL to Vacuum	Vacuum
Relative Humidity	100%	100%	100%	N/A	N/A	100%	100%	N/A
Vibration Mechanical	N/A	TBD(1) TBD(2)	N/A					
Acoustic	N/A	N/A	N/A					
Shock	N/A	TBD(1) TBD(2)						
Acceleration	N/A	4G any Direction(1) 2G Axial (2) 2G Lateral					Up to 3g-manned Up to 4g-cargo	

1. Engine supported by thrust mount
2. Engine unsupported by thrust mount
3. Engine installed in vehicle

TBD - To be determined

N/A - Not Applicable

3.1.2.5 Transportability. The engine either as an assembly or installed in the vehicle shall meet transportability requirements.

3.1.2.6 Human Performance. The principles of Human Engineering as specified for the vehicle/spacecraft shall also be applied to the rocket engine.

3.1.2.7 Safety. The engine assembly shall meet the safety requirements specified for the vehicle.

3.2 CEI DEFINITION

3.2.1 Interface Requirements. The physical, fluid transfer, and energy transfer interface requirements are specified below.

3.2.1.1 Physical Interface.

3.2.1.1.1 Envelope Requirements. Engine dimensional envelope requirements to be determined and specified in LMSC envelope drawing.

3.2.1.1.2 Connections. The following connections shall be specified as to configuration, dimension or standard fitting reference, material, location and misalignment tolerances, and fastener torque requirements when information is available.

3.2.1.1.2.1 Engine Mounting.

3.2.1.1.2.2 Pump Inlet Flanges.

3.2.1.1.2.3 Gimbal Actuator Mounting (as applicable)

3.2.1.1.2.4 Drain Lines.

3.2.1.1.2.5 Gas Actuation and Pressurization Line Ports.

3.2.1.1.2.6 Electrical Connectors.

3.2.1.1.3 Mockup. A full scale mockup shall be provided by the engine contractor to display and record rocket engine - vehicle interface agreements.

3.2.1.2 Fluid Transfer Interface.

3.2.1.2.1 Propellant Requirements.

3.2.1.2.1.1 Operation. The engine shall start and operate as specified when supplied with propellants specified in 3.3.1.4 in the temperature and pressure ranges specified in Table 1.

3.2.1.2.1.2 Chilldown. Propellant shall be supplied to the engine for pump chilldown prior to engine start. Operation in an unpumped idle mode may be used to minimize impulse propellant loss. Pressure and flow rate requirements shall be determined.

3.2.1.2.1.3 Contamination. Contamination limits shall be determined.

TABLE 1

	Engine Operation Mode		
	Pumped (Normal Rated)	Pumped Idle (10% of Normal Rated)	Unpumped Idle
Temperature			Saturated or Mixed Phase Propellants (Quality to be Determined)
Fuel	45°R		
Oxidizer	180°R		
Net Positive Suction Pressure (PSI)			
Fuel	2	0	
Oxidizer	8	0	

3.2.1.2.2 Pressurant Requirements.

3.2.1.2.2.1 Helium. The engine shall be supplied with helium as specified in 3.3.1.4 at pressures, flow rates and quantities required for rocket engine operation as established by the rocket engine contractor.

3.2.1.2.2.2 Autogenous Pressurant Requirements. The engine shall provide gaseous fuel and gaseous oxidizer for vehicle propellant tank pressurization during all normal and throttled operating modes at flow rates and pressures to be determined.

3.2.1.2.3 Plume Effects. The interaction of the engine exhaust plume with the vehicle structure, vehicle components and/or other engine assemblies shall be determined.

3.2.1.3 Energy Transfer Interface. Requirements for transfer or isolation of electrical, mechanical, fluid and acoustical energy across all vehicle/engine physical interfaces shall be as specified below.

3.2.1.3.1 Electrical Energy Requirements.

3.2.1.3.1.1 Source Power Characteristics. Characteristics of vehicle electrical power available to supply the engine electrical system shall be defined as to voltage, amperage, impedance, transients, ripple, etc. Engine requirements for vehicle power shall be derived from the following:

a. Engine electrical distribution system
b. Engine-borne computer for checkout, operation, control, malfunction, detection and corrective action initiation.
c. Nozzle extension position actuators (if required) when engine is inoperative.
d. Thrust chamber gimbal actuators (if required) when engine is inoperative.

3.2.1.3.1.2 Signal Power Characteristics. Signal power output characteristics, and input requirements, of vehicle onboard computer which will interface with the engine in accordance with 3.1.2.2.2, shall be defined:

a. Voltage
b. Amperage
c. Regulation

3.2.1.3.2 Mechanical Energy Requirements. Excitation at the engine-vehicle interface induced by the engine and the vehicle shall be determined and specified in Tables 1 and 2.

TABLE 1

	EXCITATION AT INTERFACE INDUCED BY THE ENGINE DURING OPERATION																	DURING NONOPERATION (ON GROUND HORIZONTAL)
	LOADS GENERATED BY THRUST FORCE													VIBRATION				
	STEADY STATE MAX		VARIABLE				PEAK				BENDING MOMENT			SINUSOIDAL		RANDOM		
			AXIAL		LATERAL		AXIAL		LATERAL									
	AXIAL	LATERAL	MAGNITUDE	FREQUENCY	MAGNITUDE	FREQUENCY	MAGNITUDE	DURATION	MAGNITUDE	DURATION	MAGNITUDE	RATE	ACCELERATION	BANDWIDTH	AMPLITUDE	BANDWIDTH	POWER SPECTRUM	BENDING MOMENT
	LB	LB	LB	CPS	LB	CPS	LB	SEC	LB	SEC	FT-LB	RAD/SEC	RAD/SEC^2	CPS	g	CPS	g^2/CPS	FT-LB
ENGINE MOUNT																		
PUMP PROPELLANT INLET FLANGES																		NA
GAS ACTUATION & PRESSURIZED LINE FLANGES																		NA
ELECTRICAL CONNECTORS																		NA
GIMBAL ACTUATOR MOUNTING																		

TABLE 2

INTERFACE ROCKET ENGINE NON-OPERATIVE		EXCITATION AT INTERFACE INDUCED BY VEHICLE						
		BENDING MOMENTS			VIBRATION			
					SINUSOIDAL		RANDOM	
		MAGNITUDE	RATE	ACCELERATION	BANDWIDTH	AMPLITUDE	BANDWIDTH	POWER SPECTRUM
		FT-LB	RAD/SEC	RAD/SEC^2	CPS	g	CPS	g^2/CPS
ENGINE MOUNT	REENTRY, FLIGHT MANEUVER, LANDING							
	TRANSPORTATION							
PUMP PROPELLANT INLET FLANGE	MISALIGNMENT							
GAS ACTUATION & PRESSURIZED LINE FLANGES	MISALIGNMENT							
ELECTRICAL CONNECTORS	MISALIGNMENT							
GIMBAL ACTUATOR MOUNTING	REENTRY, FLIGHT MANEUVER, LANDING							
	TRANSPORTATION							

3.2.1.3.3 Acoustical Energy Requirements.

3.2.1.3.3.1 Input to Vehicle From Engine Operation.

3.2.1.3.3.2 Input to Engine By Feedback From Vehicle During Engine Operation.

3.2.1.3.4 Auxiliary Power Requirements. The engine shall provide an auxiliary power takeoff pad on either the oxidizer or fuel turbopump assembly which is capable of delivering 150 shaft horsepower.

3.2.2 Component Identification.

-------- TO BE DETERMINED -------

3.3 DESIGN AND CONSTRUCTION

3.3.1 General Design Features.

3.3.1.1 Engine Installation. The engine shall be capable of being installed in the vehicle while the vehicle is in either a horizontal or vertical position.

3.3.1.2 Engine Weight. The rocket engine dry weight shall not exceed the following weights. The wet weight consists of propellant trapped in the engine below the inlet openings.

	DRY WEIGHT		WET WEIGHT	
	Booster	Orbiter	Fuel	Oxidizer
Bell Engine	4140	4600		
Aerospike Engine	4450	4450		

3.3.1.3 Engine Center of Gravity. The engine shall be designed with overall center of gravity as far forward as practicable. Center of gravity locations shall be specified in LMSC envelope drawing as indicated in 3.2.1.1.1.

3.3.1.4 Specification Propellants. The engine shall use a propellant combination of the following:

a. Oxidizer, Liquid Oxygen (LOX) in accordance with Military Specification MIL-P-25508D, 16 March 1962.

b. Fuel, Liquid Hydrogen (LH_2) in accordance with Military Specification MIL-P-27201, 21 May 1959.

3.3.1.5 Pressurants.

a. Engine Component Actuation. The pressurizing gas supplied to the engine for component actuation shall be helium, Bureau of Mines, Grade "A". Maximum water content shall be defined by a dewpoint of $-80^{\circ}F$ at standard atmospheric pressure. The helium gas shall have been externally processed through a nominal 10 micron filter (or finer) whose maximum orifice size shall not exceed 50 microns.

b. Vehicle Tank Pressurization. The engine shall provide gases for vehicle tank pressurization as specified in 3.2.1.2.2.2 from the oxidizer and fuel supplied to the engine.

3.3.1.6 Engine Mount. The engine mount shall be sufficiently stiff to satisfy requirements of natural frequency (to be determined).

3.3.1.7 Turbopump Assembly.

3.3.1.7.1 Control. The turbopump design shall provide for independent control of thrust and propellant mixture ratio.

3.3.1.7.2 Auxiliary Power Generation. The turbopump design shall provide auxiliary power for thrust vector control or other uses as specified in 3.2.1.3.1.1.

3.3.1.8 Propellant Flow Control. The propellant flow control components shall provide for mixture ratio control on command signal from vehicle for propellant utilization.

3.3.1.9 Thrust Chamber Assembly.

3.3.1.9.1 Thrust Vector Alignment. The thrust vector shall coincide with the geometric centerline of the nozzle within a tolerance to be determined. In the event thrust vectoring is accomplished by means other than gimballing the thrust vector in null position shall coincide with geometrical centerline of the nozzle within a tolerance to be determined.

3.3.1.9.2 Gimballed Engine. For engines incorporating gimballing to satisfy thrust vector control requirements of 3.1.1.2.2, the following characteristics of the gimballed mass shall be determined:

a. Location of center of gravity.
b. Mass moment of inertia.

3.3.1.9.3 Nozzle Extension. For thrust chambers that incorporate capability for positioning of nozzle extension to satisfy specific impulse requirements of 3.1.1.1.2, provision shall be provided to automatically position the nozzle extension for required sea level or altitude operation. In addition, provision shall be provided to retract the nozzle extension on command while engine is inoperative for reentry or landing operations.

3.3.1.10 Electrical System. The electrical system of the engine shall consist of the following:

a. Power distribution system for electrical components.
b. Instrumentation system to monitor the critical engine performance and operational parameters, to be determined.
c. Integral computer system to integrate, control and monitor engine operation to satisfy the requirements of 3.1.2.2.2. This system shall be designed to function independent of vehicle computer system but shall interface with the vehicle system to accept commands and interrogation, and to transmit appropriate response.

3.3.1.11 Flight and Ground Loading. The engine and its components shall be provided with necessary strength and rigidity to withstand the environmental and interface loads of 3.1.2.4 and 3.2.1.3.2, respectively, increased by appropriate factors of safety to be determined.

3.3.1.12 Selection of Specifications and Standards. To be determined.

3.3.1.13 Materials, Parts and Processes. To be determined.

3.3.1.14 Standard and Commercial Parts. To be determined.

3.3.1.15 Moisture and Fungus Resistance. To be determined.

3.3.1.16 Corrosion of Metal Parts. To be determined.

3.3.1.17 Interchangeability and Replaceability. To be determined.

3.3.1.18 Workmanship. To be determined.

3.3.1.19 Electromagnetic Interference. To be determined.

3.3.1.20 Identification and Marking. To be determined.

3.3.1.21 Storage. To be determined.

3.3.1.22 Material - Propellant Compatibility. To be determined.

4 QUALITY ASSURANCE PROVISIONS

4.1 CATEGORY I TEST

4.1.1 Engineering Test and Evaluation.

4.1.2 Preliminary Qualification Tests.

4.1.3 Formal Qualification Tests.

4.1.4 Reliability Tests and Analysis.

4.1.5 Engineering Critical Component Qualification.

5 PREPARATION FOR DELIVERY

6. NOTES

6.1 DEFINITIONS

6.1.1 Vehicle Launch. Vehicle Launch involves vertical takeoff from either the Eastern Test Range (ETR) or Western Test Range (WTR).

6.1.2 Orbital Insertion. Normal missions involve insertion into an elliptical orbit with subsequent insertion into a circular orbit.

6.1.3 Rendezvous. The vehicle shall have parallel motion translation along each of three axis in order to permit rendezvous with a space station or other spacecraft.

6.1.4 Space Maneuvers. Space maneuvers include orbit circularization, synergetic plane change, orbit plane change, drag makeup and other similar operations.

6.1.5 Reentry. Reentry involves necessary maneuvers for deorbit and reentry as well as subsonic flight to the point of origin.